Copy 6
RM L55I08

NACA RM L55I08

NACA

RESEARCH MEMORANDUM

(3)

HIGH-SPEED CASCADE TESTS OF THE NACA 65-$\left(12A_{10}\right)$10 AND NACA 65-$\left(12A_2I_{8b}\right)$10 COMPRESSOR BLADE SECTIONS

By James C. Dunavant, James C. Emery, Howard C. Walch, and Willard R. Westphal

Langley Aeronautical Laboratory
Langley Field, Va.

NATIONAL ADVISORY COMMITTEE FOR AERONAUTICS

WASHINGTON

December 21, 1955

NACA RM L55I08

NATIONAL ADVISORY COMMITTEE FOR AERONAUTICS

RESEARCH MEMORANDUM

HIGH-SPEED CASCADE TESTS OF THE NACA 65-$(12A_{10})10$ AND NACA 65-$(12A_2I_{8b})10$ COMPRESSOR BLADE SECTIONS

By James C. Dunavant, James C. Emery, Howard C. Walch, and Willard R. Westphal

SUMMARY

Two-dimensional porous-wall cascade tests of the NACA 65-$(12A_{10})10$ and NACA 65-$(12A_2I_{8b})10$ blade sections were made at Mach numbers from 0.3 to choking in most cases. Data were obtained at solidities of 1.0 and 1.5 at inlet-air angles of 45° and 60° for both blade sections. With a solid-wall modification to the cascade tunnel, schlieren observations were made of the flow in cascade at a solidity of 1.5 and inlet-air angle of 45° and at a solidity of 1.0 and inlet-air angle of 60°.

Test results for the NACA 65-$(12A_{10})10$ blade section show that the turning angles measured at low speed do not change significantly as the speed increases until the critical Mach number is exceeded. Because of increasing separation from the highly cambered trailing-edge region, the turning angles for the NACA 65-$(12A_2I_{8b})10$ blade section decreased as much as 4° from low speed to critical speed. The high-speed performance of the NACA 65-$(12A_{10})10$ and the NACA 65-$(12A_2I_{8b})10$ blade sections is largely determined by the passage area distribution. The angle of attack for best operation at high Mach numbers is higher than the design angle of attack selected at low speed to have pressure distributions that are free of peaks.

INTRODUCTION

Conventional compressors frequently have used the uniformly loaded NACA 65-$(C_{l_0}A_{10})10$ blade section for which low-speed cascade data are

available in reference 1. In order to obtain high critical speeds, the A_2I_{8b} mean line having most of the loading in the trailing-edge region was devised and low-speed cascade tests of blade sections using this mean line are reported in reference 2. Rotor tests of the A_2I_{8b} mean line at Mach numbers up to 1.13 (ref. 3) were highly successful. These two blade sections representing two significantly different types of loading were selected for the first high-speed tests in the porous-wall cascade where detailed examination of blade passage flows could be made to determine the manner in which high subsonic speeds affect blade performance and whether design information obtained in low-speed testing is satisfactorily correct at high speeds.

Two-dimensional porous-wall cascade tests of the NACA 65-$(12A_{10})10$ and the NACA 65-$(12A_2I_{8b})10$ blade sections were made at Mach numbers from 0.30 to a high subsonic Mach number that frequently choked the cascade and produced blade-surface Mach numbers above 1.4. Cascade configurations were solidities of 1.0 and 1.5, and inlet-air angles of both 45° and 60° for both blade sections. With a solid-wall modification to the cascade, schlieren observations were made at several angles of attack for cascade configurations of solidity 1.5 and inlet-air angle 45° and solidity 1.0 and inlet-air angle 60°.

SYMBOLS

A	flow area
c	blade chord
C_{l_o}	camber, expressed as design lift coefficient of isolated airfoil
C_w	momentum-loss coefficient
F_c	ratio of wake momentum loss to integrated total-pressure loss in wake
M	Mach number
p	static pressure
P	total pressure
q	dynamic pressure, $\frac{1}{2}\rho V^2$

[redacted]

s	tangential spacing between blades
S	pressure coefficient, $\frac{p_1 - p_l}{q_1}$
V	velocity
w	wake width
α	angle of attack: angle between entering flow direction and chord
β	air angle measured from perpendicular to blade row
δ	wake blockage
θ	turning angle
ρ	density
σ	solidity: chord-spacing ratio, c/s

Subscripts:

1	upstream of blade row, undisturbed stream
2	downstream of blade row
cr	critical, condition of first attainment of sonic velocity on blade surface
l	local, as on blade surface
T	throat of blade passage

APPARATUS AND METHODS

The Langley 7-Inch High-Speed Cascade

A schematic diagram of the Langley 7-inch high-speed cascade is shown in figure 1. The flow enters the 40-inch-diameter upstream duct and settling chamber through three 50-mesh screens and is accelerated smoothly through inlet fairings into a channel 7-3/8 inches wide with a maximum height of 22 inches. Upper and lower inlet fairings are adjustable vertically to match the vertical height of the particular cascade under test. The upper and lower walls of the test section are

[redacted]

attached to and move with the inlet fairings. These walls end downstream in flexible fairings which are adjusted to simulate another blade surface. The lower flexible wall is made of porous material placed over a suction chamber to prevent separation. The side walls carry the test-section walls, the blade row, instruments, and other equipment which remains fixed relative to the blade row. The side walls can be rotated for a 0° to 66° range of inlet flow angles relative to the cascade. The cascade is equipped with slots on all four walls which protrude 3/16-inch into the channel and reduce its width to 7 inches just ahead of the blade row. Suction chambers enclose the slot exteriors and are connected to a suction system for removal of the wall boundary layers.

In order to meet the requirement of two-dimensional flow, which will be discussed in detail later, the cascade was equipped with porous, removable side-wall sections into which the blade row is affixed. The porous-wall sections are constructed of layers of rolled monel filter cloth backed with a perforated steel plate and have exterior chambers which also connect to the suction system. The porosity of these walls must be such that the amount of flow through the surface is sufficient to remove the boundary layer for most of the test conditions, yet not so porous as to induce recirculation. The material selected was satisfactory for tests at most speeds. At the higher Mach numbers the flow through the test-section porous surfaces fell short of that required and the flow was not two dimensional. Data are marked when flow removal was insufficient. For schlieren observations these porous test-section walls were replaced with solid walls having approximately 5- by 7-inch glass windows.

Flow Surveys

Three total-pressure rakes were installed for wall boundary-layer survey. The first was positioned ahead of the side wall slot; the second, behind; and the third, on the lower wall ahead of the slot. A wide range of slot-chamber pressures were investigated. A comparison of the wall boundary-layer profiles showed the most effective slot-chamber pressure was less than the test-section static pressure by about 20 percent of the test-section impact pressure $P - p$.

The test section was surveyed upstream of a typical cascade set at an inlet-air angle of $\beta_1 = 60^\circ$ to determine the uniformity of the flow under the usual operating conditions. Uniform upstream and downstream static pressure distributions were set by varying the upper and lower wall slot pressures and by varying the position of the flexible upper and lower wall ends. Then flow angle and total pressure were measured at two positions, the first a quarter-test-section height from the lower wall and the second a quarter-test-section height from the upper wall.

[redacted]

Shown in figure 2 are the flow angles and total pressures measured ahead of the blade row. There is a deviation of approximately 1° in the test-section flow. No correction has been applied to the data for this deviation.

The temperature of the flow upstream was maintained at from 150° to 160° F at high speeds to avoid any possible condensation effects. This temperature was sufficient even under highly humid local conditions (for example, 90° F and 70-percent relative humidity) to reduce the relative humidity to 20 percent in the upstream duct without the use of air-drying equipment. According to reference 4, at 20-percent relative humidity the flow is essentially free of condensation for Mach numbers greater than the maximum entering Mach number of 1.0 obtained in these tests.

Test Procedure

For a typical cascade test the following quantities were measured: (1) the total pressure in the upstream duct; (2) upstream static pressures measured by 10 or more orifices located one chord length upstream of the blade row (but downstream of the wall boundary-layer removal slot as shown in fig. 1); (3) downstream static pressures measured by from 8 to 10 orifices approximately one-half chord length downstream of the blade row; (4) upper and lower blade-surface static pressures measured by 21 orifices located at midspan of the center blade; (5) turning angle measured approximately one chord length downstream of the blades at midspan and behind the four centermost passage exits; and (6) the total pressure in the wake of the center blade at midspan which was measured by a 26-tube rake. When measuring turning angles, care was taken to insure that the readings were not affected by the wake of the blades. For this purpose the two yaw tubes were very closely spaced and the total pressure tubes were mounted 1/2 inch to each side. Turning angle was recorded only when full total pressure was present at the two outer tubes.

The accuracy of the turning angle is dependent not only on the survey instrument and its position behind the passage but also on the setting of the slot suction pressures, the porous-wall chamber pressures, and the flexible walls. The instrument is estimated to be accurate to $\pm 0.3^{\circ}$ and turning angle is repeatable for any test to $\pm 1.0^{\circ}$. The turning angles presented are the measured angles and are not altered for change in axial velocity across the cascade.

The necessity of porous-wall boundary-layer removal to produce cascade data which would be two dimensional and in agreement with blower data was established in reference 5 for low speeds. Two-dimensional flow (no spanwise convergence or divergence of the stream tubes) was

maintained in these high-speed tests whenever possible. In order to achieve this condition the wall boundary layers were removed to prevent any decrease in passage width which would otherwise increase downstream velocity. As the boundary layers are removed from the blade-passage end walls, blade-row pressure rise increases and the downstream velocity decreases. Thus, changes in porous-wall test chamber pressures were used to adjust boundary-layer removal and hence prevent stream-tube convergence. To establish that two-dimensional flow was present, cascade turning angles were measured and used to calculate an ideal value of the downstream impact pressure $(P_1 - p_2)$ for the particular upstream impact pressure $(P_1 - p_1)$. The porous-wall chamber pressure was adjusted until the value of $(P_1 - p_2)$ was equal to the ideal value of $(P_1 - p_2)$ plus a small excess proportional to the amount of wake blockage present. Changes in turning angle or the wake resulting from the new flow conditions required readjustment of the amount of boundary layer removed.

For some high-angle-of-attack, high-pressure-rise cascade configurations, attempts to establish the static-pressure rise required for two-dimensional flow resulted in separation from the blade upper surfaces, especially at the higher Mach numbers. Since no useful data can be obtained with the blade in a badly separated condition, the requirement for two-dimensional flow was relaxed and the cascade did represent a passage that converged spanwise. In relaxing the two-dimensional requirement and hence the pressure rise, turning angles increase over the two-dimensional value. Examination of the data shows that for some conditions without sharply defined separation the effects of separation are still present regardless of whether the flow is two dimensional or not.

For flow observations by the schlieren method, the requirement of two-dimensional flow was waived. The resulting test-section pressure rise was usually less than that obtained with the porous-wall setup. This difference in pressure rise sometimes caused a change in flow separation on the blades which was evident in comparison of wake-loss coefficients.

Reduction of Data

A momentum-loss coefficient was calculated from the measured total pressure loss by the method of reference 6 for calculating wake force. Momentum loss was calculated from the downstream conditions and is expressed in coefficient form based on the dynamic pressure upstream of

the cascade. Hence,

$$C_{w_1} = F_c \int_0^w \frac{P_1 - P_2}{q_1 c} dw$$

where F_c (determined from ref. 6) is the ratio of the momentum-loss coefficient to the total pressure-loss coefficient for an assumed wake shape as a function of the maximum total pressure loss and Mach number.

A calculated check of the two dimensionality of the flow was made for all tests. Tests are considered two dimensional if the test pressure rise $\frac{P_2 - P_1}{q_1}$ is greater than 90 percent of the ideal pressure rise calculated from the entering Mach number, inlet-air angle, turning angle, and the wake blockage of the test. The wake blockage was calculated for a number of assumed cosine-shaped wakes all having equal momentum loss but different widths and heights. It was found that the wake blockages for all practical purposes were equal except for wakes having velocities less than 0.6 of the free-stream velocity. Such a condition would correspond to a wake taken practically at the trailing edge of a blade section. For these tests with the wakes measured almost a chord downstream it was concluded that the wake blockage would be proportional to the total-pressure loss. To obtain the exact relationship the wake blockages of a number of the test wakes were calculated and plotted against the integrated total-pressure loss, and the following relationship for the wake blockage δ was indicated:

$$\frac{\delta}{c} = 0.51 \int_0^w \frac{P_1 - P_2}{q_2 c} dw$$

The ideal pressure rise for the cascade was obtained from the displacement thickness and isentropic relationships. This ideal value was compared to the measured pressure rise to determine the maximum Mach number for which the tests are considered two dimensional.

PRESENTATION OF RESULTS

The results of the porous-wall cascade tests are presented in figures 3 to 52. A list of the cascade configurations tested and corresponding

[redacted]

figure numbers are tabulated in table 1. For each blade setting, four to six pressure distributions representative of the variation of surface pressures throughout the Mach number range tested are given. The downstream static pressure $\frac{p_1 - p_2}{q_1}$ is indicated on the pressure distributions by the horizontal line at 100-percent chord. The variation of turning angle, momentum-loss coefficient, and pressure rise are presented in figures immediately following each pressure-distribution figure. The limit of two dimensionality of the tests is indicated by the vertical line on the section characteristics, figures 3 to 52. Schlieren figures 53 to 67 contain five to eight representative schlieren photographs and are followed by figures showing the variation of turning angle, momentum-loss coefficient, and pressure rise obtained in the schlieren test. (See table I.) In figures 68 to 75, turning angle is plotted against angle of attack at $M_1 = 0.30$ and at critical speed. Turning angles measured in the low-speed cascade tunnel (refs. 1 and 2) are also plotted for comparison. In figures 76 to 83 momentum-loss coefficients at various constant Mach numbers are plotted for the angles of attack tested.

DISCUSSION OF RESULTS

Turning angles.- Good correlation of turning angle was obtained between tests of the 65-$(12A_{10})$10 blade section made in the low-speed cascade ($M_1 < 0.15$ and Reynolds number = 245,000 and 444,000 in ref. 1) and tests made in the high Mach number cascade at $M_1 = 0.30$ (Reynolds number = 550,000). Figures 68 to 71 show the turning angles to be nearly equal at these speeds. At critical speed the turning angles are essentially unchanged from the $M_1 = 0.30$ values. (See figs. 68 to 71.) Mach number had negligible effect on the turning angle of the 65-$(12A_{10})$10 blade section until supersonic velocities occurred on the blade surface and momentum losses increased. At speeds above critical, turning angles decreased due to the lower pressures over the blade lower surface caused by a decrease in the angle of attack locally (discussed later) and/or by separation on either blade surface. The separation, which may or may not be caused by a shock, reduces the blade-row pressure rise and hence reduces the downstream pressure which largely determines the lower surface pressure over the rearward portion of the blade.

The turning angles measured for the 65-$(12A_2I_{8b})$10 blade section are affected greatly by the unusual highly curved portion of the loaded trailing edge of the airfoils. The variation of turning angle with Mach number is shown in figures 28 to 52 and the variation of turning

[redacted]

angle with angle of attack is shown in figures 72 to 75. For the 65-$(12A_2I_{8b})$10 blade section the turning angles obtained in the high Mach number cascade tunnel at $M_1 = 0.30$ were in agreement with turning angles measured at low speed. Increasing the Mach number to critical, lowered the turning angle as much as 4° in some cases while other tests showed no decrease in turning angle. The turning angle usually decreased rapidly as the losses increased.

The jog in the turning angle, angle-of-attack plots for the 65-$(12A_2I_{8b})$10 blade section (figs. 73 to 75) is a result of the shift of the minimum pressure and boundary-layer transition point from the trailing-edge region at low angles of attack to the leading edge at high angles of attack. Low turning angles are produced when the transition is near the leading edge because the turbulent boundary layer thickens along the blade surface and may separate sooner in the highly curved trailing-edge region. A like phenomenon is found in tests of isolated airfoils and is discussed in reference 7. Pressure distributions at $\beta_1 = 60^\circ$ and $\sigma = 1.0$ (fig. 72) indicate laminar separation is occurring ahead of the highly curved trailing edge.

The highly curved trailing edge of the 65-$(12A_2I_{8b})$10 blade section is conducive to separation. The extent of the separation and hence the turning angle is determined by the required pressure rise and the condition of the boundary layer approaching the curved portion, and results in irregular turning-angle variations.

High-speed loss increase.- Except for angles of attack at which the flow is separated at low speed, the momentum-loss coefficient (see figs. 3 to 27) increased rapidly for the 65-$(12A_{10})$10 blade section at Mach numbers of from 0.75 to 0.85, about 0.05 to 0.10 greater than the critical Mach number. This behavior is similar to that of isolated airfoils. For the Mach numbers at which the momentum loss increased the maximum blade surface Mach numbers were between 1.09 and 1.26. The total pressure loss across a normal shock at these Mach numbers would not have produced this increase in momentum-loss coefficient. The distribution of the losses measured in the total-pressure surveys made in the passage behind the blade row indicate the losses originate on the blade surface rather than in the passage. Schlieren photographs, figures 53 to 59, indicate increased separation of boundary layer from the blade surface.

The momentum loss for the 65-$(12A_2I_{8b})$10 blade section was usually greater than for the 65-$(12A_{10})$10 blade section because of separation of flow from the trailing edge.

[redacted]

In figures 76 to 83 momentum-loss coefficients at various constant Mach numbers are plotted for the angles of attack tested. The useful angle-of-attack range is bordered by high-loss regions. At low speed, peaked blade surface velocities at high and low angles of attack result in thick and separated boundary layers producing the high losses that limit the useful angle-of-attack range. Since higher speeds accentuate peaked velocities it was expected that higher losses would be measured in the angle-of-attack regions having peaked low speed pressure distributions. Useful angle-of-attack range does decrease at higher Mach numbers for both blade sections as shown in figures 76 to 83.

Passage area distribution.- At high speeds the passage area distribution and minimum throat area determine some important blade operating characteristics. For 65-$(12A_{10})$10 and 65-$(12A_2I_{8b})$10 blade cascades at inlet-air angles greater than 40° the throat area extends from a lower surface point very near the leading edge to an upper surface point near midchord. When the throat area is less than the upstream flow area (see fig. 84), compressibility effects accentuate the throat contraction and cause a disproportionate increase of the velocities in the throat region. The pressure distribution shows the formation of velocity peaks near the leading edge on the lower surface, locally decreasing the loading, and near midchord on the upper surface, increasing the loading. A result of this shift of the loading rearward is to increase the adverse pressure gradient over the rear portion of the upper surface and thereby increase boundary-layer growth and the tendency to separate. Typical examples of the rearward shift of loading can be seen in figures 22 and 47. At choke the pressure over the upper surface decreases from a high value at the leading edge to a minimum at the throat (near midchord) while the lower surface pressure at the leading edge is a minimum. Hence, the blade sections appear to operate at a lower angle of attack at high speed than at low speed.

For high angles of attack at which the cascade did not choke, the upwash and hence the surface pressures in the leading-edge region is greatly influenced by the proximity of the upper surface of the upstream blade. Increased interference from the upper surface of the upstream blade due to compressibility even at Mach numbers below critical causes a decrease in the upwash as Mach number increases. Above critical speed the blade-surface shocks terminate a supersonic region through which the pressure influences of the rearward parts cannot be propagated and thereby eliminate their effect on the flow field ahead of the blades and thus decrease the upwash. Hence, the effective angle of attack of the leading edge decreases at high speeds. The effects of this angular change can be seen in the pressure distributions of the tests. (For example, see fig. 4.) Near the leading edge the downsweeping flow slightly lowers the velocities on the upper surface and greatly increases the lower surface velocities as Mach number is increased. Evaluation of the data at critical speed indicates that the effective angle of

[redacted]

attack is 3.5° lower than at low speeds. Increasing the design angle of attack by a comparable amount for high-speed operation appears to be feasible since the low momentum loss (figs. 76 to 83) indicates this angle-of-attack increase would decrease high-speed losses. This is in agreement with the results of most transonic rotor tests which show a marked increase in efficiency as the angle of attack is raised 3° to 4° above the design point selected from low-speed cascade data. The increase in work alone with no decrease in losses would not produce the marked increase in efficiency. (For example, see fig. 11 of ref. 3.)

A too rapid increase in the passage area either from the upstream stream tube (A_1 in fig. 84) to the throat A_T (usually found at a high-air inlet angle, high angle-of-attack condition), or from the throat to just downstream of the throat A_2 (usually a high air-inlet angle, low angle-of-attack condition) probably causes separation and high losses. The occurrence of high losses in the tests contained herein cannot definitely be attributed to this cause although the 65-$(12A_{10})10$ and 65-$(12A_2I_{8b})10$ blade sections did perform poorest at $\beta = 60°$ and $\sigma = 1.0$, conditions for which divergence of the passage from upstream to the throat was maximum.

For many design conditions, especially at low inlet-air angles, the minimum passage (throat) area is critical and may determine a maximum entering Mach number or influence blade section and angle-of-attack selection. Transonic compressors are designed with particular attention given to the ratio of throat to upstream area. Throat areas are given for the 65-$(C_{l_o}A_{10})10$ and 65-$(C_{l_o}A_2I_{8b})10$ blade series in figures 85 and 86 as the ratio of throat area A_T to spacing ($s = A_1/\cos \beta_1$). This ratio divided by $\cos \beta_1$ yields the throat to upstream area ratio A_T/A_1 which determines the maximum entering Mach number. In figures 85 and 86 the throat to spacing area ratio $\frac{A_T}{A_1} \cos \beta_1$ is plotted against $(\beta_1 - \alpha)$, σ and C_{l_o} by the carpet-plotting method (see ref. 8) for accurate interpolation. Briefly, the carpet plot presented herein was made displacing like points of $(\beta_1 - \alpha)$ and C_{l_o} to a horizontal scale proportional to the solidity. Thus, to interpolate between solidities it is necessary only to fair a line between like points of $(\beta_1 - \alpha)$ and C_{l_o} at the three given solidities and read the line at the horizontal distance proportional to the difference between a given solidity value and the desired solidity.

Pressure rise across cascade.- Under ideal conditions the pressure rise across the cascade would be controlled by the blade configuration and the flow removed through the side wall; however, losses from separation have a large effect on the actual pressure rise obtained.

[redacted]

Increasing the amount of flow removed through porous side walls normally produces a higher pressure rise across the cascade. As greater amounts of flow are removed through the porous wall the pressure rise across the cascade increases to a maximum and the blade-surface boundary layer separates to decrease the pressure rise. Thus, to avoid separation many tests, particularly those at high Mach numbers, were made at the highest pressure rise condition obtainable, since no two-dimensional flow was possible under these conditions. The pressure rise across the cascade $\frac{p_2 - p_1}{q_1}$ obtained in the tests at $M_1 = 0.60$ and 0.80 is presented in figure 87. The pressure rise for the 65-$(12A_{10})$10 blade section shown in figure 87(a) decreased between $M_1 = 0.60$ and $M_1 = 0.80$ and is less than the pressure rise of the 65-$(12A_2I_{8b})$10 blade section at like conditions. Separation limited the pressure rise for the 65-$(12A_{10})$10 blade section at $\beta_1 = 60^\circ$ and $\sigma = 1.0$ (fig. 87(a)). At $\beta = 45^\circ$ and $\sigma = 1.0$ the pressure rise also decreases between $M_1 = 0.60$ and $M_1 = 0.80$; however, the maximum pressure rise was not obtained in these tests due to insufficient boundary-layer removal capacity (fig. 87(b)). In figures 87(c) and 87(d) choking in the throat precludes high entering Mach number at low angles of attack; hence, there is a decrease in the range of angles of attack at which $M_1 = 0.80$ can be attained from the range at which $M_1 = 0.60$ is attained. A similar angle-of-attack shift may be seen in momentum-loss coefficient variation, figures 76 to 83.

SUMMARY OF RESULTS

High-speed, two-dimensional cascade tests were made of the NACA 65-$(12A_{10})$10 and the NACA 65-$(12A_2I_{8b})$10 blade sections. From data obtained in these tests and in the low-speed tests of the blade sections reported in NACA RM L51G31 and NACA RM L53I30b, the following results are summarized:

(1) Turning angles measured at low speed (upstream Mach number less than 0.15) for the uniformly loaded NACA 65-$C_{l_o}A_{10}$ 10 blade sections are sufficiently accurate for design purposes at Mach numbers up to critical. For the NACA 65-C_l A_2I_{8b} 10 blade series increasing separation from the highly cambered trailing-edge region may cause the turning angle to decrease as much as 4° between upstream Mach number of 0.3 and the critical speed.

(2) The high-speed performance of NACA 65-$(C_{l_o}A_{10})$10 and NACA 65-$(C_{l_o}A_2I_{8b})$10 blade configuration is largely determined by the passage area distribution through the cascade.

[redacted]

(3) The angle of attack for best operation at high Mach numbers is higher than the design angle of attack selected to have pressure distributions that are free of peaks at low speeds.

(4) The angle-of-attack range for low losses at high Mach numbers is less than that at low speeds.

Langley Aeronautical Laboratory,
National Advisory Committee for Aeronautics,
Langley Field, Va., September 8, 1955.

REFERENCES

1. Herrig, L. Joseph, Emery, James C., and Erwin, John R.: Systematic Two-Dimensional Cascade Tests of NACA 65-Series Compressor Blades at Low Speeds. NACA RM L51G31, 1951.

2. Erwin, John R., Savage, Melvyn, and Emery, James C.: Two-Dimensional Low-Speed Cascade Investigation of NACA Compressor Blade Sections Having a Systematic Variation in Mean-Line Loading. NACA RM L53I30b, 1953.

3. Savage, Melvyn, Erwin, John R., and Whitley, Robert P.: Investigation of an Axial-Flow Compressor Rotor Having NACA High-Speed Blade Sections (A_2I_{8b} Series) at Mean Radius Relative Inlet Mach Numbers up to 1.13. NACA RM L53G02, 1953.

4. Lindsey, Walter F., and Chew, William L.: The Development and Performance of Two Small Tunnels Capable of Intermittent Operation at Mach Numbers Between 0.4 and 4.0. NACA TN 2189, 1950.

5. Erwin, John R., and Emery, James C.: Effect of Tunnel Configuration and Testing Technique on Cascade Performance. NACA Rep. 1016, 1951. (Supersedes NACA TN 2028.)

6. Heaslet, Max A.: Theoretical Investigation of Methods for Computing Drag From Wake Surveys at High Subsonic Speeds. NACA WR W-1, 1945. (Formerly NACA ARR 5C21.)

7. Abbott, Ira H., Von Doenhoff, Albert E., and Stivers, Louis S., Jr.: Summary of Airfoil Data. NACA Rep. 824, 1945. (Supersedes NACA WRL-560.)

8. Felix, A. Richard: Summary of 65-Series Compressor-Blade Low-Speed Cascade Data by Use of the Carpet-Plotting Technique. NACA RM L54H18a, 1954.

[redacted]

TABLE I.- CASCADE CONFIGURATIONS TESTED

Blade section	Solidity	Inlet air angle, deg	Angle of attack, deg	Type of Data	Figure
65-(12A10)10	1.0	60	7.1	Porous wall	3
			9.3	Schlieren	53
			11.1	Porous wall	4
			12.3	Schlieren	54
			11.3	Porous wall	5
			15.3	Schlieren	55
			17.1	Porous wall	6
			20.1	Porous wall	7
		45	7.0	Porous wall	8
			10.0	Porous wall	9
			12.0	Porous wall	10
			14.0	Porous wall	11
			17.0	Porous wall	12
			20.0	Porous wall	13
			23.0	Porous wall	14
	1.5	60	9.8	Porous wall	15
			12.8	Porous wall	16
			15.8	Porous wall	17
			18.8	Porous wall	18
			21.8	Porous wall	19
			24.8	Porous wall	20
		45	8.5	Schlieren	56
			8.5	Porous wall	21
			11.5	Schlieren	57
			12.2	Porous wall	22
			14.5	Schlieren	58
			15.2	Porous wall	23
			17.5	Schlieren	59
			18.2	Porous wall	24
			20.6	Porous wall	25
			23.6	Porous wall	26
			25.6	Porous wall	27
65-(12A2I25)10	1.0	60	8.0	Porous wall	28
			8.1	Schlieren	60
			11.0	Porous wall and schlieren	29 and 61
			14.0	Porous wall	30
			14.1	Schlieren	62
			17.0	Porous wall	31
			17.1	Schlieren	63
			19.0	Porous wall	32
			19.1	Schlieren	64
		45	5.0	Porous wall	33
			8.0	Porous wall	34
			11.0	Porous wall	35
			14.0	Porous wall	36
			17.0	Porous wall	37
			20.0	Porous wall	38
			23.0	Porous wall	39
			26.0	Porous wall	40
	1.5	60	10.5	Porous wall	41
			13.5	Porous wall	42
			16.5	Porous wall	43
			19.5	Porous wall	44
			22.5	Porous wall	45
		45	7.5	Porous wall	46
			10.5	Porous wall	47
			13.5	Porous wall and schlieren	48 and 65
			16.5	Porous wall and schlieren	49 and 66
			19.5	Porous wall	50
			20.5	Schlieren	67
			22.5	Porous wall	51
			25.5	Porous wall	52

[redacted]

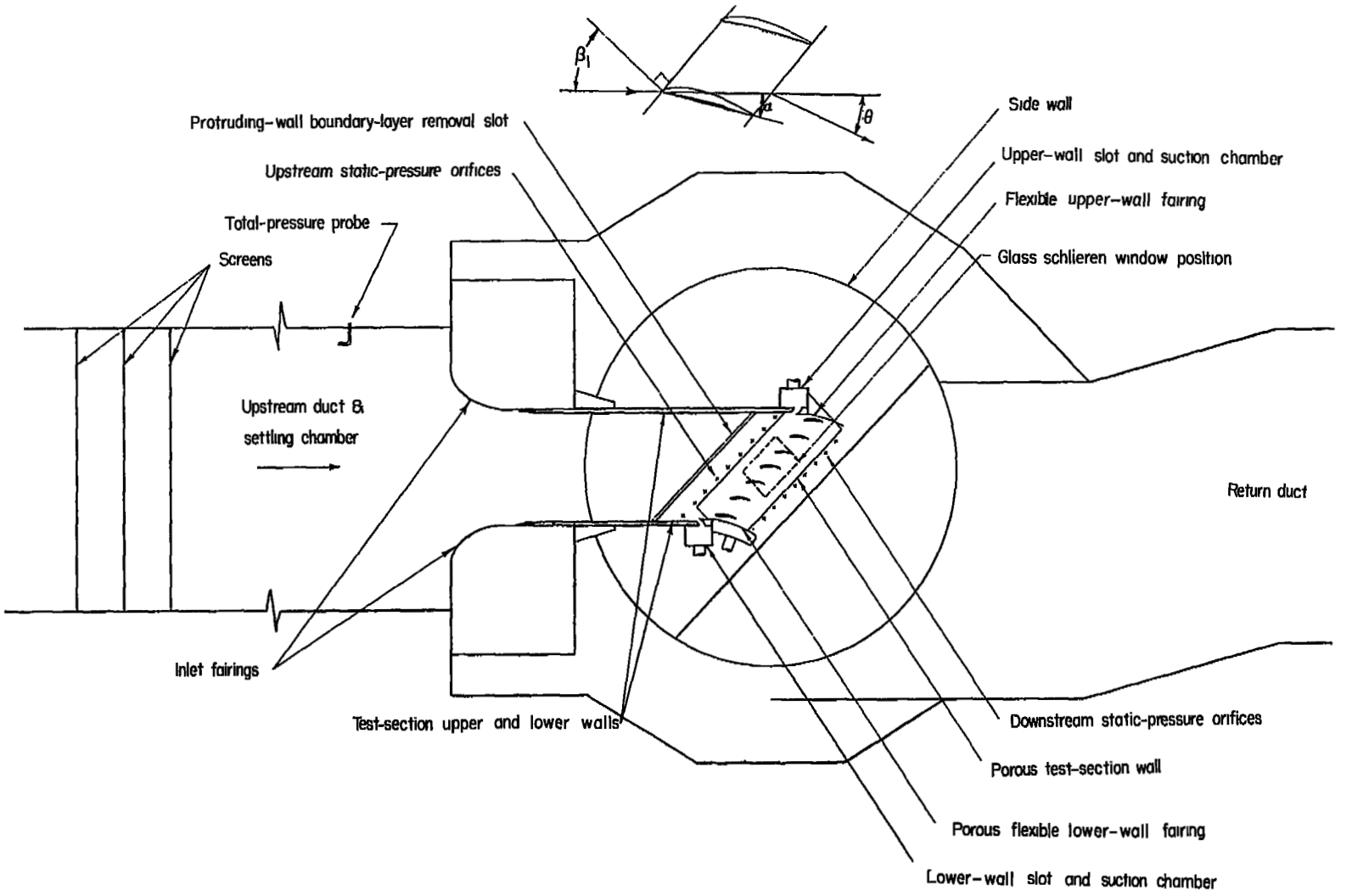

Figure 1.- Cross-sectional view of the Langley 7-inch high-speed cascade tunnel.

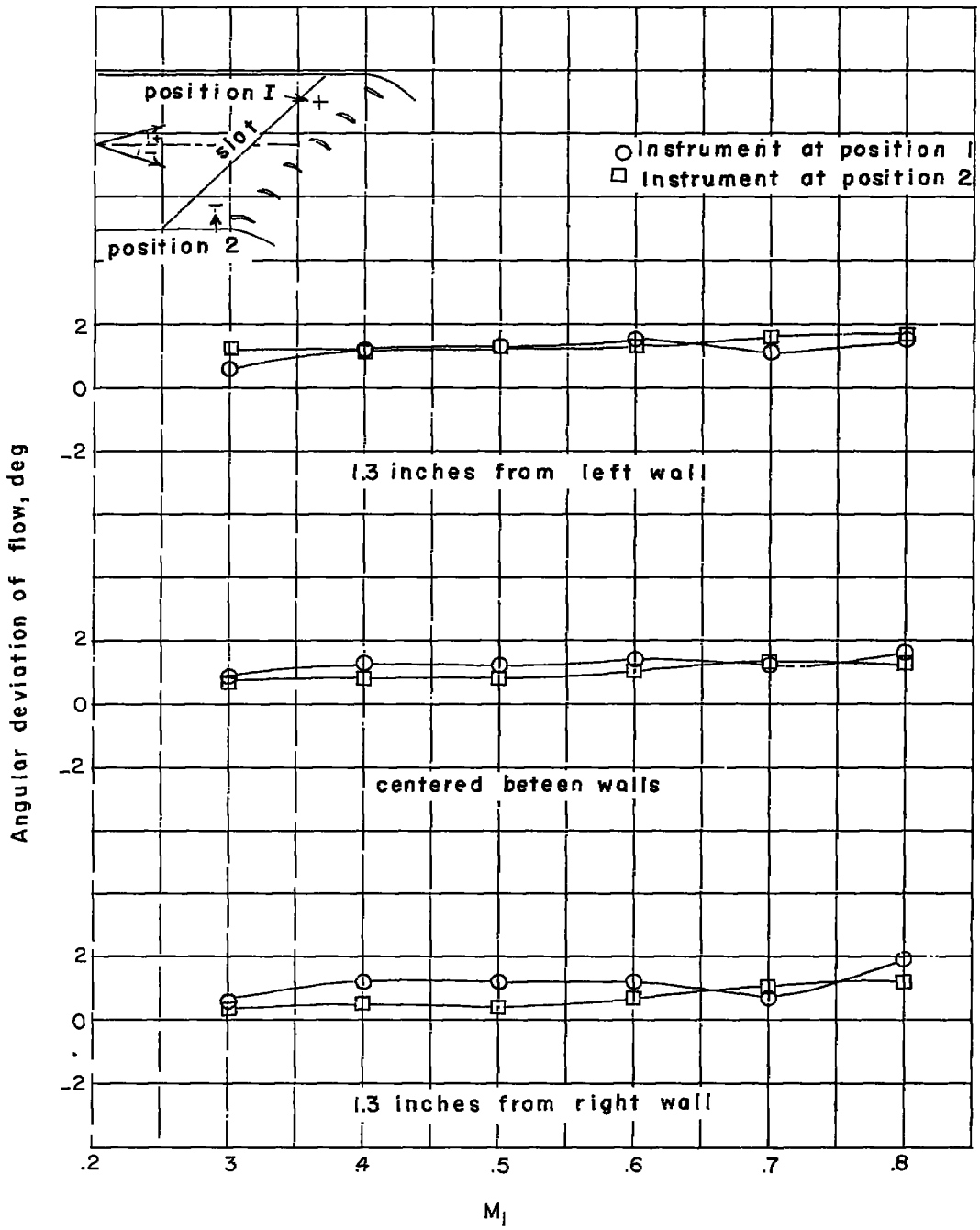

(a) Angular deviation of flow downstream of wall boundary-layer removal slot and upstream of blade row. $\beta = 60^{\circ}$.

Figure 2.- Cascade tunnel calibration.

[redacted]

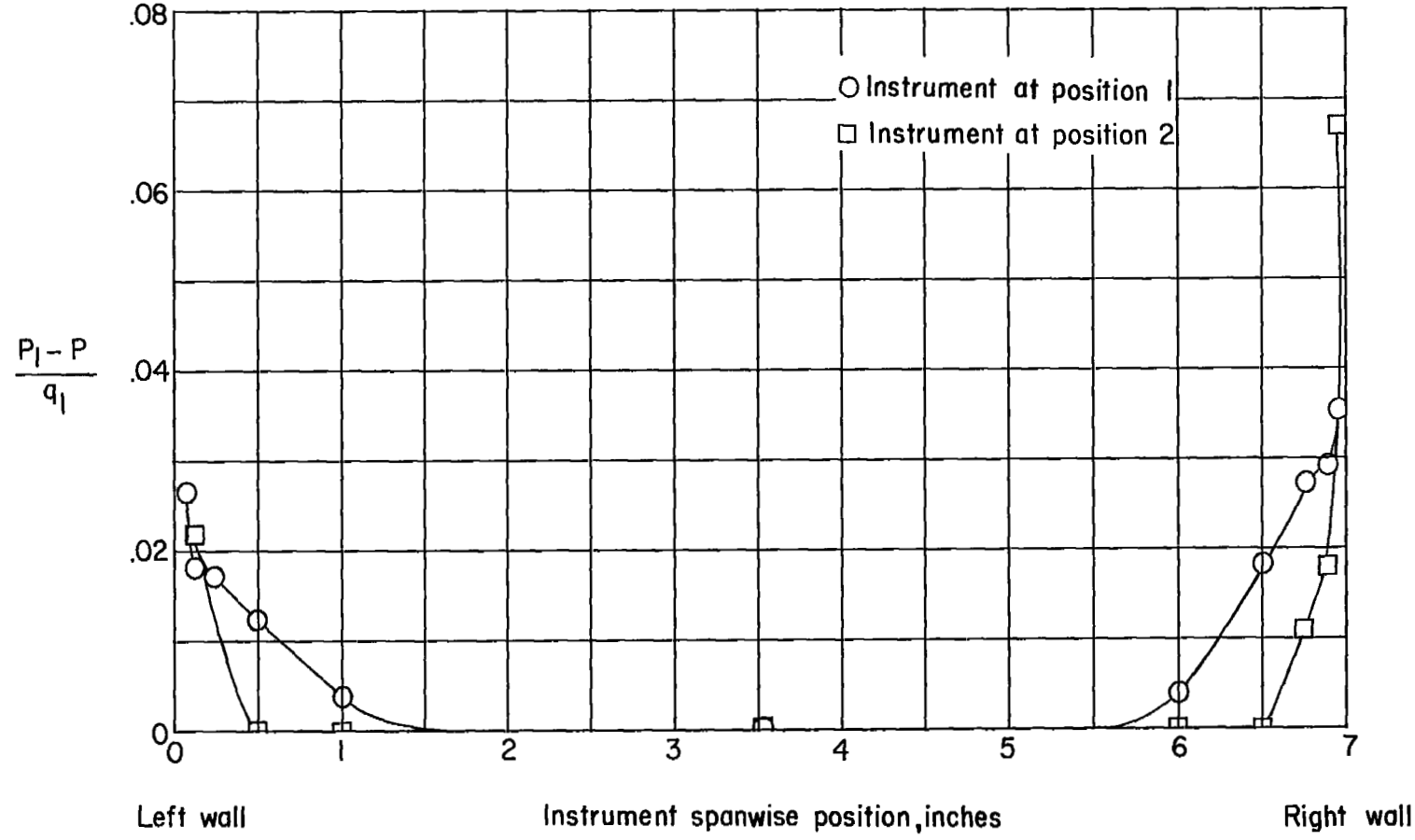

(b) Spanwise total pressure distribution downstream of wall boundary-layer removal slot and upstream of blade row. $\beta_1 = 60^\circ$; $M_1 = 0.500$.

Figure 2.- Concluded.

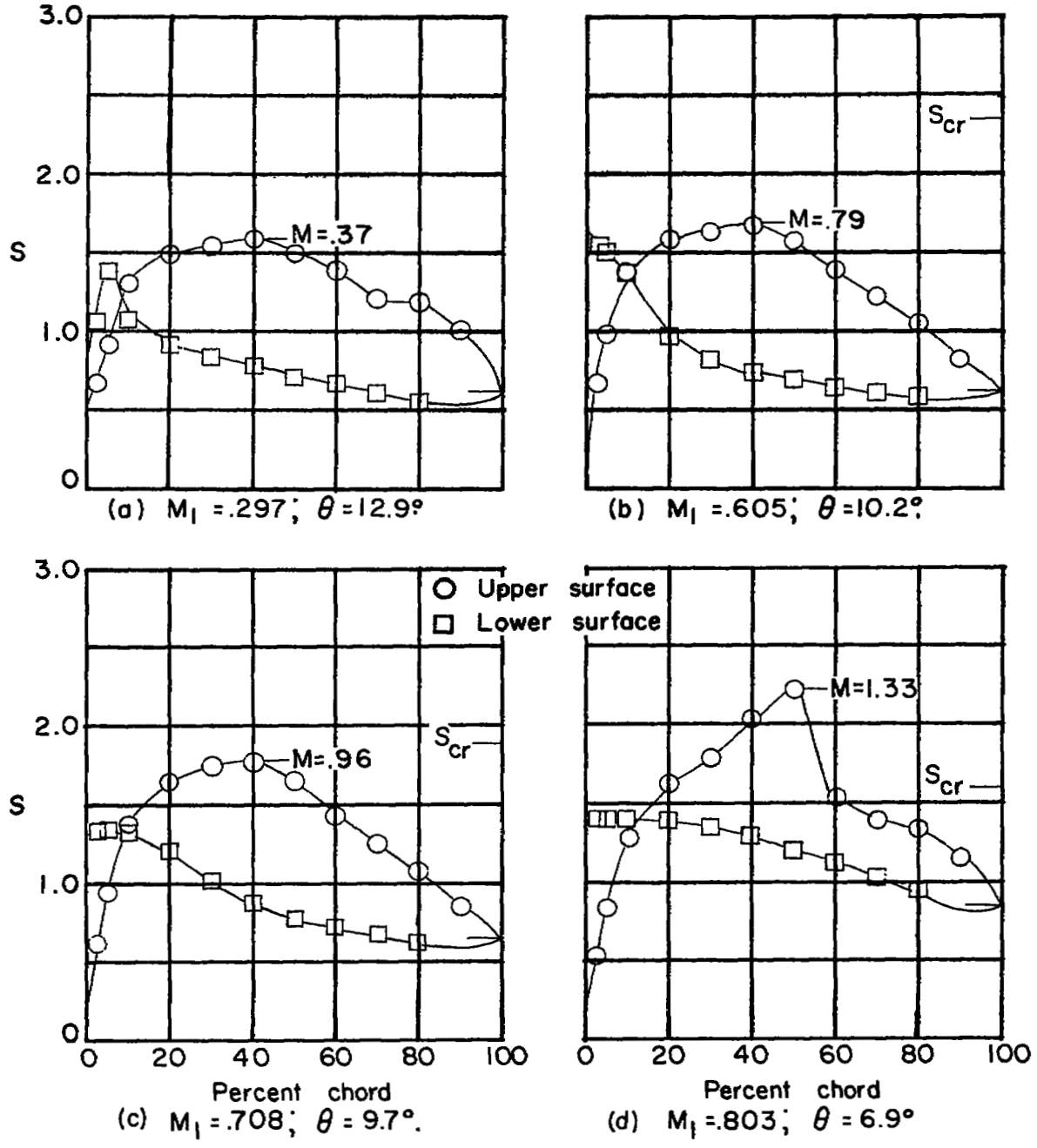

Figure 3 .— Blade-surface pressure distributions and section characteristics for the cascade combination. β_1 = 60°; σ =1.0 ; α = 7.1° ; and blade section, NACA 65-($12A_{10}$)10.

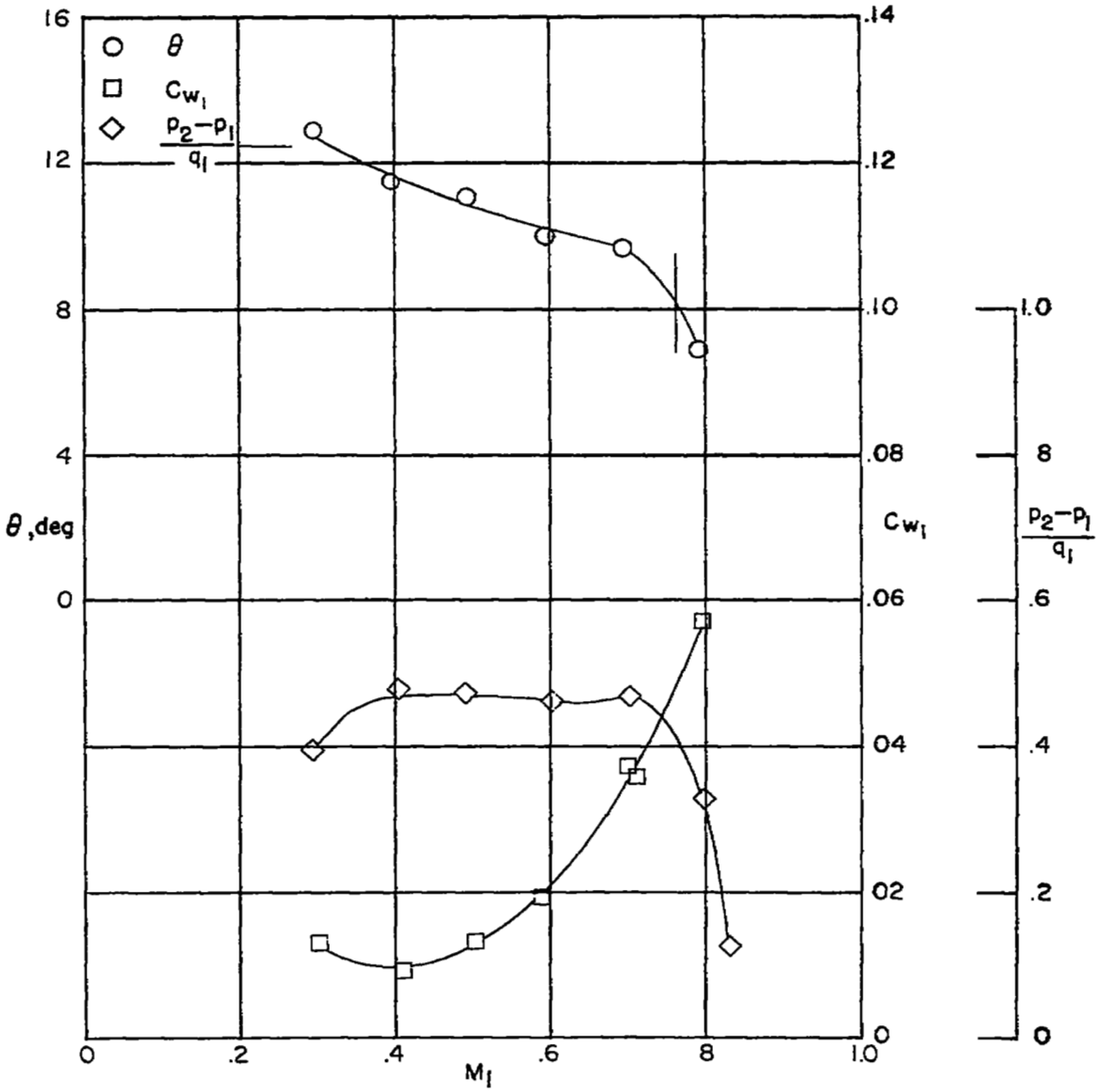

(e) Section characteristics. Tests are two dimensional for Mach numbers up to the vertical line. The horizontal line indicates low-speed turning angle given in reference 1.

Figure 3 .— Concluded.

[redacted]

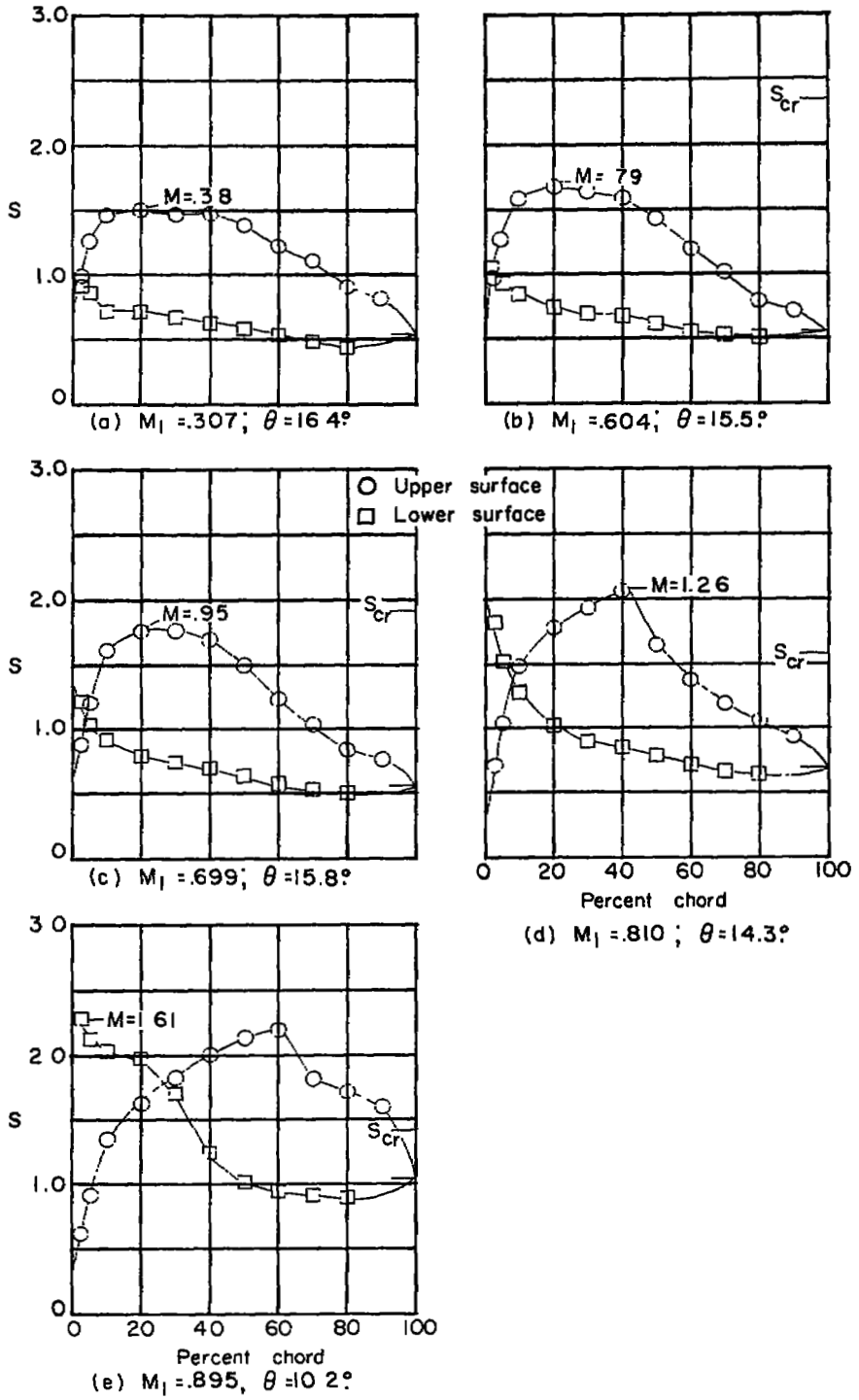

Figure 4 .— Blade-surface pressure distributions and section characteristics for the cascade combination, β_1 =60°; σ =1.0 ; α =11.1°; and blade section, NACA 65-(12A_{10})10.

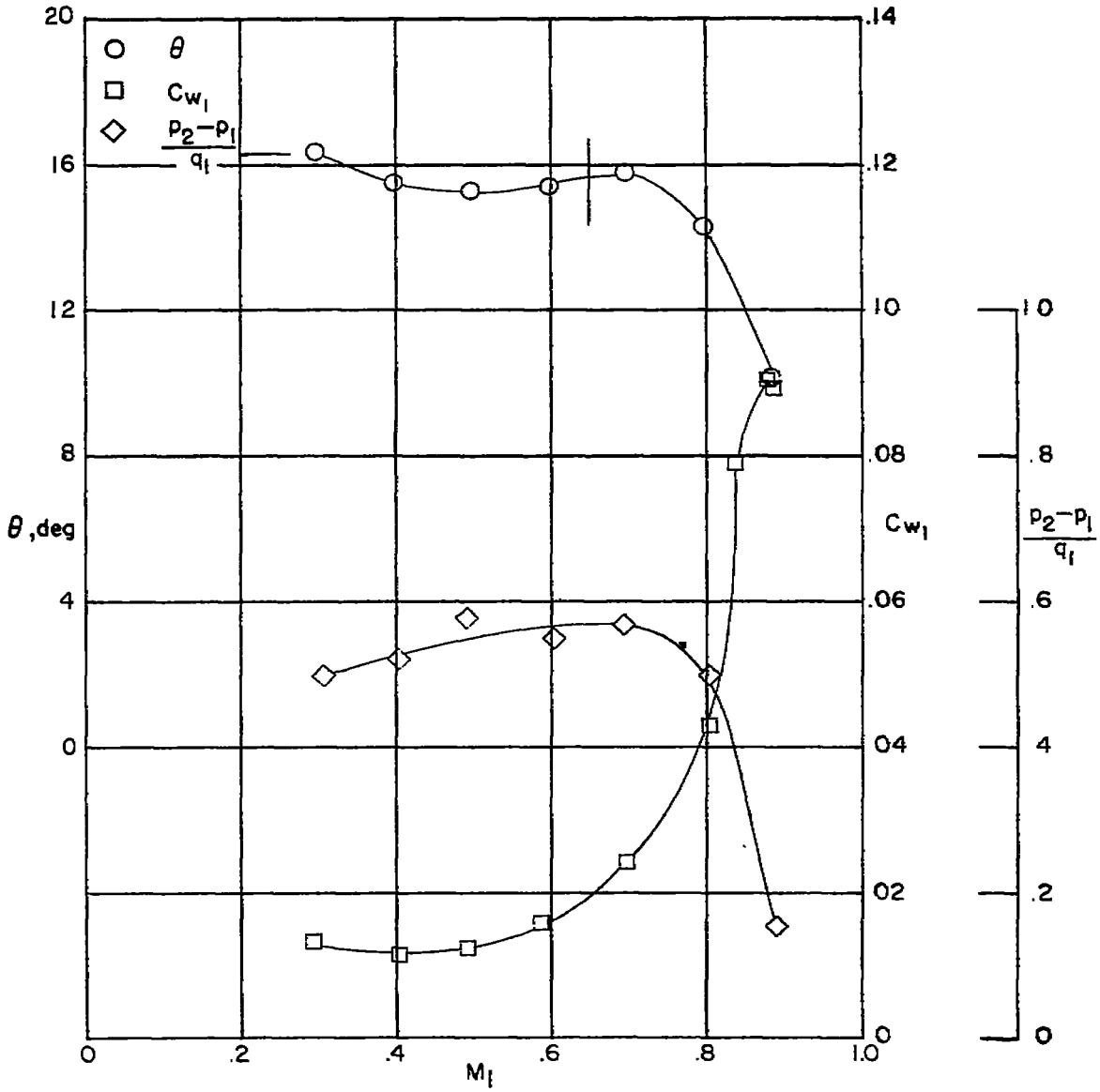

(f) Section characteristics. Tests are two dimensional for Mach numbers up to the vertical line. The horizontal line indicates low-speed turning angle given in reference 1.

Figure 4.— Concluded.

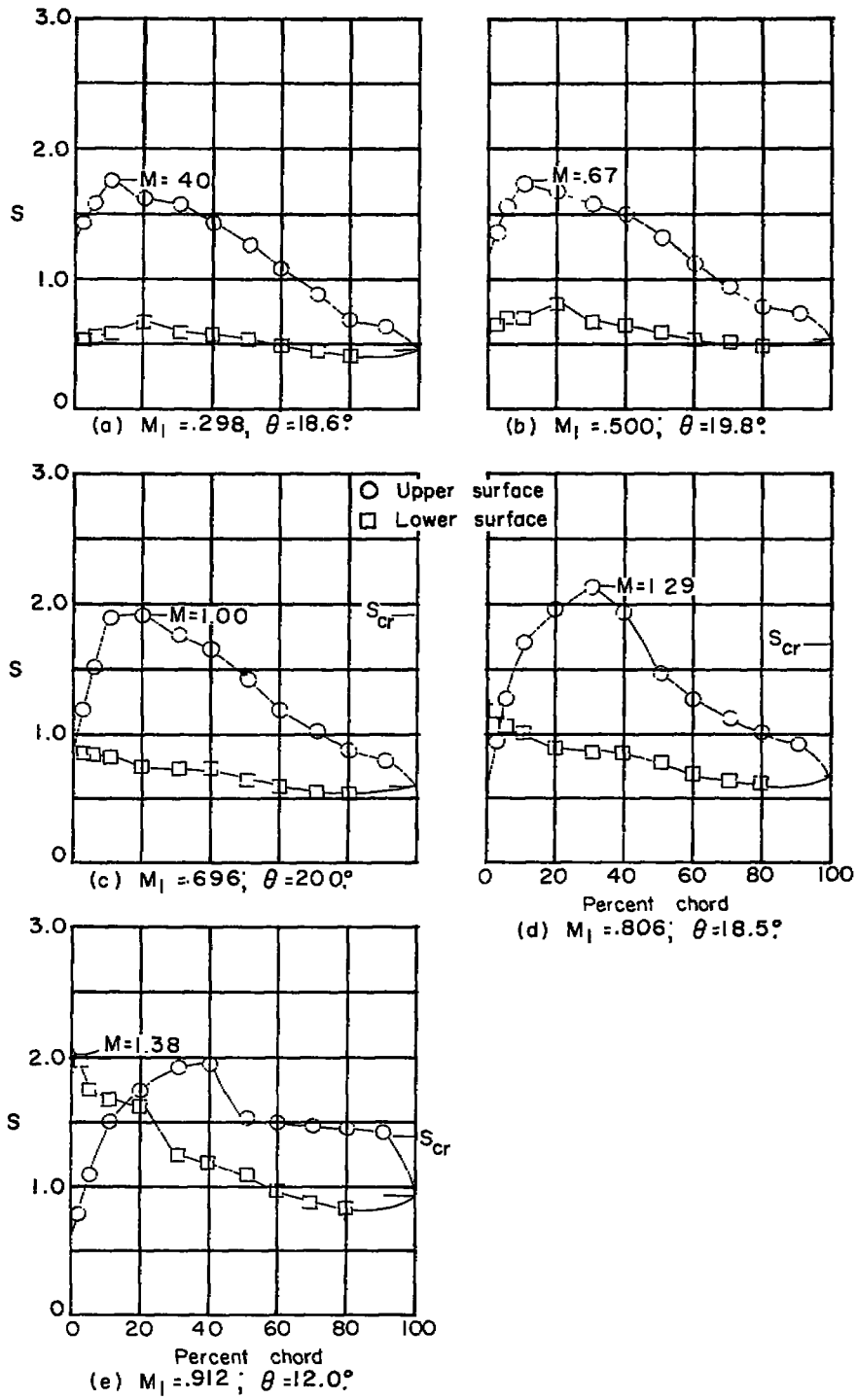

Figure 5 .— Blade-surface pressure distributions and section characteristics for the cascade combination. β_1 =60°; σ =1.0 ; α =14.3°; and blade section, NACA 65-(12A_{10})10.

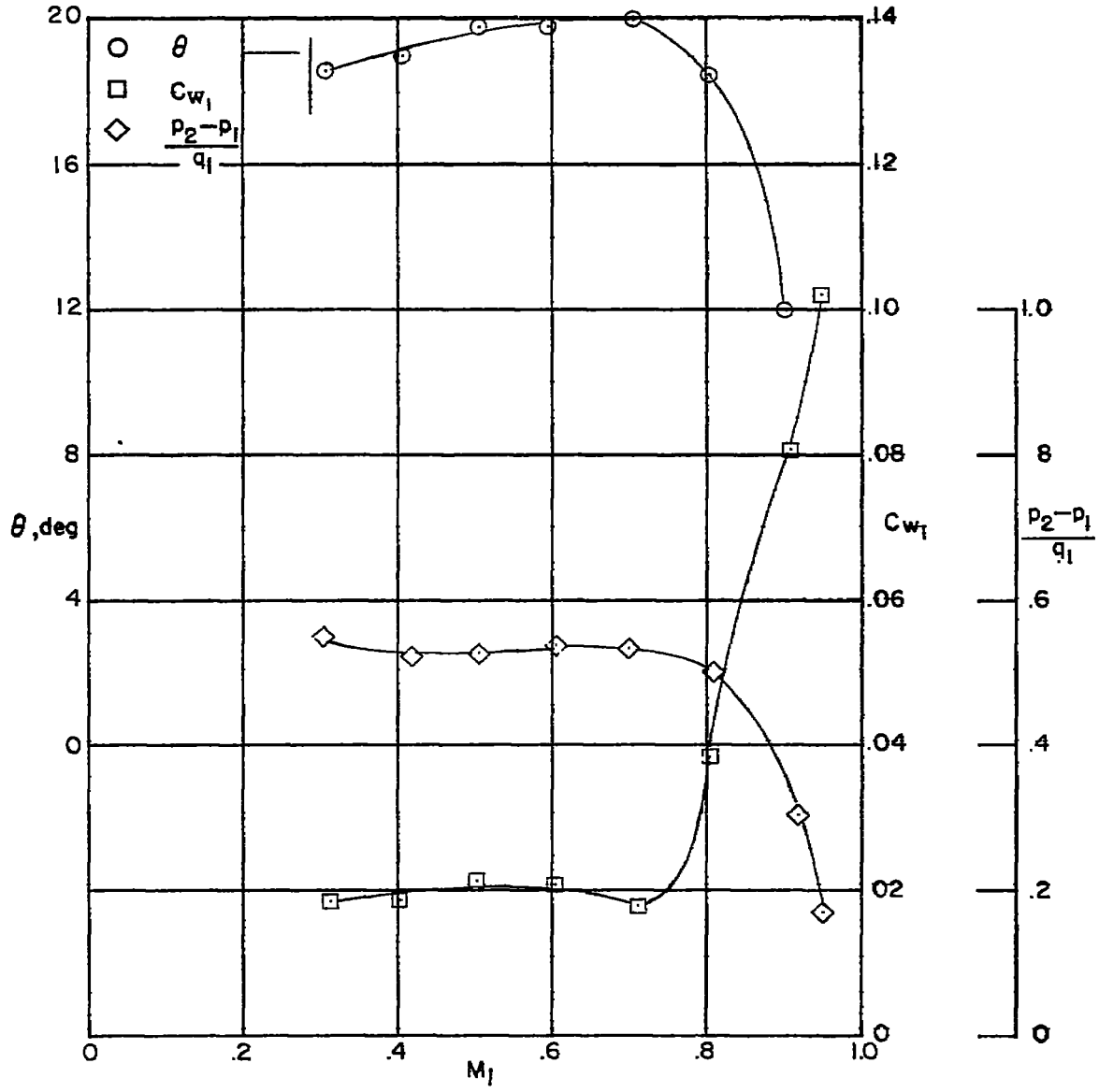

(f) Section characteristics. Tests are two dimensional for Mach numbers up to the vertical line The horizontal line indicates low-speed turning angle given in reference 1.

Figure 5 .— Concluded.

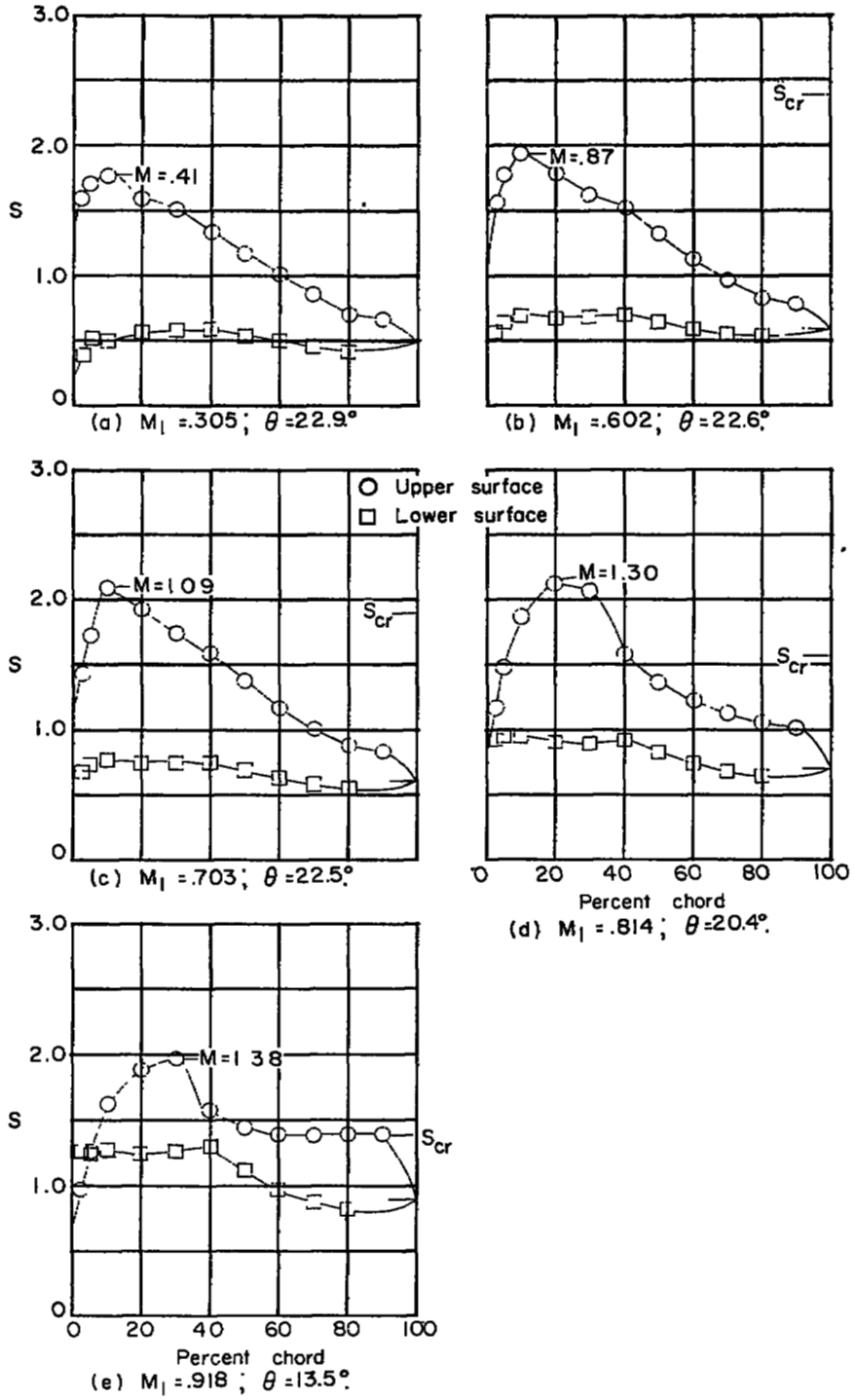

Figure 6 .— Blade-surface pressure distributions and section characteristics for the cascade combination. β_1 =60°; σ =1.0 ; α =17.1°; and blade section, NACA 65-($12A_{10}$)10.

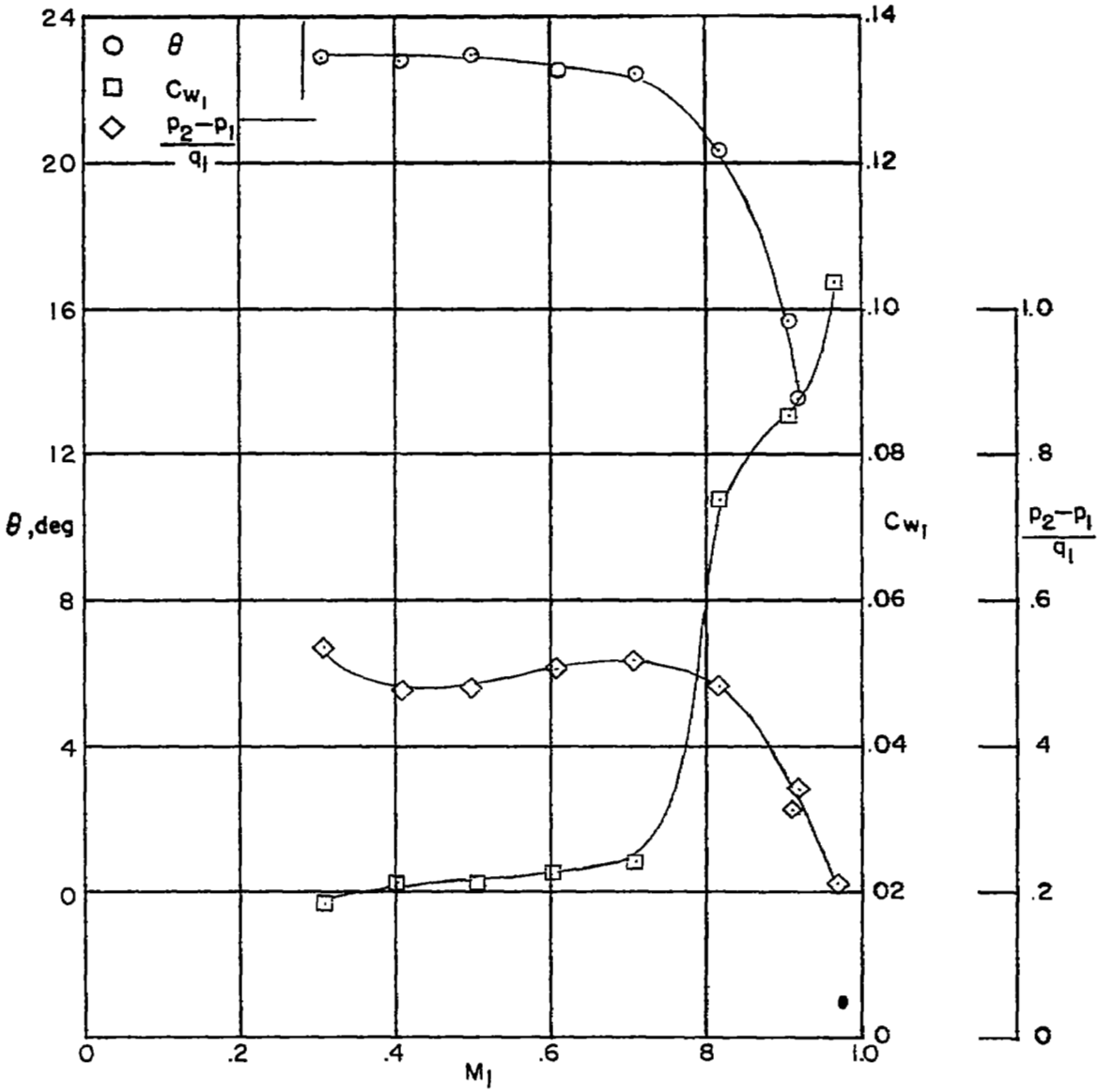

(f) Section characteristics. Tests are two dimensional for Mach numbers up to the vertical line. The horizontal line indicates low-speed turning angle given in reference 1.

Figure 6.— Concluded.

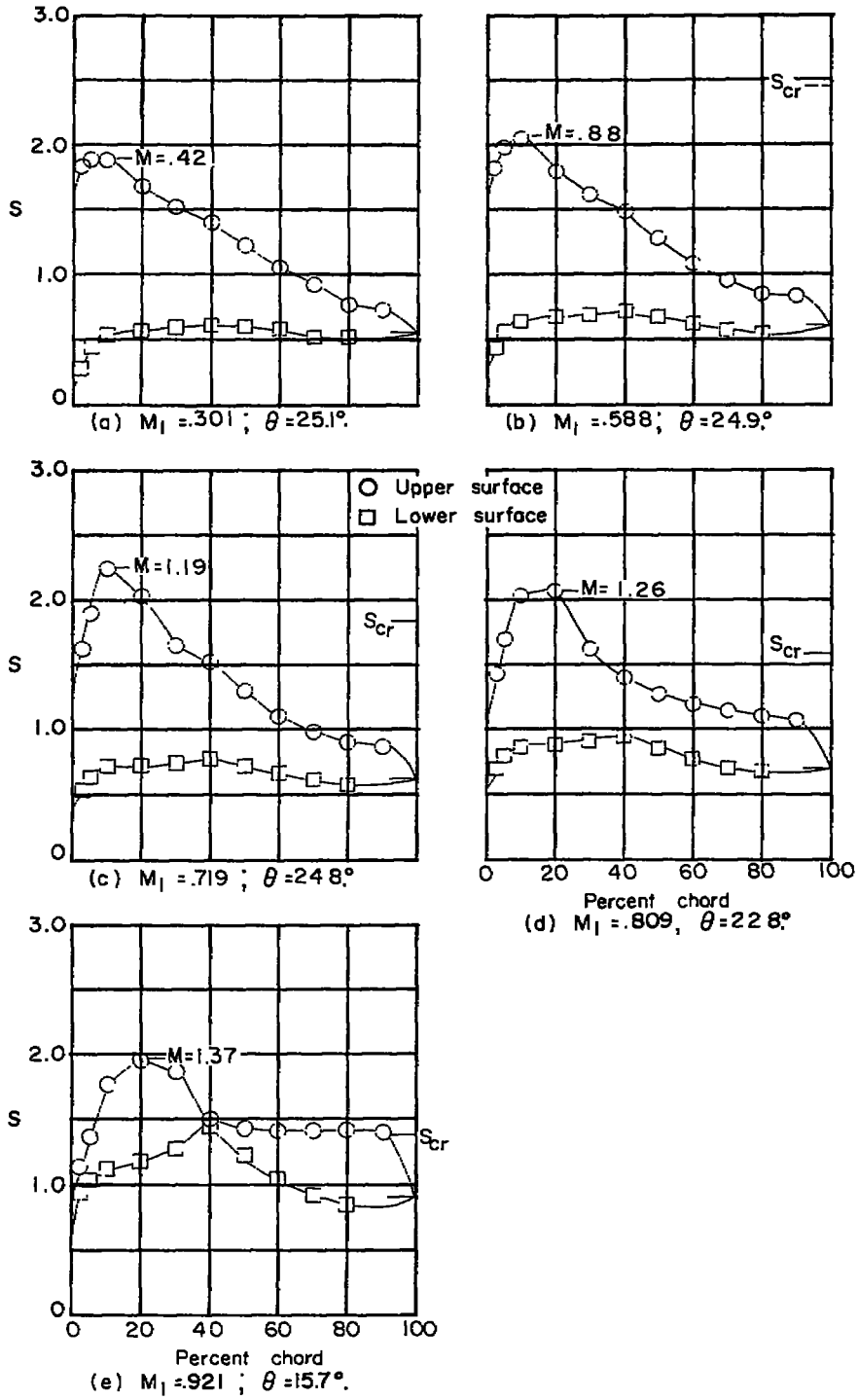

Figure 7 .— Blade-surface pressure distributions and section characteristics for the cascade combination. β_1 =60° ; σ =1.0 ; α =20.1°; and blade section, NACA 65-(12A_{10})10.

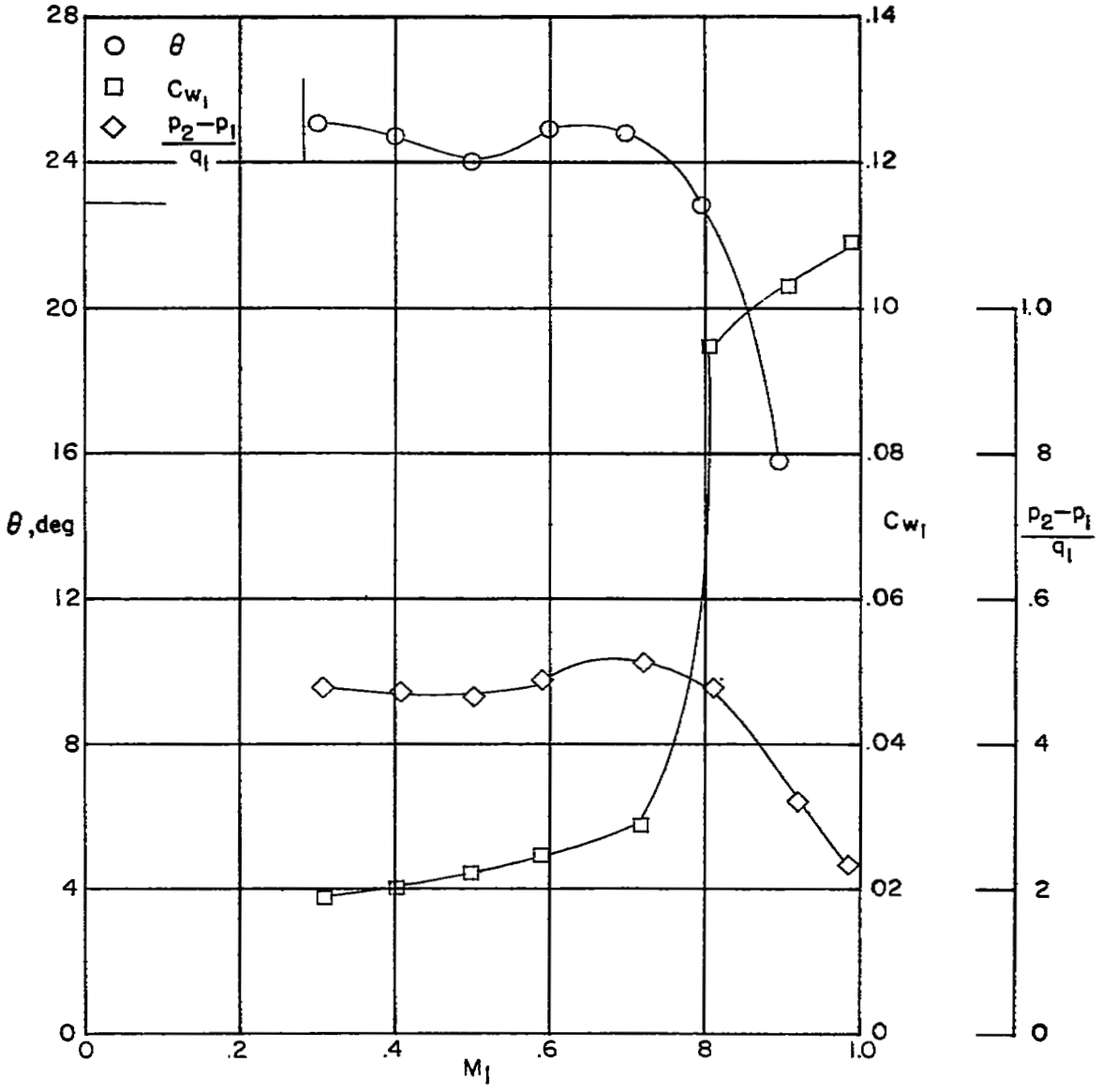

(f) Section characteristics. Tests are two dimensional for Mach numbers up to the vertical line. The horizontal line indicates low-speed turning angle given in reference 1.

Figure 7 .— Concluded.

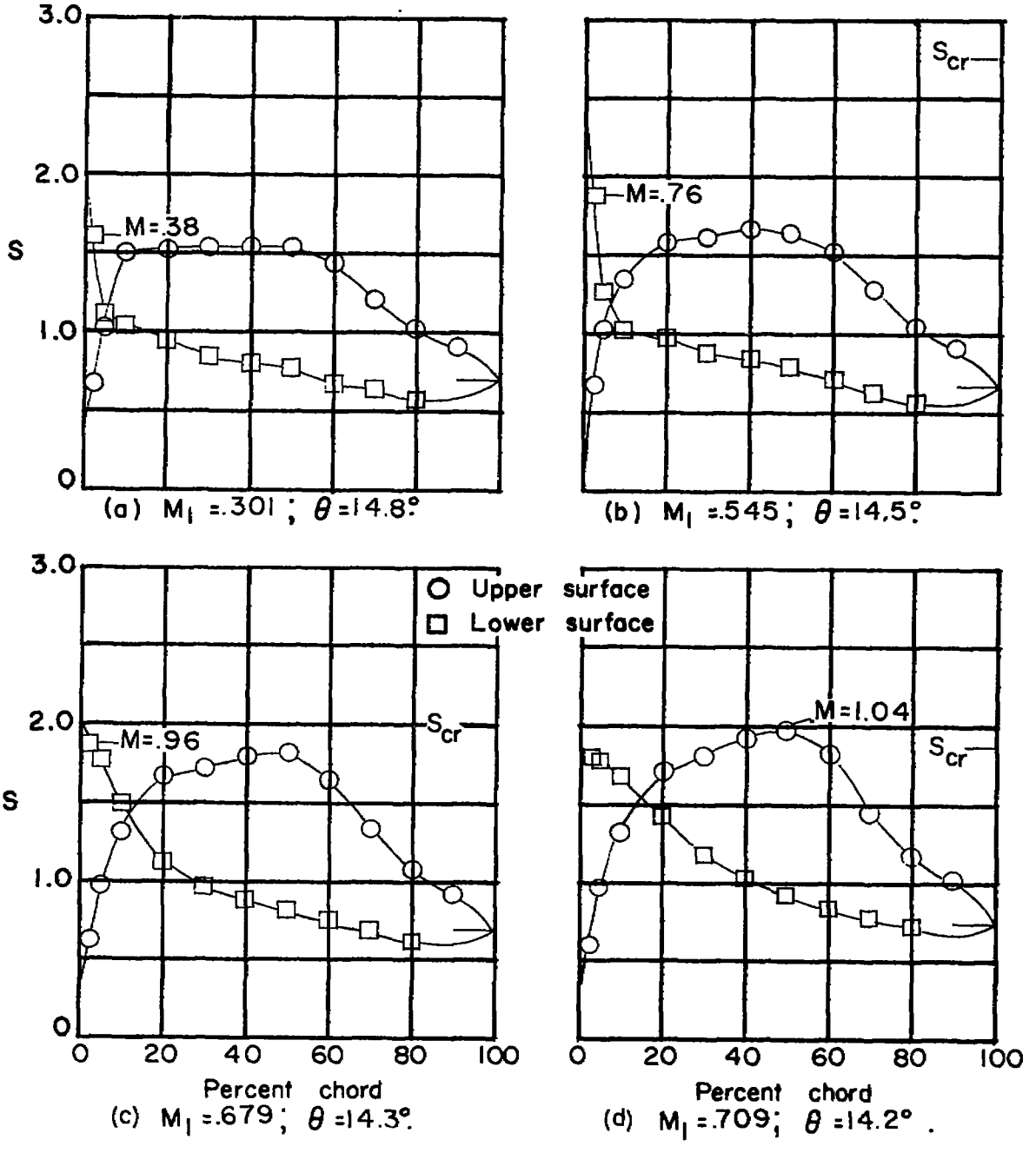

Figure 8 .— Blade-surface pressure distributions and section characteristics for the cascade combination. β_1 =45°; σ = 1.0 ; α = 7.0°; and blade section, NACA 65-$(12A_{10})$10.

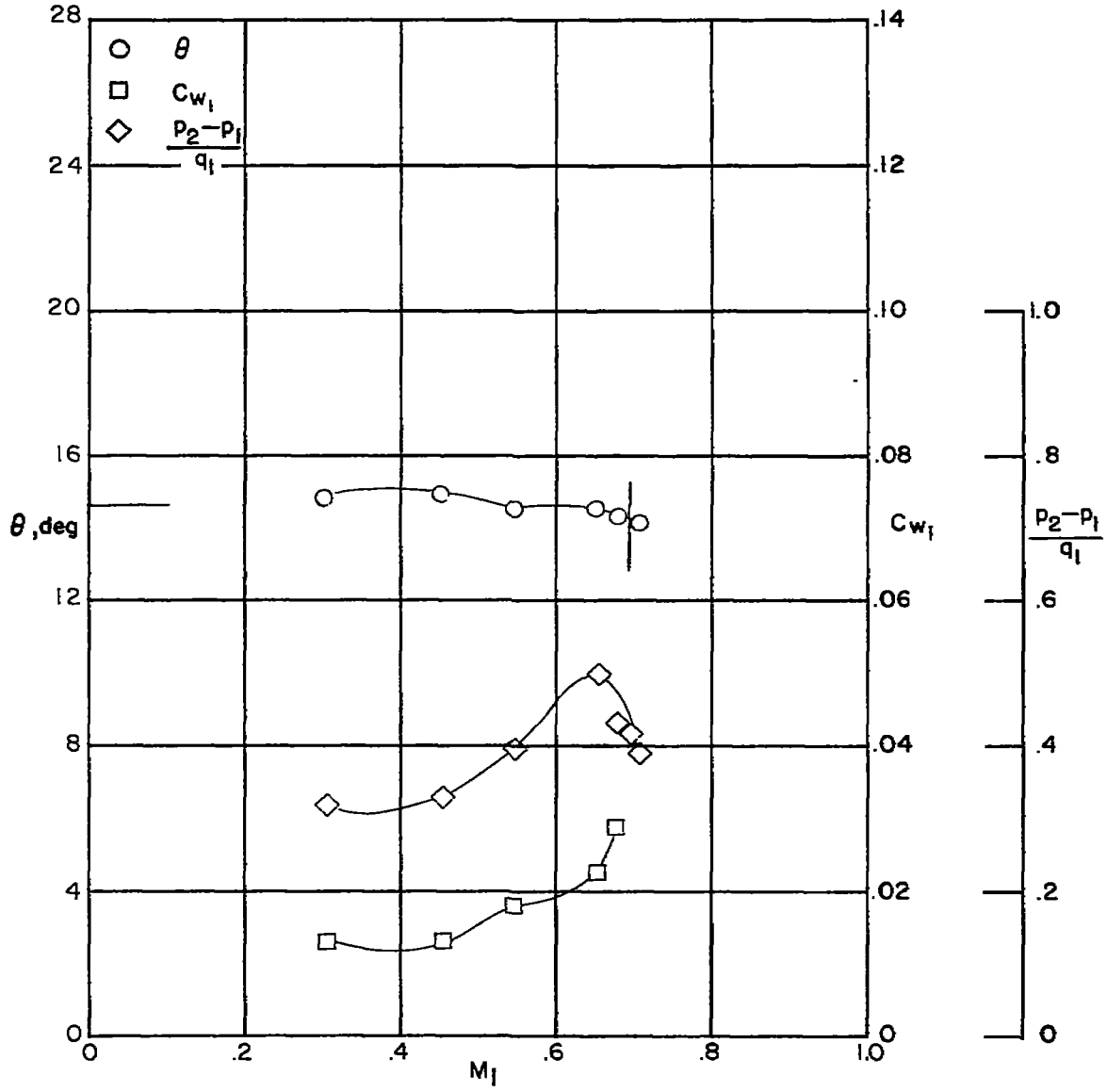

(e) Section characteristics. Tests are two dimensional for Mach numbers up to the vertical line. The horizontal line indicates low-speed turning angle given in reference 1.

Figure 8 .— Concluded.

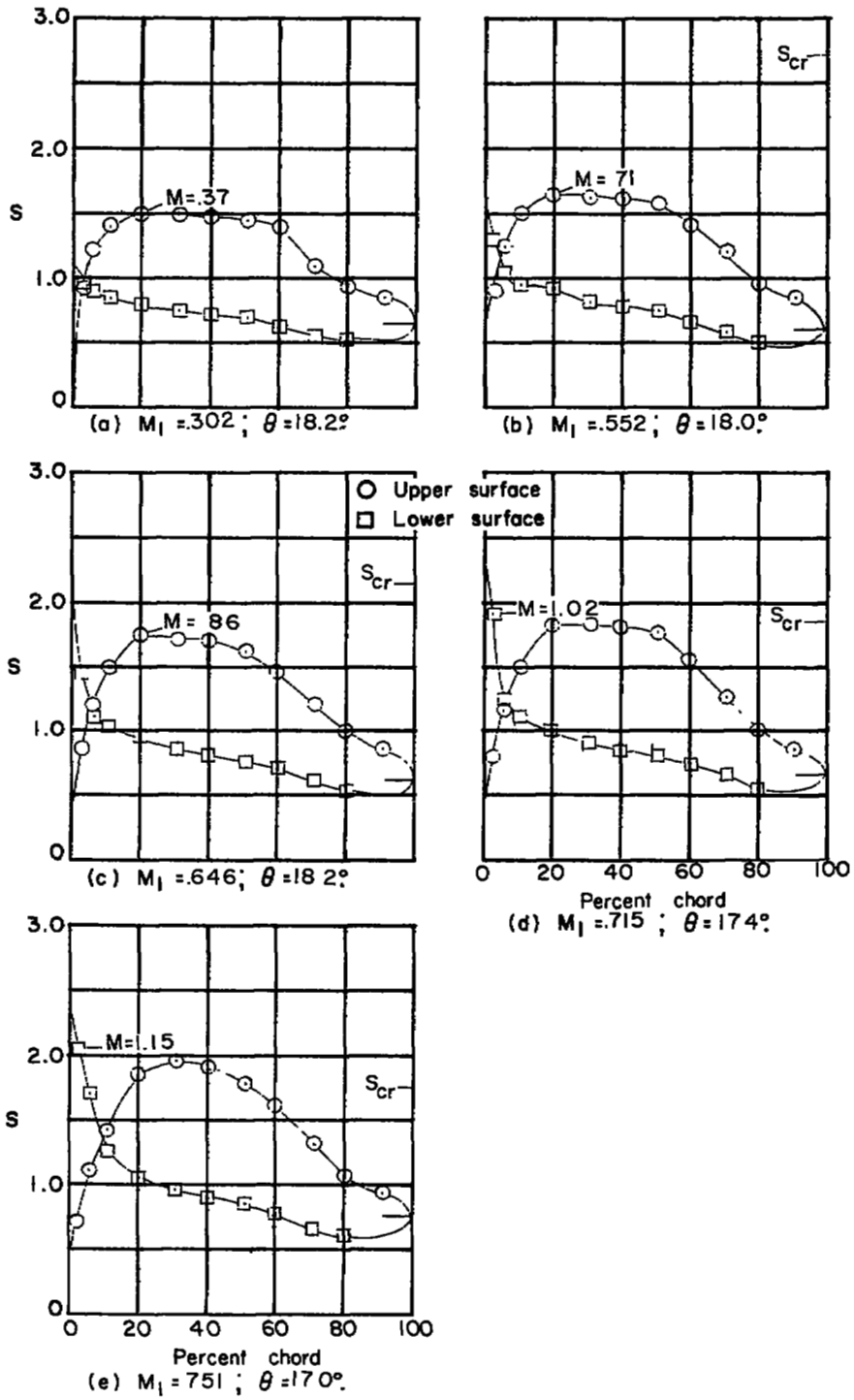

Figure 9 .— Blade-surface pressure distributions and section characteristics for the cascade combination. β_1 =45°; σ =1.0 ; α =10.0°; and blade section, NACA 65-($12A_{10}$)10.

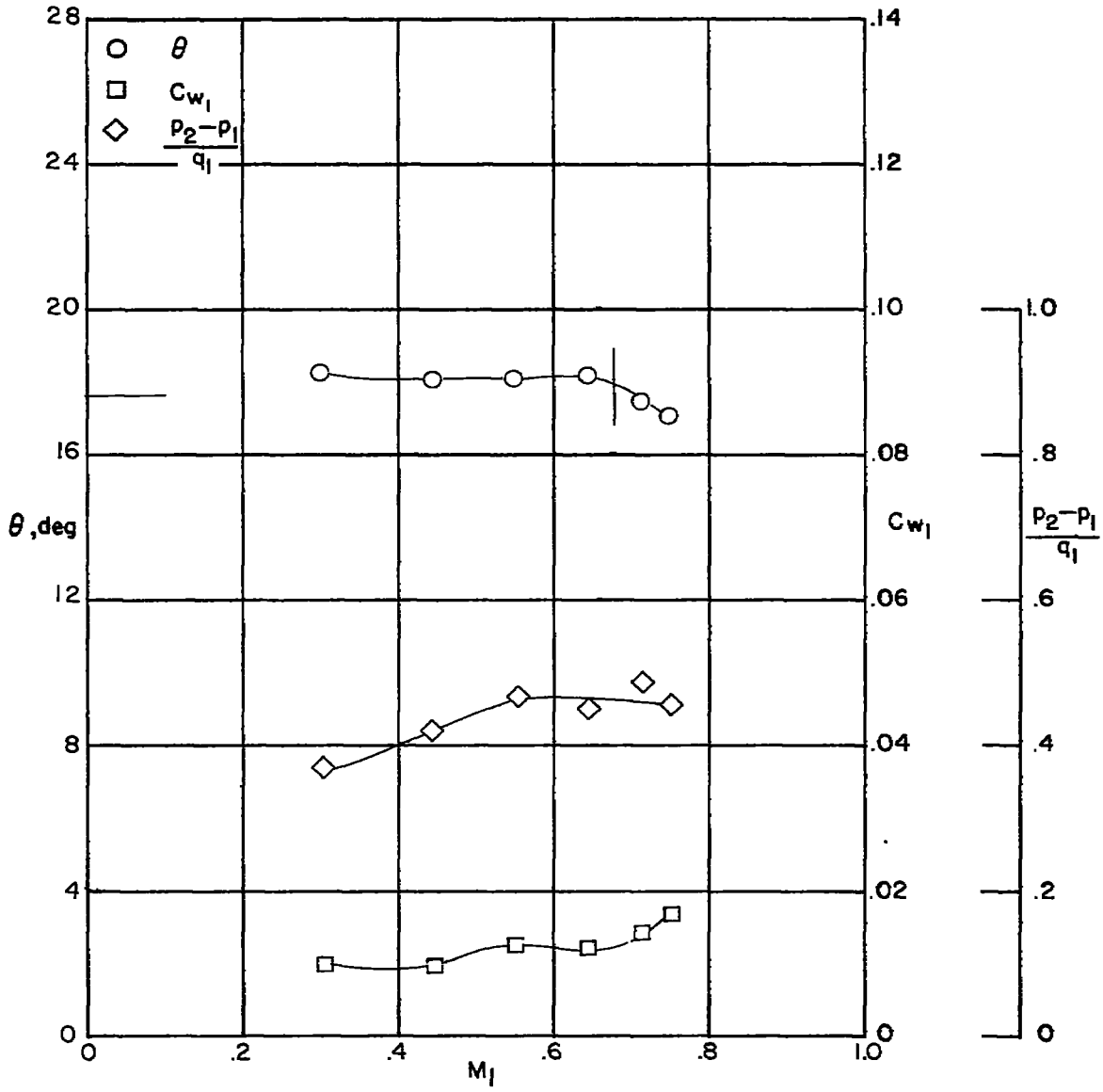

(f) Section characteristics. Tests are two dimensional for Mach numbers up to the vertical line. The horizontal line indicates low-speed turning angle given in reference 1.

Figure 9 .— Concluded.

[redacted]

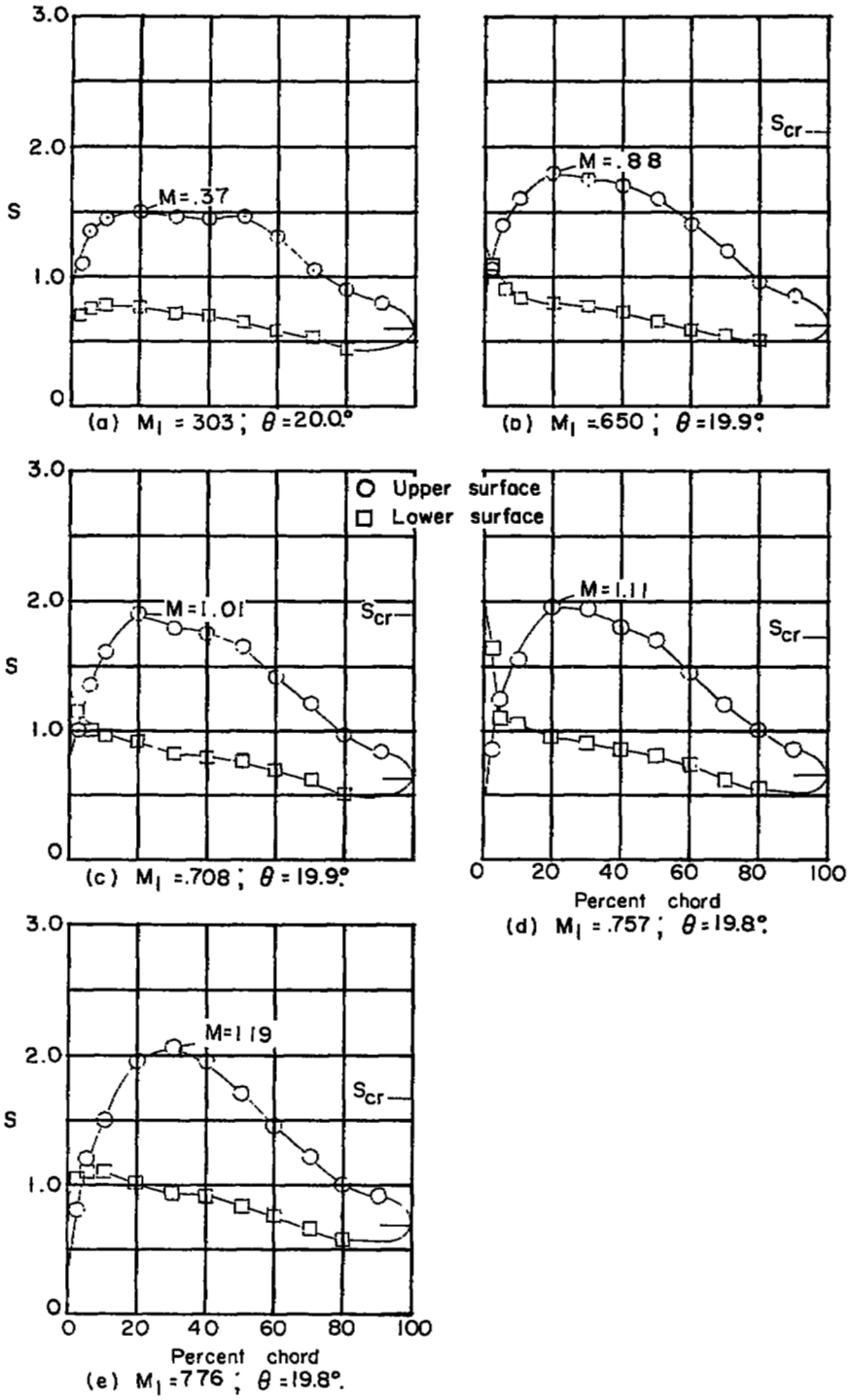

Figure 10 .— Blade-surface pressure distributions and section characteristics for the cascade combination, β_1 =45°; σ = 1.0 ; α =12.0°; and blade section, NACA 65-(12A_{10})10.

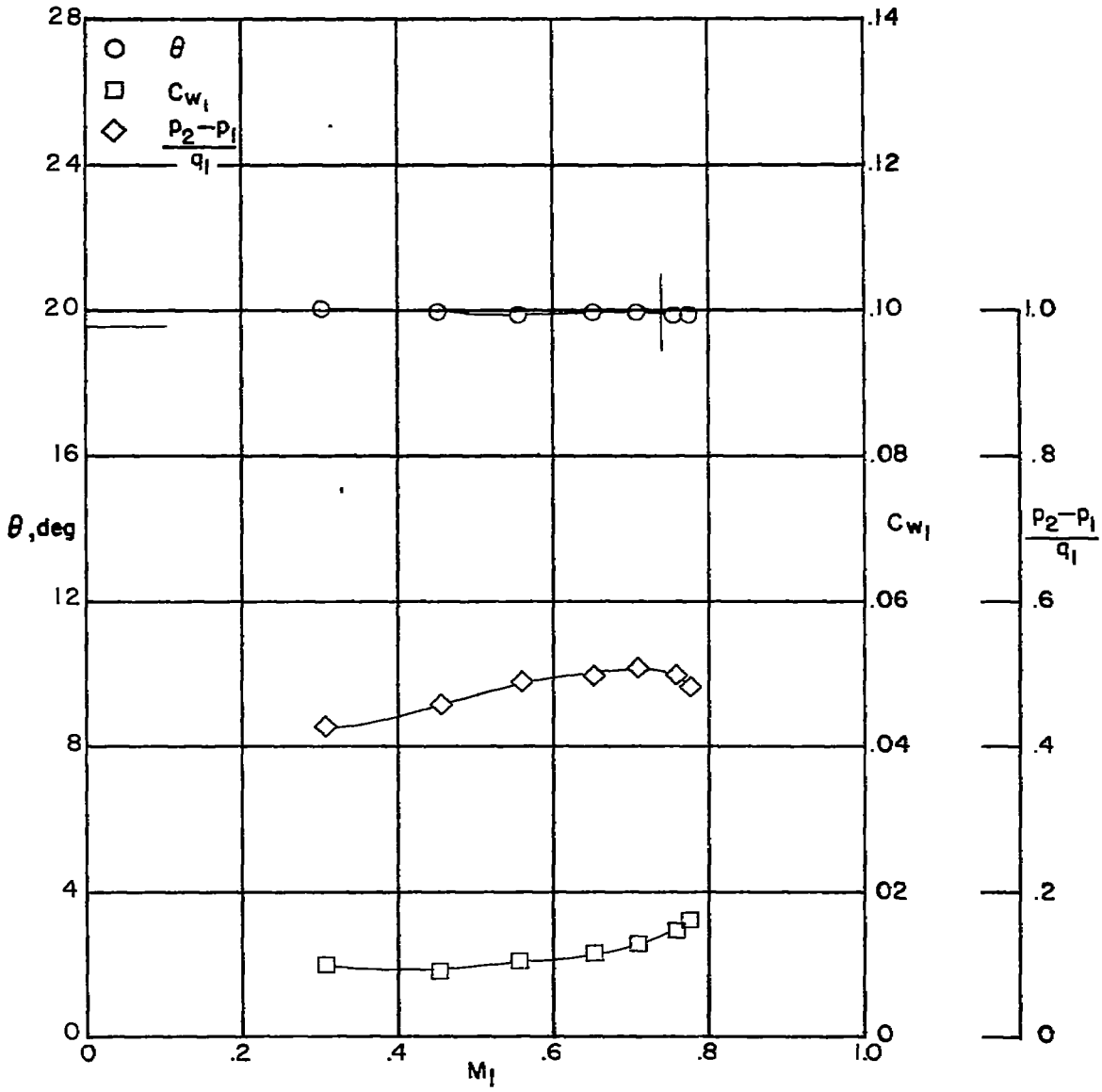

(f) Section characteristics. Tests are two dimensional for Mach numbers up to the vertical line. The horizontal line indicates low-speed turning angle given in reference 1.

Figure 10 .— Concluded.

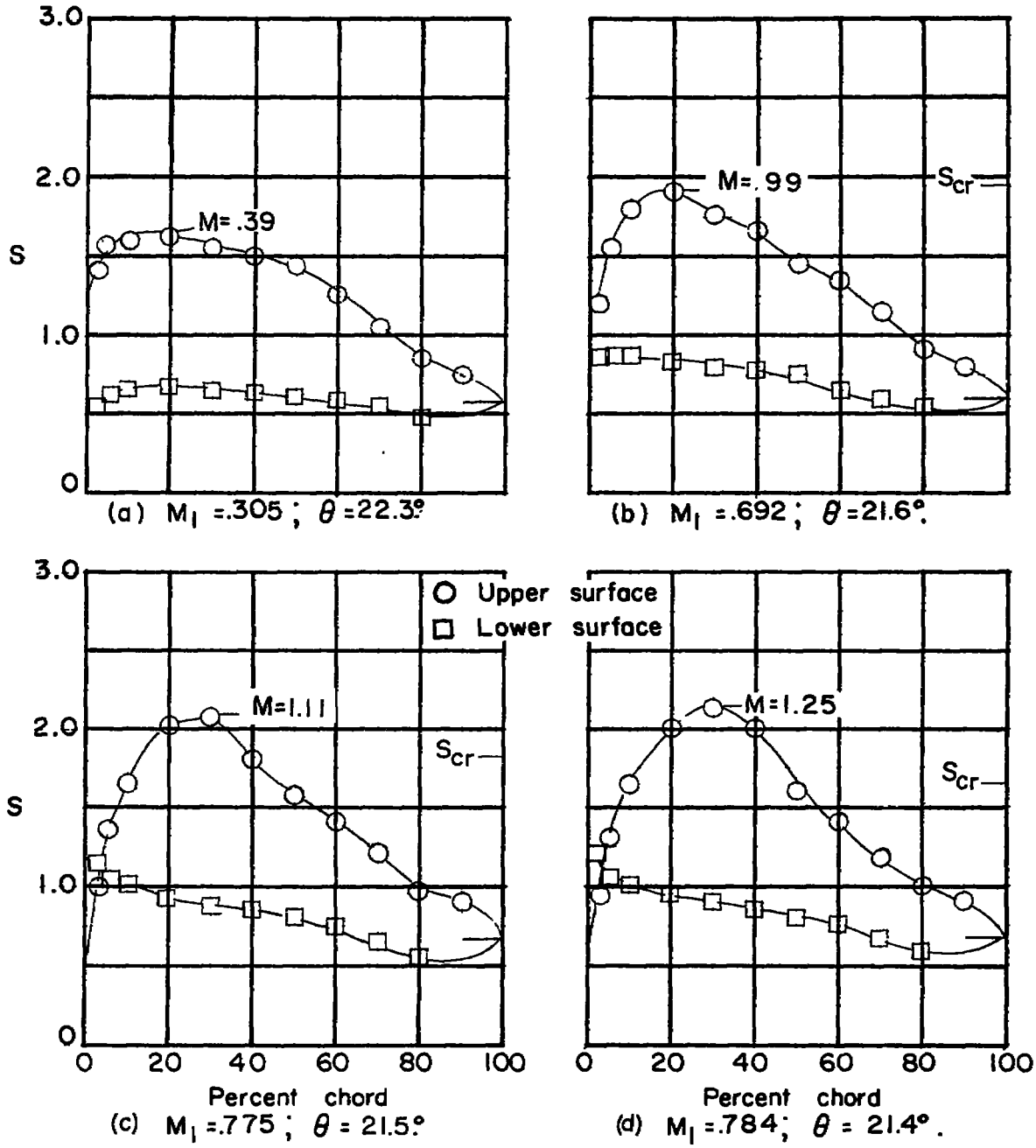

Figure 11 .— Blade-surface pressure distributions and section characteristics for the cascade combination. β_1 =45°; σ =1.0 ; α =14.0°; and blade section, NACA 65-($12A_{10}$)10.

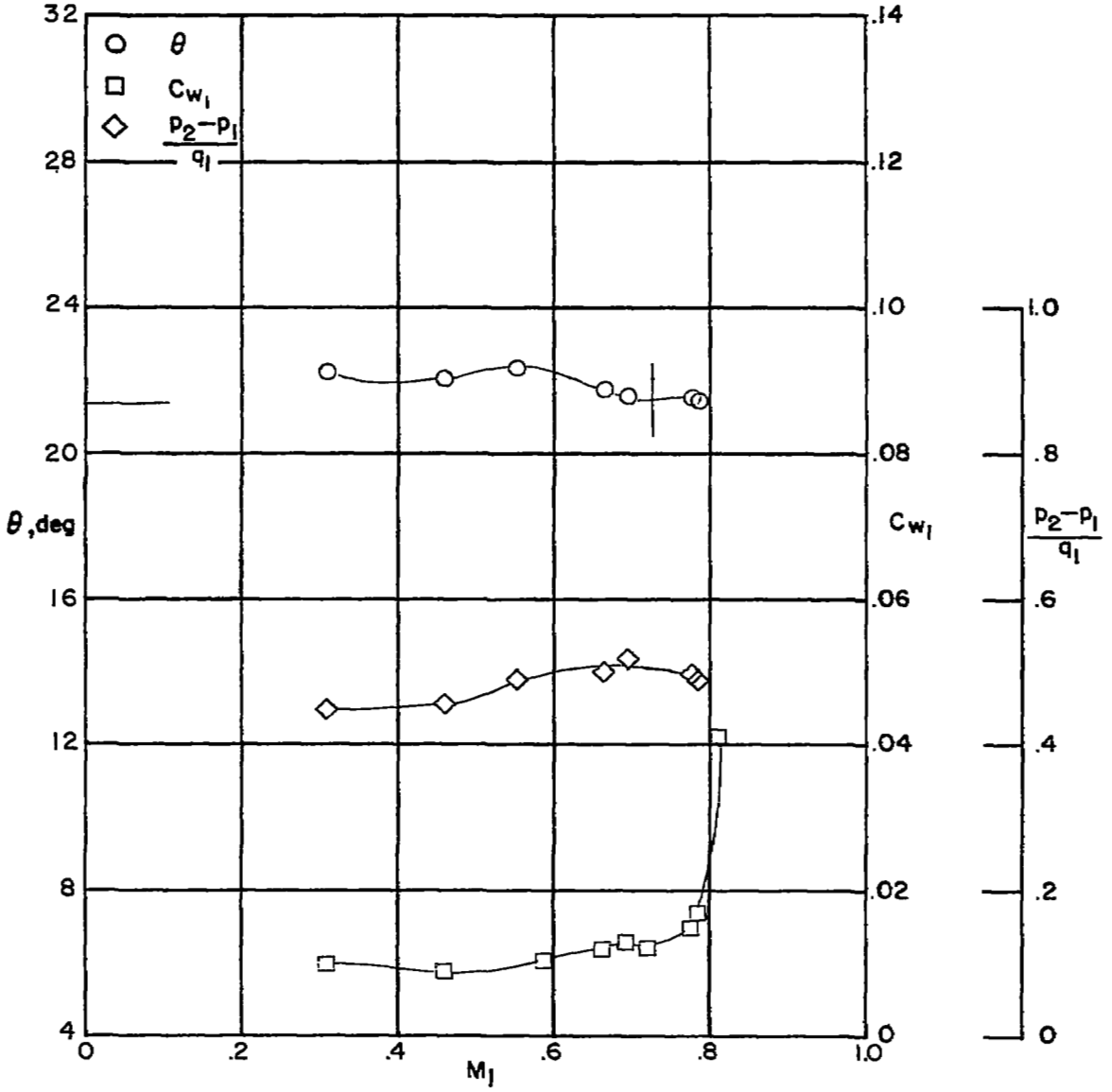

(e) Section characteristics. Tests are two dimensional for Mach numbers up to the vertical line. The horizontal line indicates low-speed turning angle given in reference 1.

Figure 11 .— Concluded.

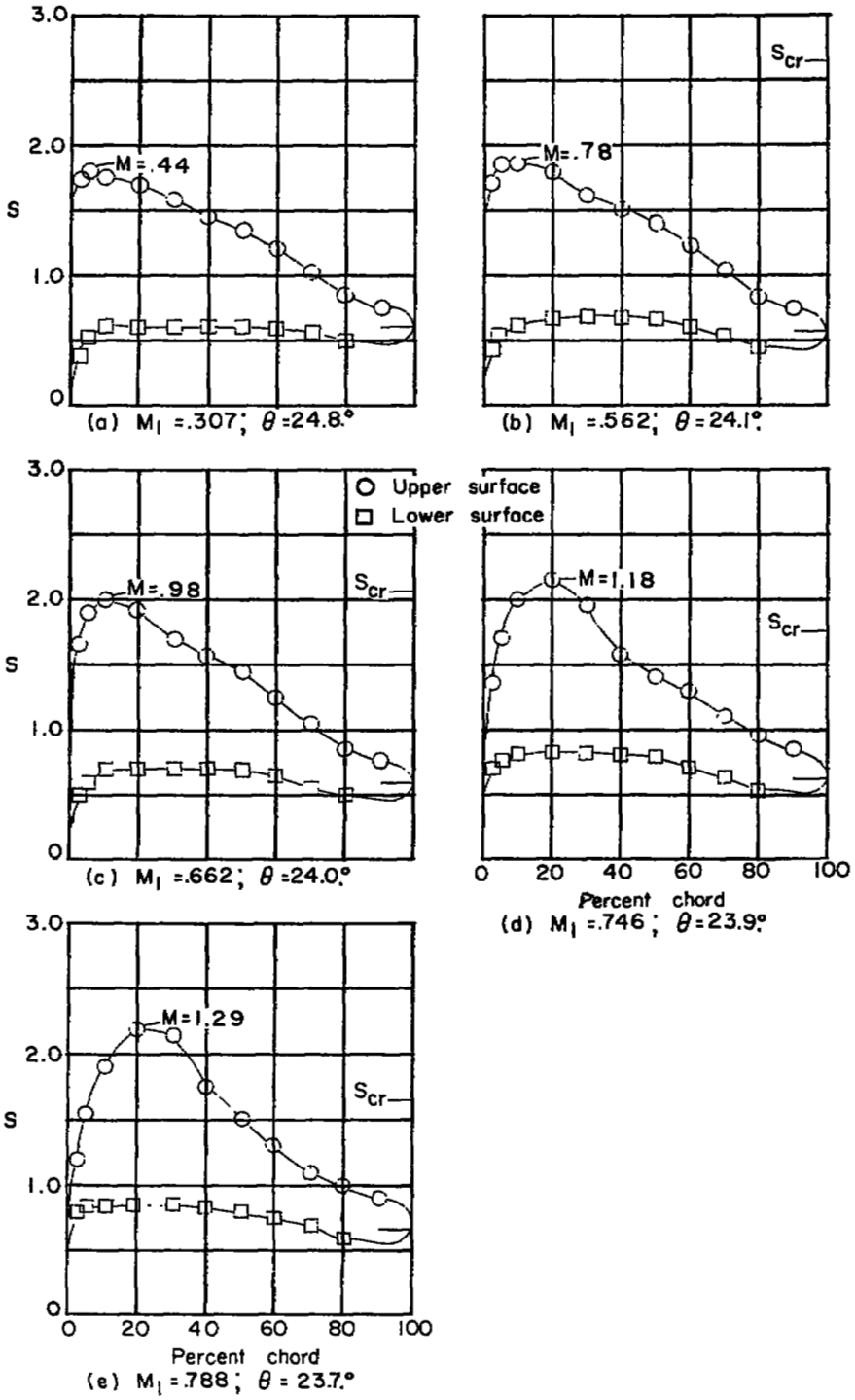

Figure 12 .— Blade-surface pressure distributions and section characteristics for the cascade combination · β_1 =45°; σ =1.0 ; α =17.0°; and blade section, NACA 65-($12A_{10}$)10.

[redacted]

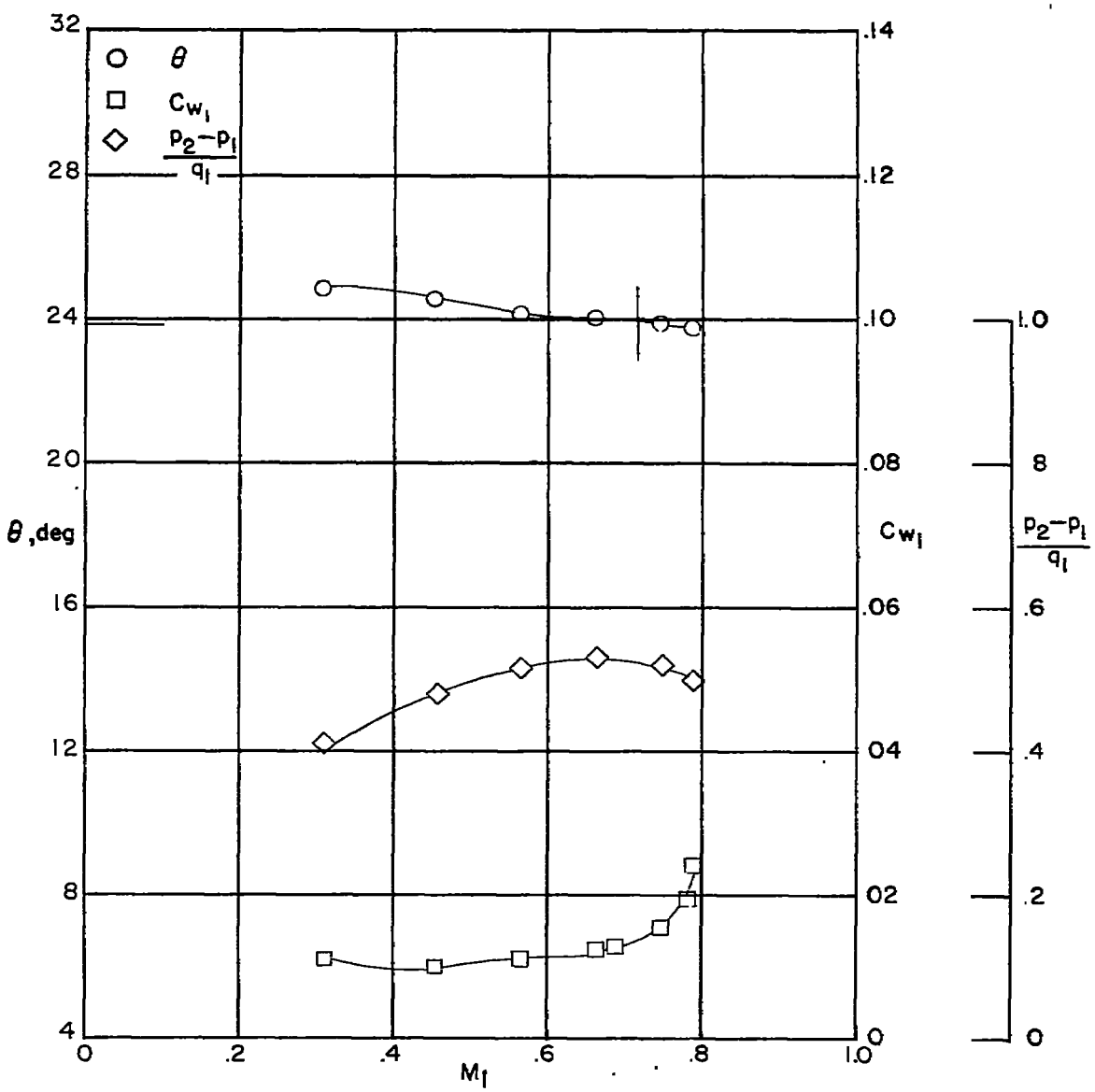

(f) Section characteristics. Tests are two dimensional for Mach numbers up to the vertical line. The horizontal line indicates low-speed turning angle given in reference 1.

Figure 12 .— Concluded.

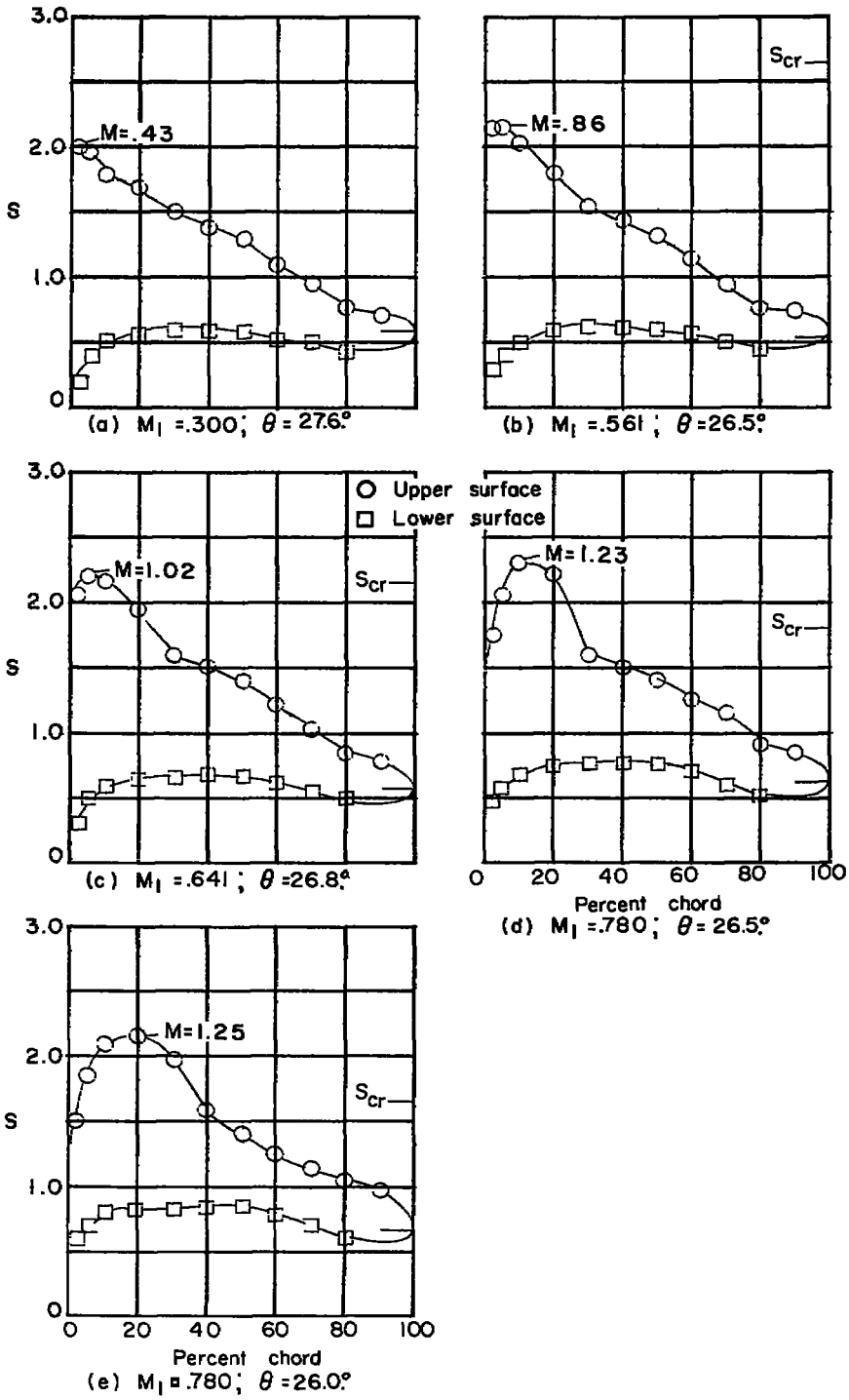

Figure 13 .— Blade-surface pressure distributions and section characteristics for the cascade combination, β_1 =45°; σ =1.0 ; α =20.0° and blade section, NACA 65-($12A_{10}$)10.

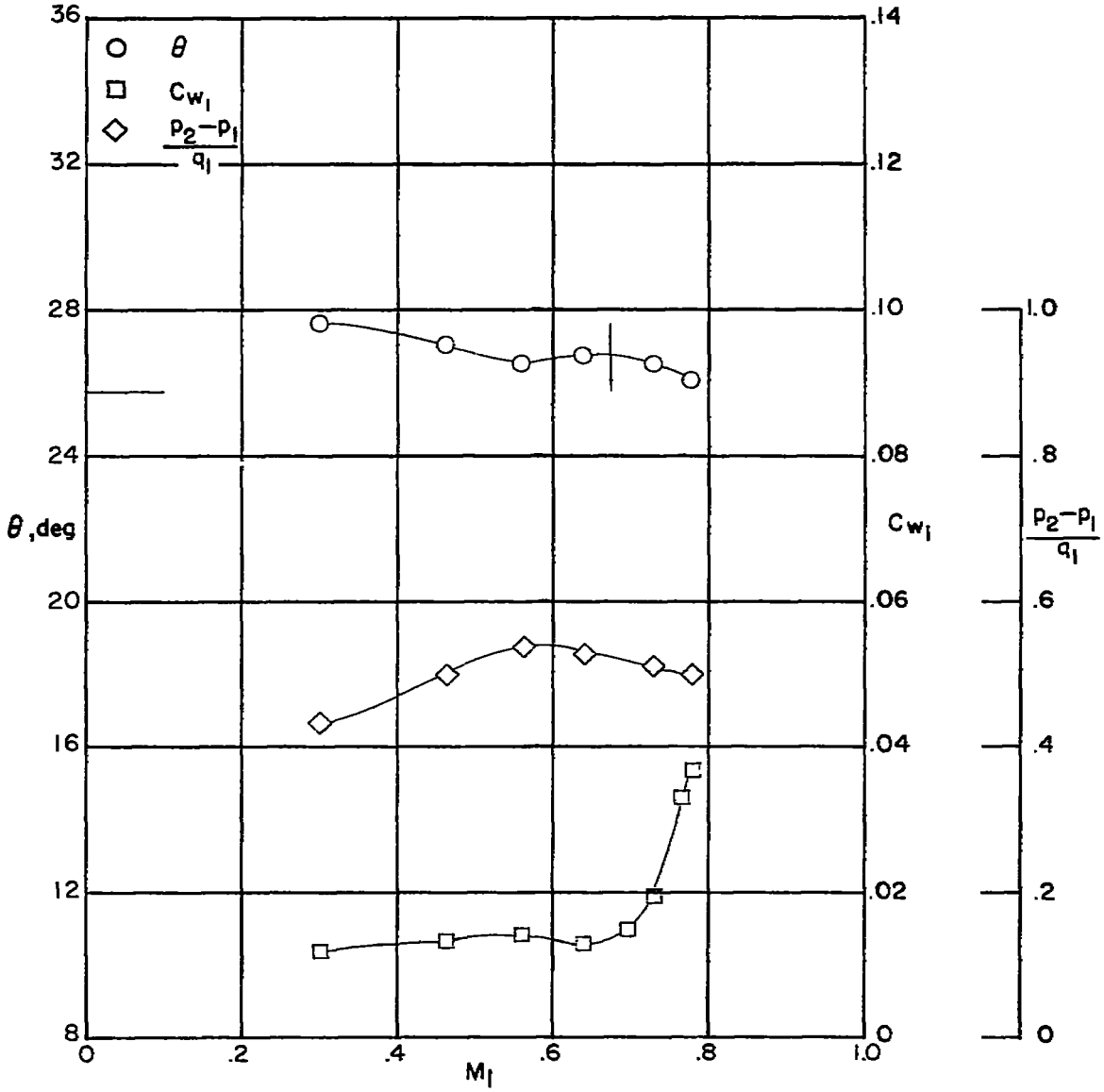

(f) Section characteristics. Tests are two dimensional for Mach numbers up to the vertical line. The horizontal line indicates low-speed turning angle given in reference 1.

Figure 13 .— Concluded.

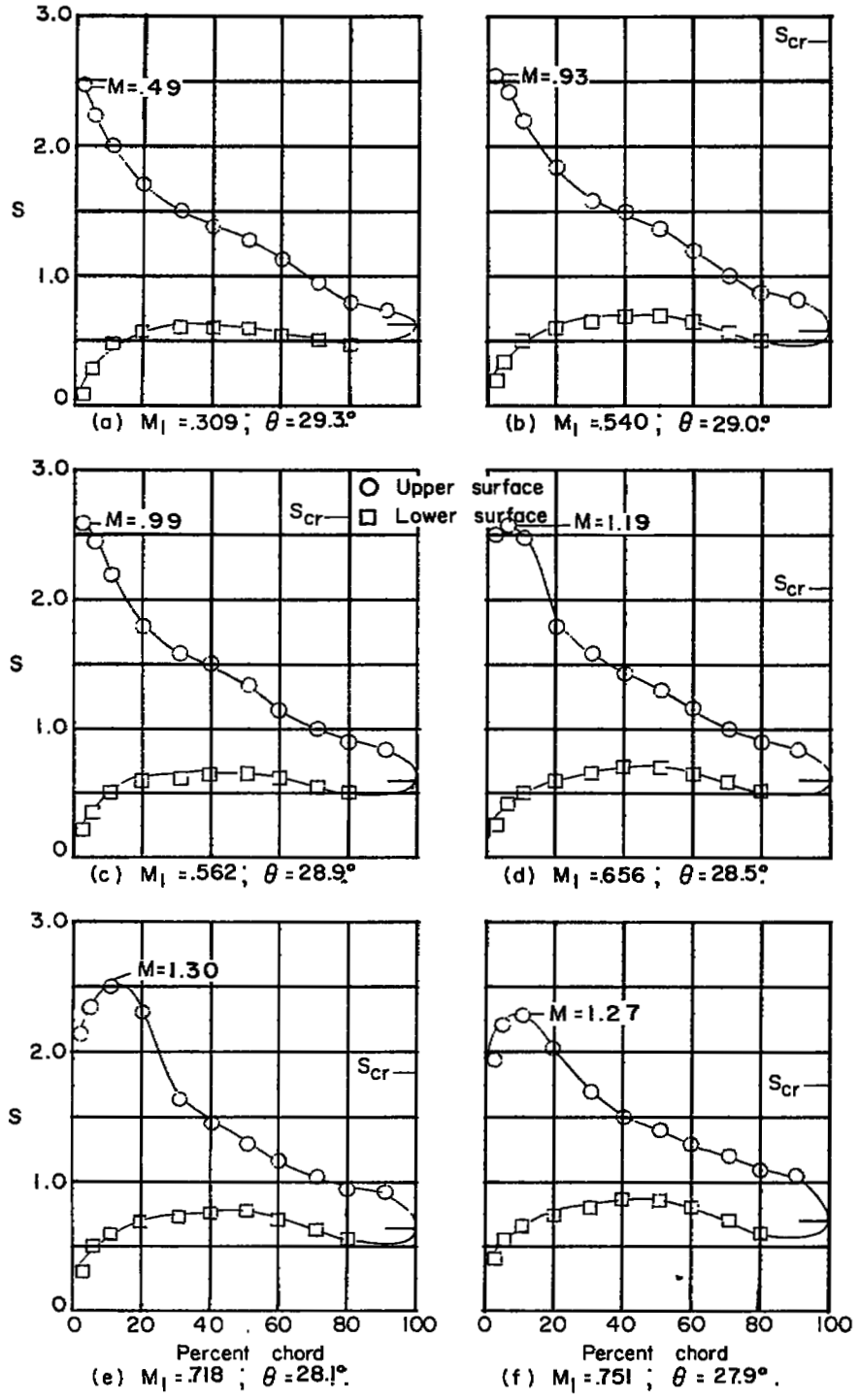

Figure 14 .— Blade-surface pressure distributions and section characteristics for the cascade combination, β_1 =45°; σ =1.0 ; α =23.0°; and blade section, NACA 65-($12A_{10}$)10.

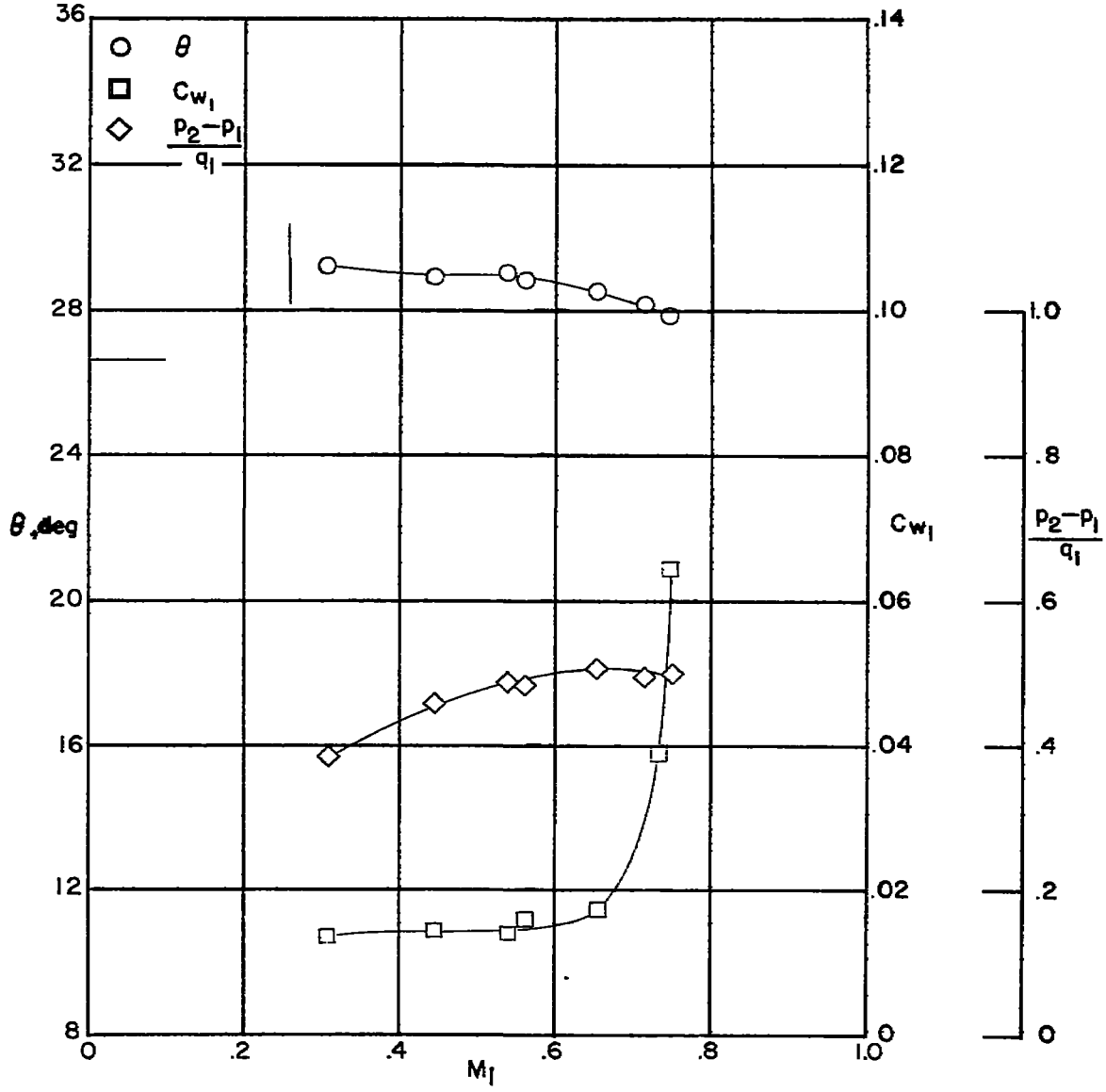

(g) Section characteristics. Tests are two dimensional for Mach numbers up to the vertical line. The horizontal line indicates low-speed turning angle given in reference 1.

Figure 14 .— Concluded.

[redacted]

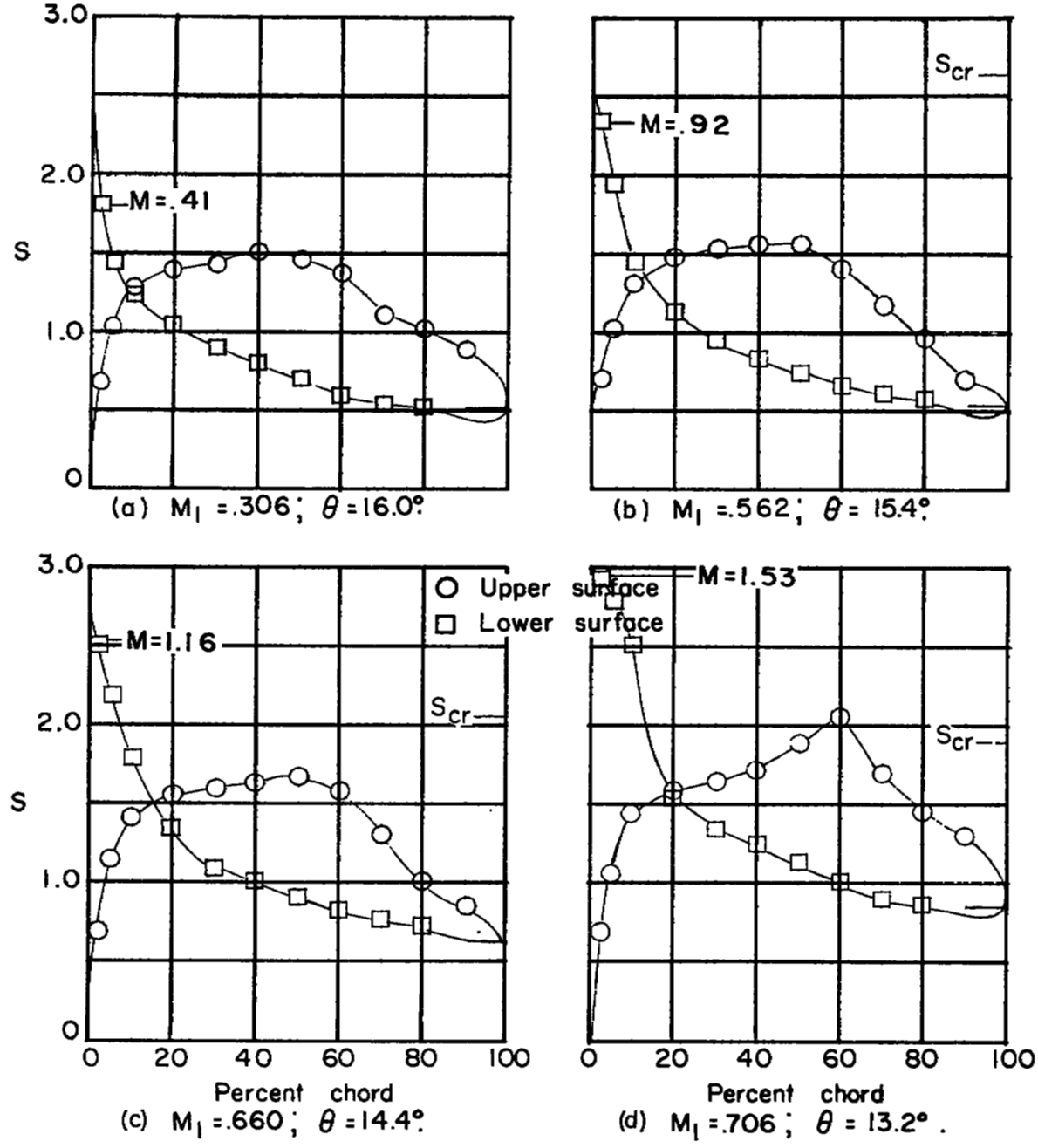

Figure 15 .— Blade-surface pressure distributions and section characteristics for the cascade combination. β_1 = 60°; σ =1.5 ; α = 9.8°; and blade section, NACA 65-(12 A_{10})10.

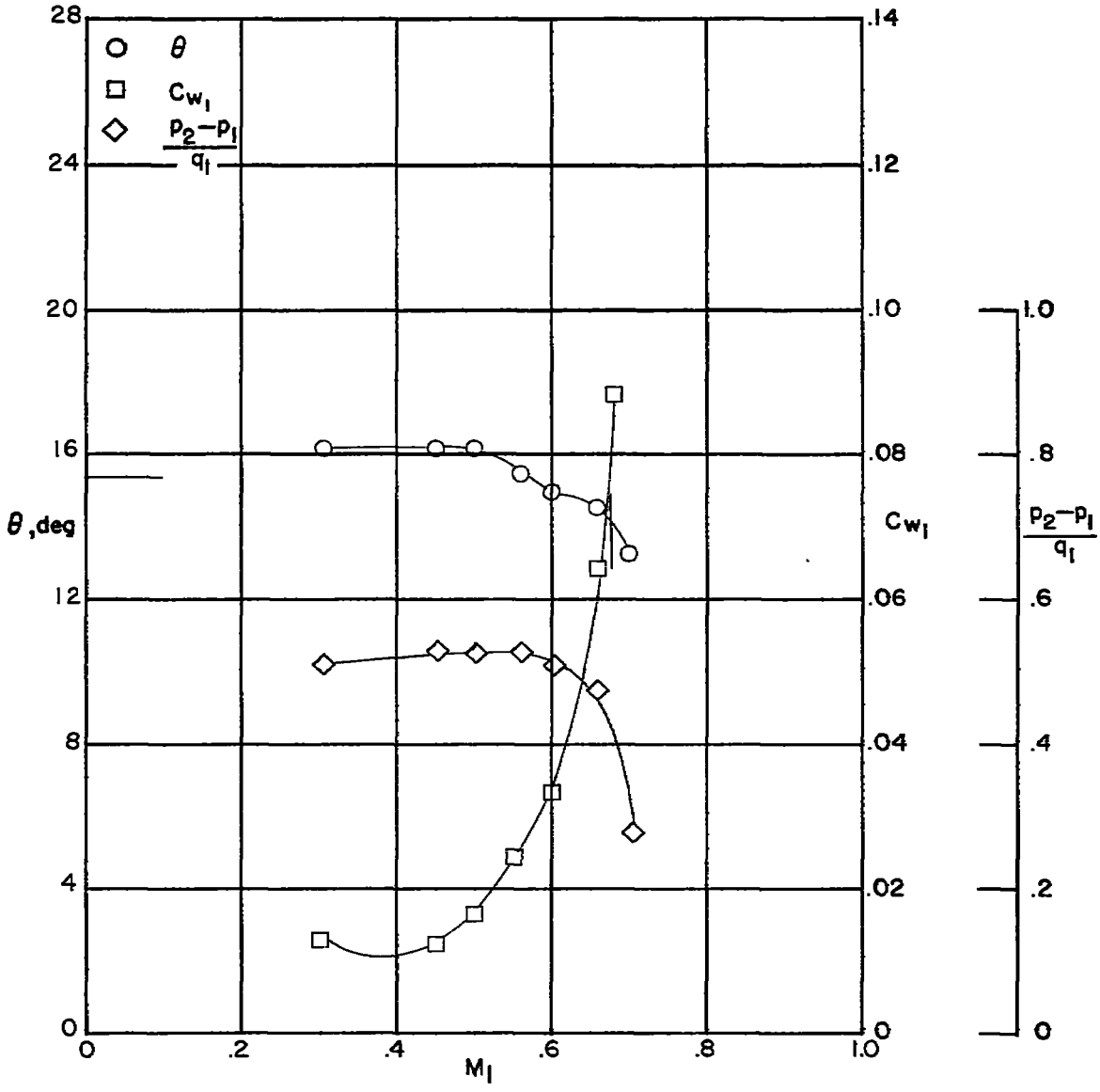

(e) Section characteristics. Tests are two dimensional for Mach numbers up to the vertical line. The horizontal line indicates low-speed turning angle given in reference 1.

Figure 15.— Concluded.

[redacted]

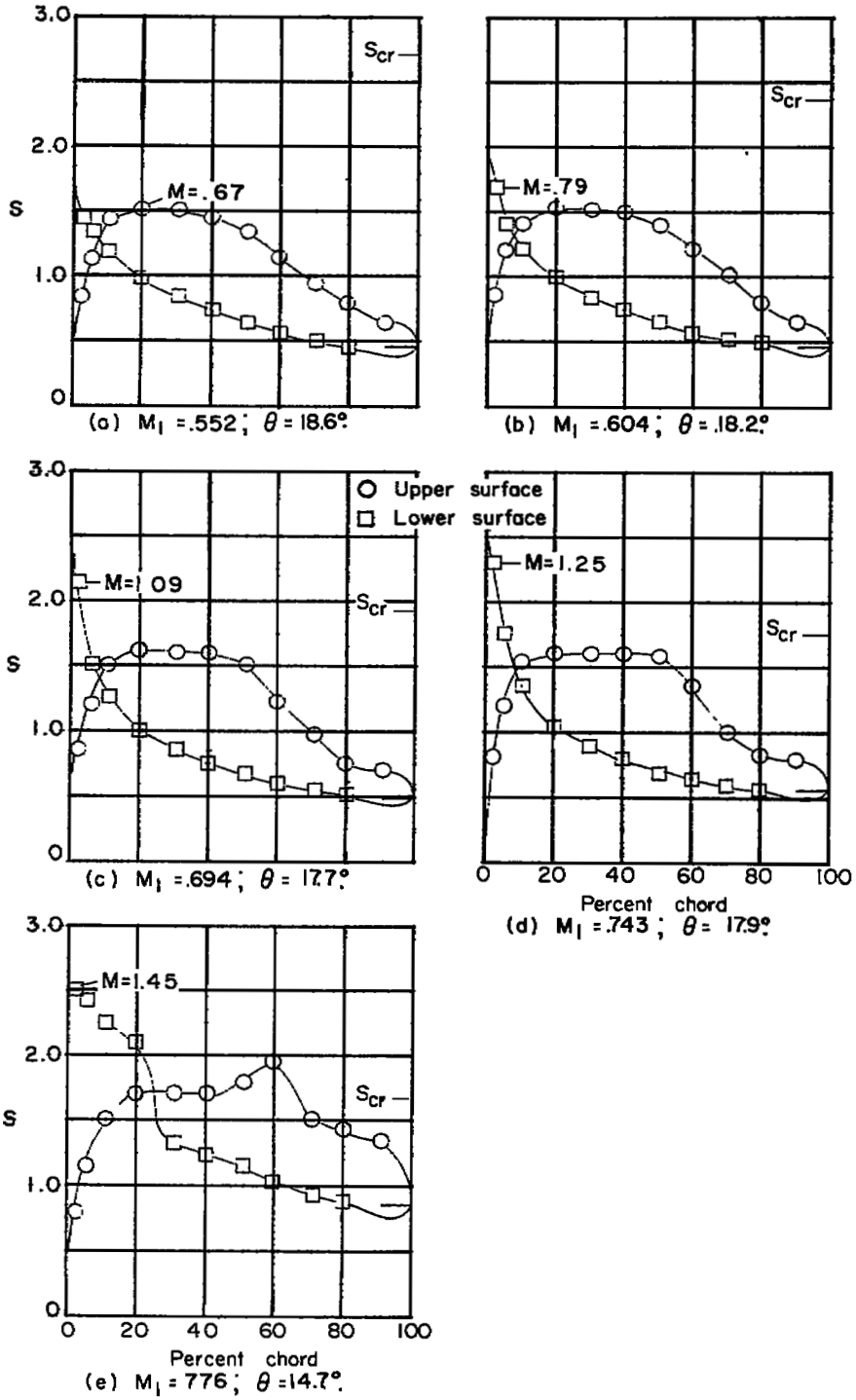

Figure 16 .— Blade-surface pressure distributions and section characteristics for the cascade combination. β_1 =60 ; σ =1.5 ; α =12.8°; and blade section, NACA 65-($12A_{10}$)10.

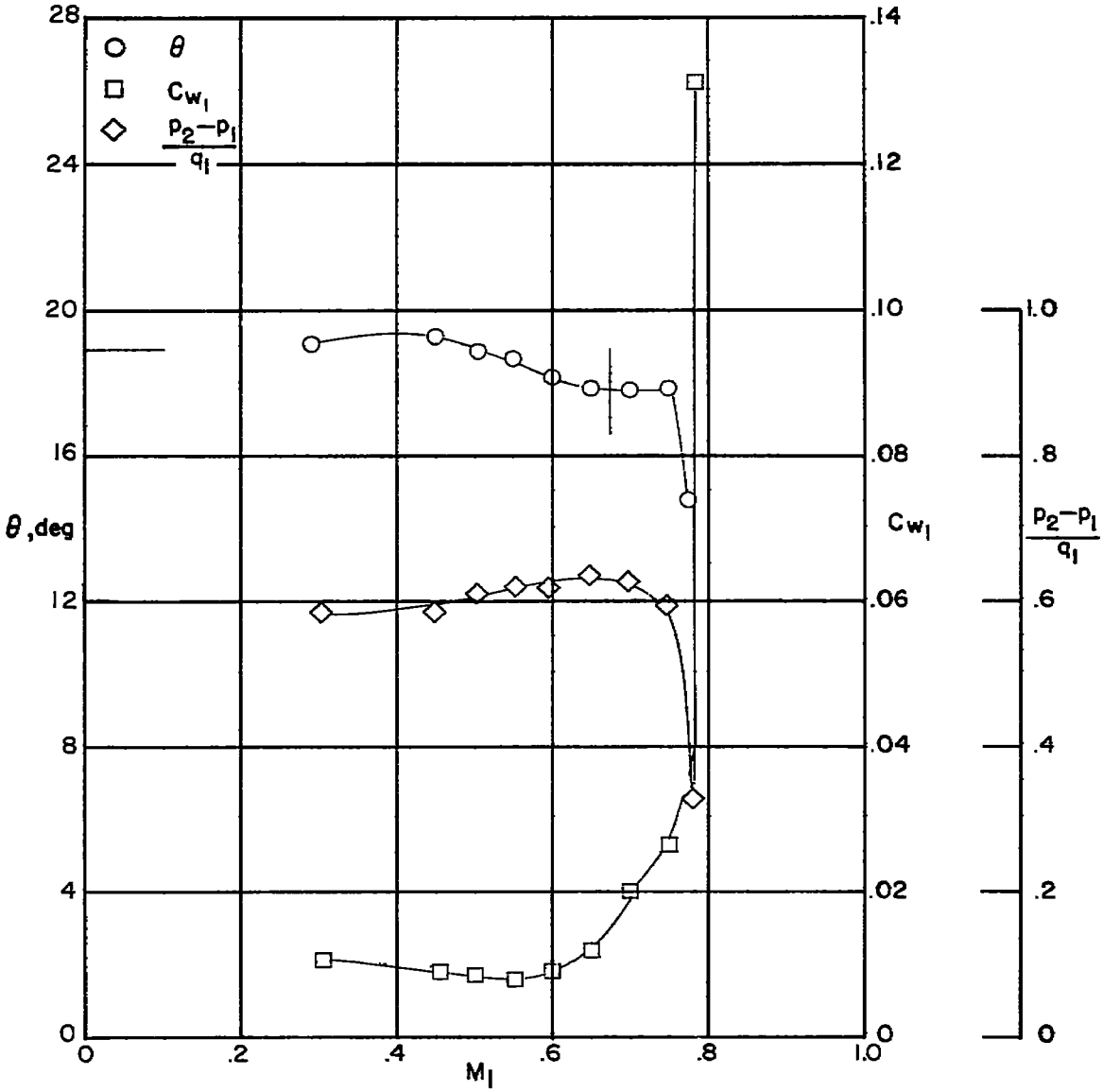

(f) Section characteristics. Tests are two dimensional for Mach numbers up to the vertical line. The horizontal line indicates low-speed turning angle given in reference 1

Figure 16 .— Concluded.

[redacted]

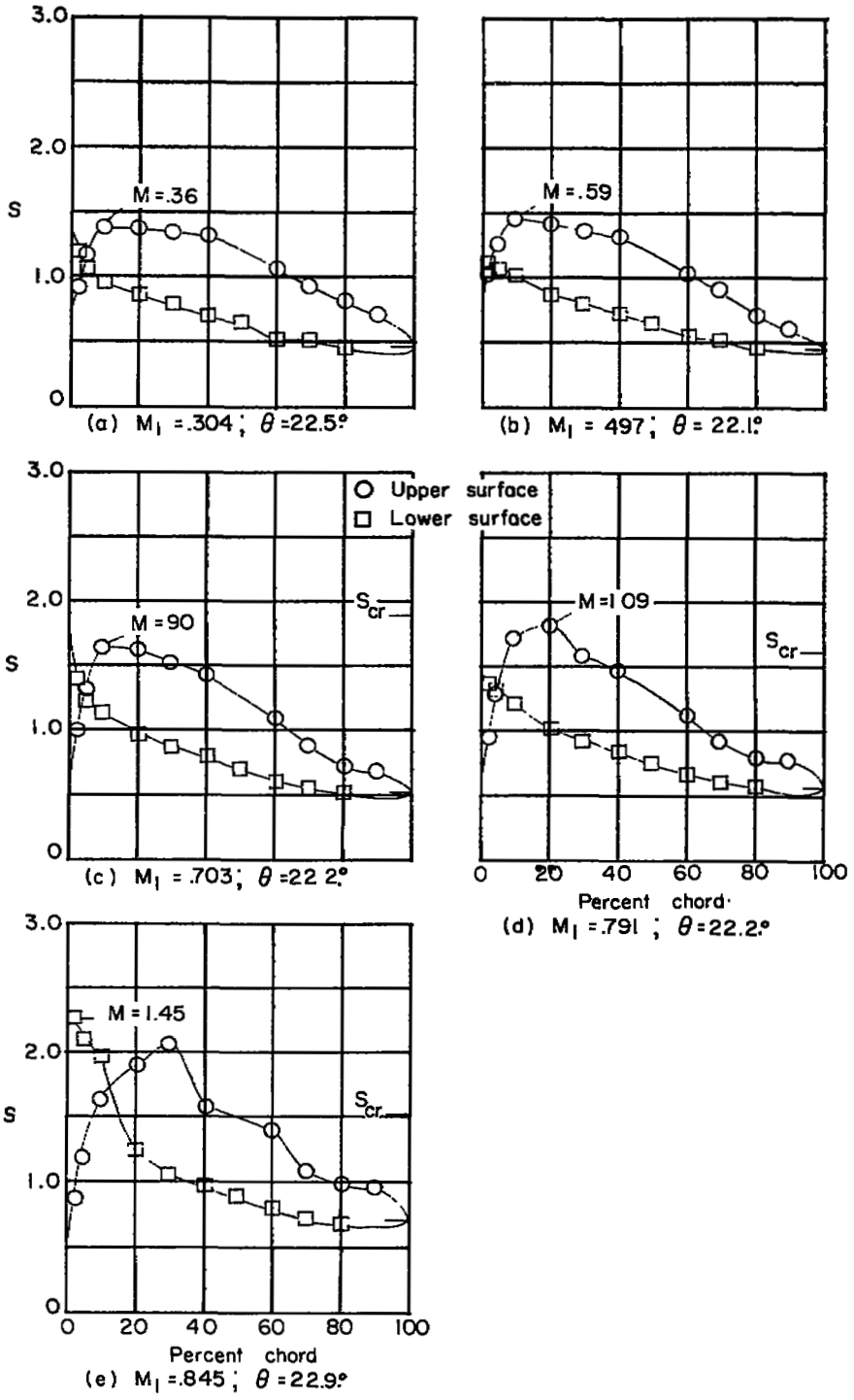

Figure 17.— Blade-surface pressure distributions and section characteristics for the cascade combination. β_1 = 60°; σ = 1.5; α = 15.8°; and blade section, NACA 65-($12A_{10}$)10.

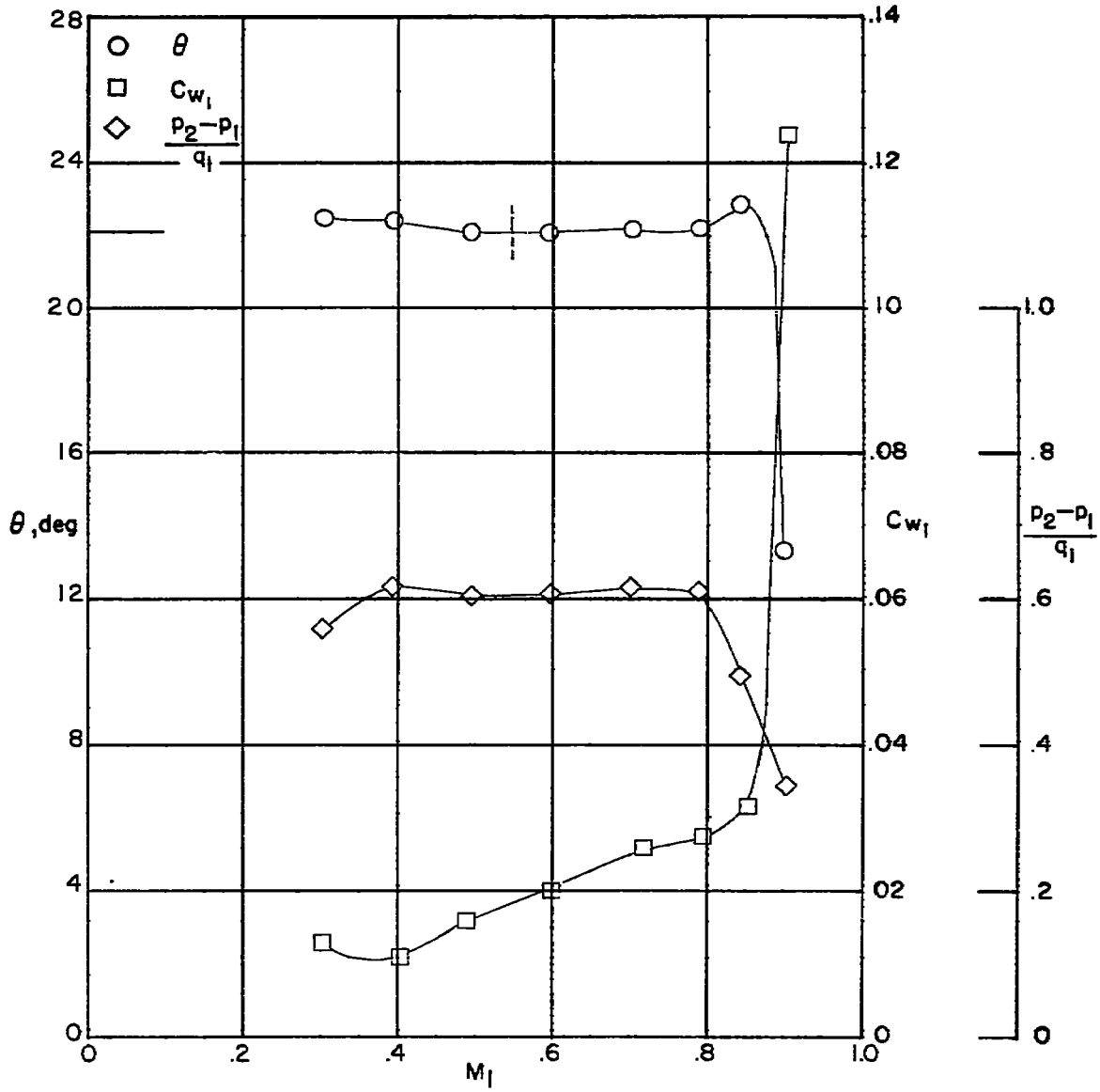

(f) Section characteristics. Tests are two dimensional for Mach numbers up to the vertical line. The horizontal line indicates low-speed turning angle given in reference 1.

Figure 17 .— Concluded.

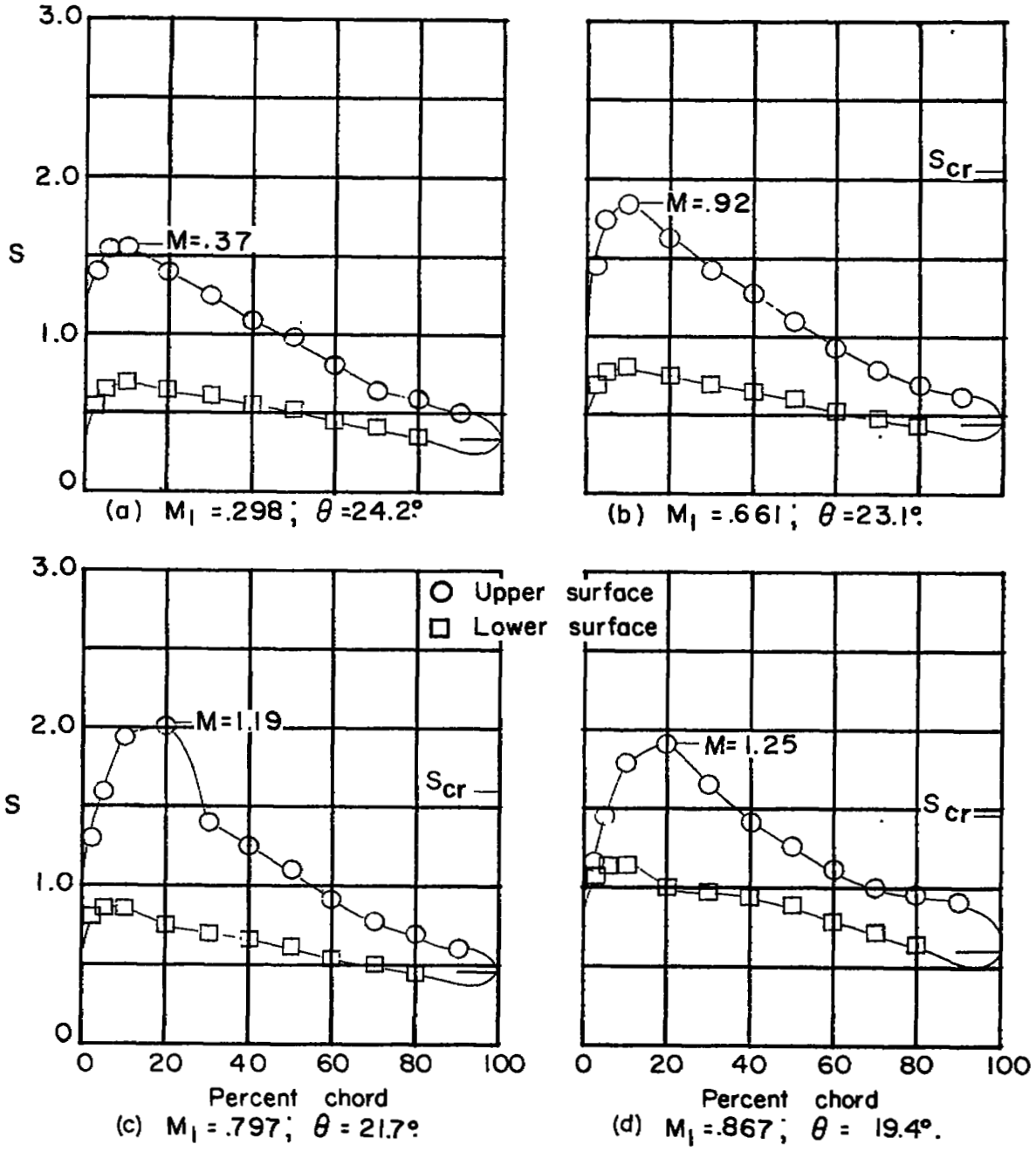

Figure 18 — Blade-surface pressure distributions and section characteristics for the cascade combination. β_1 = 60°; σ =1.5 ; α =18.8°; and blade section, NACA 65-($12A_{10}$)10.

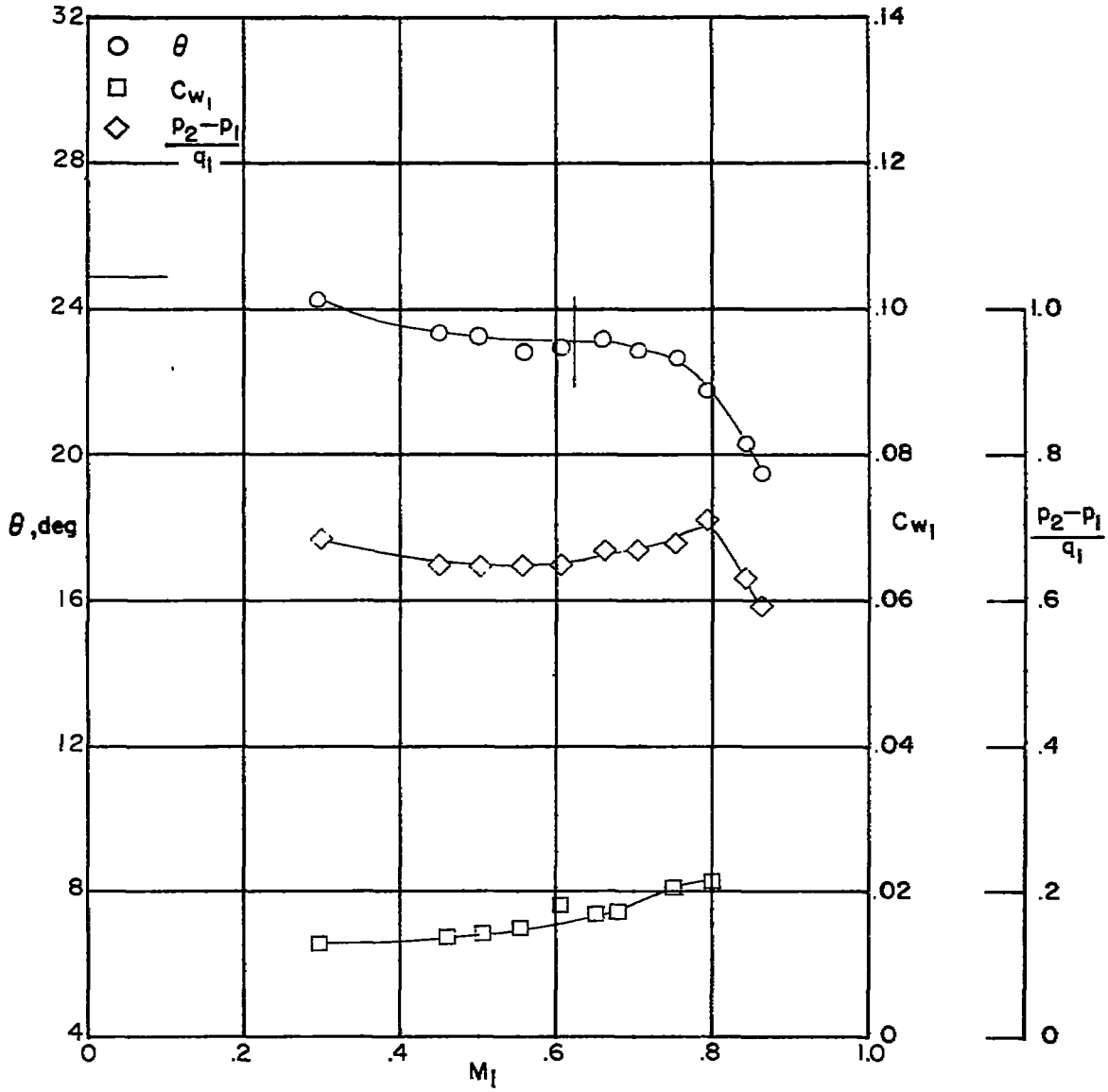

(e) Section characteristics. Tests are two dimensional for Mach numbers up to the vertical line. The horizontal line indicates low-speed turning angle given in reference 1.

Figure 18 .— Concluded.

[redacted]

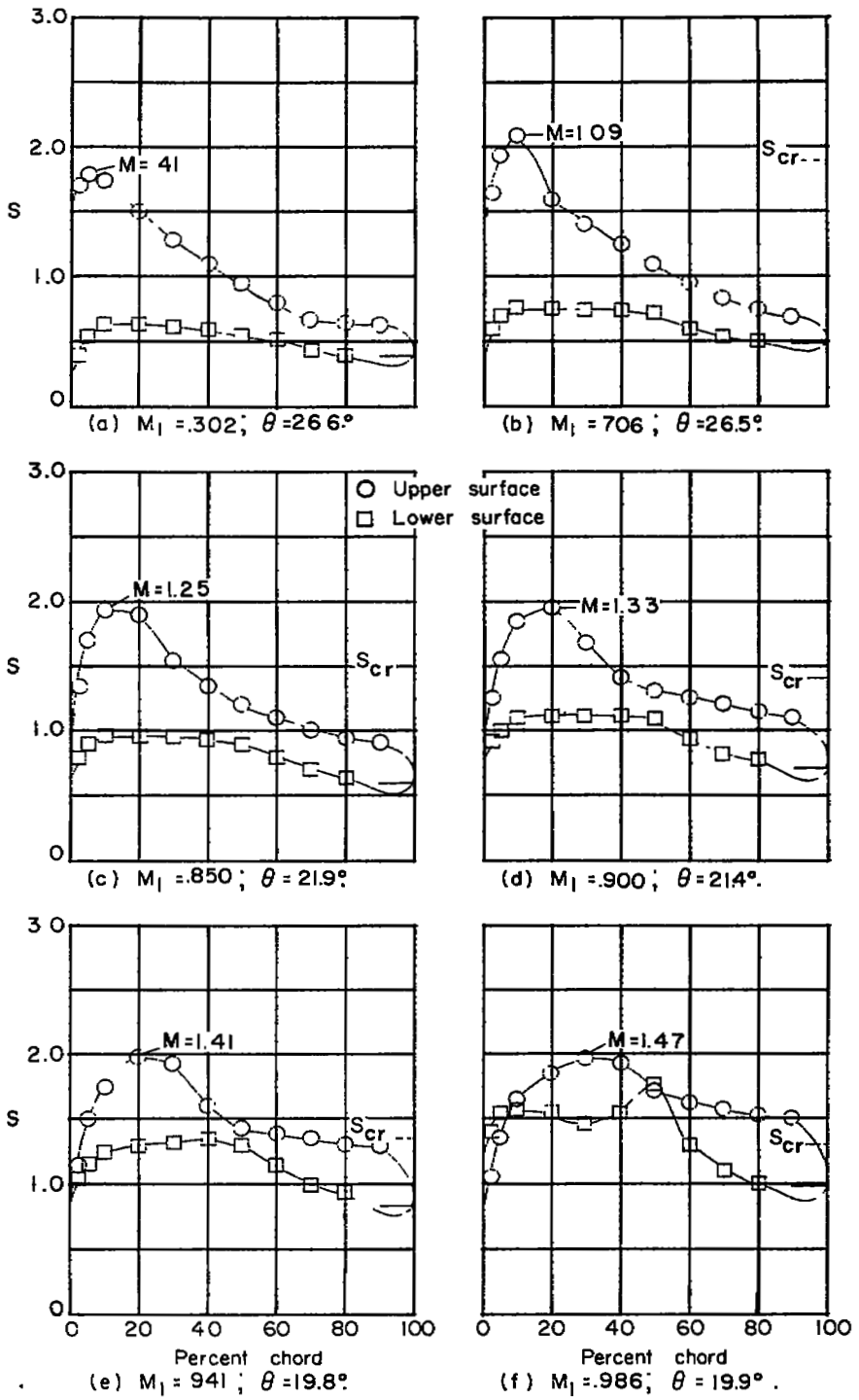

Figure 19.— Blade-surface pressure distributions and section characteristics for the cascade combination. β_1 =60°; σ =1.5; α =21.8°; and blade section, NACA 65-($12A_{10}$)10.

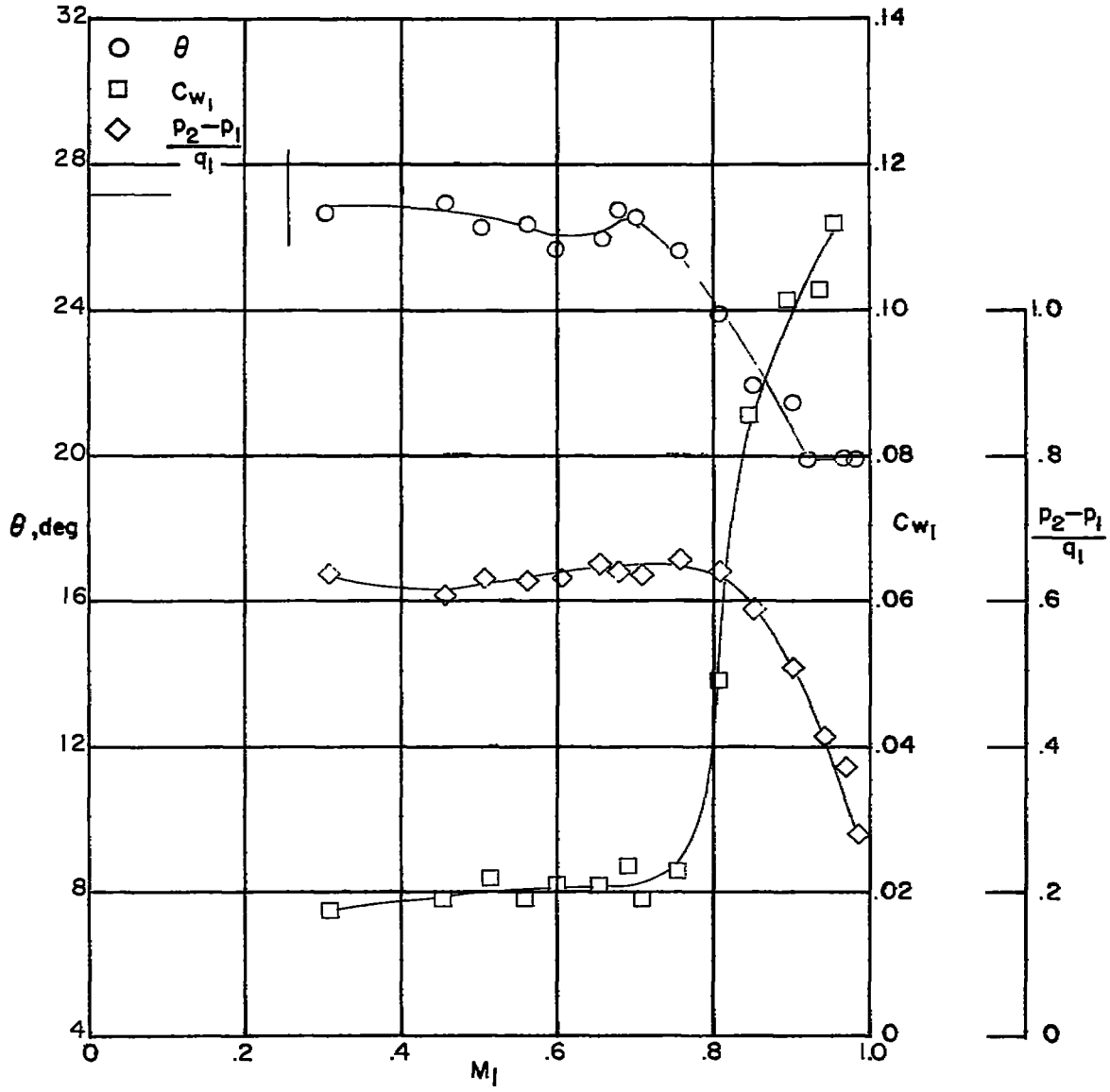

(g) Section characteristics. Tests are two dimensional for Mach numbers up to the vertical line. The horizontal line indicates low-speed turning angle given in reference 1.

Figure 19.— Concluded.

[redacted]

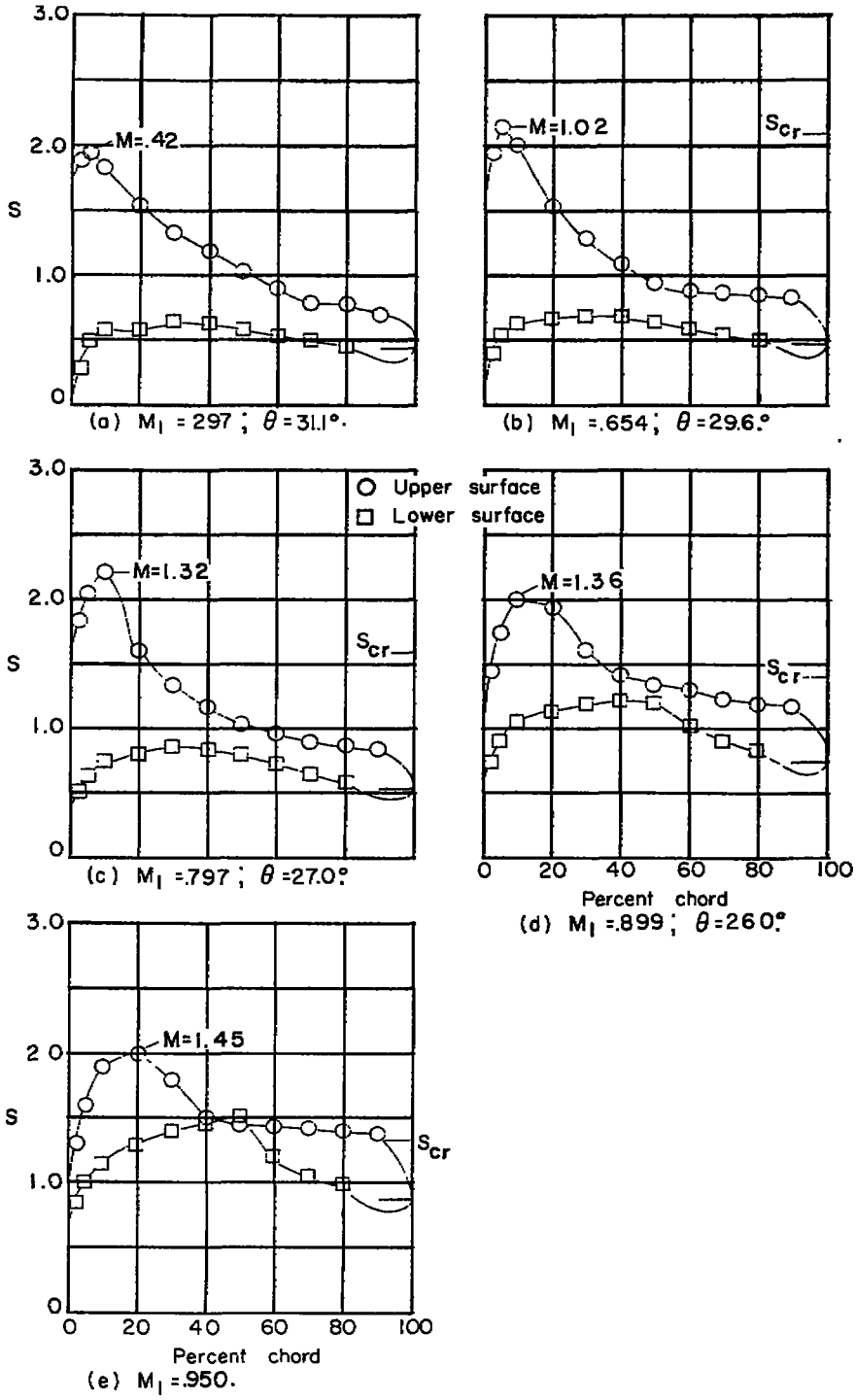

Figure 20.— Blade-surface pressure distributions and section characteristics for the cascade combination. β_1 = 60°; σ = 1.5 ; α = 24.8°; and blade section, NACA 65-($12A_{10}$)10.

[redacted]

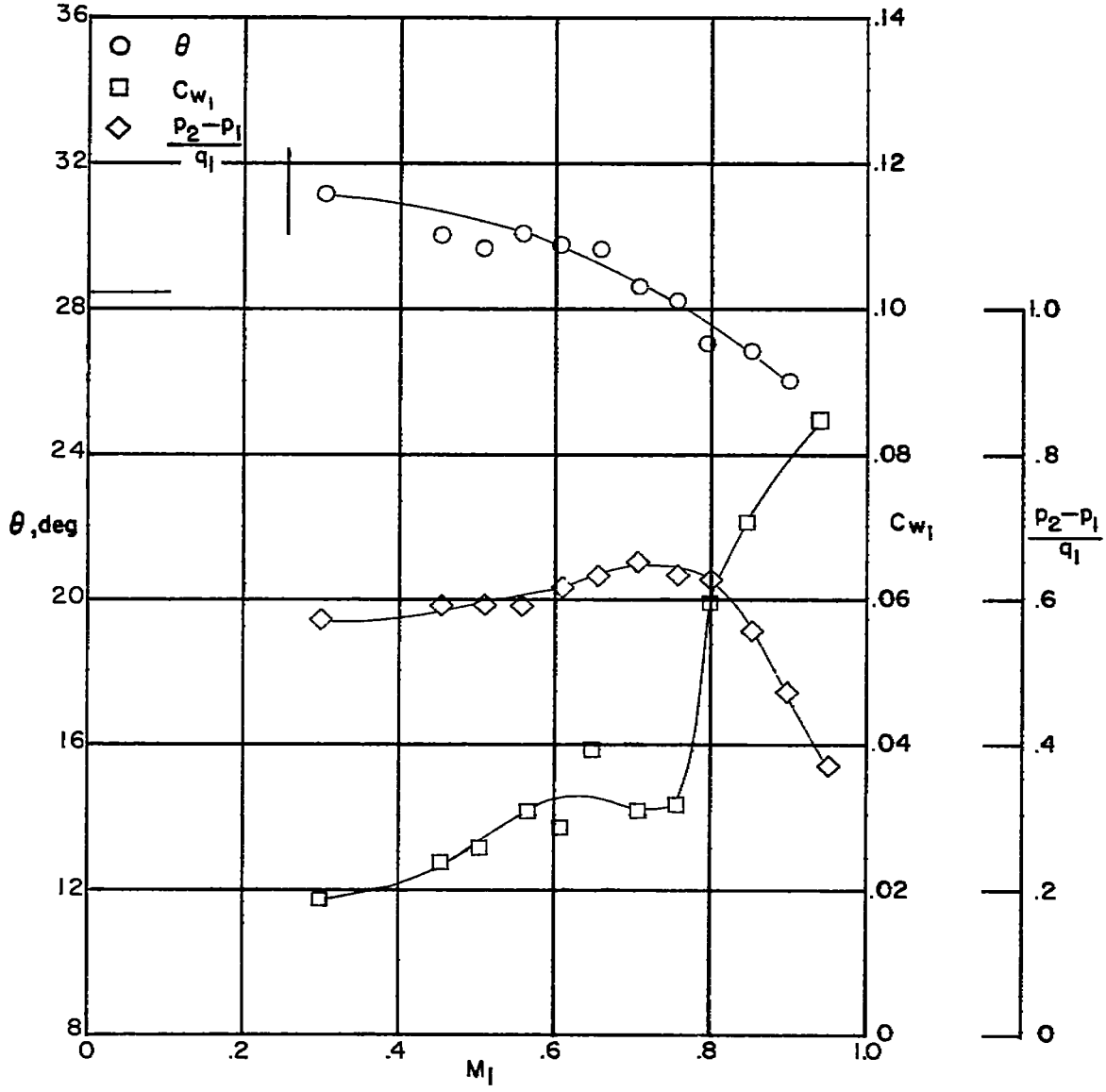

(f) Section characteristics. Tests are two dimensional for Mach numbers up to the vertical line. The horizontal line indicates low-speed turning angle given in reference 1

Figure 20.— Concluded.

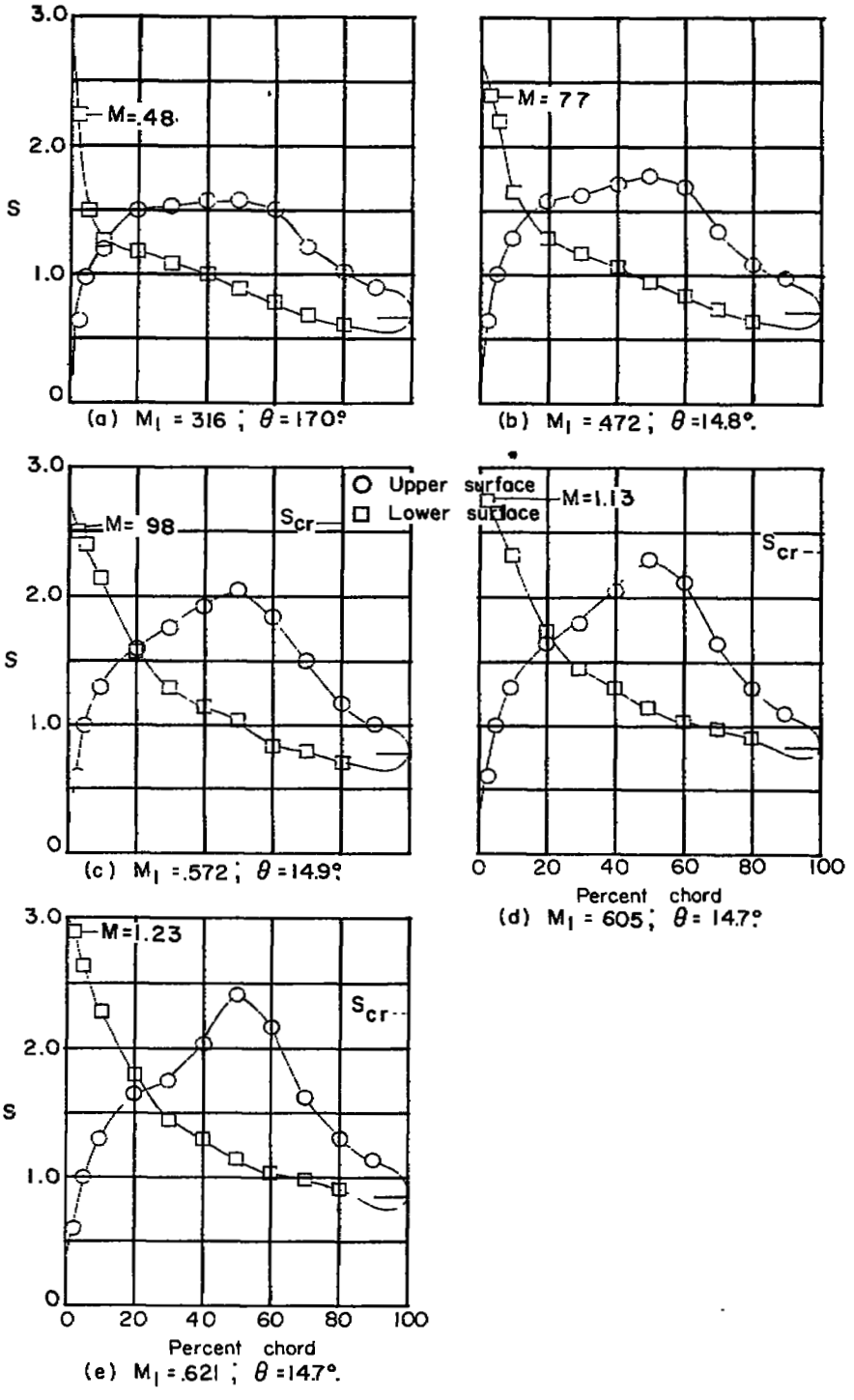

Figure 21 .— Blade-surface pressure distributions and section characteristics for the cascade combination. β_1 = 45 ; σ = 1.5 ; α = 8.6°; and blade section, NACA 65-($12A_{10}$)10.

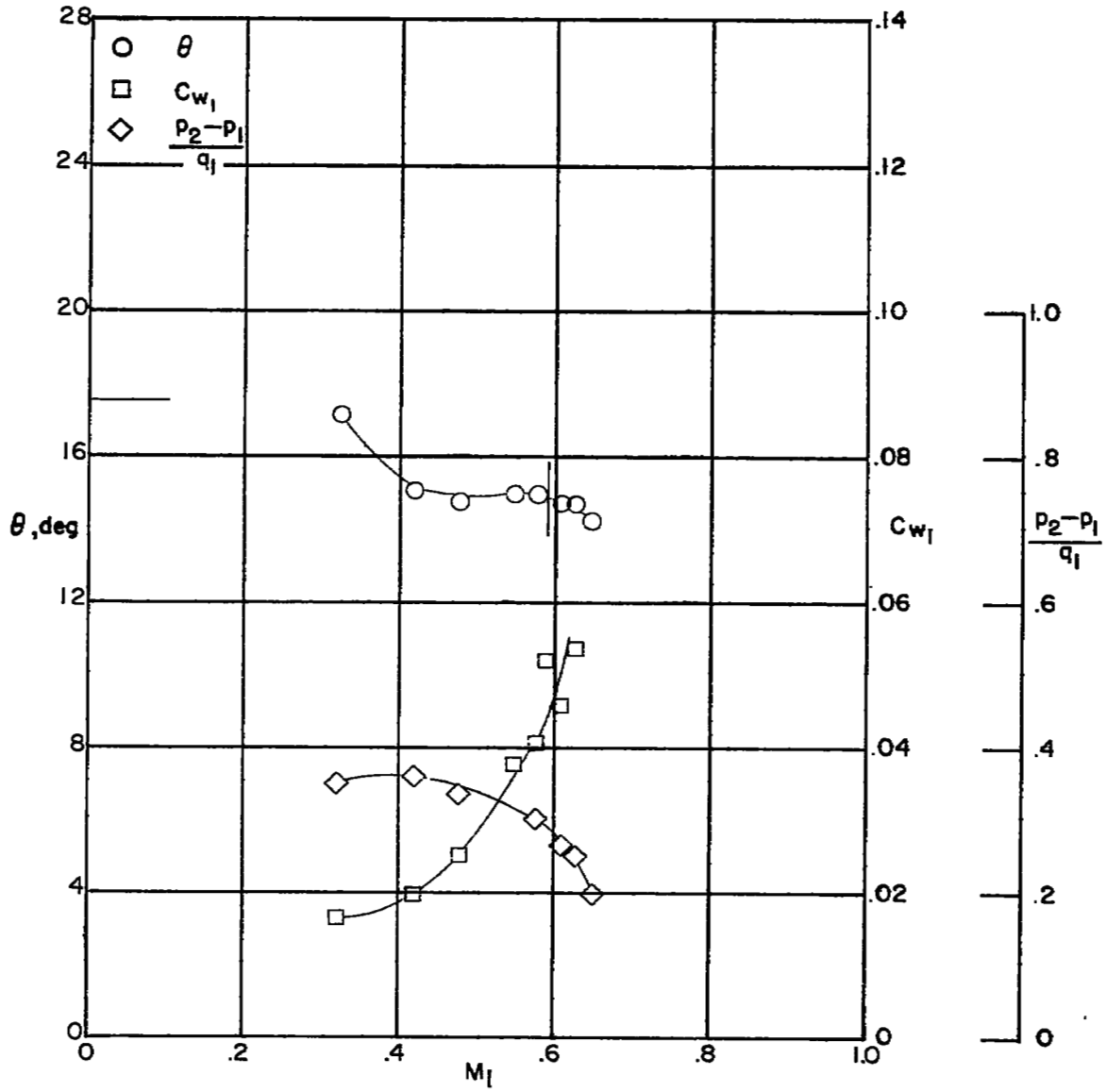

(f) Section characteristics. Tests are two dimensional for Mach numbers up to the vertical line. The horizontal line indicates low-speed turning angle given in reference 1.

Figure 21 .— Concluded.

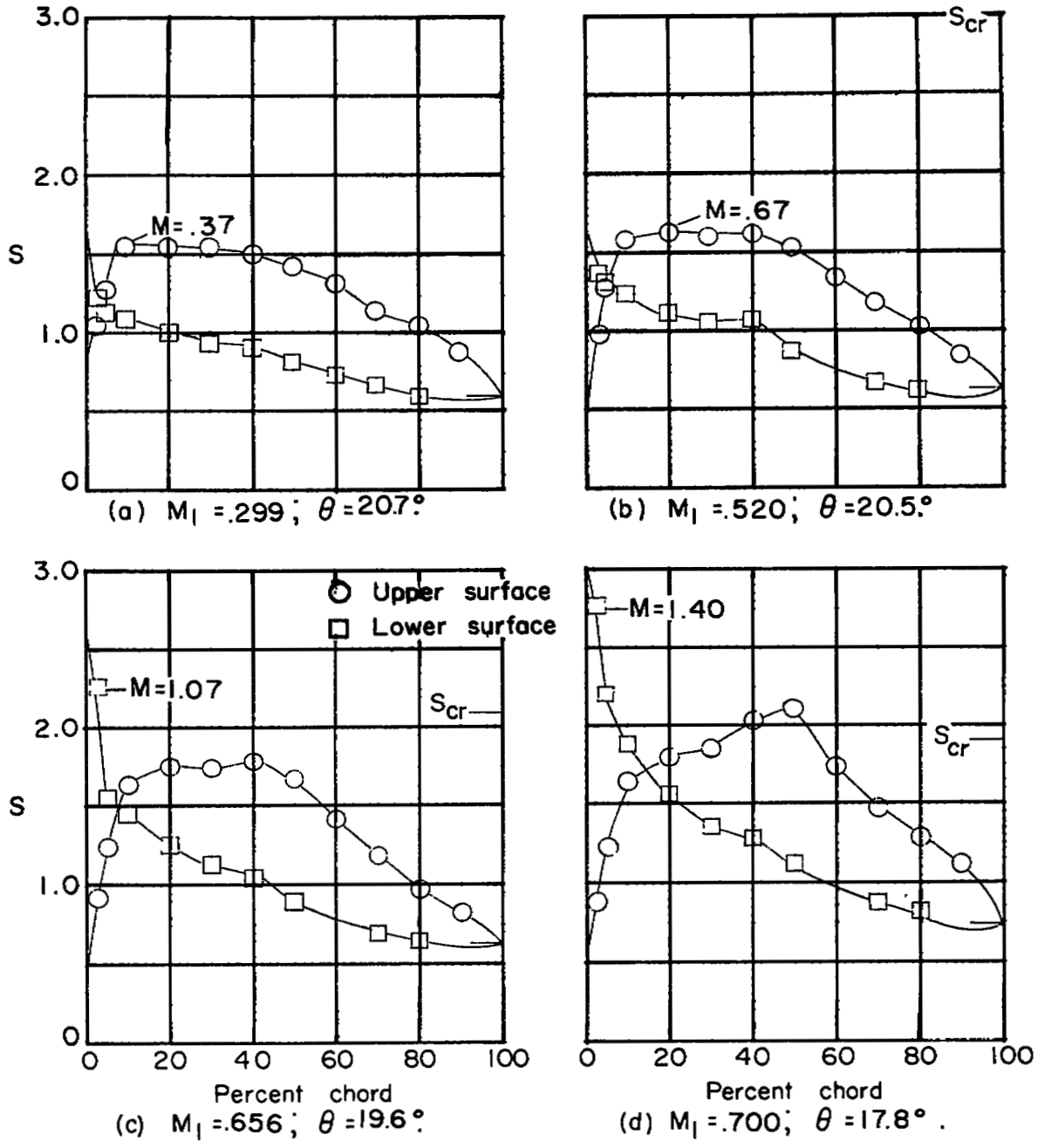

Figure 22.— Blade-surface pressure distributions and section characteristics for the cascade combination · β_1 = 45°; σ = 1.5 ; α =12.2°; and blade section, NACA 65-($12A_{10}$)10.

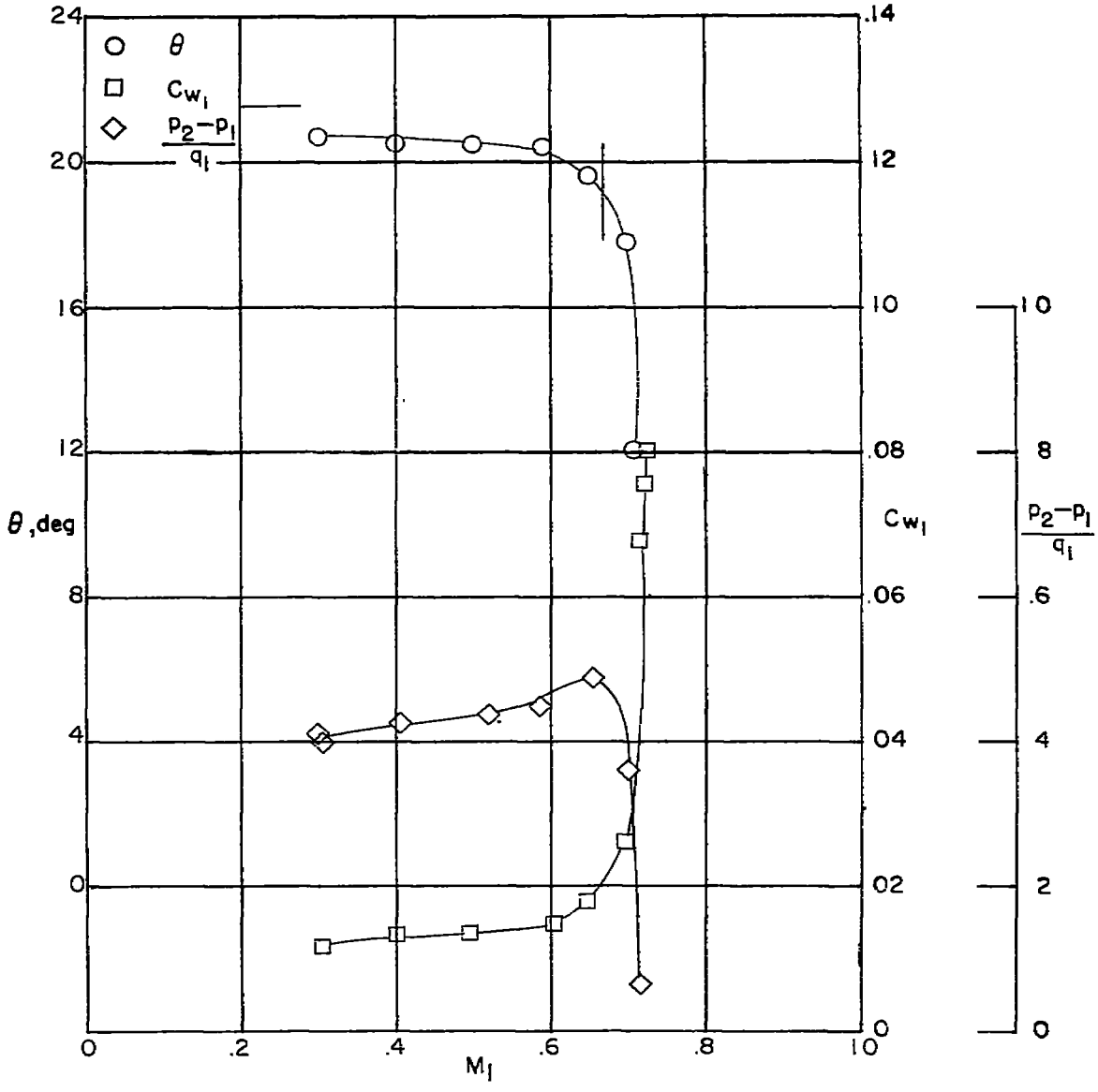

(e) Section characteristics. Tests are two dimensional for Mach numbers up to the vertical line. The horizontal line indicates low-speed turning angle given in reference 1

Figure 22.— Concluded.

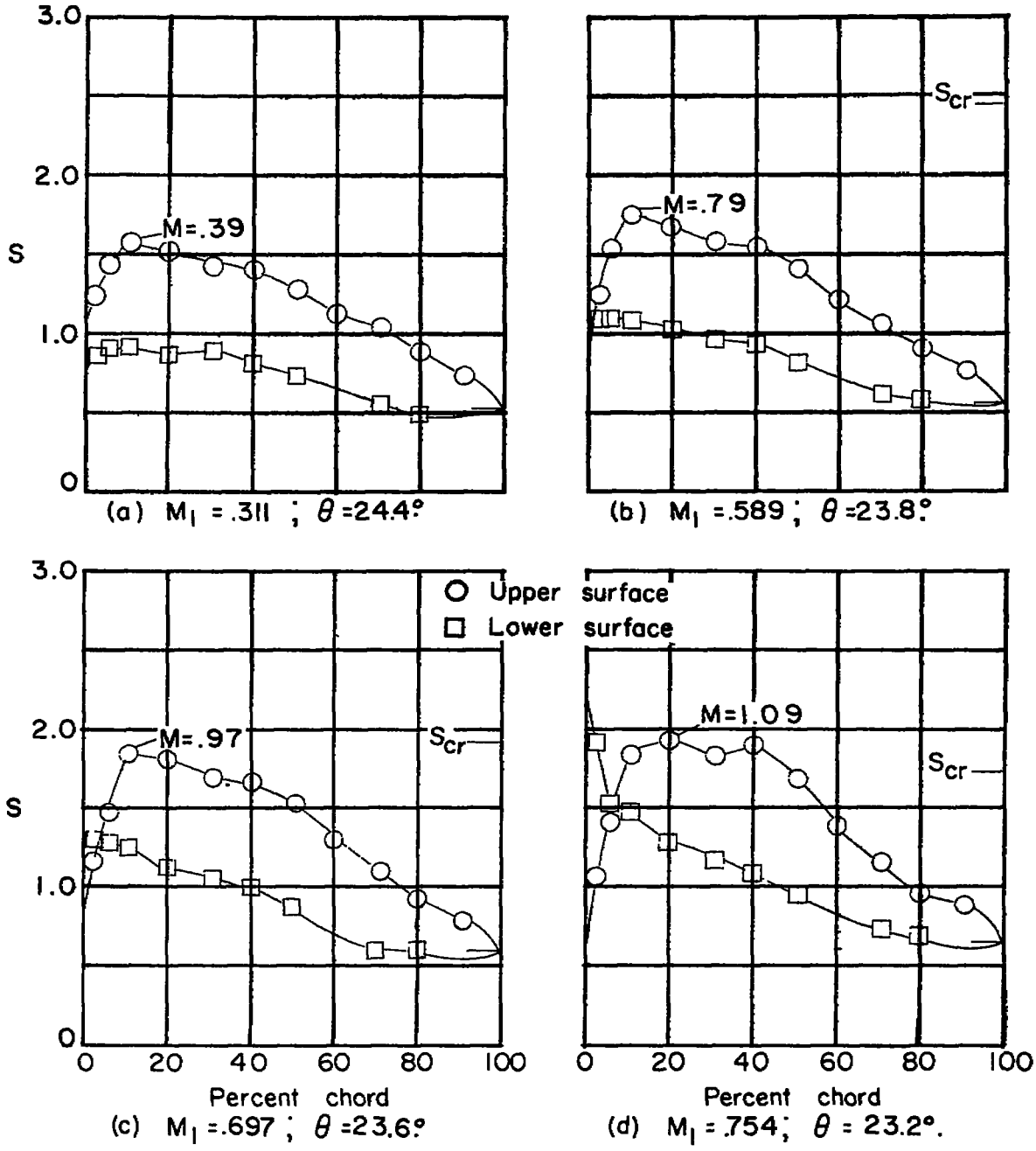

Figure 23.— Blade-surface pressure distributions and section characteristics for the cascade combination. β =45° ; σ = 1.5 ; α =15.2°; and blade section, NACA 65-($12A_{10}$)10.

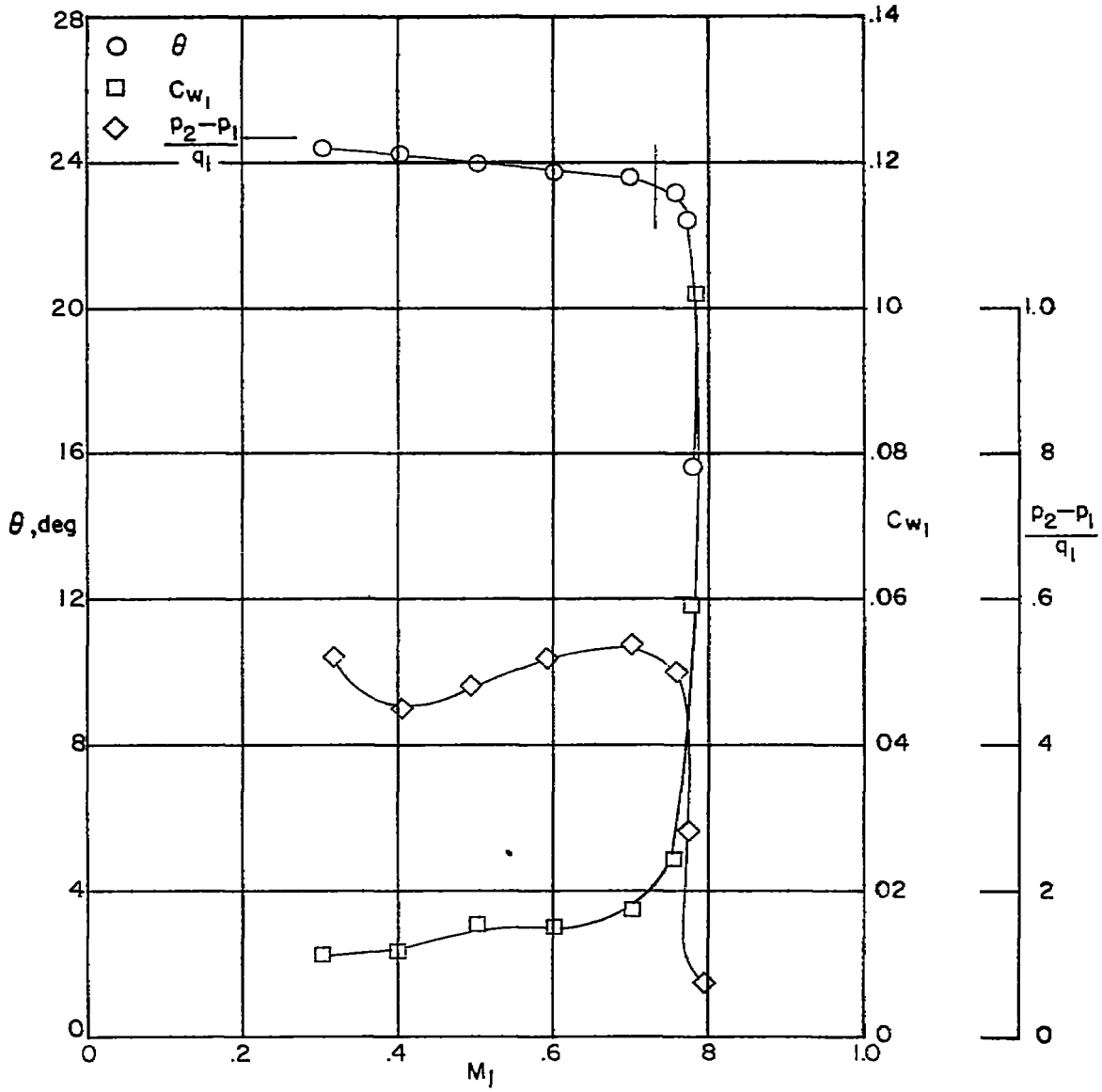

(e) Section characteristics. Tests are two dimensional for Mach numbers up to the vertical line. The horizontal line indicates low-speed turning angle given in reference 1.

Figure 23.— Concluded.

[redacted]

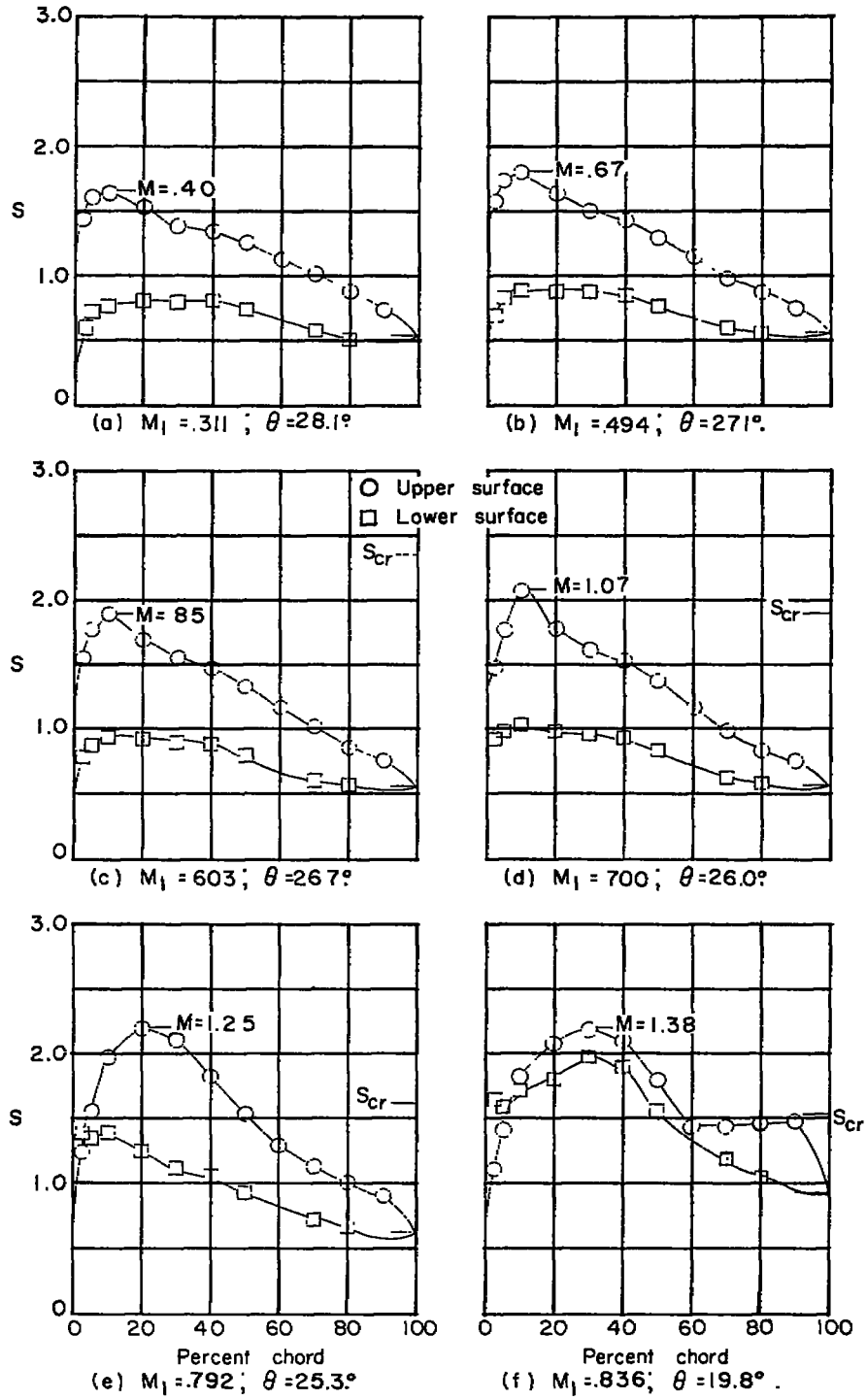

Figure 24.— Blade-surface pressure distributions and section characteristics for the cascade combination. β_1 =45° ; σ =1.5 ; α =18.2°; and blade section, NACA 65-($12A_{10}$)10.

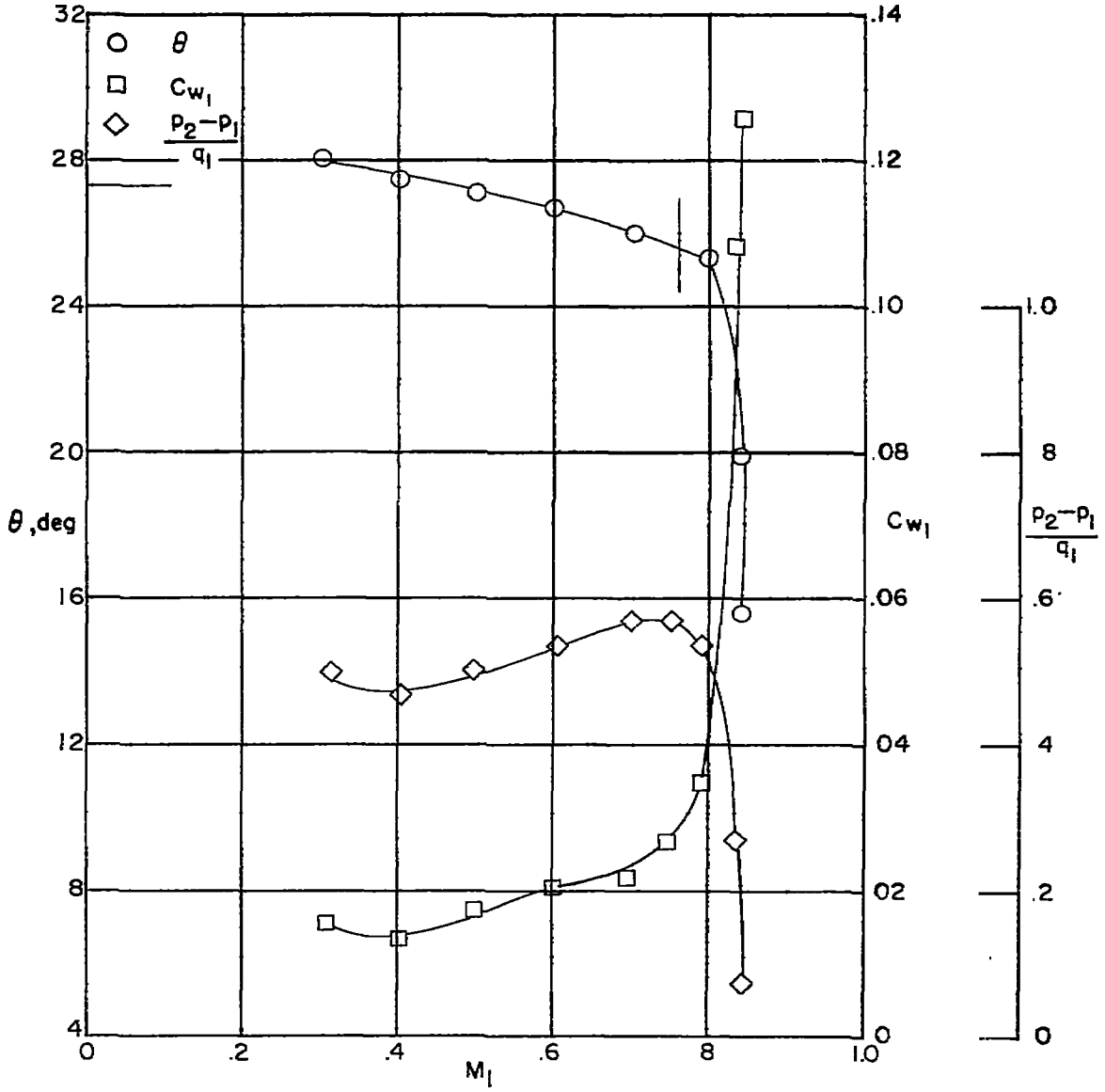

(g) Section characteristics. Tests are two dimensional for Mach numbers up to the vertical line. The horizontal line indicates low-speed turning angle given in reference 1.

Figure 24 .— Concluded.

[redacted]

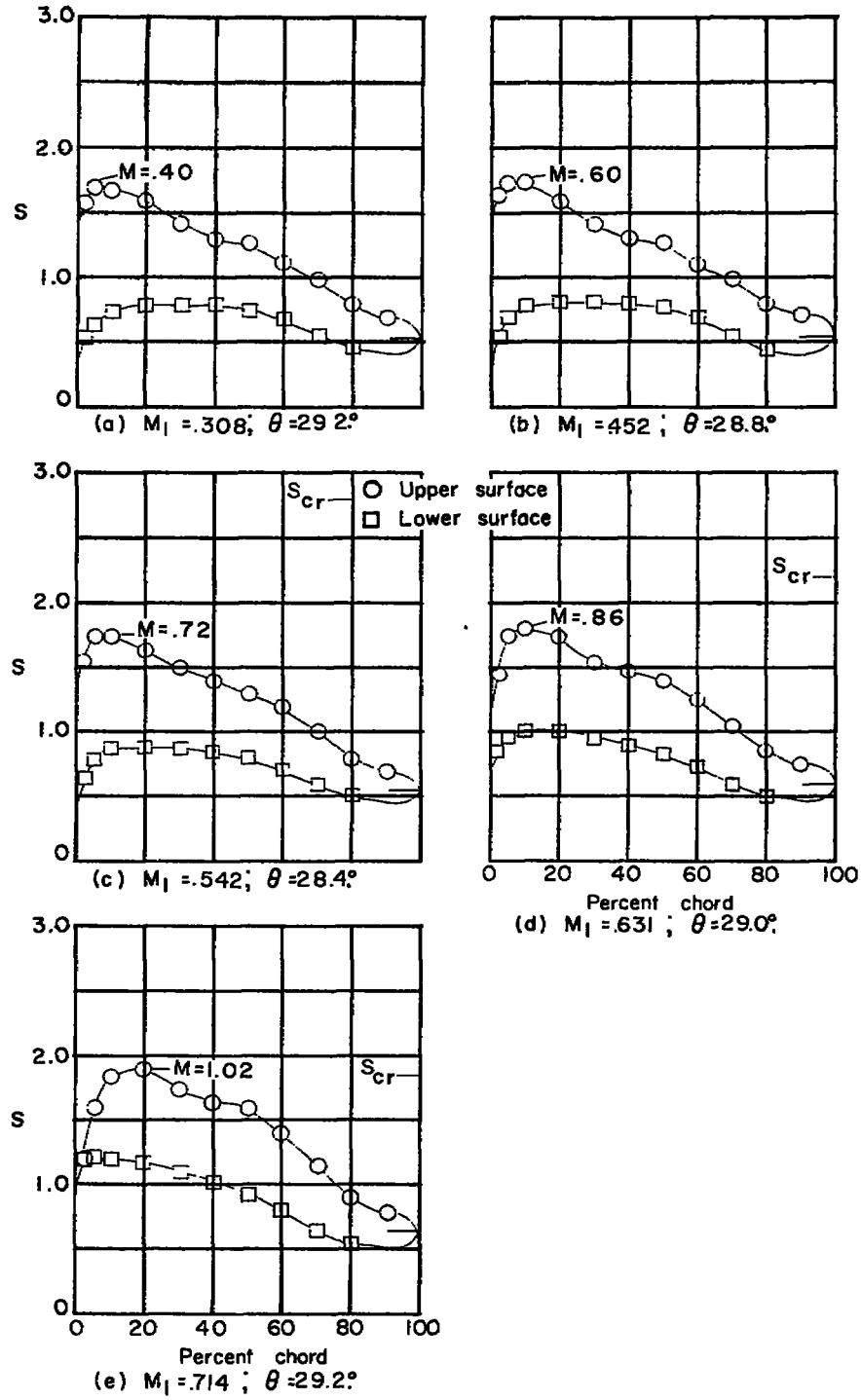

Figure 25.— Blade-surface pressure distributions and section characteristics for the cascade combination. β_1 = 45°; σ =1.5 ; α =20.6°; and blade section, NACA 65-($12A_{10}$)10.

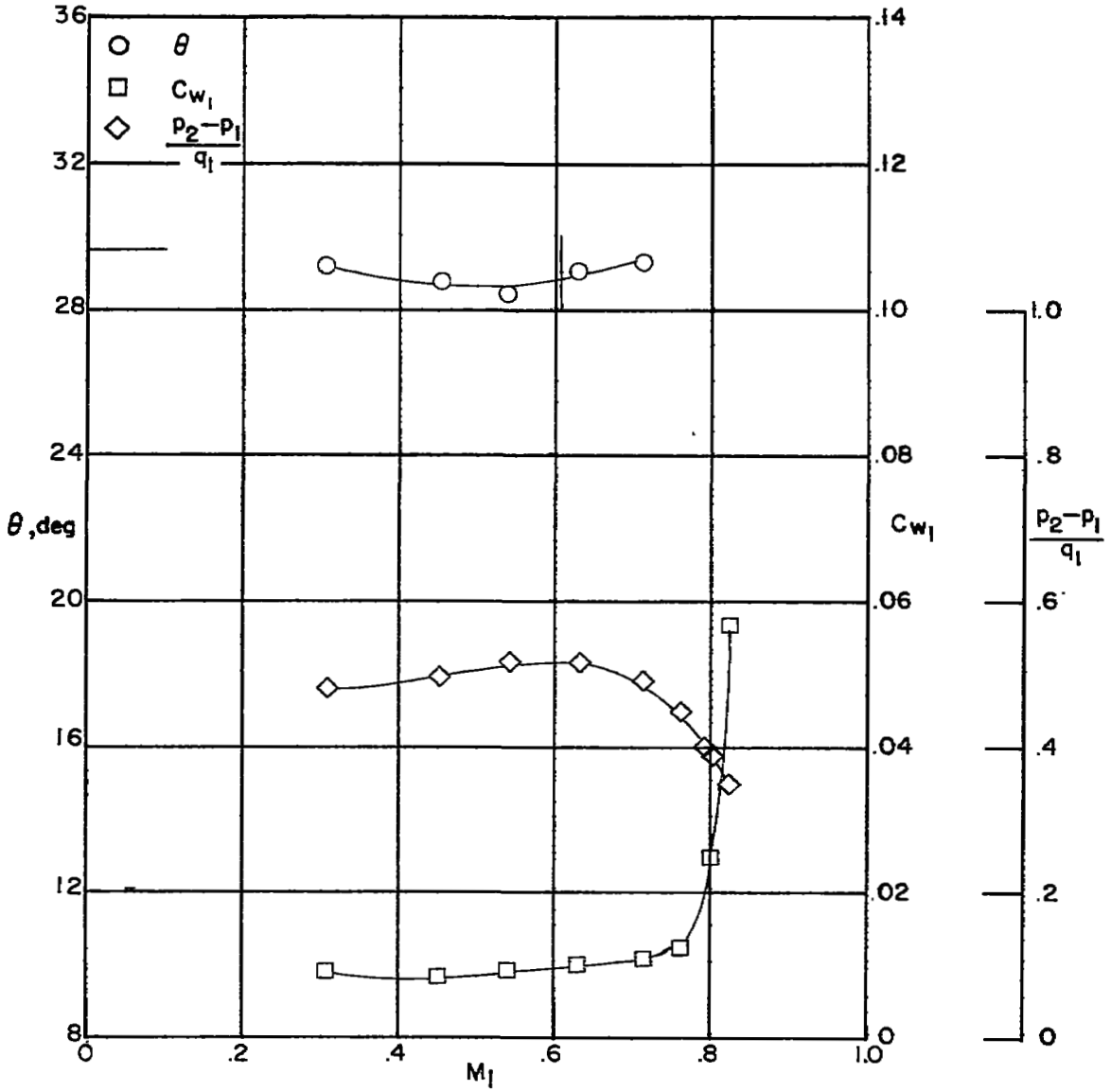

(f) Section characteristics. Tests are two dimensional for Mach numbers up to the vertical line. The horizontal line indicates low-speed turning angle given in reference 1.

Figure 25 .— Concluded.

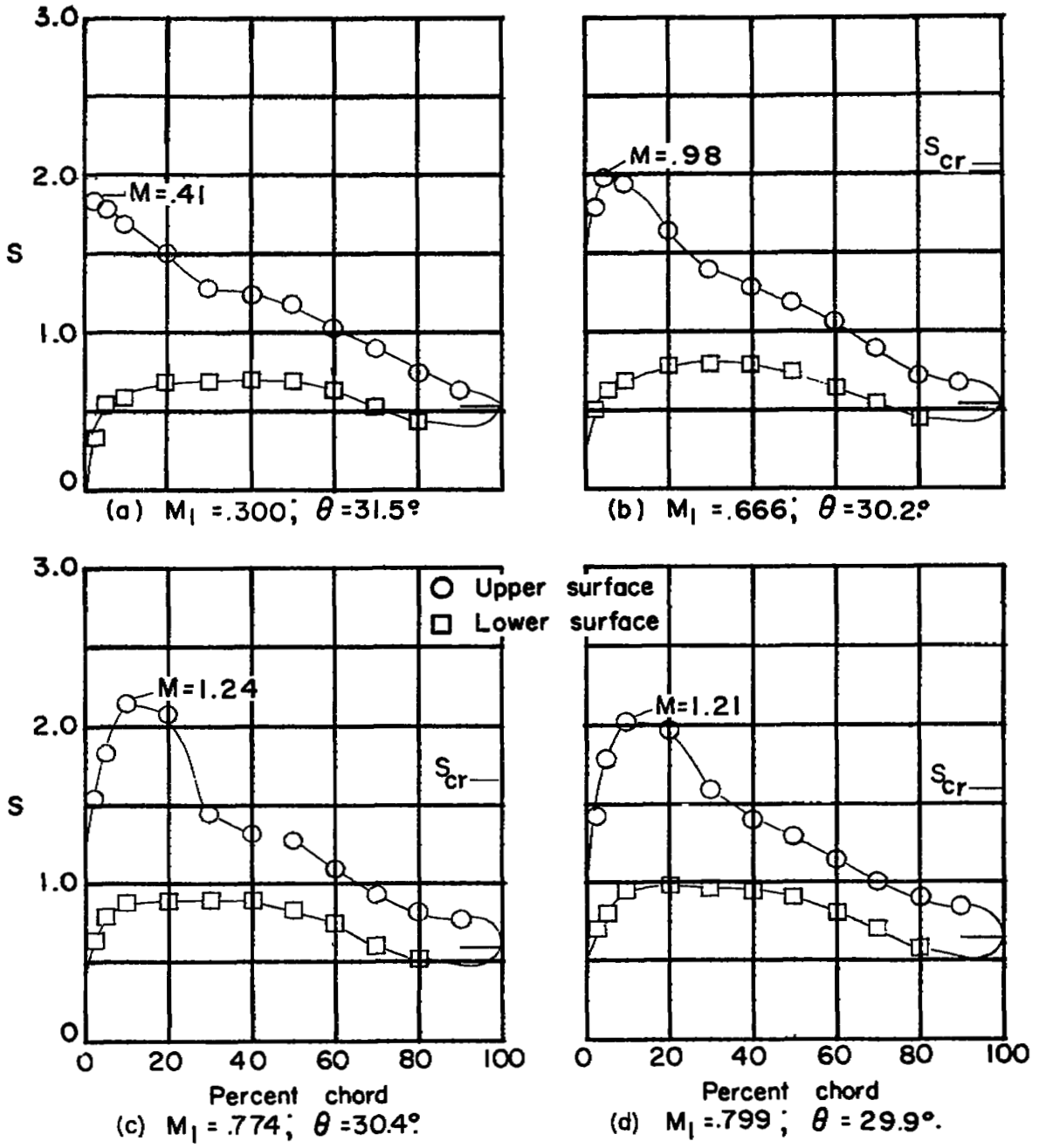

Figure 26.— Blade-surface pressure distributions and section characteristics for the cascade combination. $\beta_1 = 45$; $\sigma = 1.5$; $\alpha = 23.6°$; and blade section, NACA 65-($12A_{10}$)10.

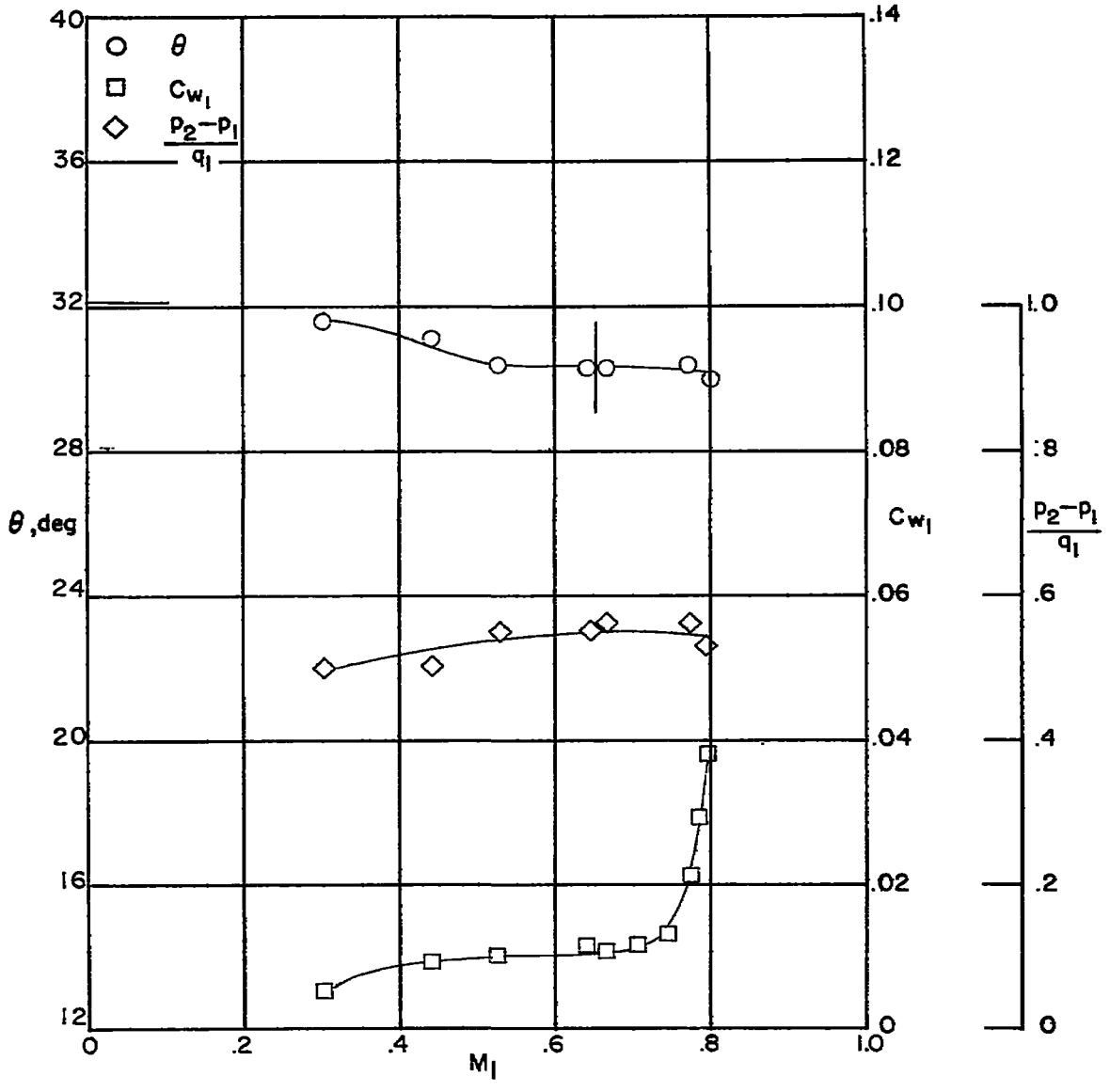

(e) Section characteristics. Tests are two dimensional for Mach numbers up to the vertical line. The horizontal line indicates low-speed turning angle given in reference 1.

Figure 26.— Concluded.

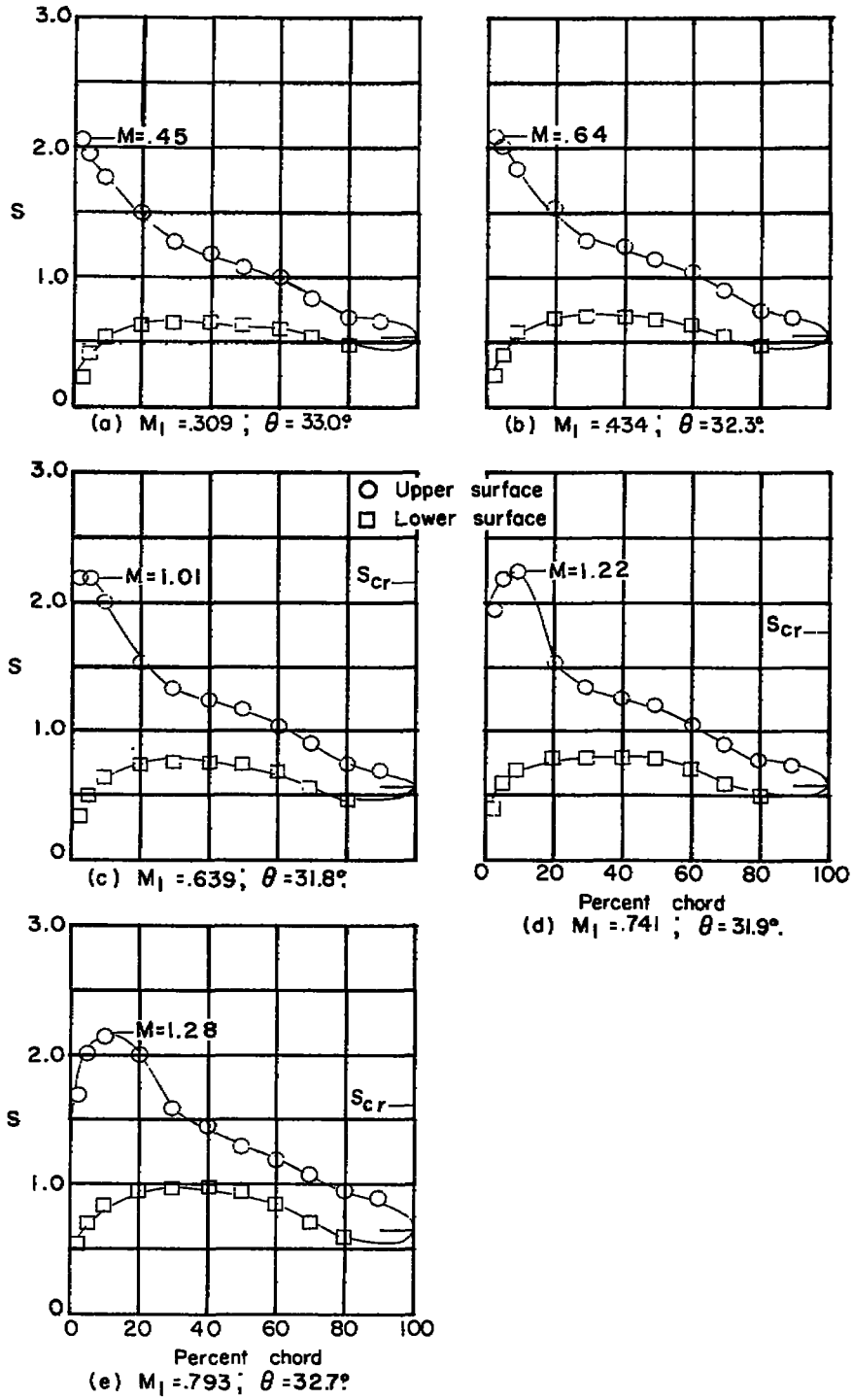

Figure 27.— Blade-surface pressure distributions and section characteristics for the cascade combination. β_1 = 45°; σ = 1.5 ; α = 25.6°; and blade section, NACA 65-($12A_{10}$)10.

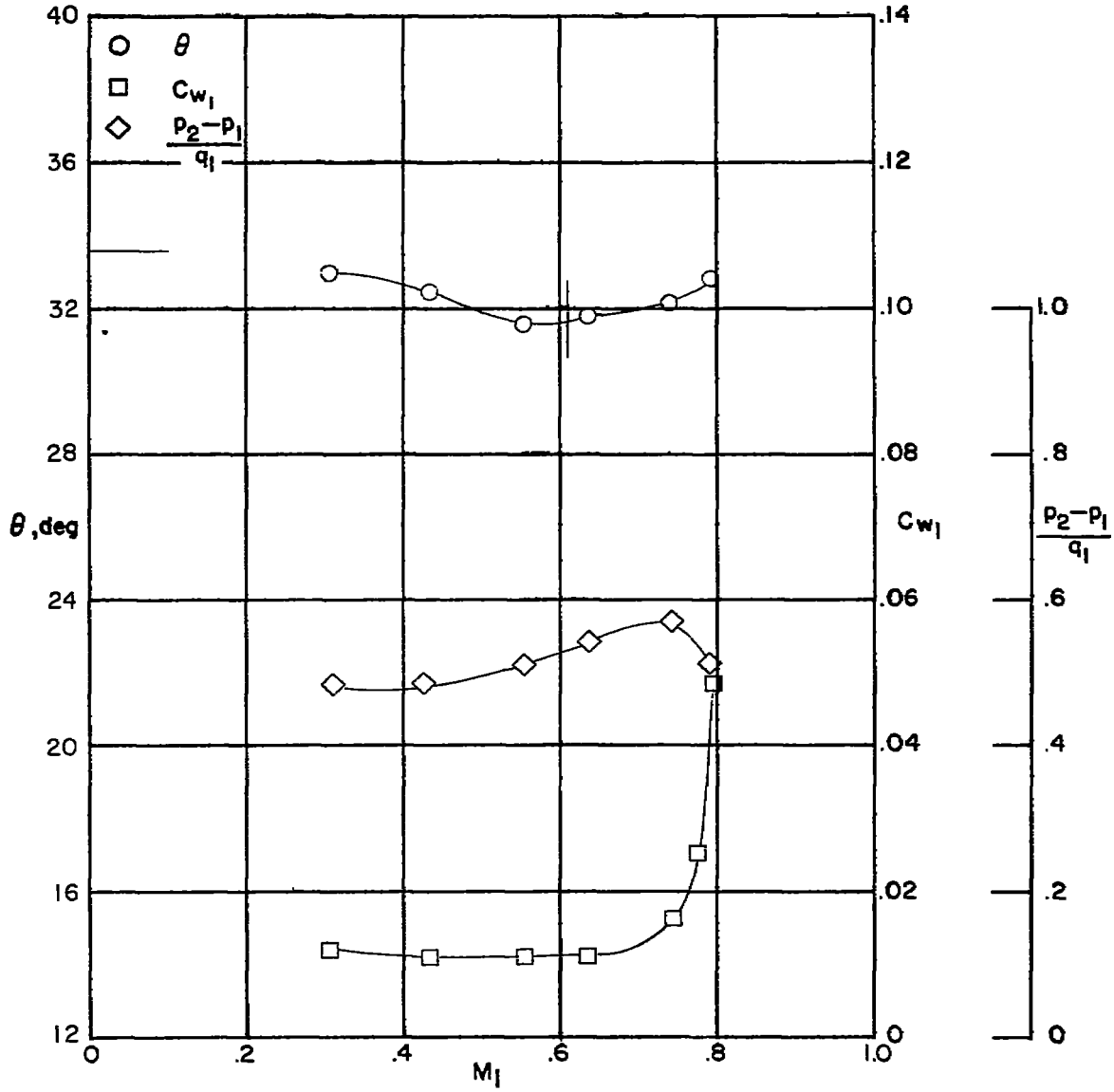

(f) Section characteristics. Tests are two dimensional for Mach numbers up to the vertical line. The horizontal line indicates low-speed turning angle given in reference 1.

Figure 27.— Concluded.

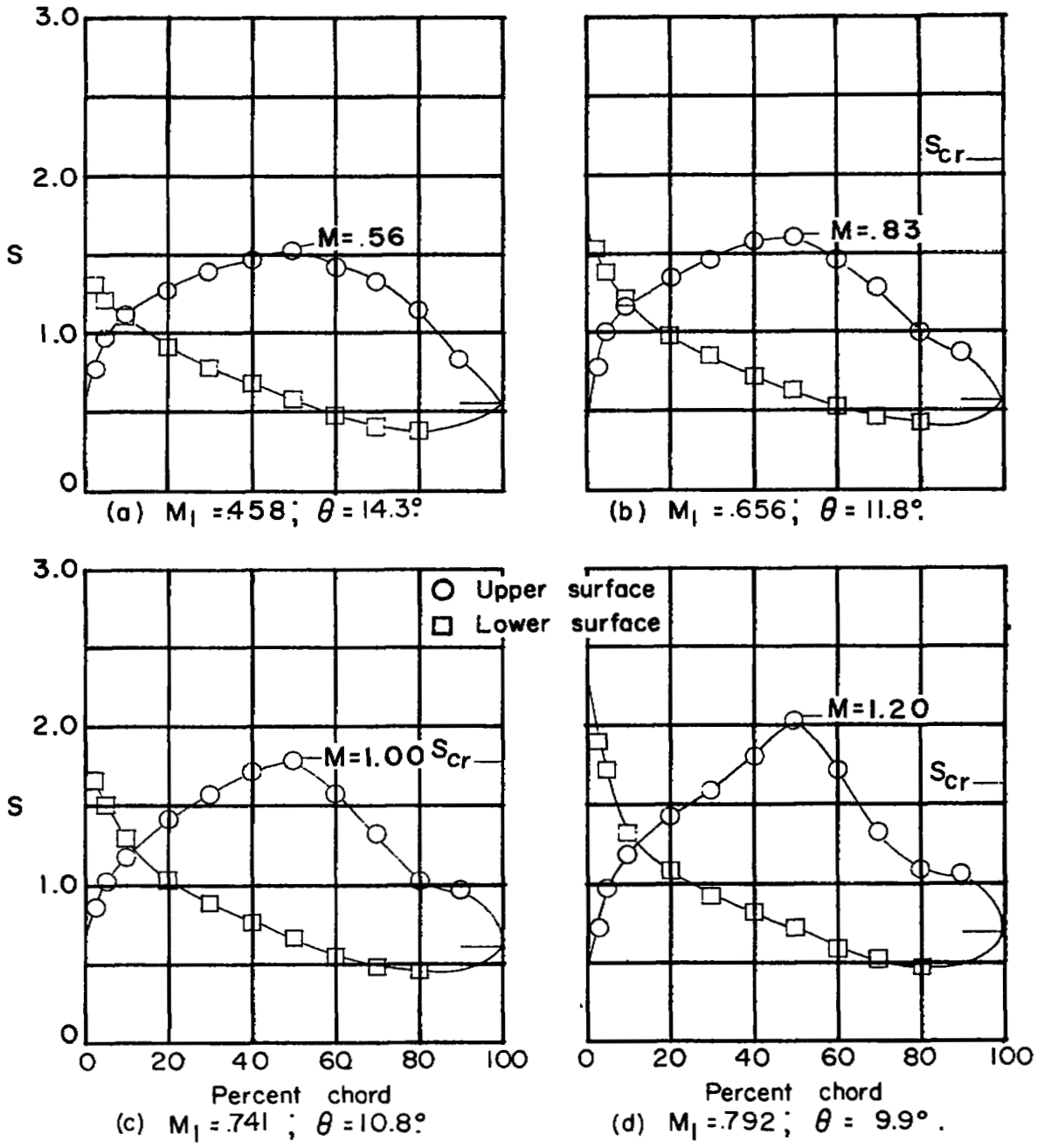

Figure 28.— Blade-surface pressure distributions and section characteristics for the cascade combination. β_1 = 60°; σ = 1.0 ; α = 8.0°; and blade section, NACA 65-($12A_2I_{8b}$)10.

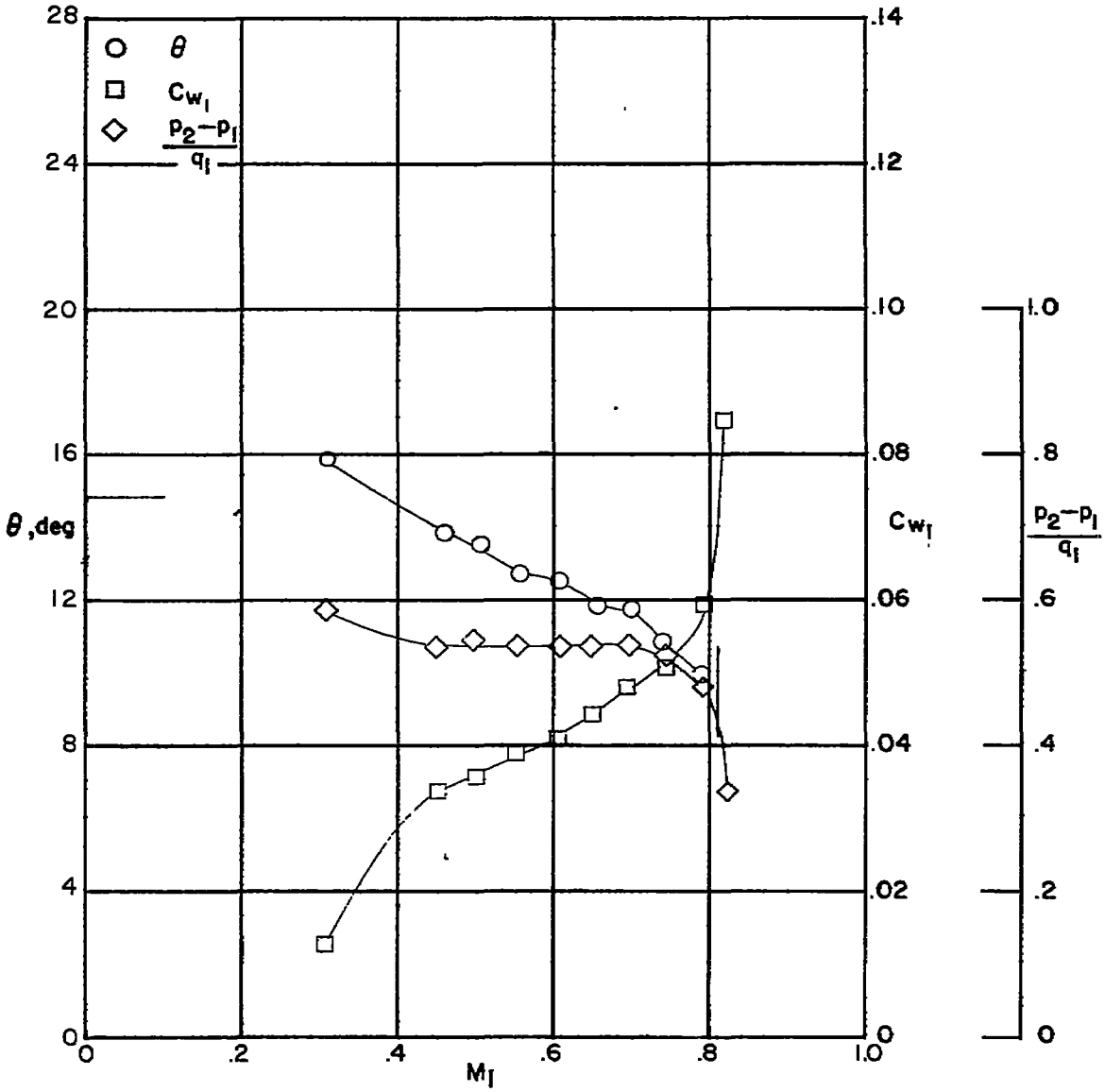

(e) Section characteristics. Tests are two dimensional for Mach numbers up to the vertical line. The horizontal line indicates low-speed turning angle given in reference 2.

Figure 28.— Concluded.

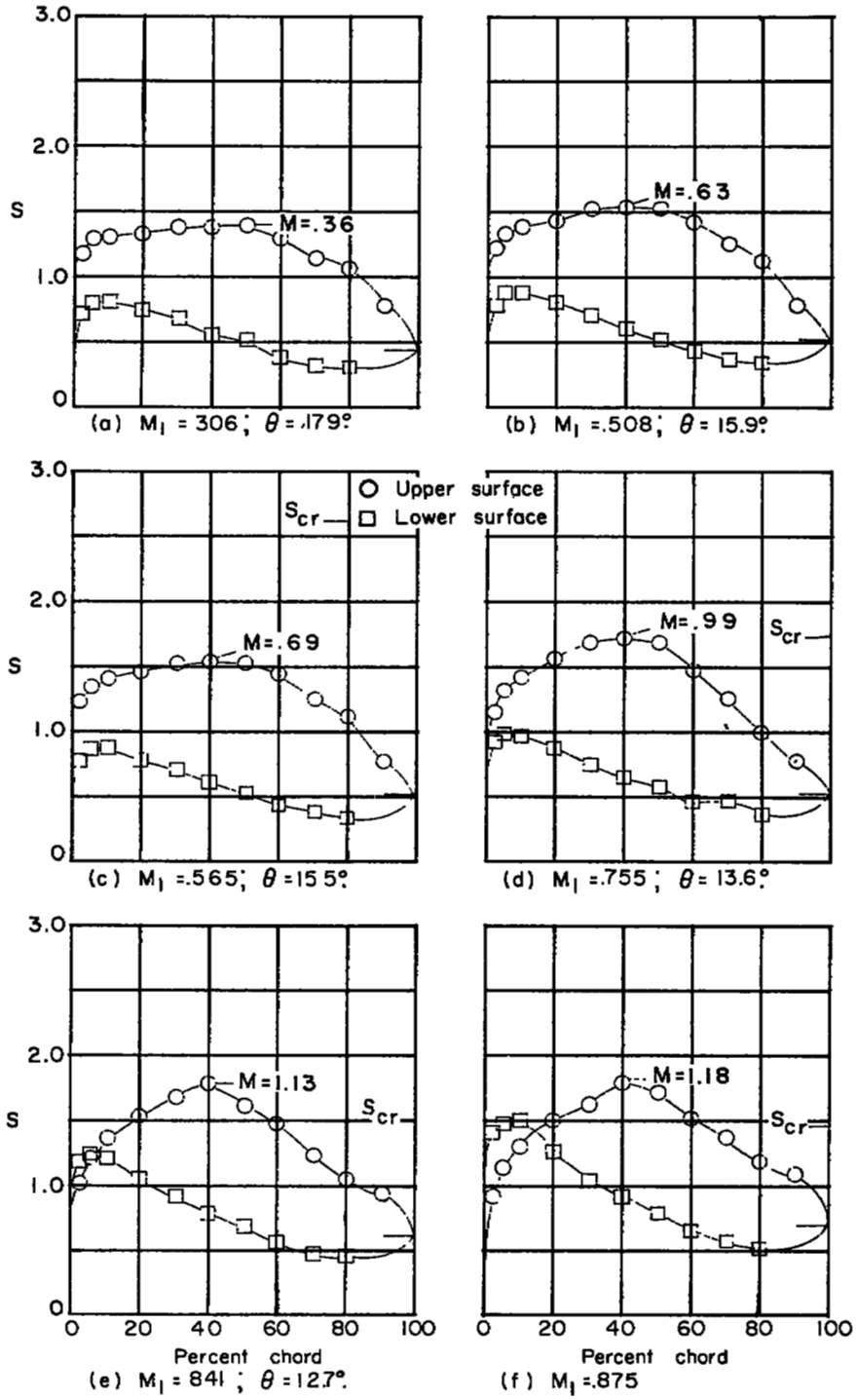

Figure 29.— Blade-surface pressure distributions and section characteristics for the cascade combination. $\beta_1 = 60°$; $\sigma = 1.0$; $\alpha = 11.0°$; and blade section, NACA 65-(12 A_2 I_{8b})10.

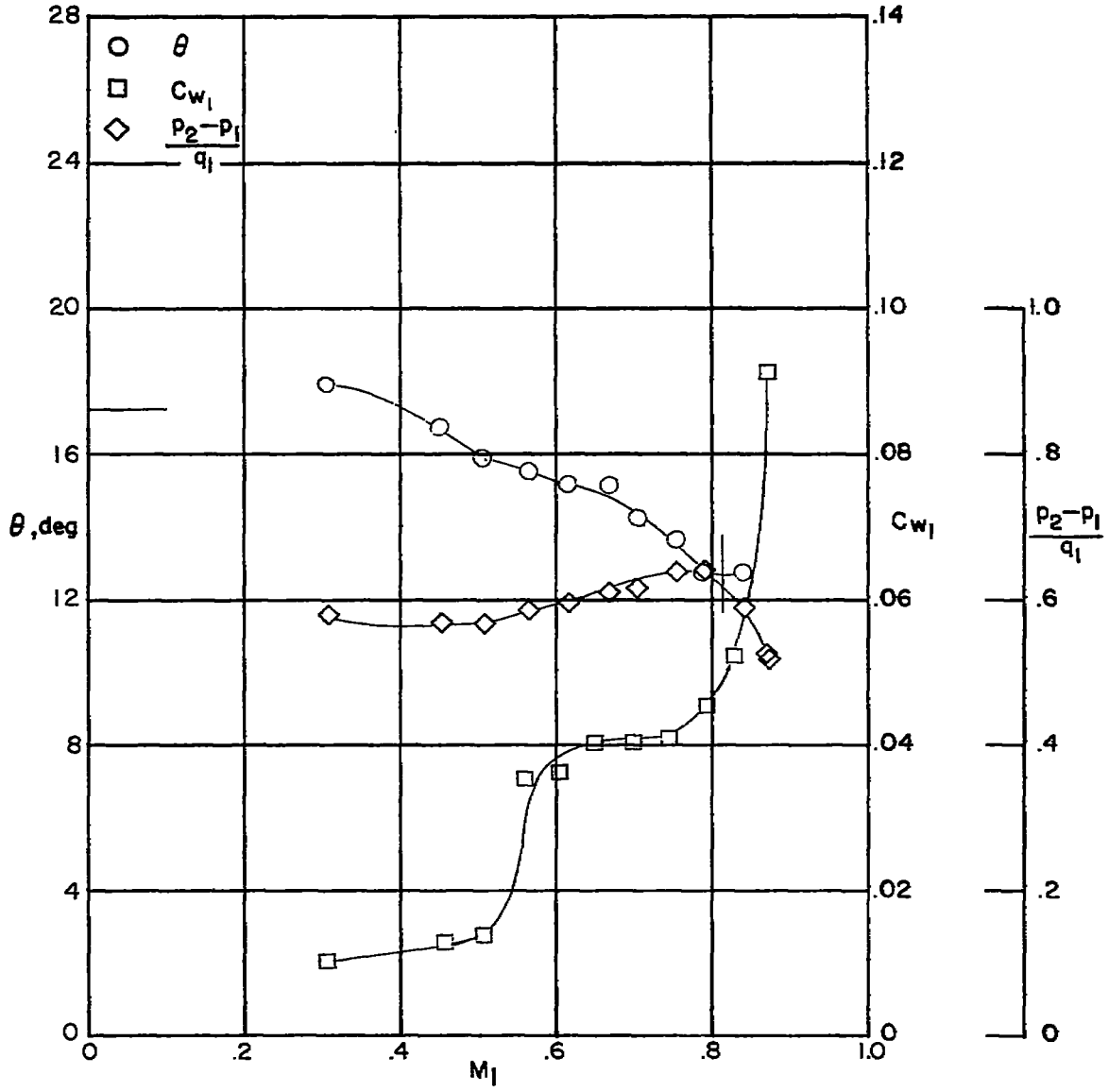

(g) Section characteristics. Tests are two dimensional for Mach numbers up to the vertical line. The horizontal line indicates low-speed turning angle given in reference 2.

Figure 29.— Concluded.

[redacted]

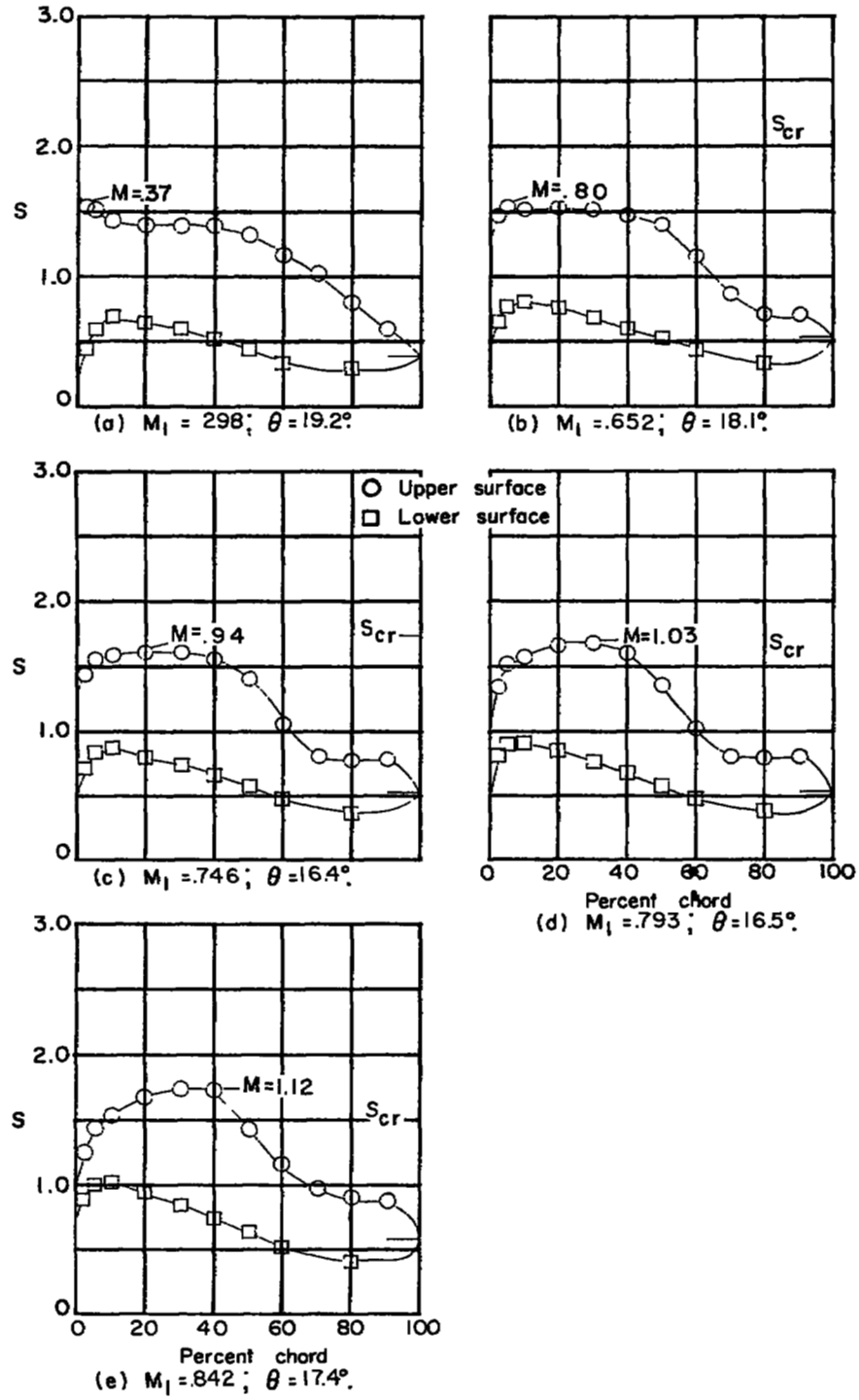

Figure 30.— Blade-surface pressure distributions and section characteristics for the cascade combination. β_1 = 60°; σ = 1.0 ; α =14.0°; and blade section, NACA 65-($12A_2I_{8b}$)10.

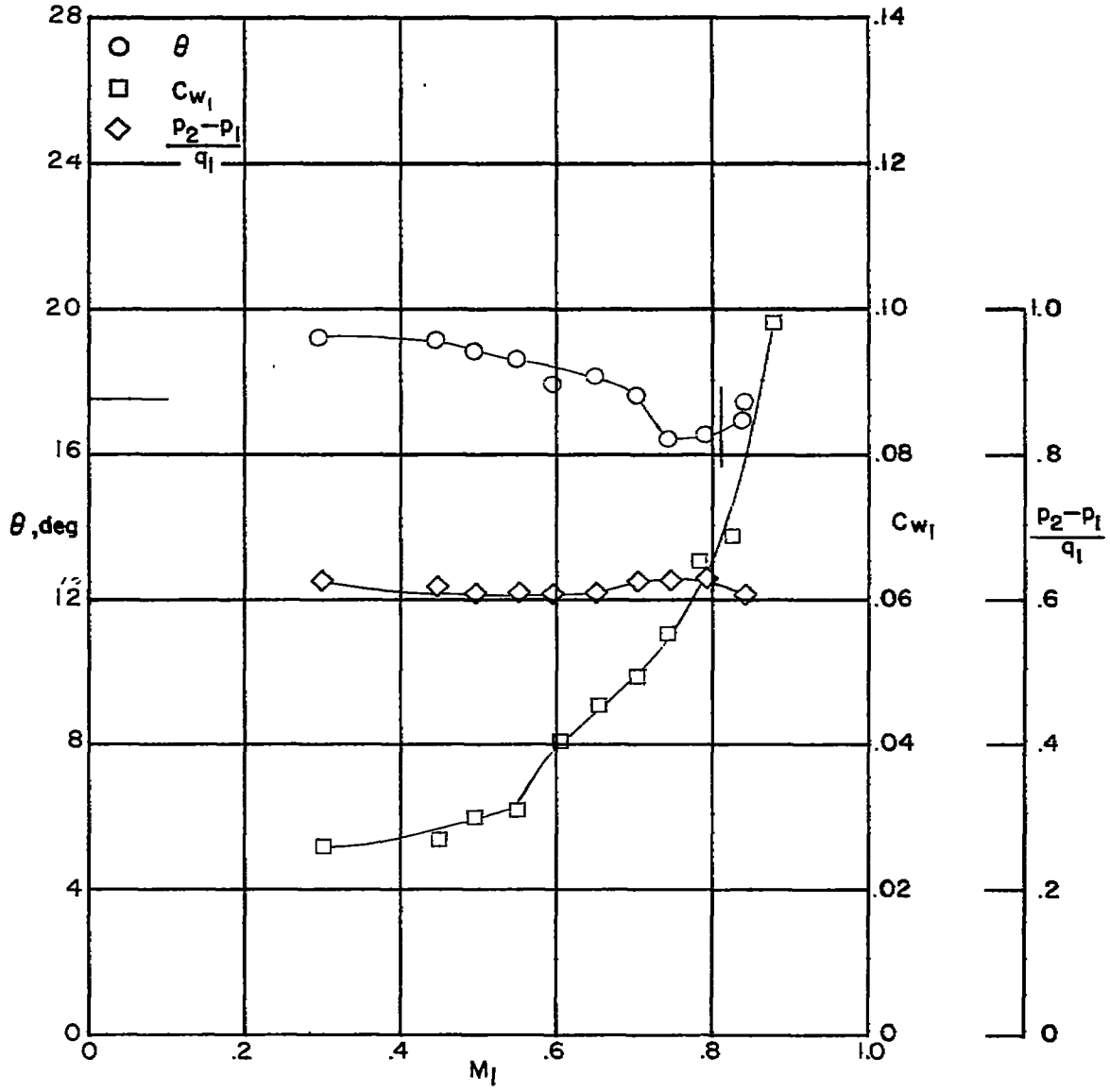

(f) Section characteristics. Tests are two dimensional for Mach numbers up to the vertical line. The horizontal line indicates low-speed turning angle given in reference 2.

Figure 30'.— Concluded.

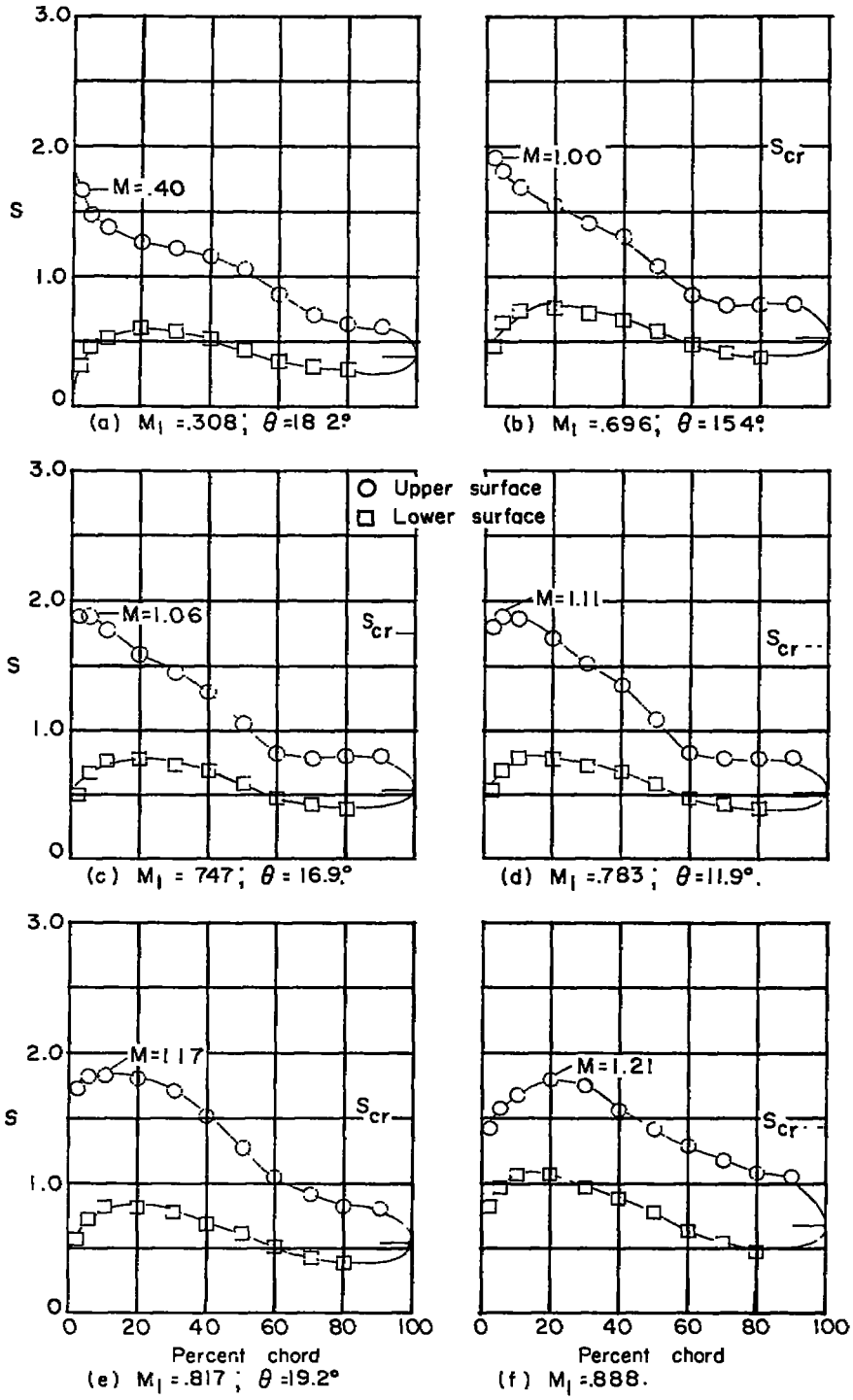

Figure 31 .— Blade-surface pressure distributions and section characteristics for the cascade combination. $\beta_1 = 60°$; $\sigma = 1.0$; $\alpha = 17.0°$; and blade section, NACA 65-($12A_2I_{8b}$)10.

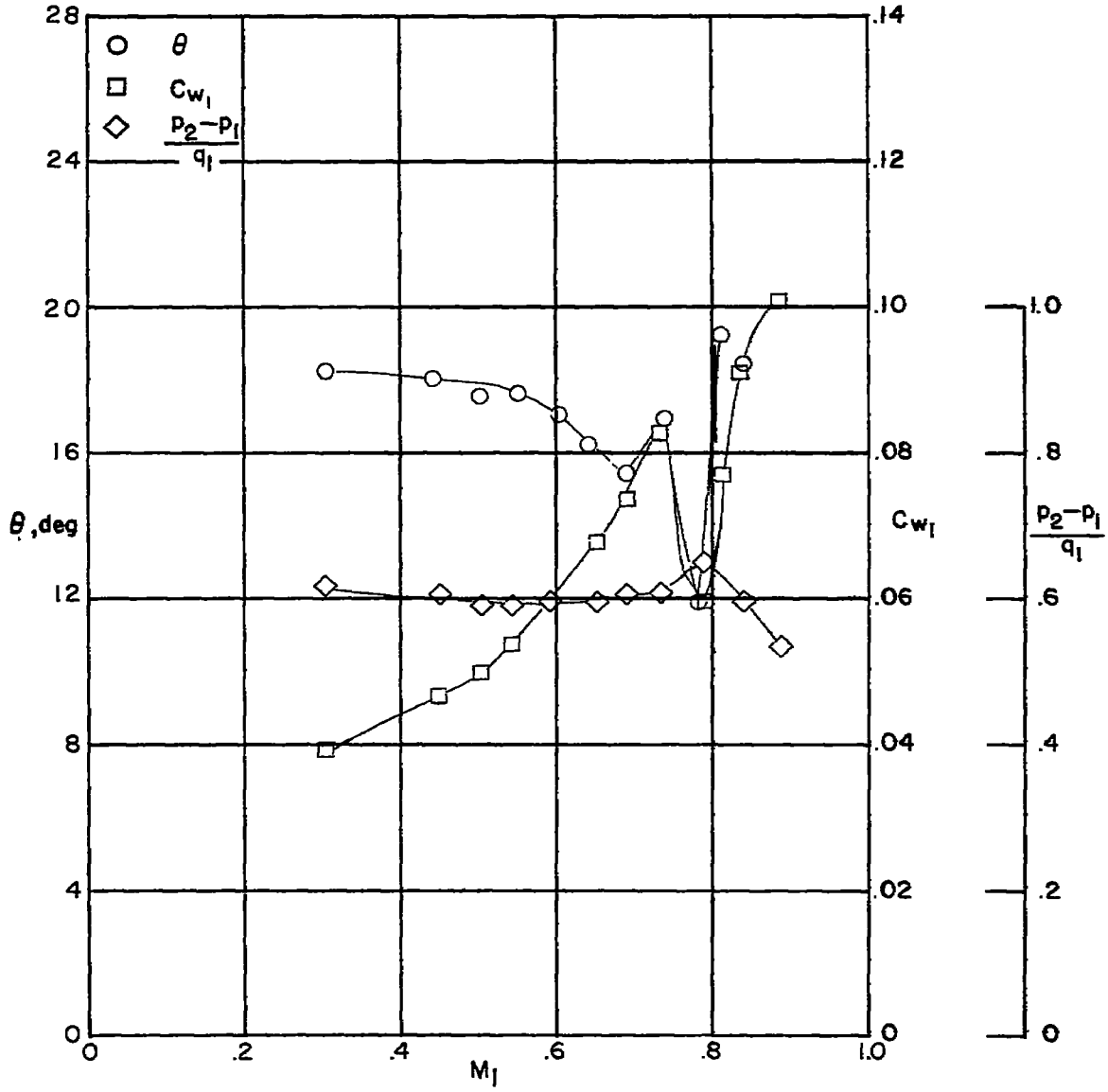

(g) Section characteristics. Tests are two dimensional for Mach numbers up to the vertical line.

Figure 31 .— Concluded.

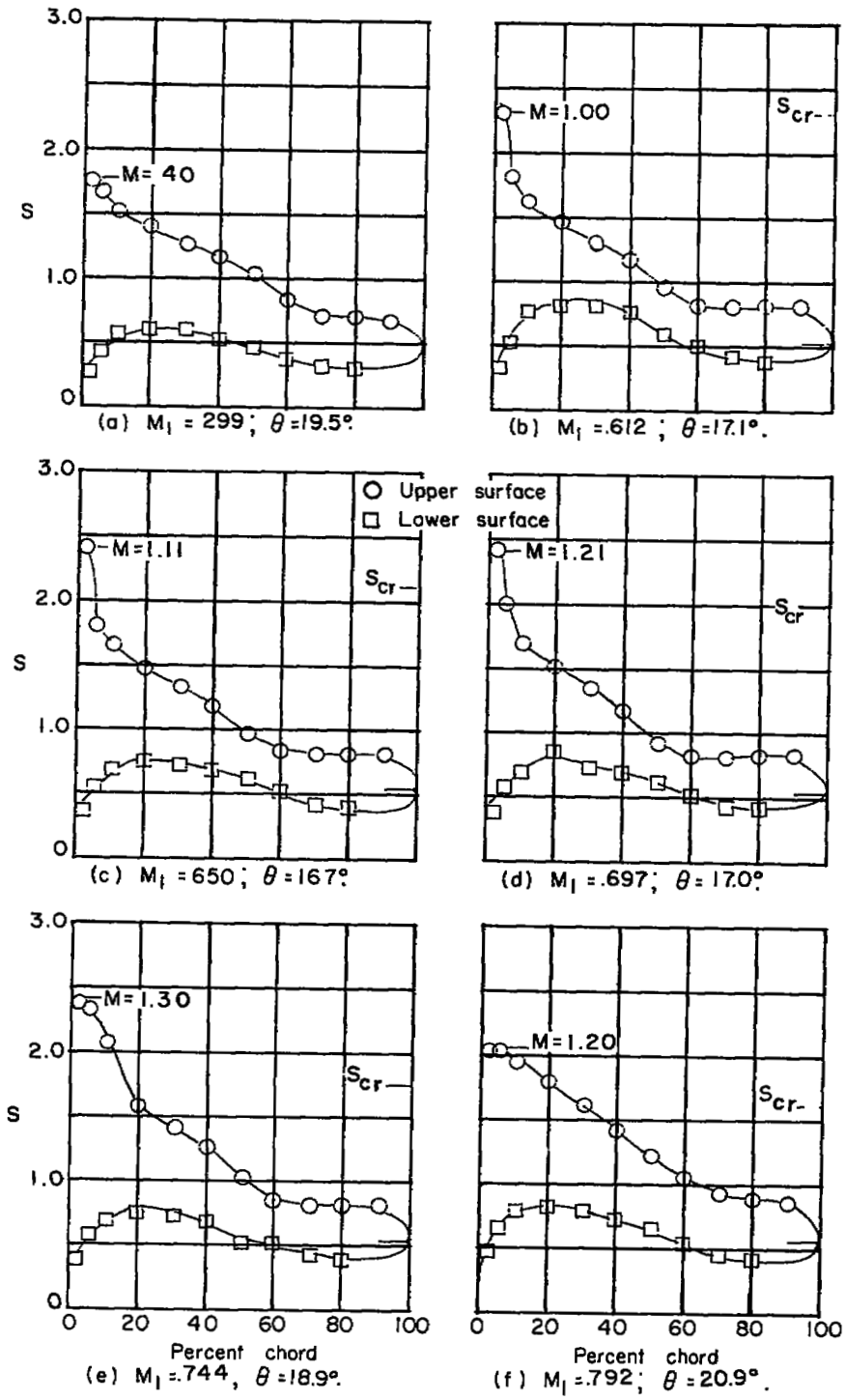

Figure 32 .— Blade-surface pressure distributions and section characteristics for the cascade combination. β_1 = 60°; σ = 1.0 ; α = 19.0°; and blade section, NACA 65-(12 A_2 $I_{8\,b}$)10.

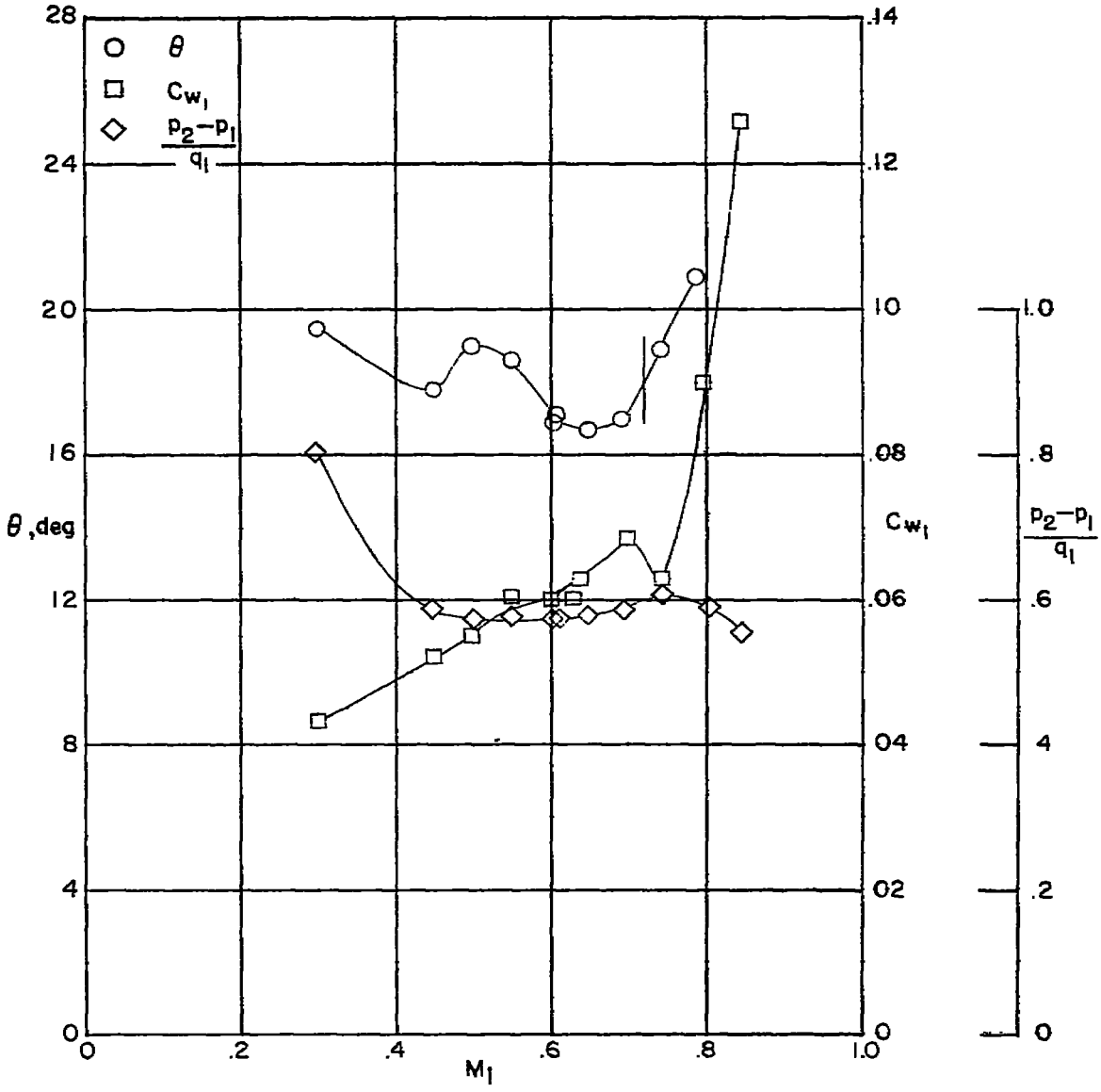

(g) Section characteristics. Tests are two dimensional for Mach numbers up to the vertical line

Figure 32 .— Concluded.

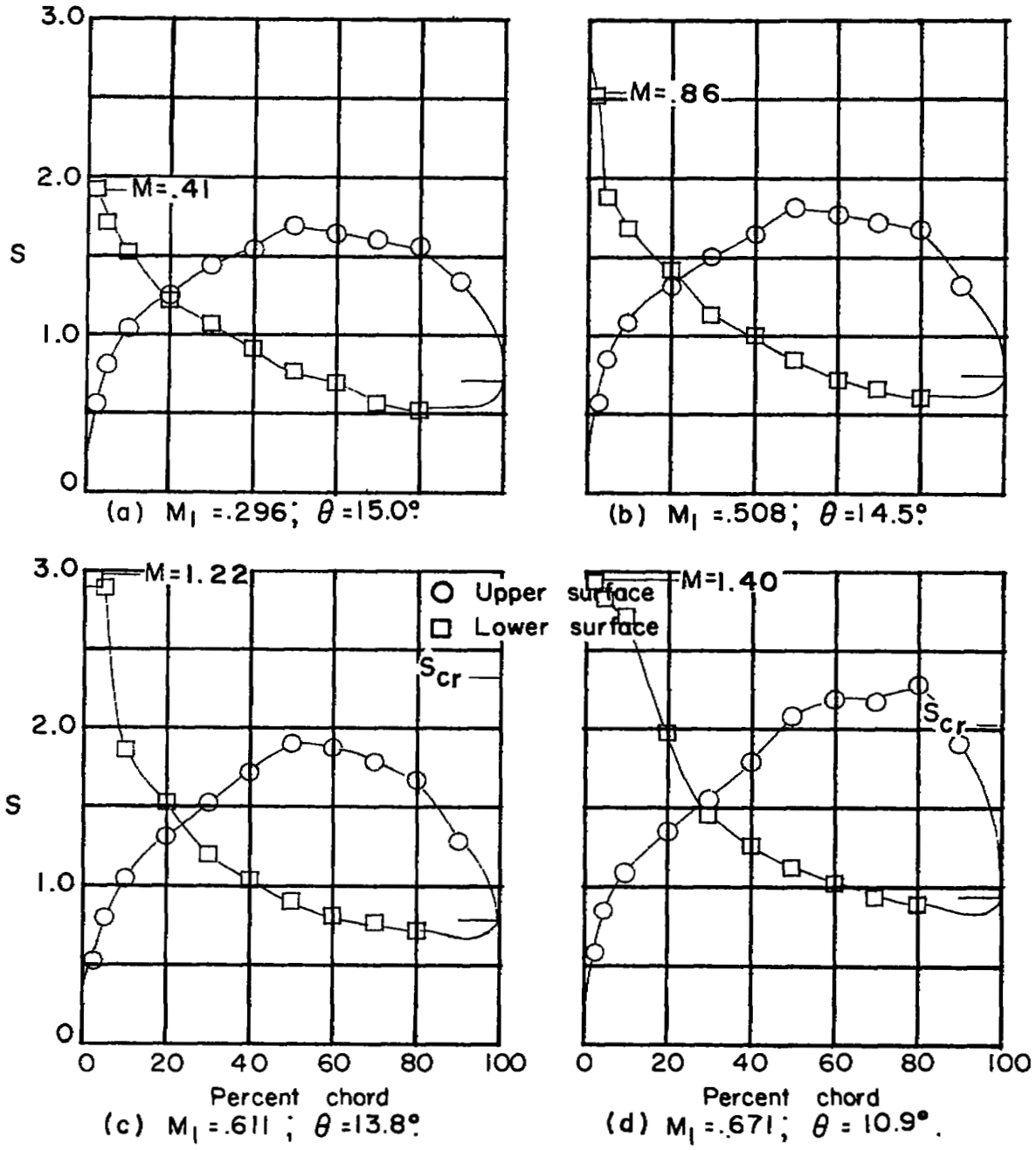

Figure 33.— Blade-surface pressure distributions and section characteristics for the cascade combination, β_1 = 45°, σ = 1.0 , α = 5.0°, and blade section, NACA 65-($12A_2I_{8b}$)10.

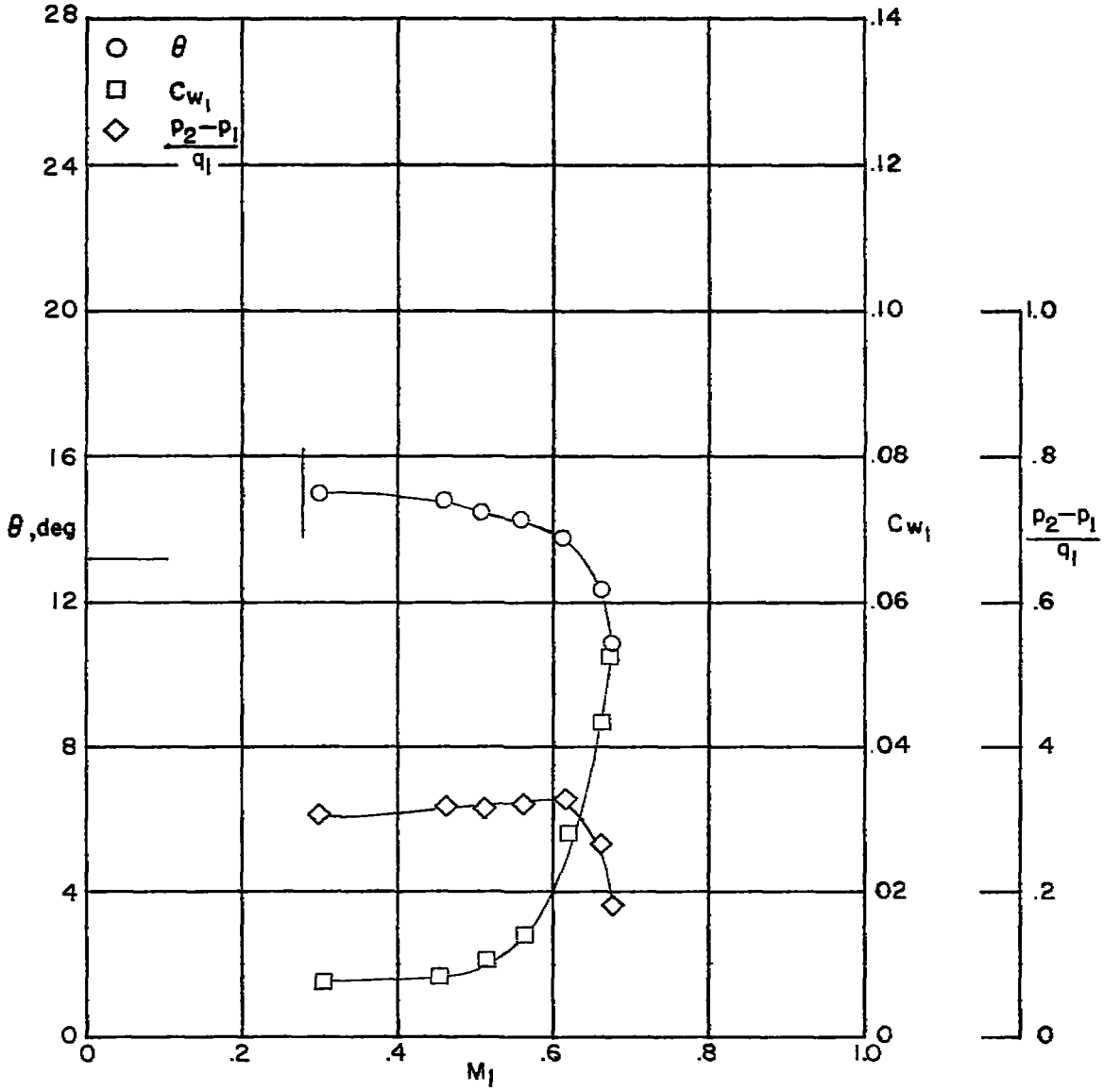

(e) Section characteristics. Tests are two dimensional for Mach numbers up to the vertical line. The horizontal line indicates low-speed turning angle given in reference 2.

Figure 33.— Concluded.

[redacted]

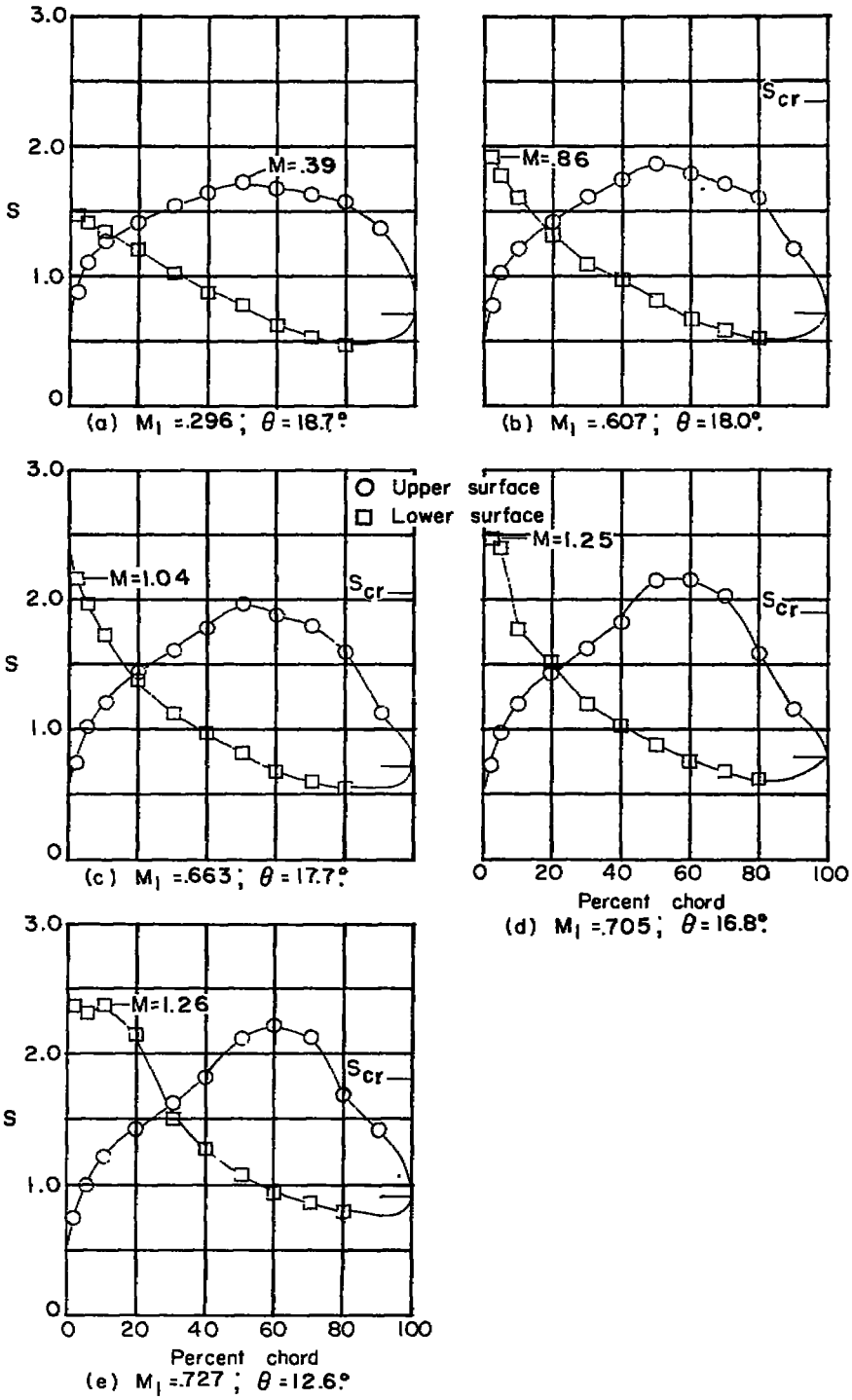

Figure 34.— Blade-surface pressure distributions and section characteristics for the cascade combination. β_1 = 45°; σ = 1.0; α = 8.0°; and blade section, NACA 65-($12A_2$ I_{8b})10.

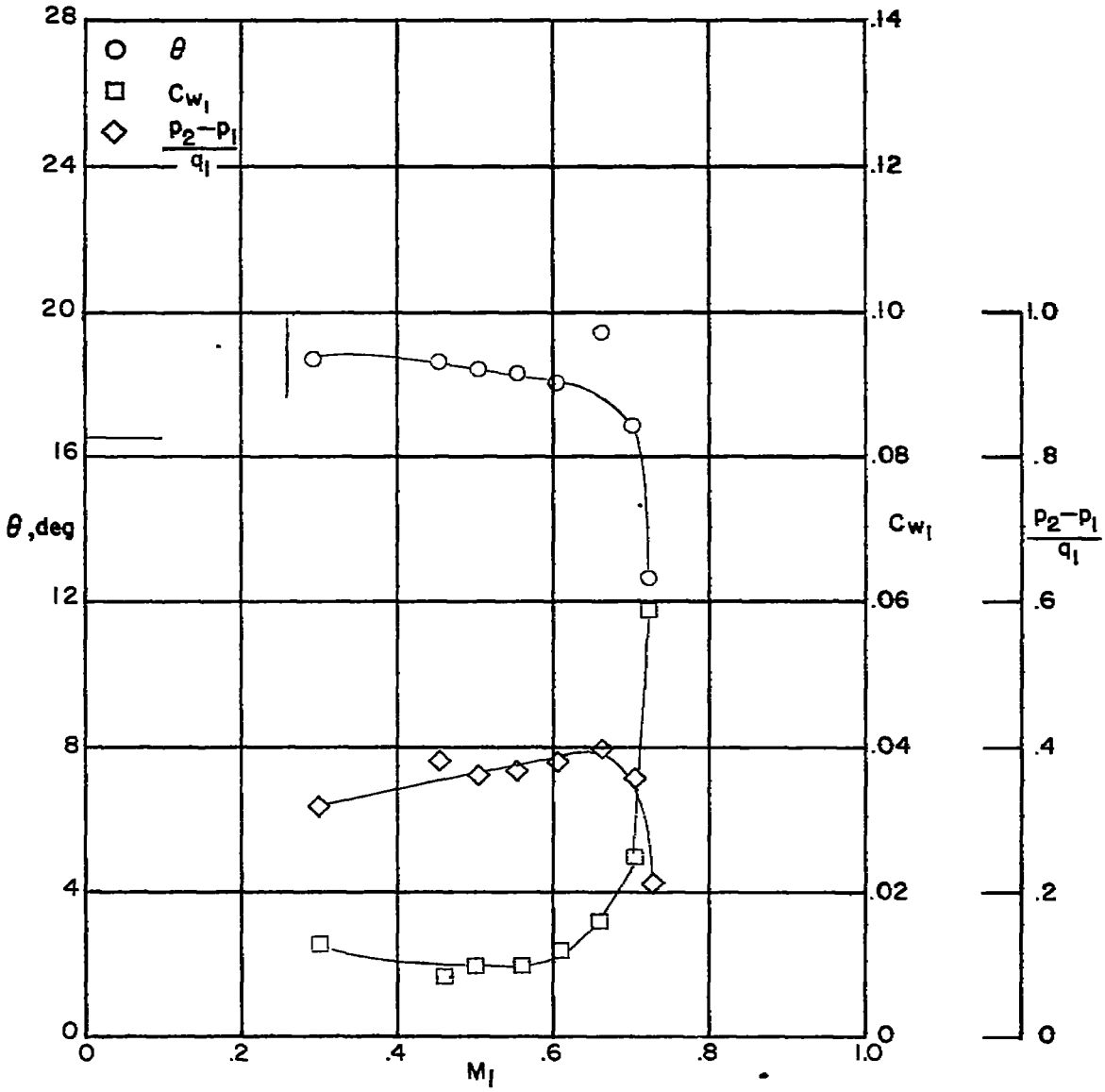

(f) Section characteristics. Tests are two dimensional for Mach numbers up to the vertical line. The horizontal line indicates low-speed turning angle given in reference 2

Figure 34 .— Concluded .

[redacted]

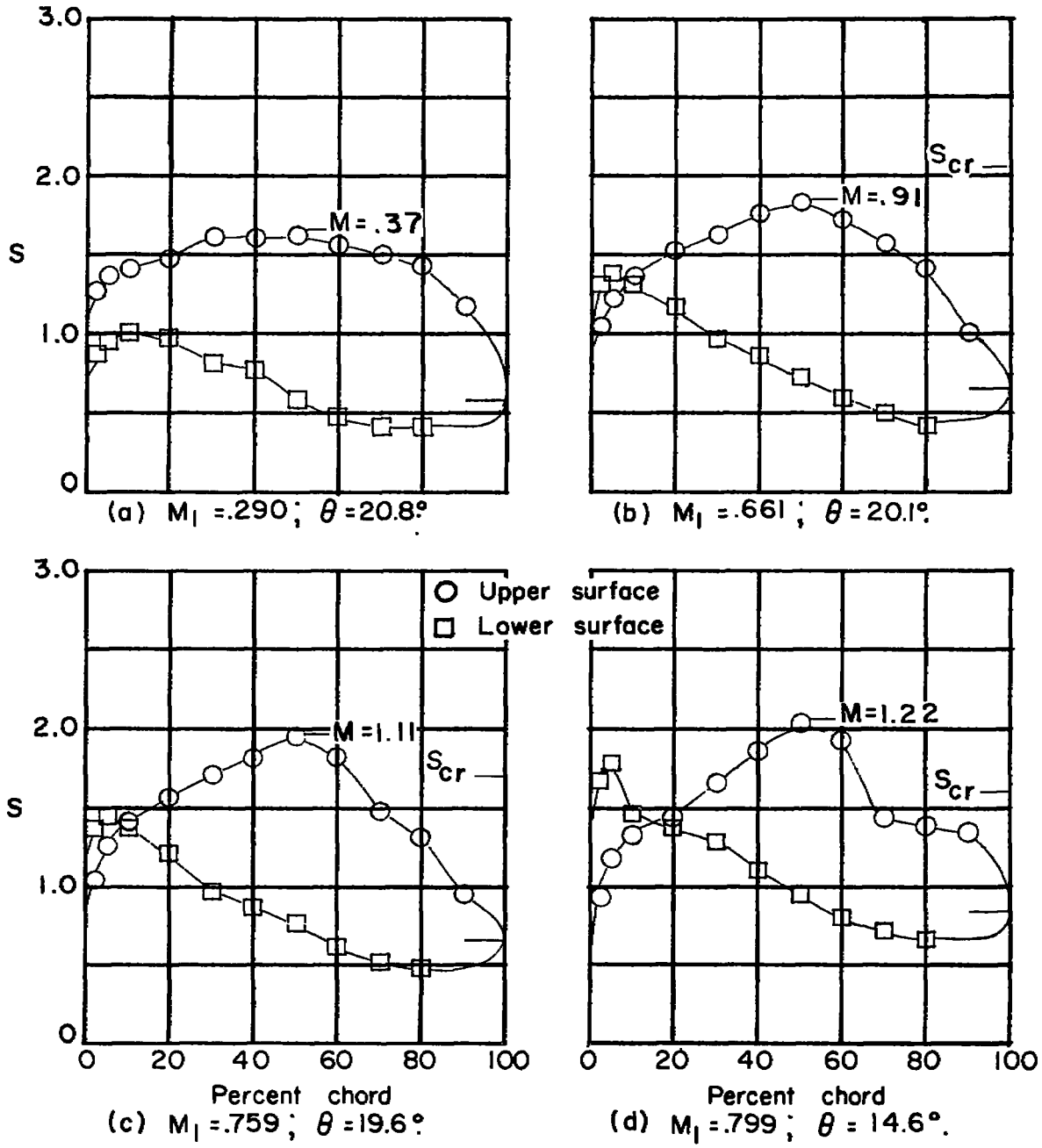

Figure 35.— Blade-surface pressure distributions and section characteristics for the cascade combination. β_1 = 45°; σ = 1.0; α = 11.0°; and blade section, NACA 65-($12A_2$ I_{8b})10.

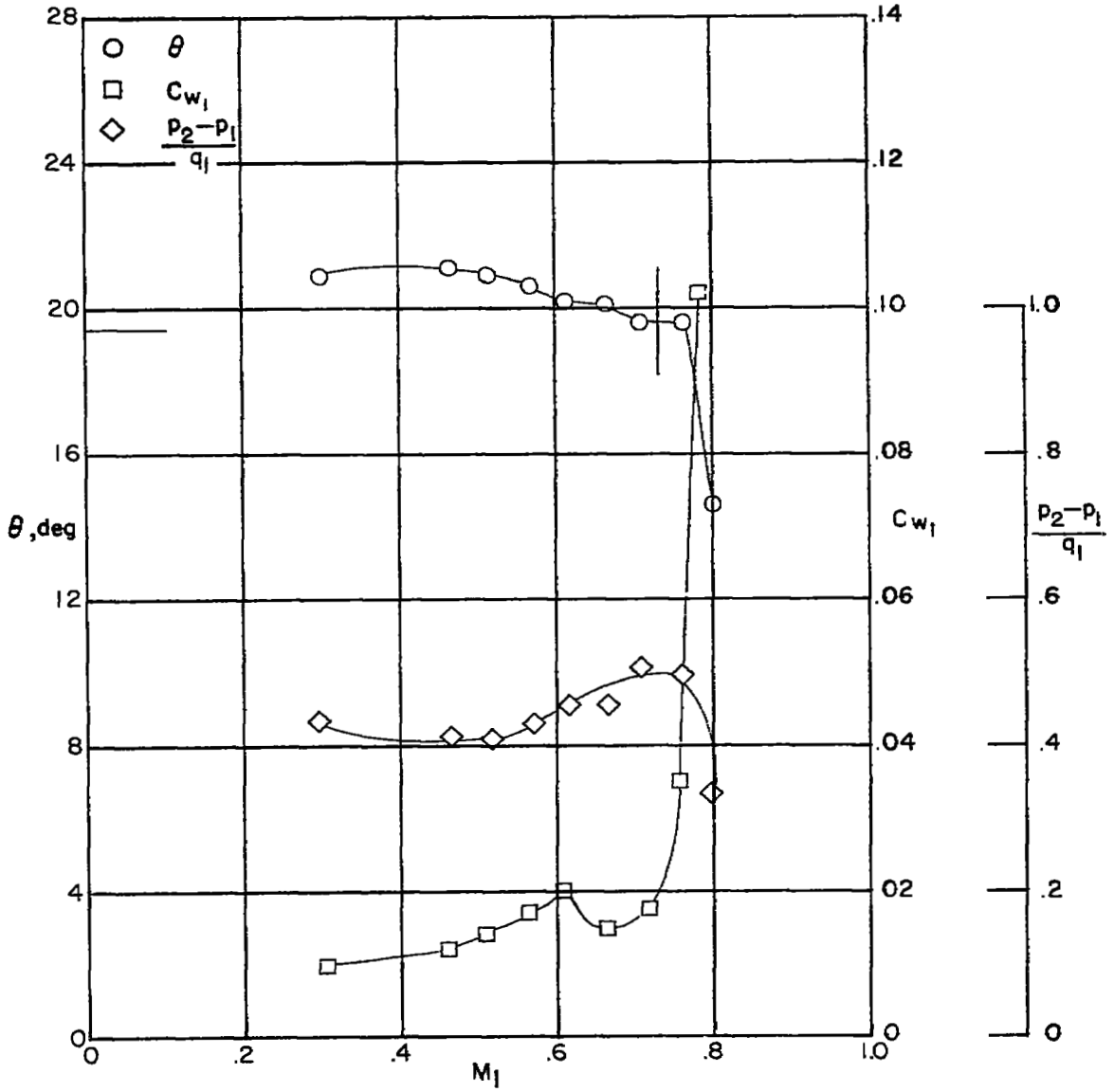

(e) Section characteristics. Tests are two dimensional for Mach numbers up to the vertical line. The horizontal line indicates low-speed turning angle given in reference 2

Figure 35 .— Concluded.

[redacted]

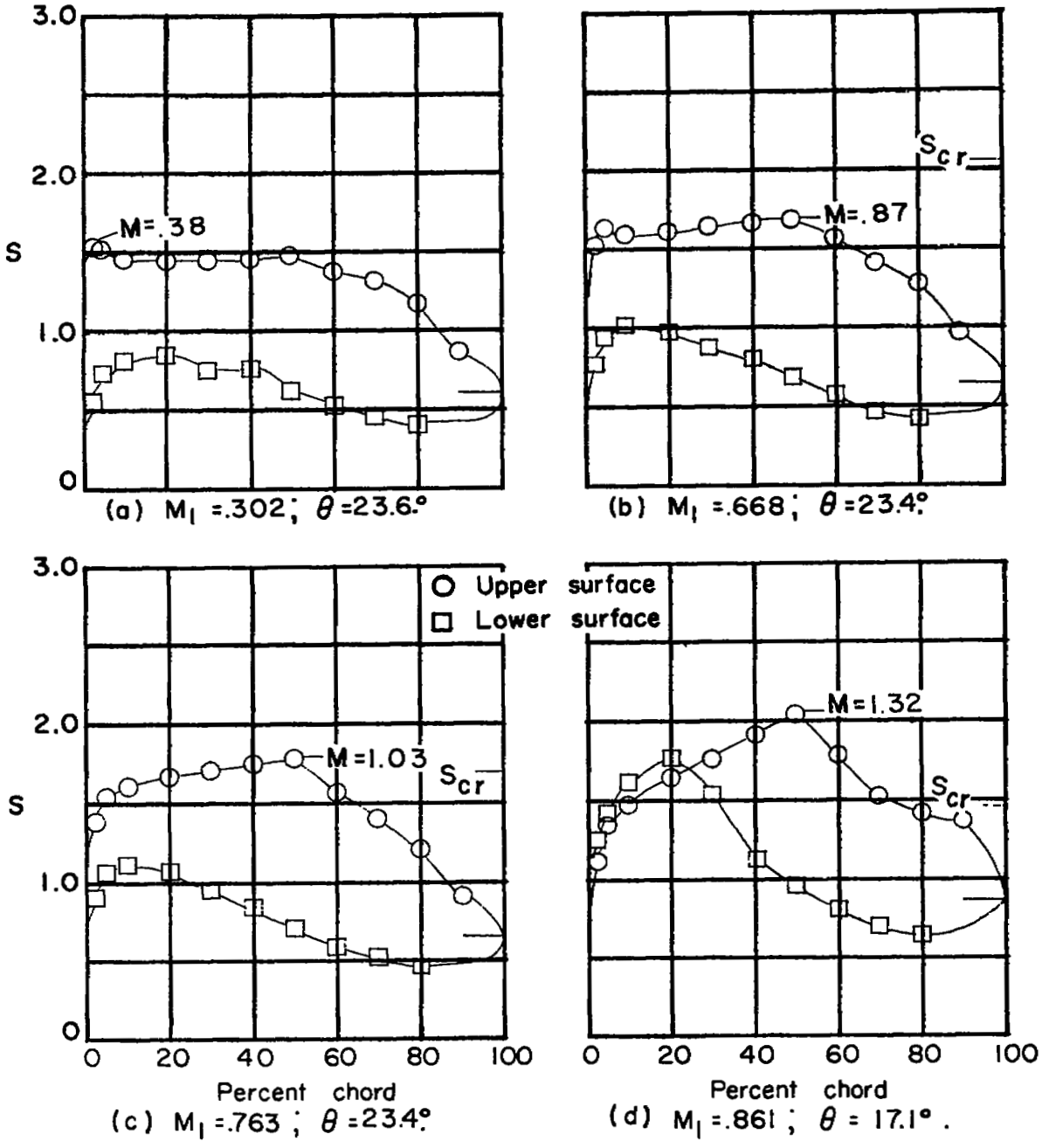

Figure 36.— Blade-surface pressure distributions and section characteristics for the cascade combination. β_1 = 45°; σ = 1.0; α =14.0°; and blade section, NACA 65-($12A_2$ I_{8b})10..

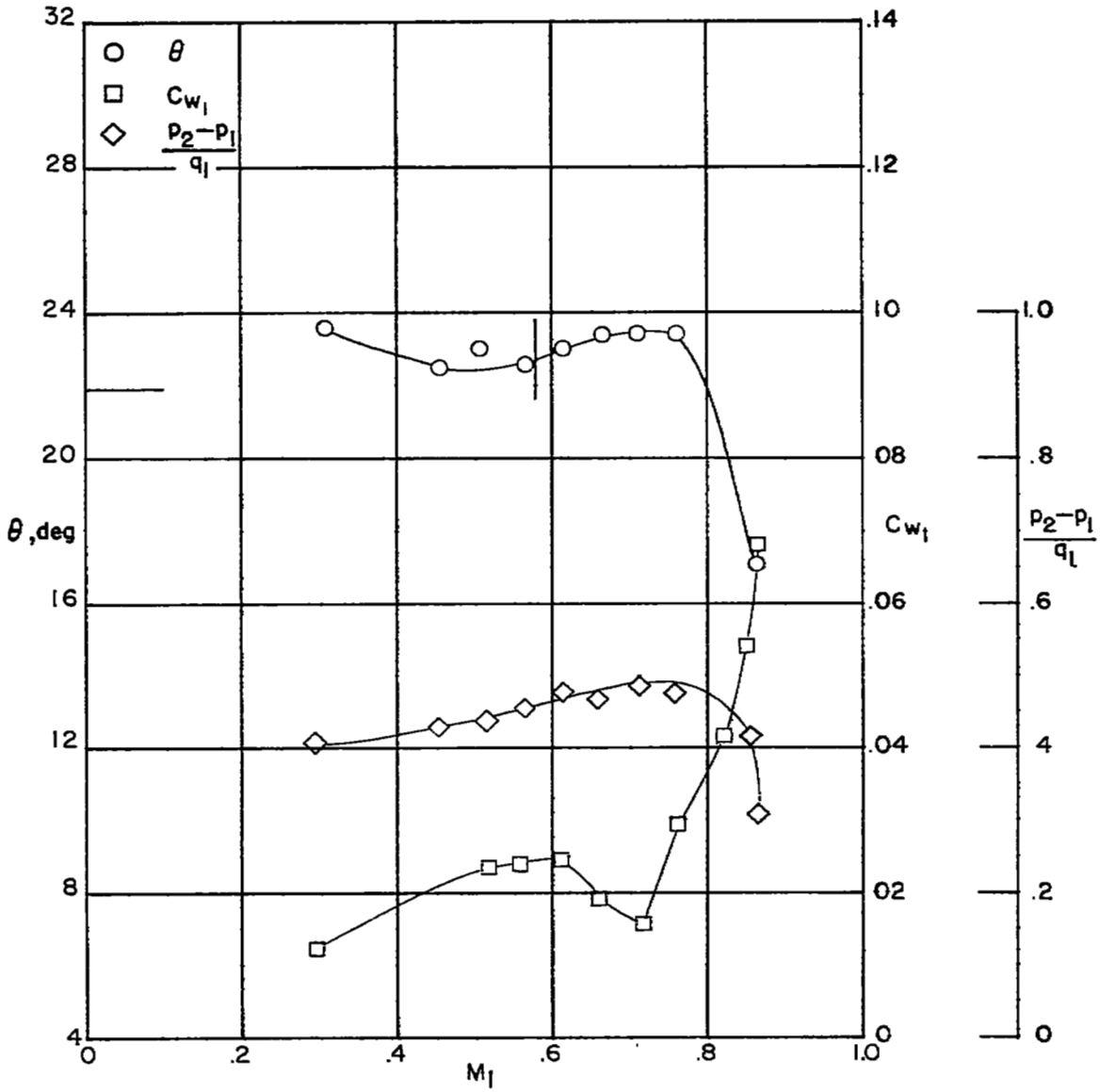

(e) Section characteristics. Tests are two dimensional for Mach numbers up to the vertical line The horizontal line indicates low-speed turning angle given in reference 2.

Figure 36 .— Concluded.

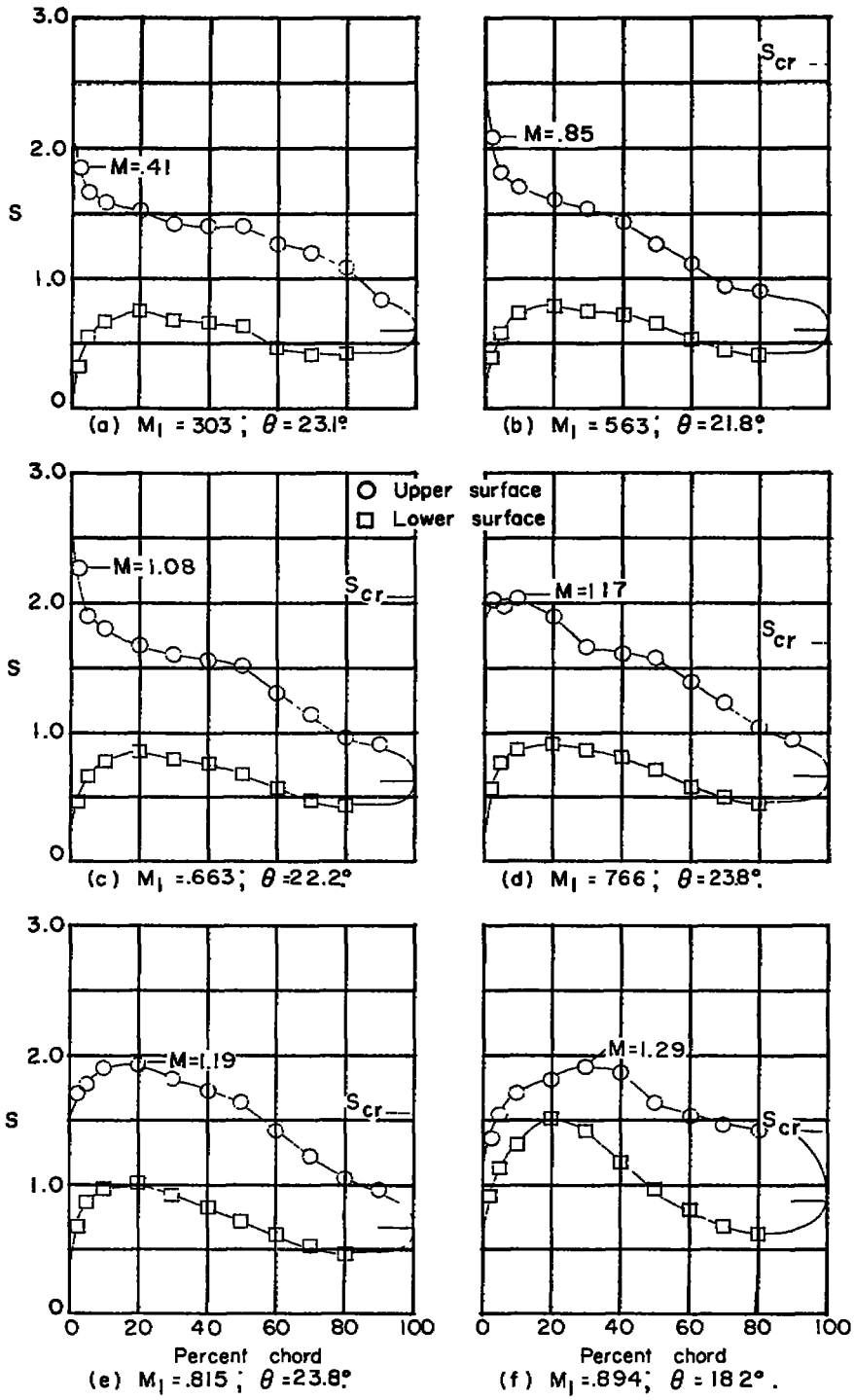

Figure 37 .— Blade-surface pressure distributions and section characteristics for the cascade combination. β_1 = 45°; σ = 1.0 ; α = 17.0°; and blade section, NACA 65-($12A_2I_{8b}$)10.

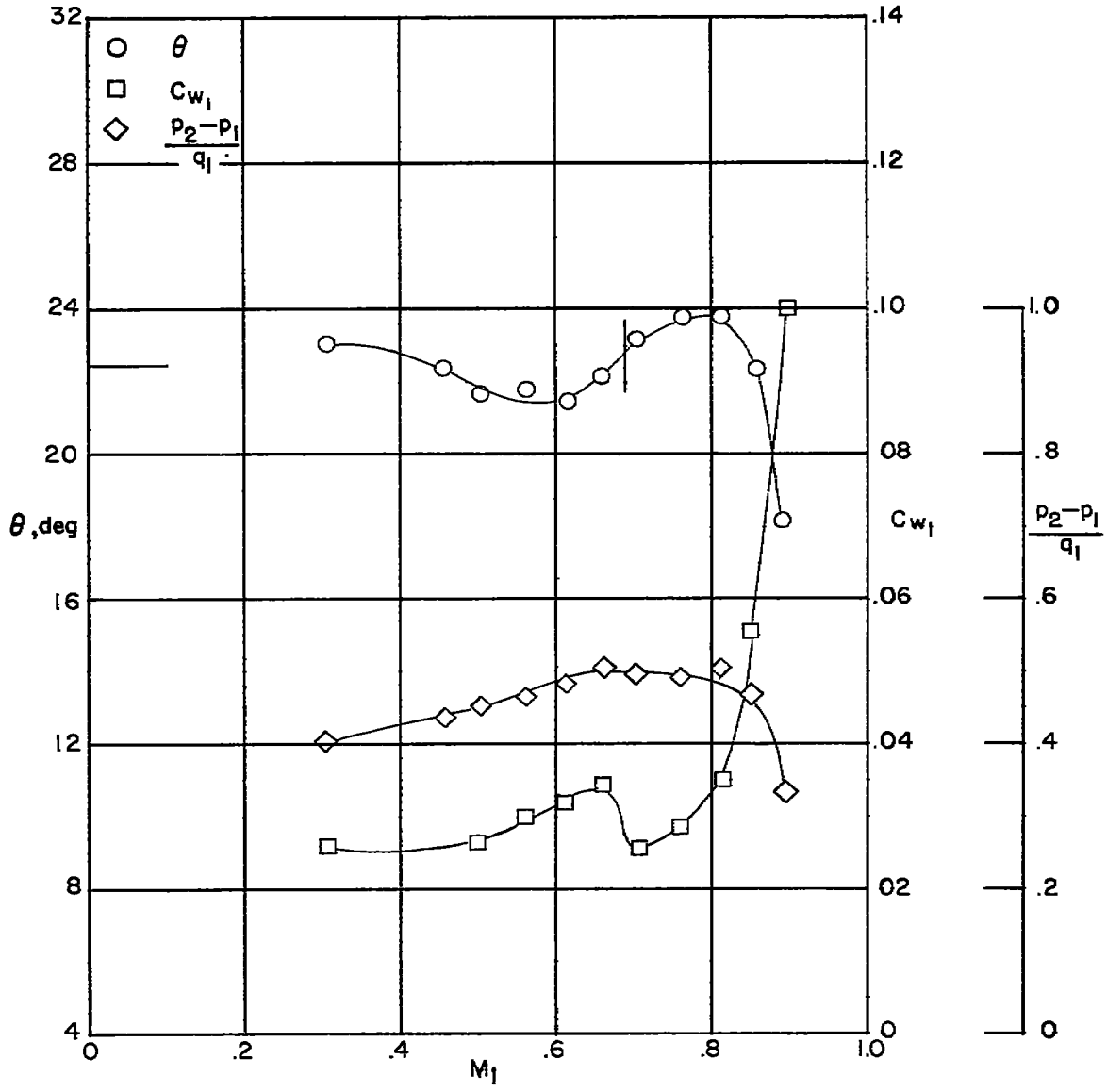

(g) Section characteristics. Tests are two dimensional for Mach numbers up to the vertical line The horizontal line indicates low-speed turning angle given in reference 2.

Figure 37 .— Concluded.

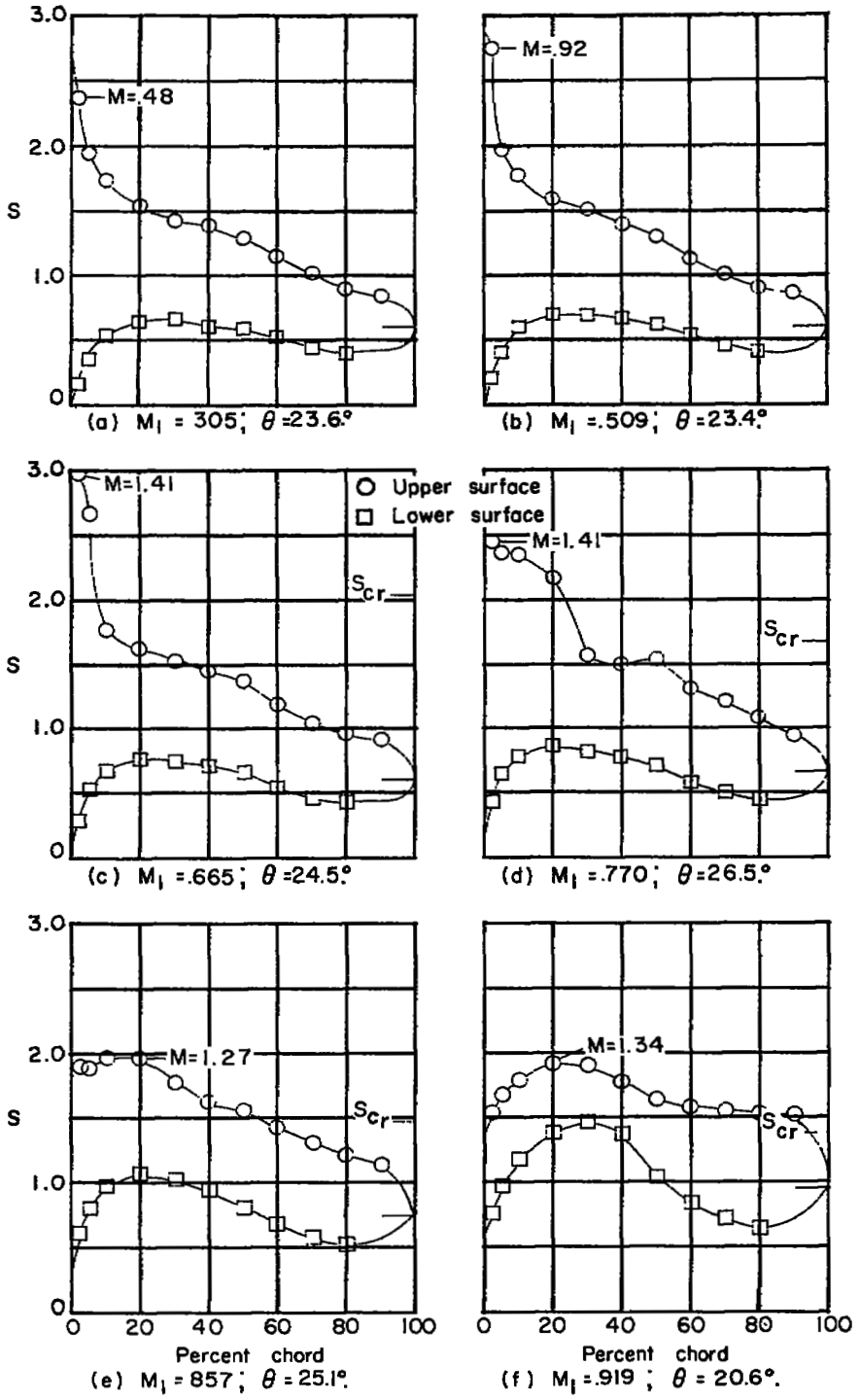

Figure 38.— Blade-surface pressure distributions and section characteristics for the cascade combination. β_1 = 45°; σ =1.0 ; α =200; and blade section, NACA 65-($12A_2I_{8b}$)10.

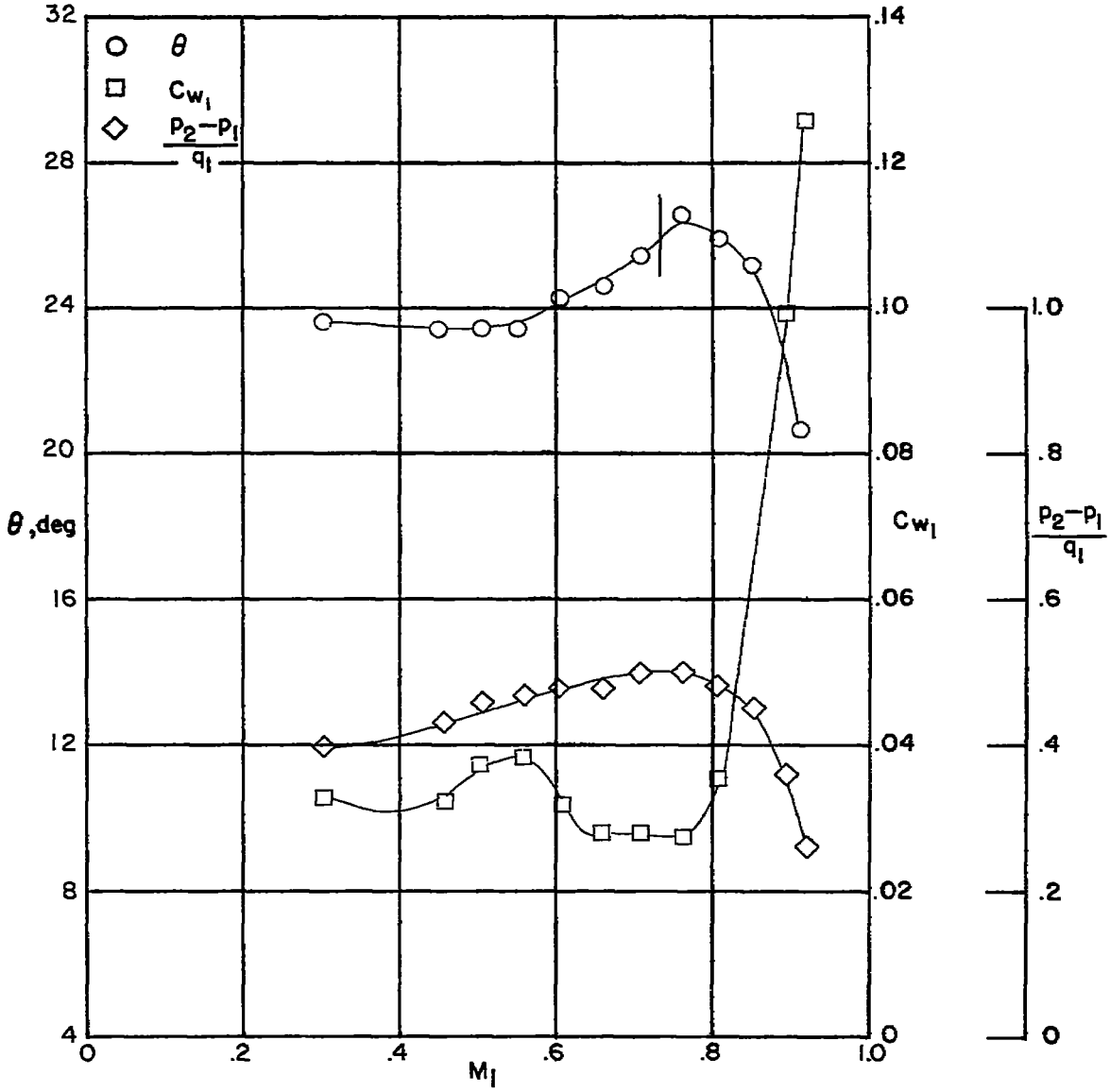

(g) Section characteristics. Tests are two dimensional for Mach numbers up to the vertical line.

Figure 38.— Concluded.

[redacted]

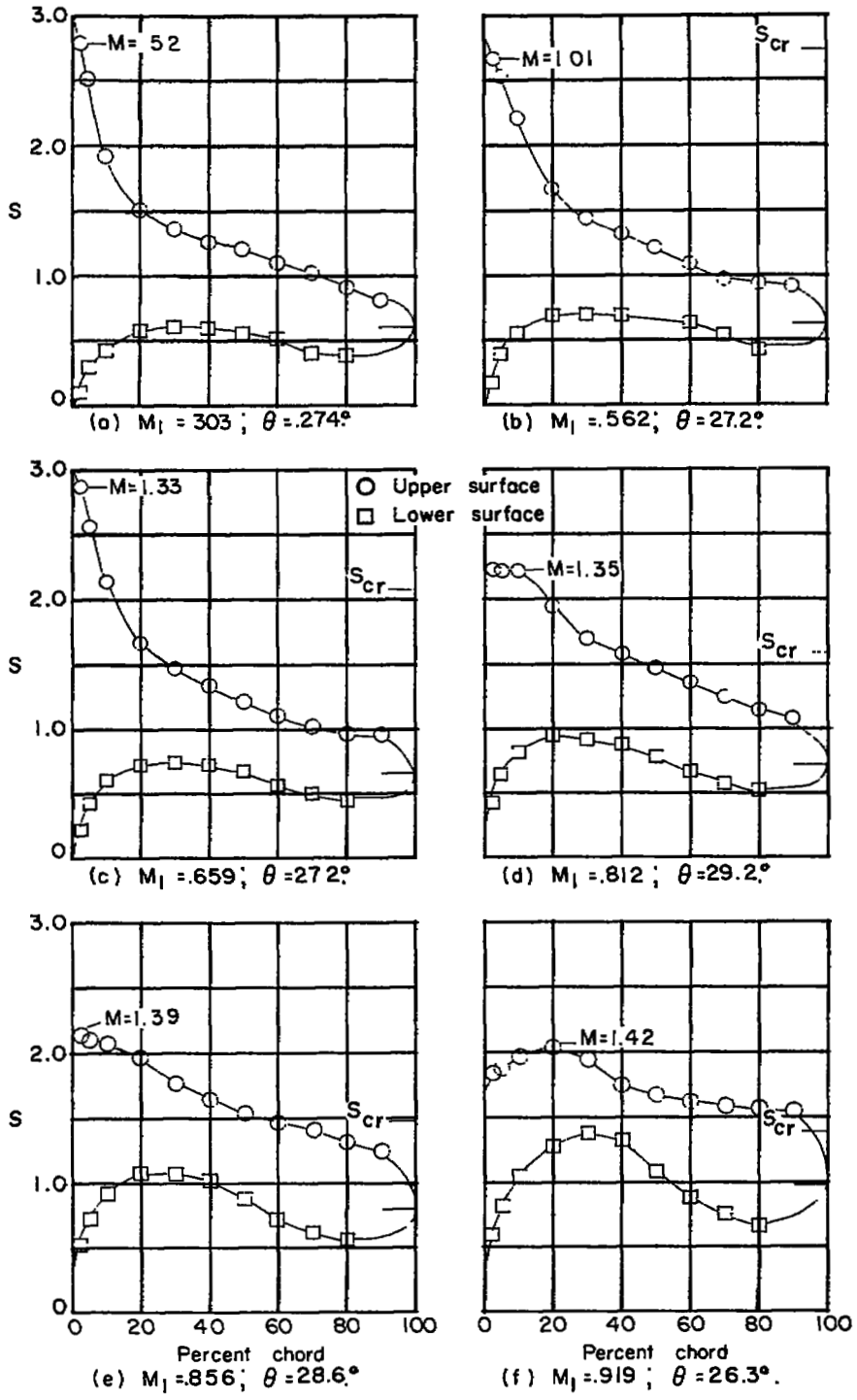

Figure 39.— Blade-surface pressure distributions and section characteristics for the cascade combination $\beta_1 = 45°$; $\sigma = 1.0$; $\alpha = 23.0°$; and blade section, NACA 65-($12A_2$ I_{8b})10.

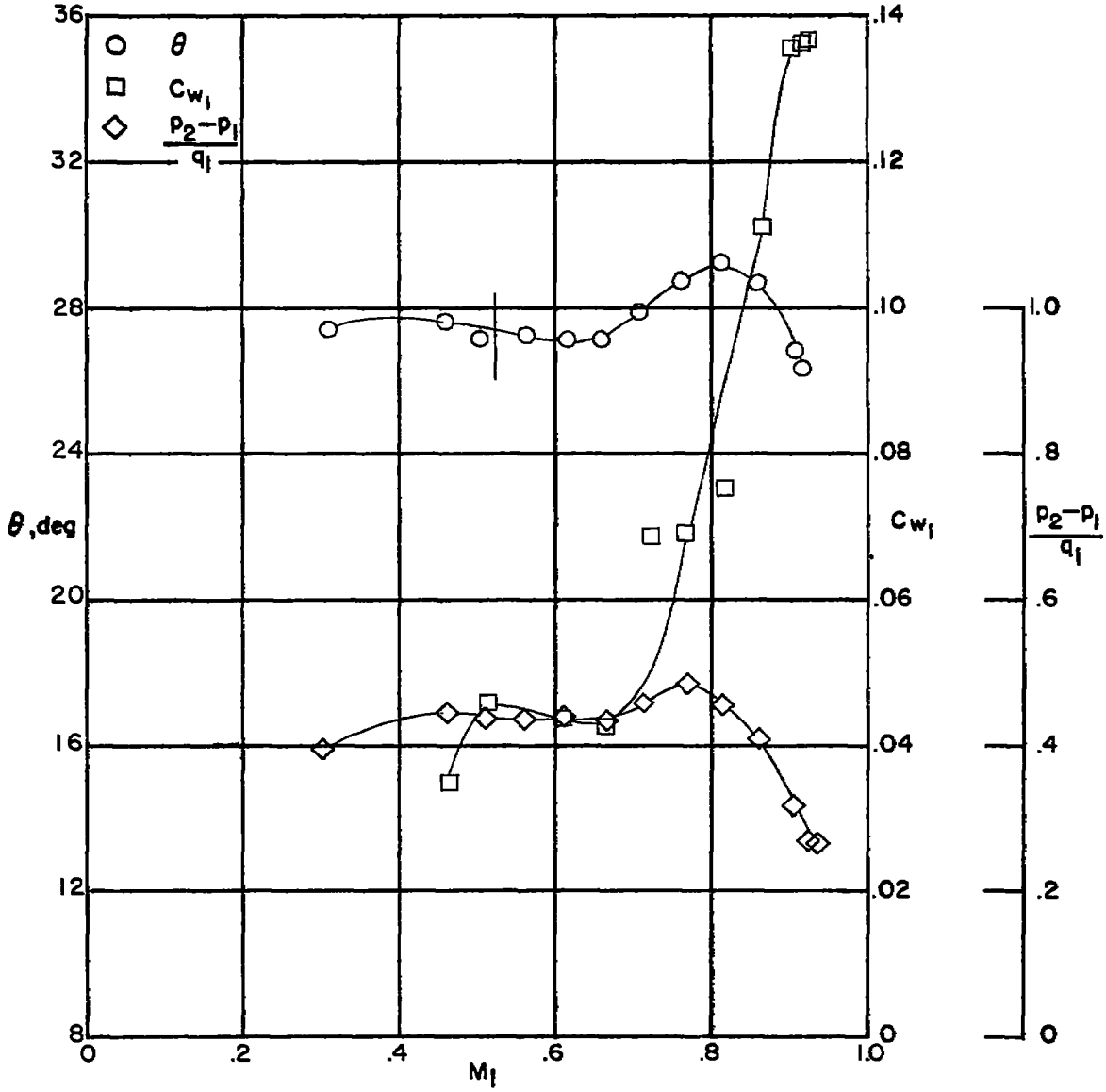

(g) Section characteristics. Tests are two dimensional for Mach numbers up to the vertical line.

Figure 39 .— Concluded.

[redacted]

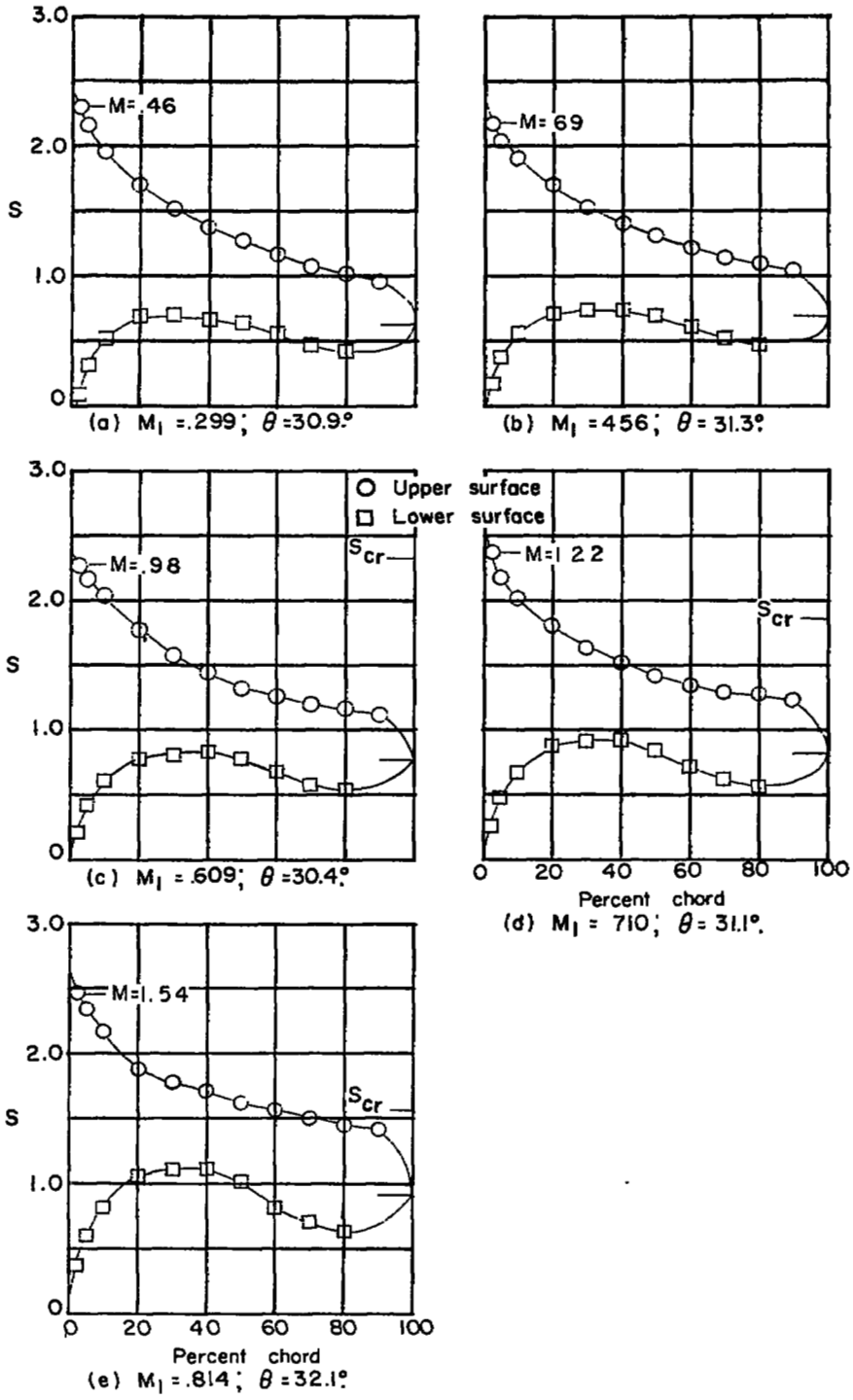

Figure 40.— Blade-surface pressure distributions and section characteristics for the cascade combination. β_1 = 45°; σ = 1.0 ; α = 26.0°; and blade section, NACA 65-($12A_2I_{8b}$)10.

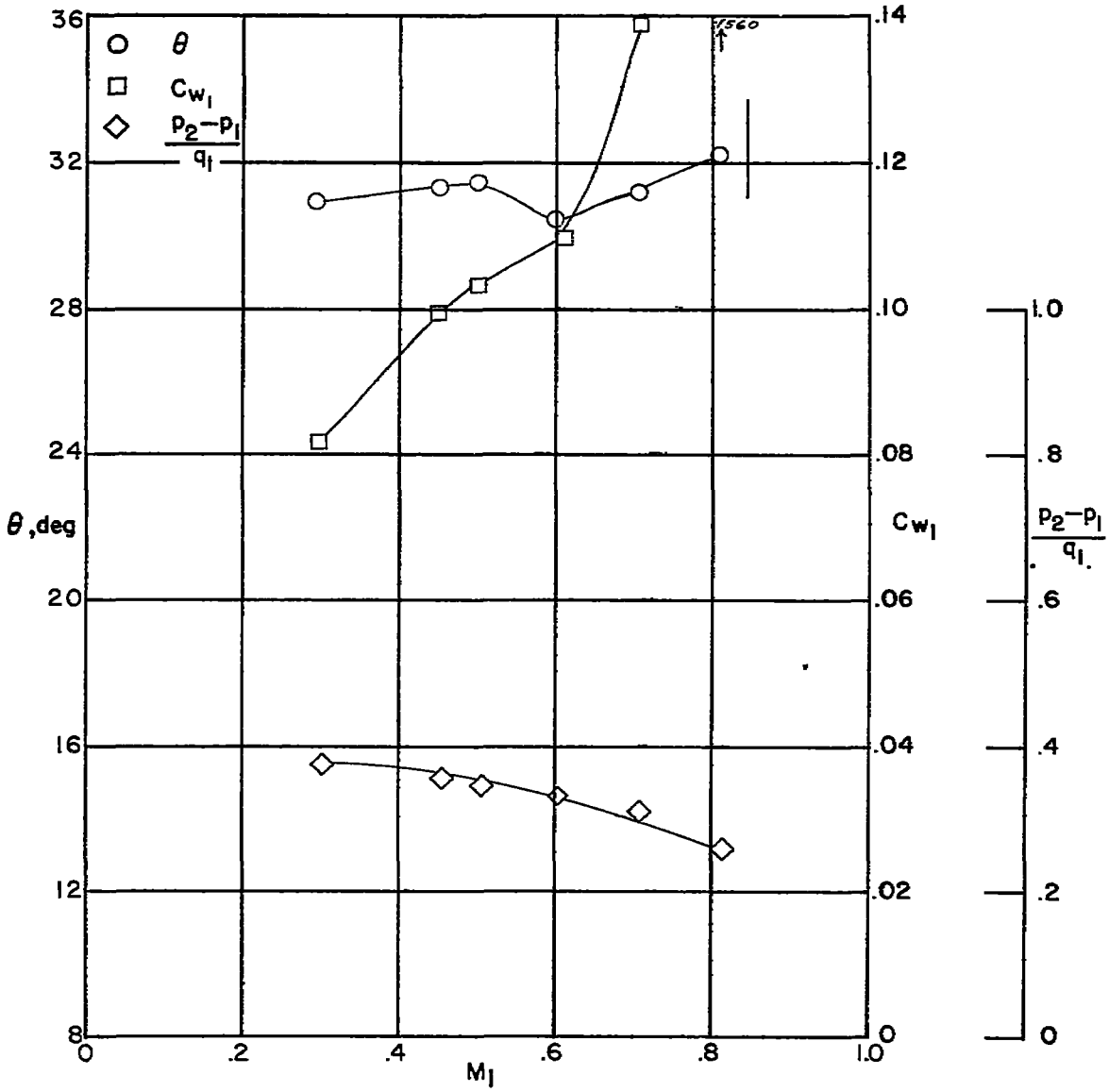

(f) Section characteristics. Tests are two dimensional for Mach numbers up to the vertical line.

Figure 40.— Concluded.

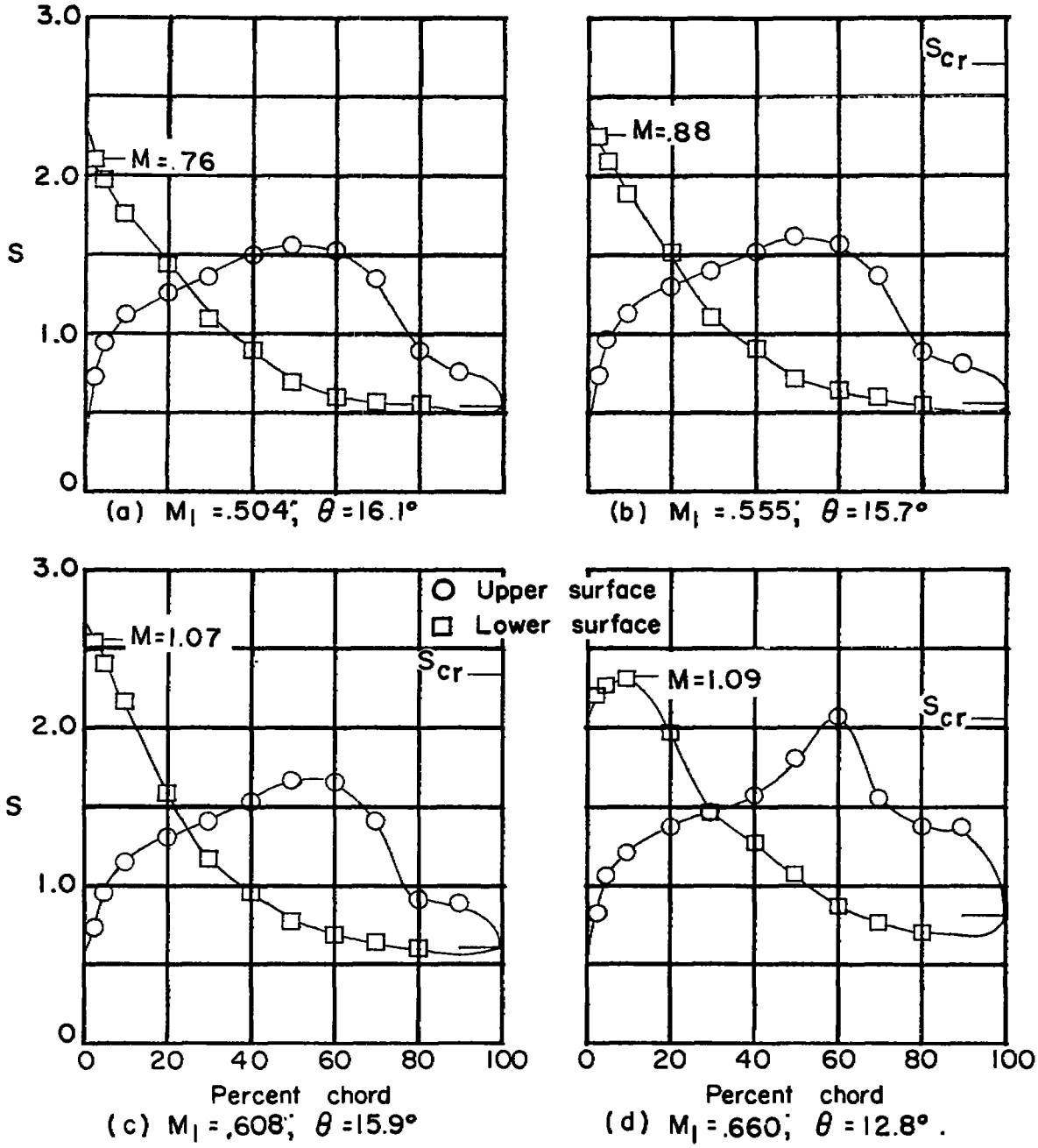

Figure 41. — Blade-surface pressure distributions and section characteristics for the cascade combination - $\beta_1 = 60°$; $\sigma = 1.5$; $\alpha = 10.5°$; and blade section, NACA 65-(12A_2 I_{8b})10.

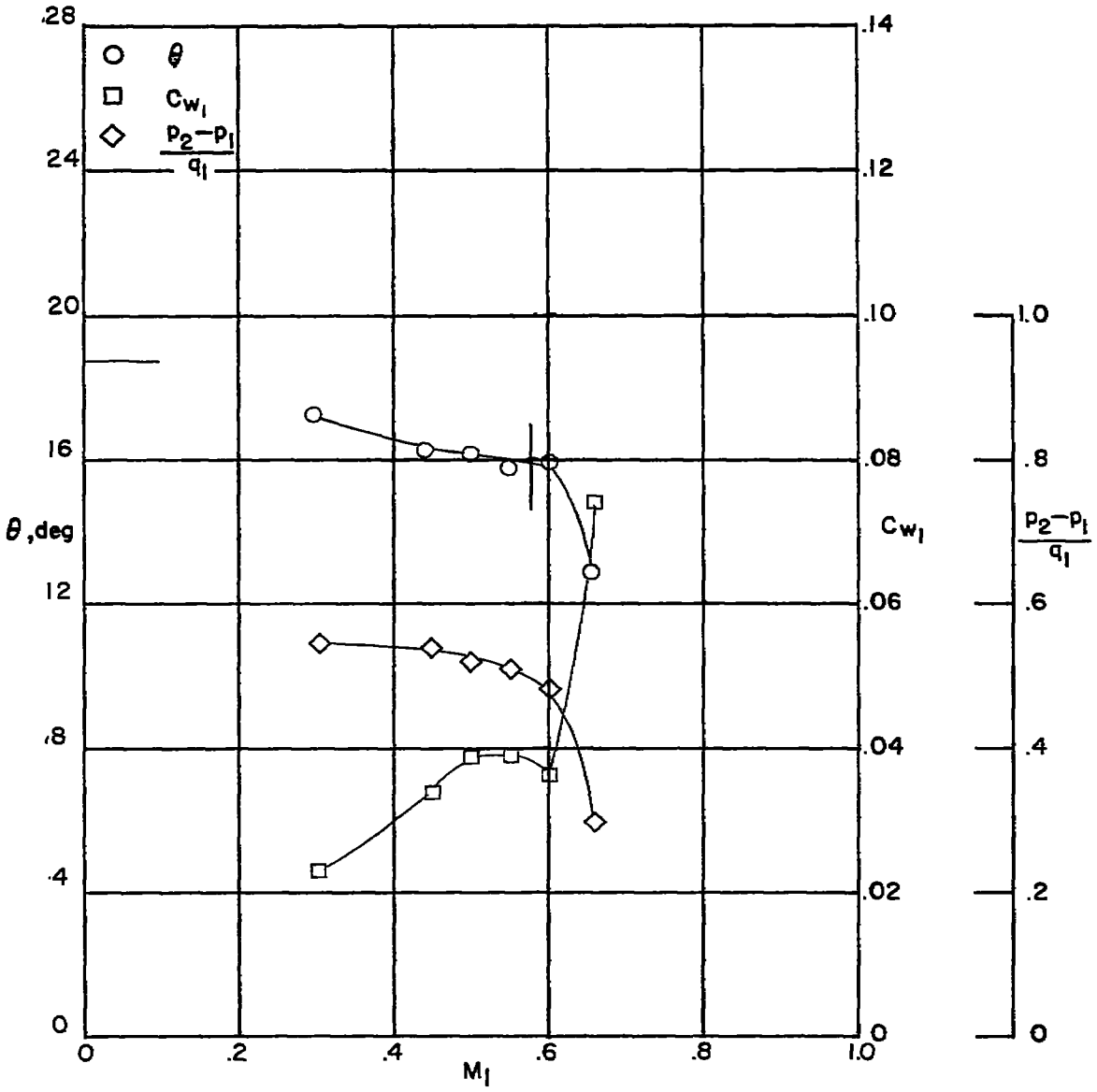

(e) Section characteristics. Tests are two dimensional for Mach numbers up to the vertical line. The horizontal line indicates low-speed turning angle given in reference 2.

Figure 41 .— Concluded.

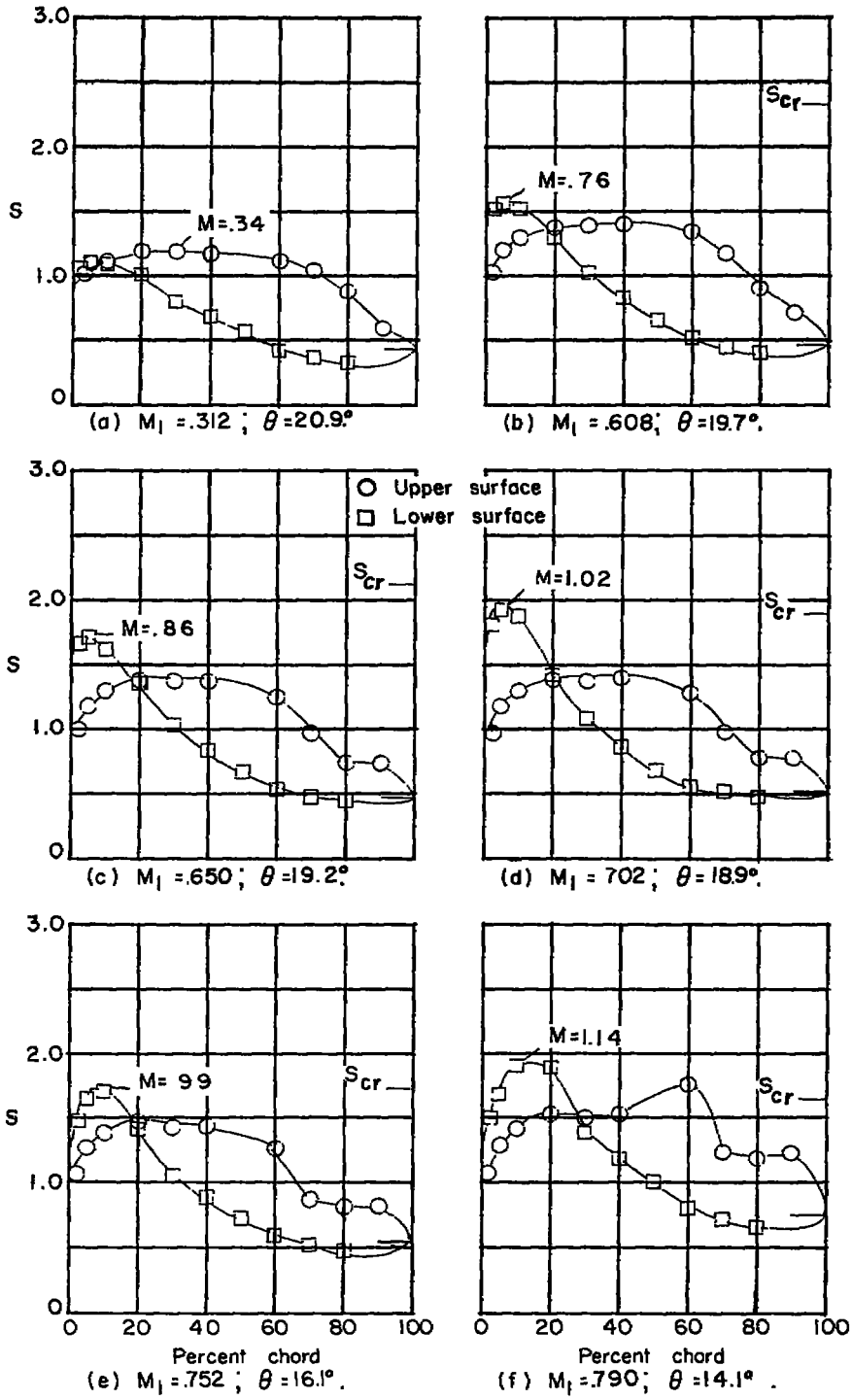

Figure 42 .— Blade-surface pressure distributions and section characteristics for the cascade combination. β_1 = 60 ; σ = 1.5 ; α =13.5°; and blade section, NACA 65-$(12A_2I_{8b})$10.

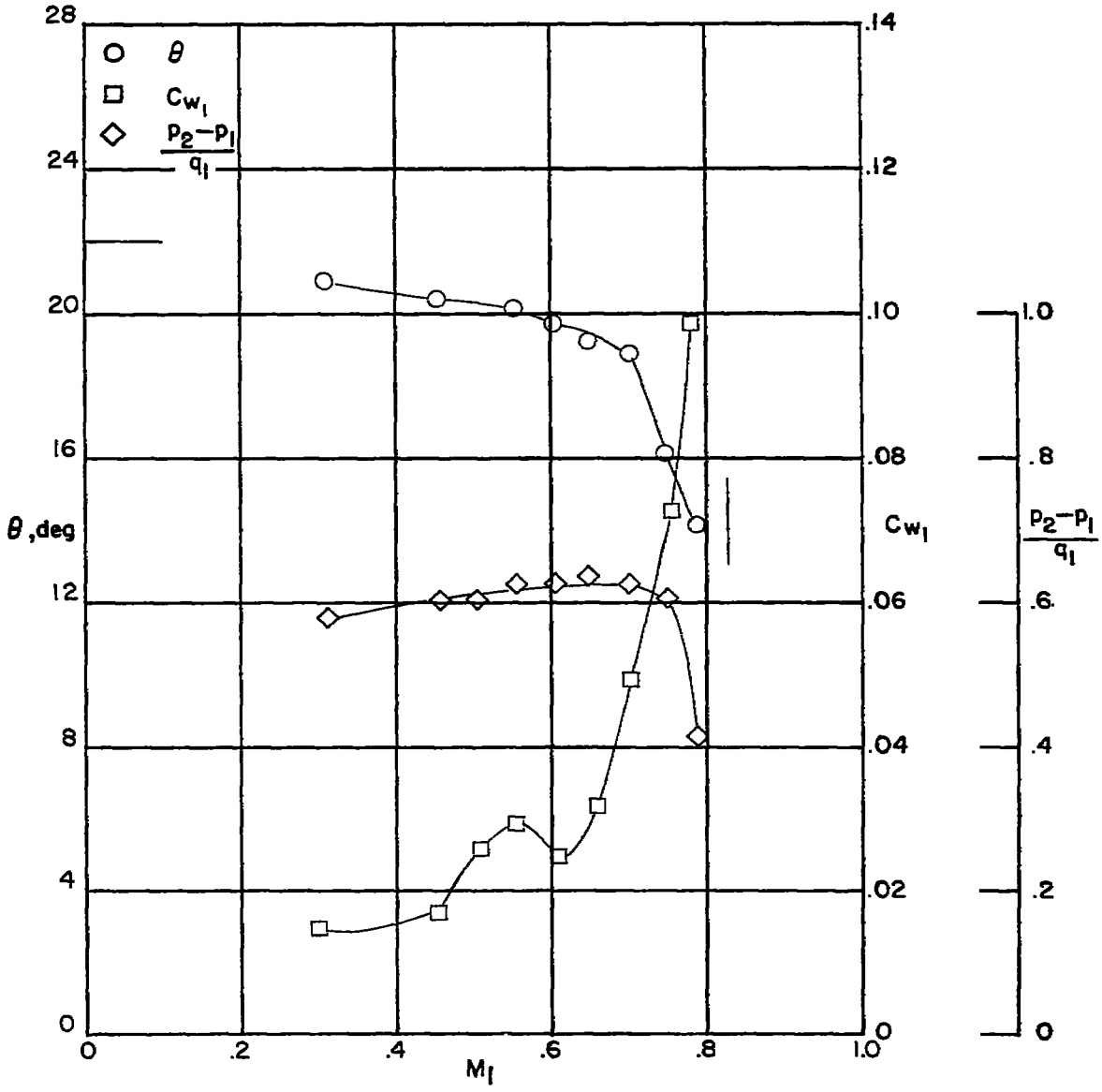

(g) Section characteristics. Tests are two dimensional for Mach numbers up to the vertical line. The horizontal line indicates low-speed turning angle given in reference 2

Figure 42 .— Concluded.

[redacted]

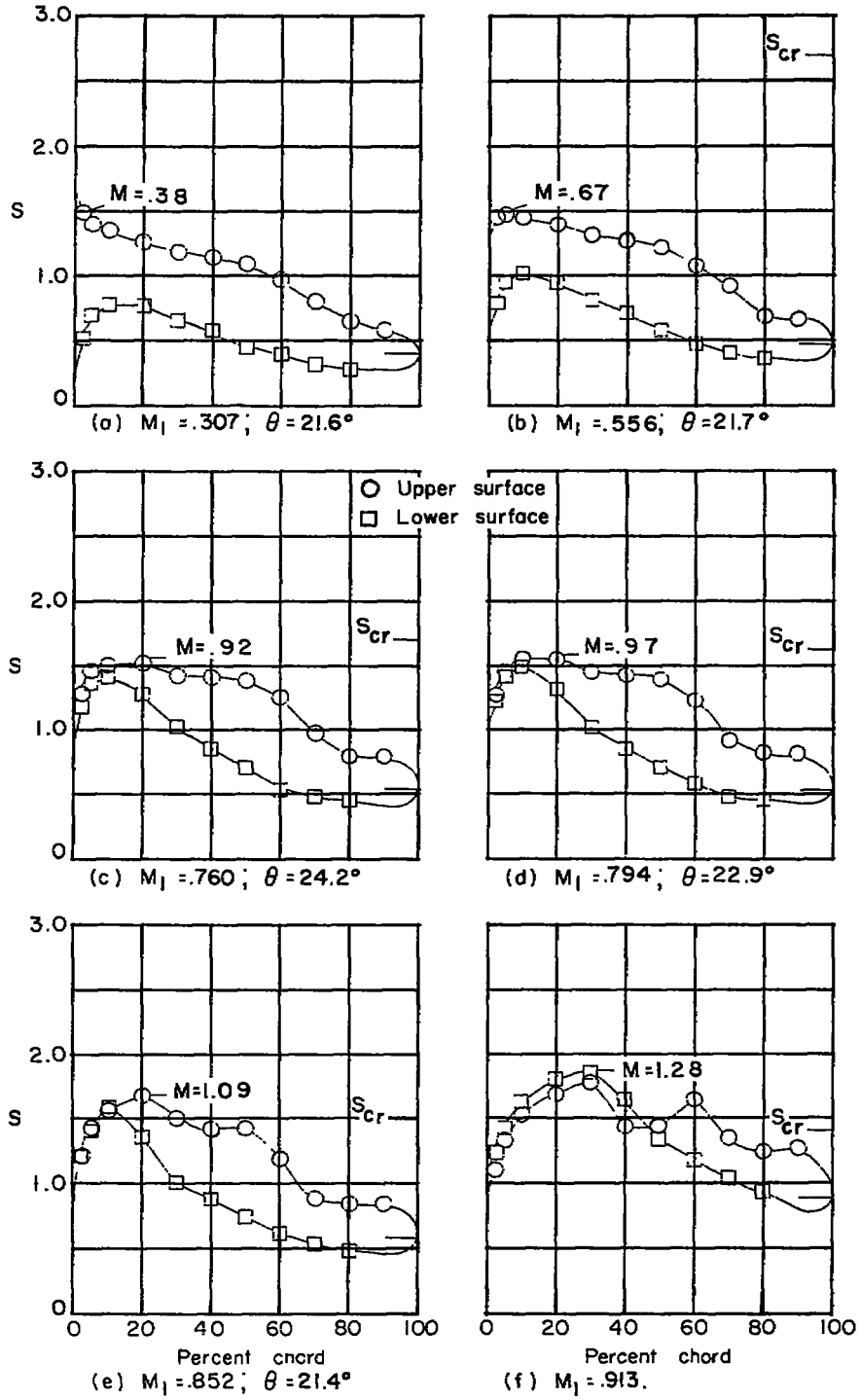

Figure 43.— Blade-surface pressure distributions and section characteristics for the cascade combination. β_1 = 60°; σ =1.5 ; α =16.5°; and blade section, NACA 65-($12A_2I_{8b}$)10.

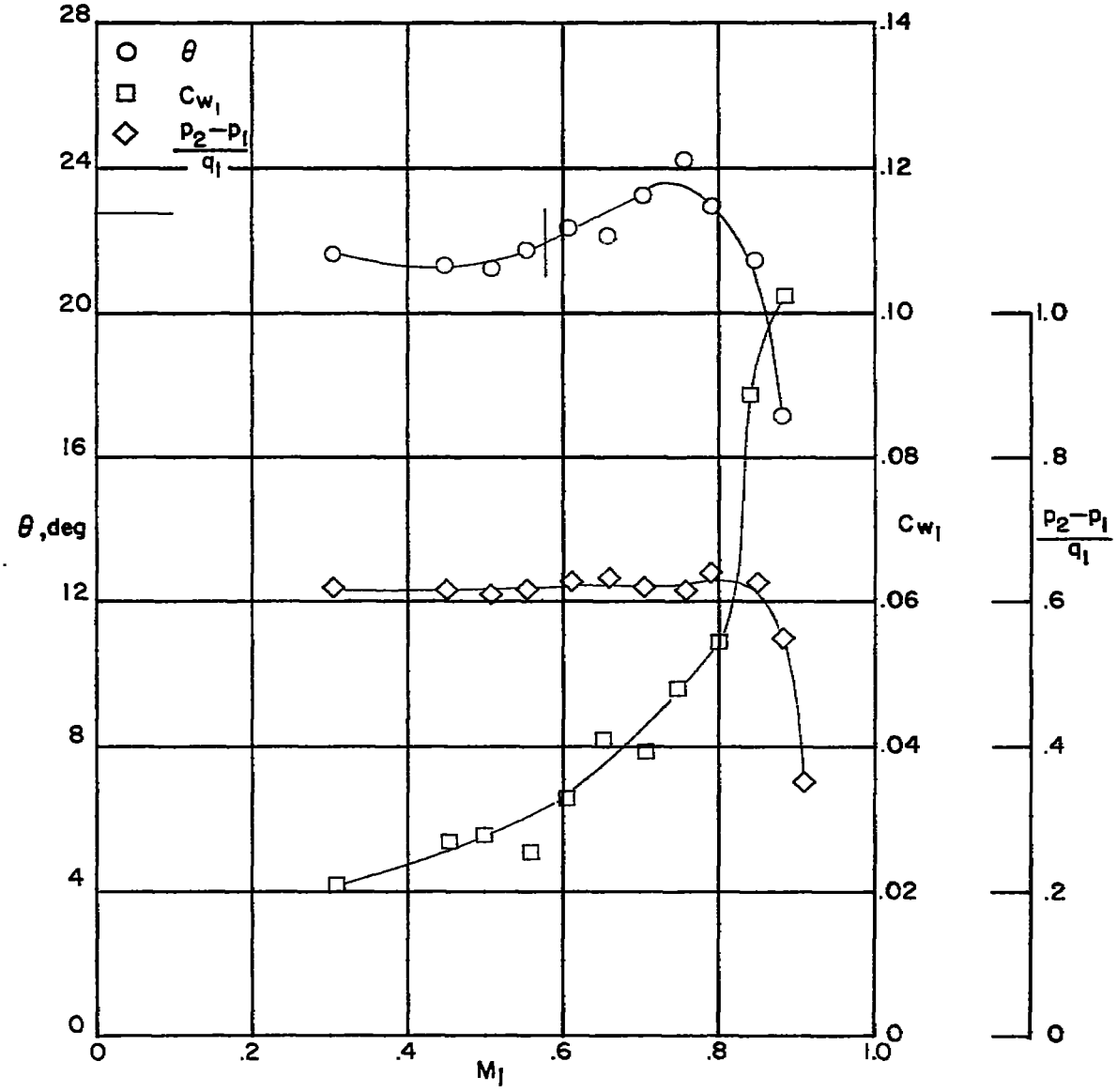

(g) Section characteristics. Tests are two dimensional for Mach numbers up to the vertical line. The horizontal line indicates low-speed turning angle given in reference 2.

Figure 43 .— Concluded.

[redacted]

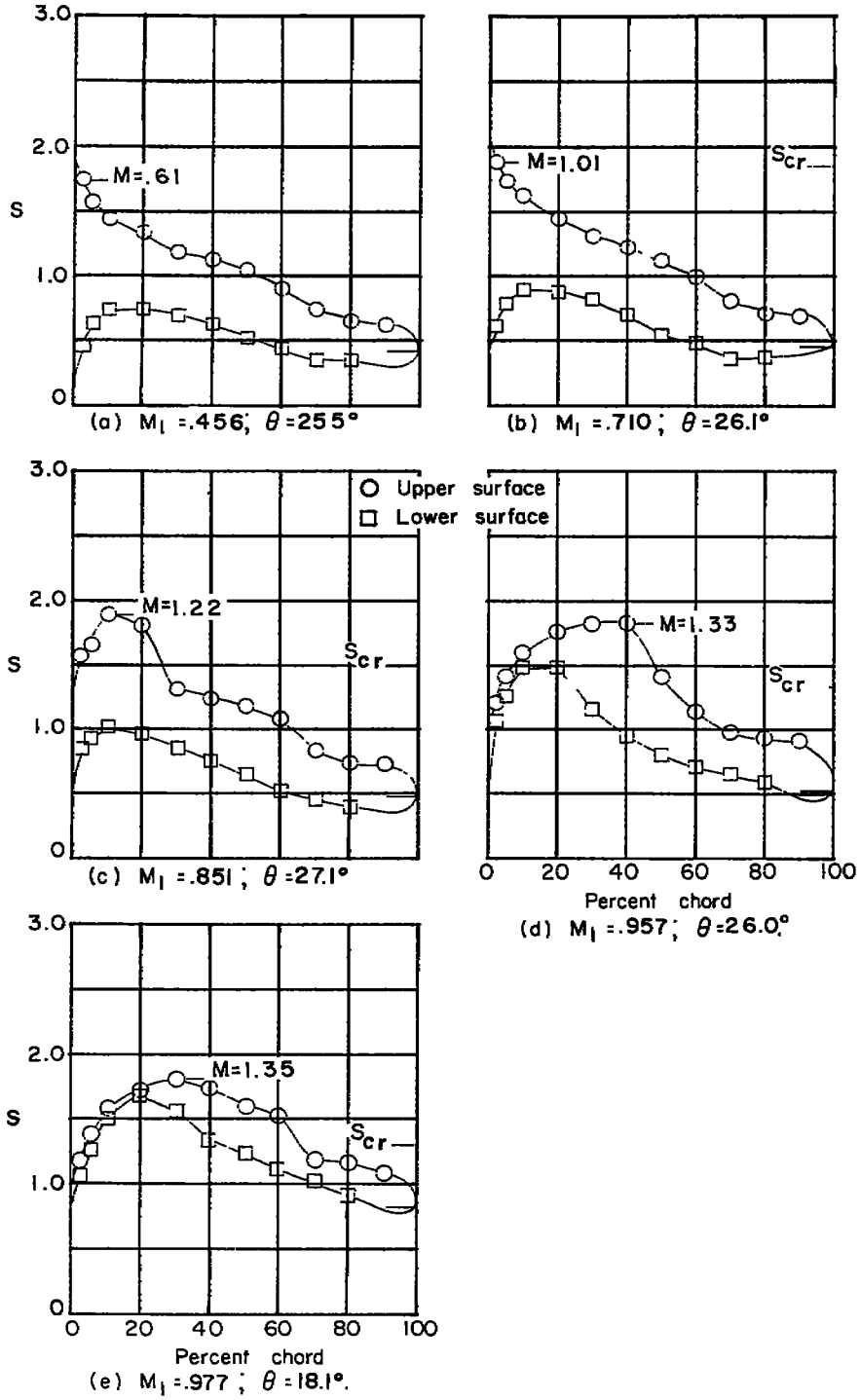

Figure 44.— Blade-surface pressure distributions and section characteristics for the cascade combination: β_1 =60°; σ =1.5; α =19.5°; and blade section, NACA 65-($12A_2I_{8b}$)10.

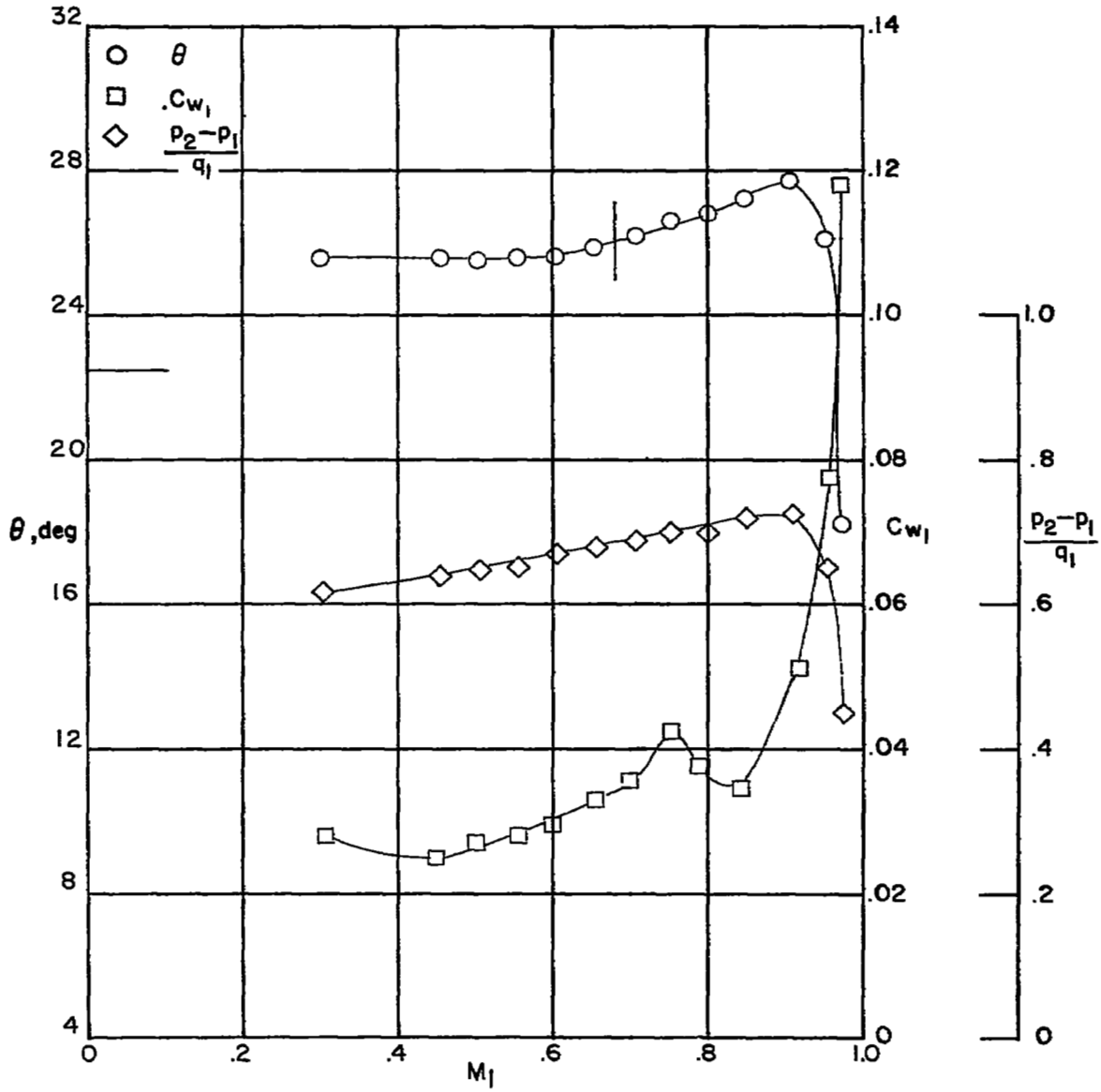

(f) Section characteristics. Tests are two dimensional for Mach numbers up to the vertical line. The horizontal line indicates low-speed turning angle given in reference

Figure 44.— Concluded.

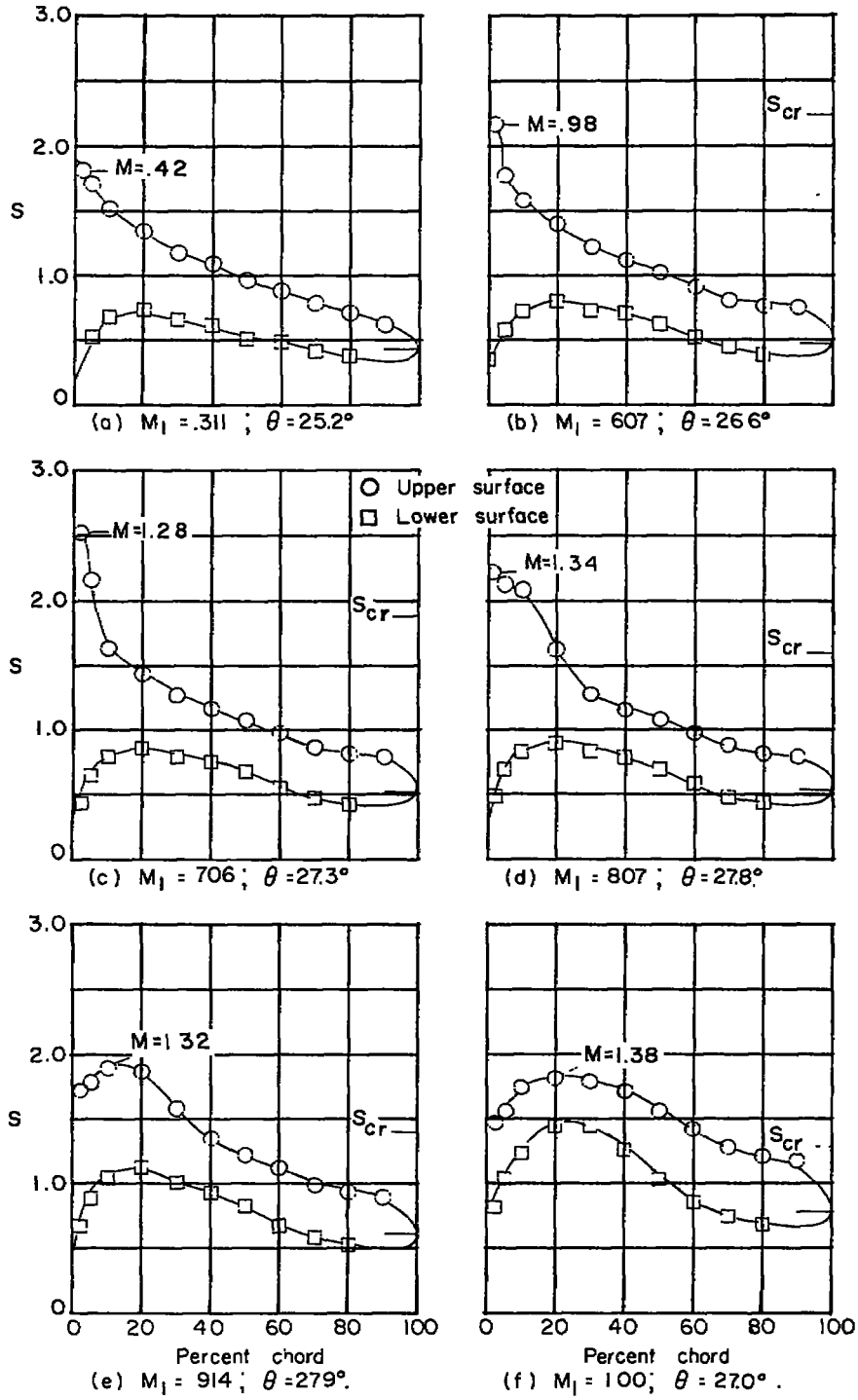

Figure 45.— Blade-surface pressure distributions and section characteristics for the cascade combination. β_1 = 60°; σ = 1.5 ; α = 22.5°; and blade section, NACA 65-$(12A_2I_{8b})$10.

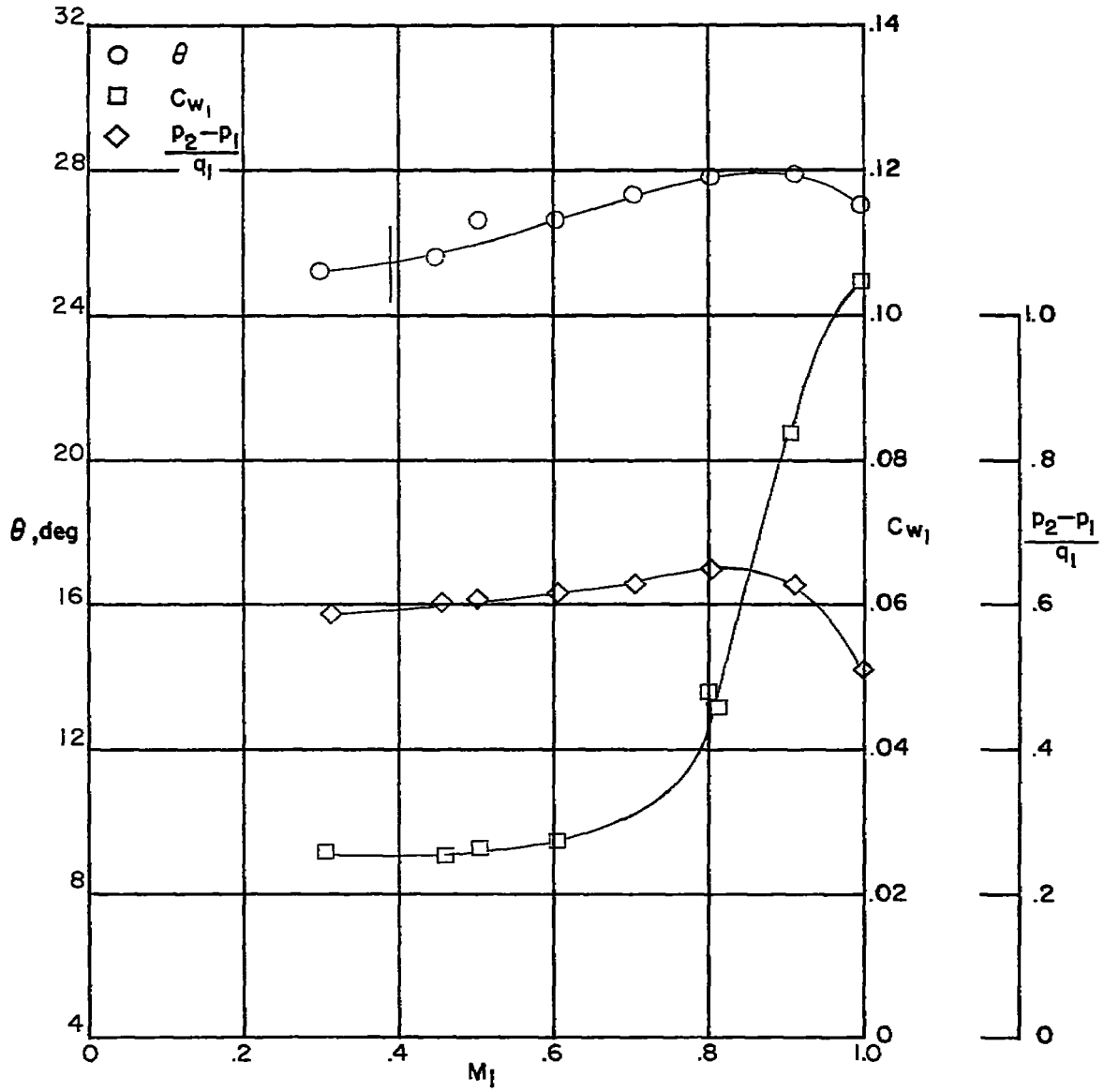

(g) Section characteristics. Tests are two dimensional for Mach numbers up to the vertical line.

Figure 45.— Concluded.

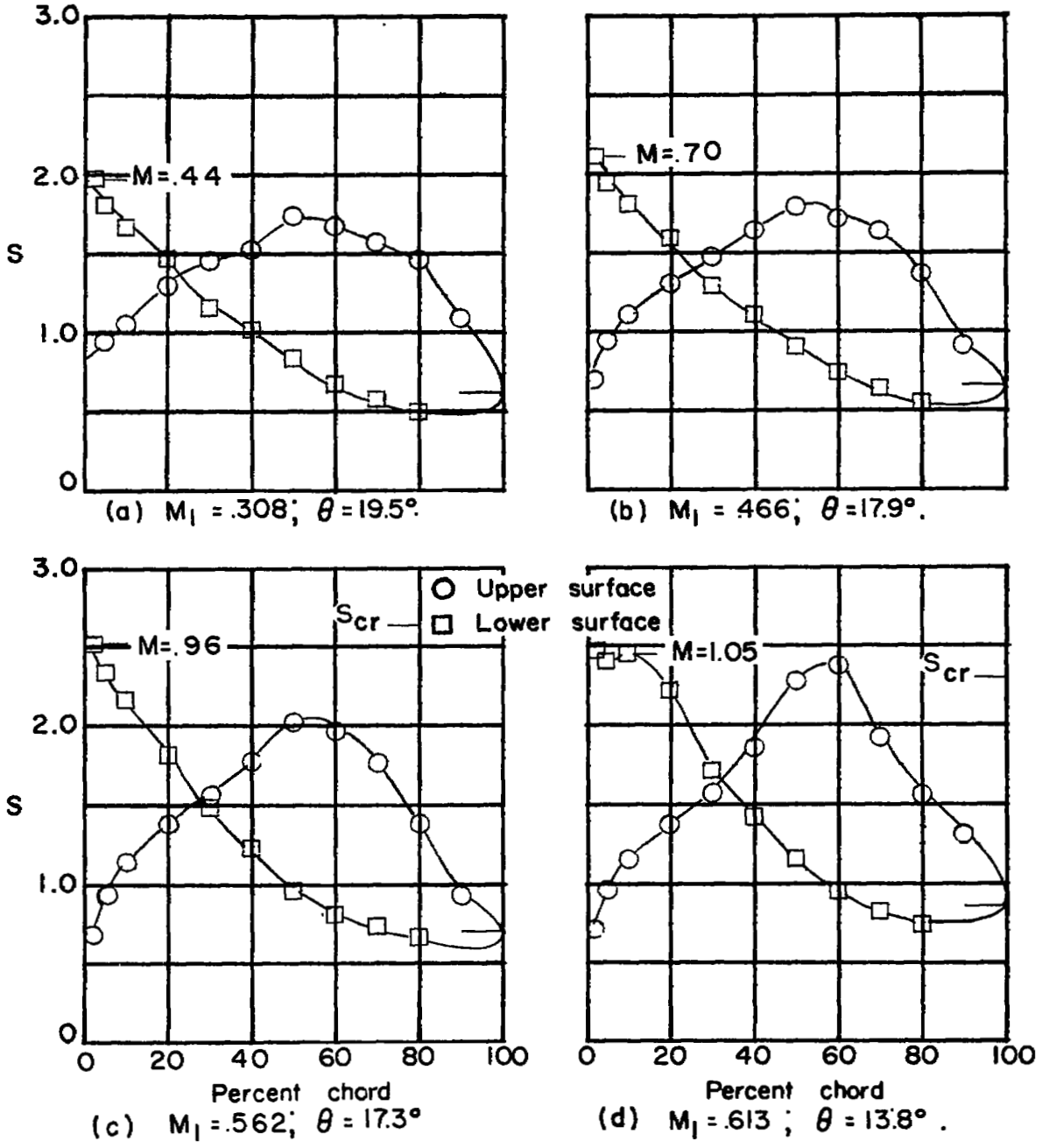

Figure 46.— Blade-surface pressure distributions and section characteristics for the cascade combination. $\beta_1 = 45°$; $\sigma = 1.5$; $\alpha = 7.5°$; and blade section, NACA 65-($12A_2I_{8b}$)10.

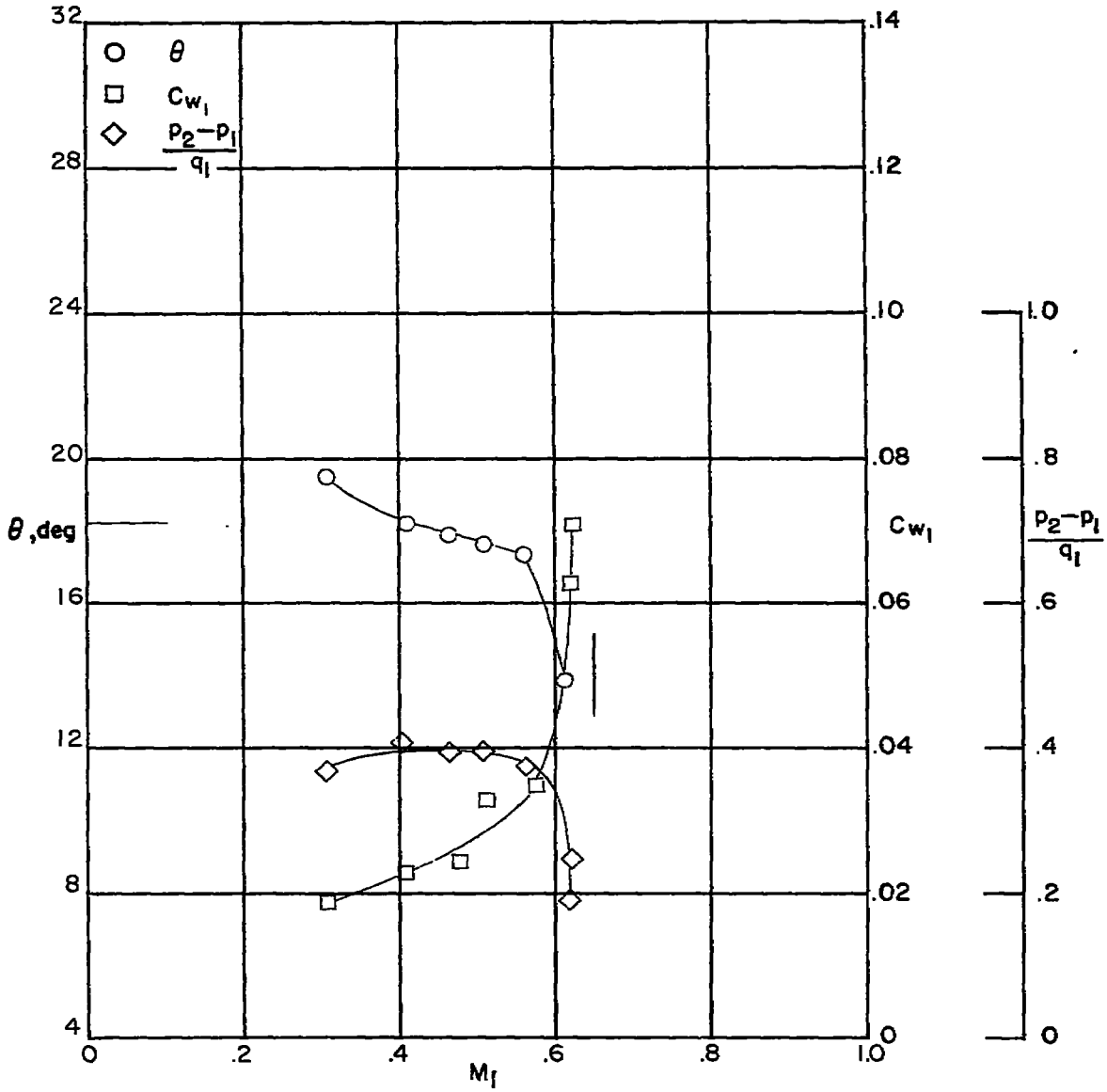

(e) Section characteristics. Tests are two dimensional for Mach numbers up to the vertical line. The horizontal line indicates low-speed turning angle given in reference 2

Figure 46.— Concluded.

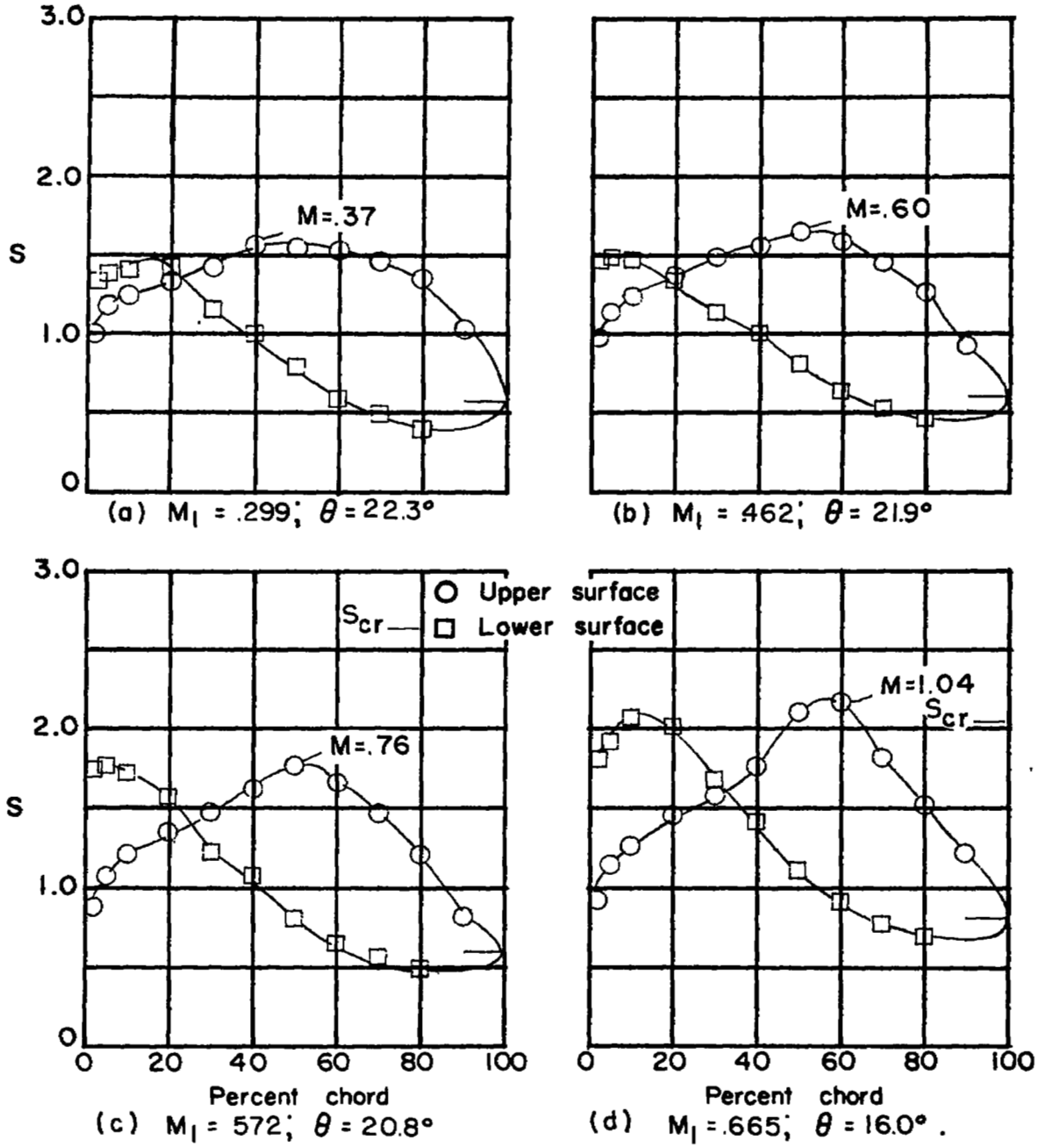

Figure 47.— Blade-surface pressure distributions and section characteristics for the cascade combination. $\beta_1 = 45°$; $\sigma = 1.5$; $\alpha = 10.5°$; and blade section, NACA 65-($12A_2I_{8b}$)10.

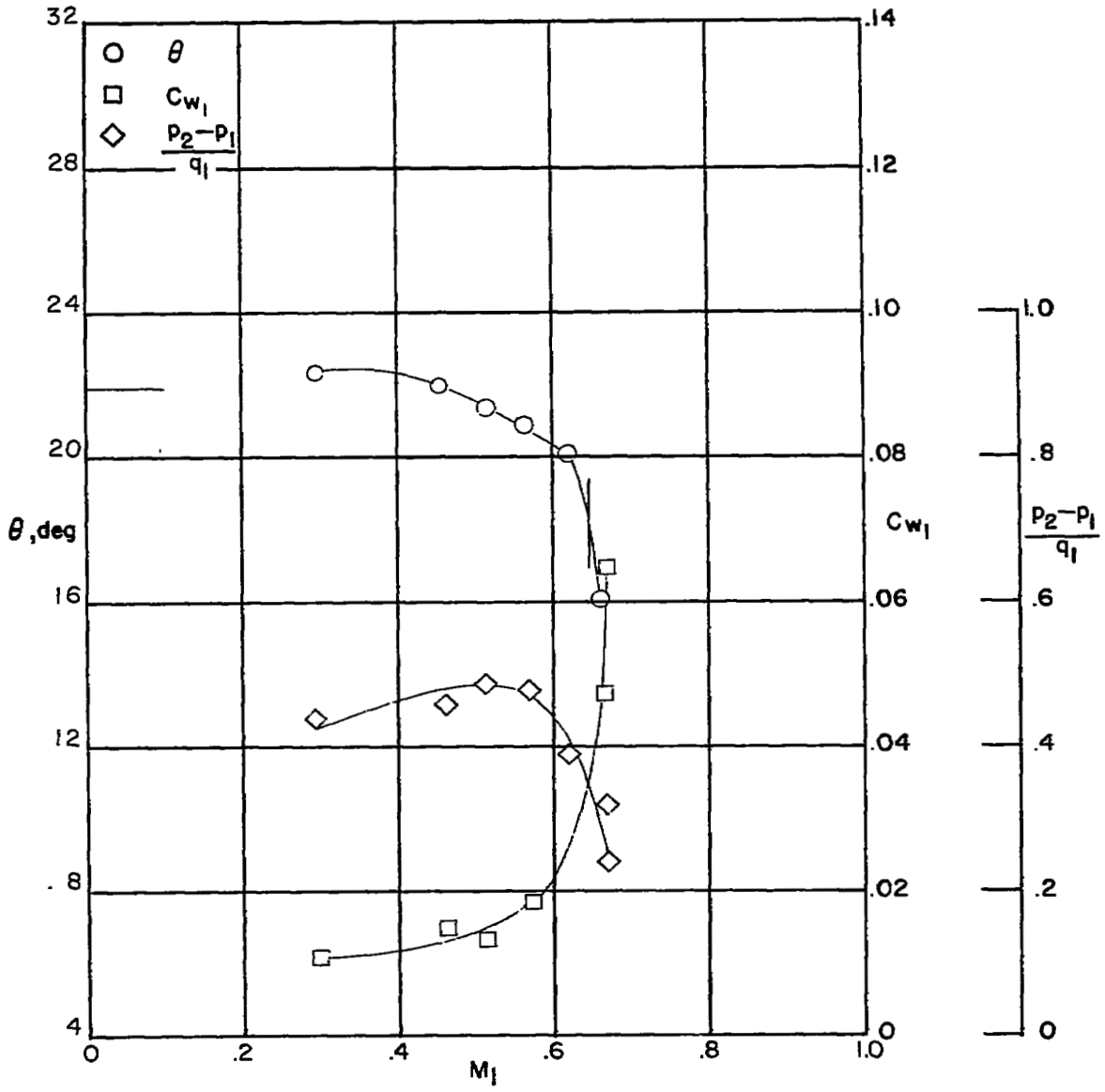

(e) Section characteristics. Tests are two dimensional for Mach numbers up to the vertical line. The horizontal line indicates low-speed turning angle given in reference 2.

Figure 47 .— Concluded.

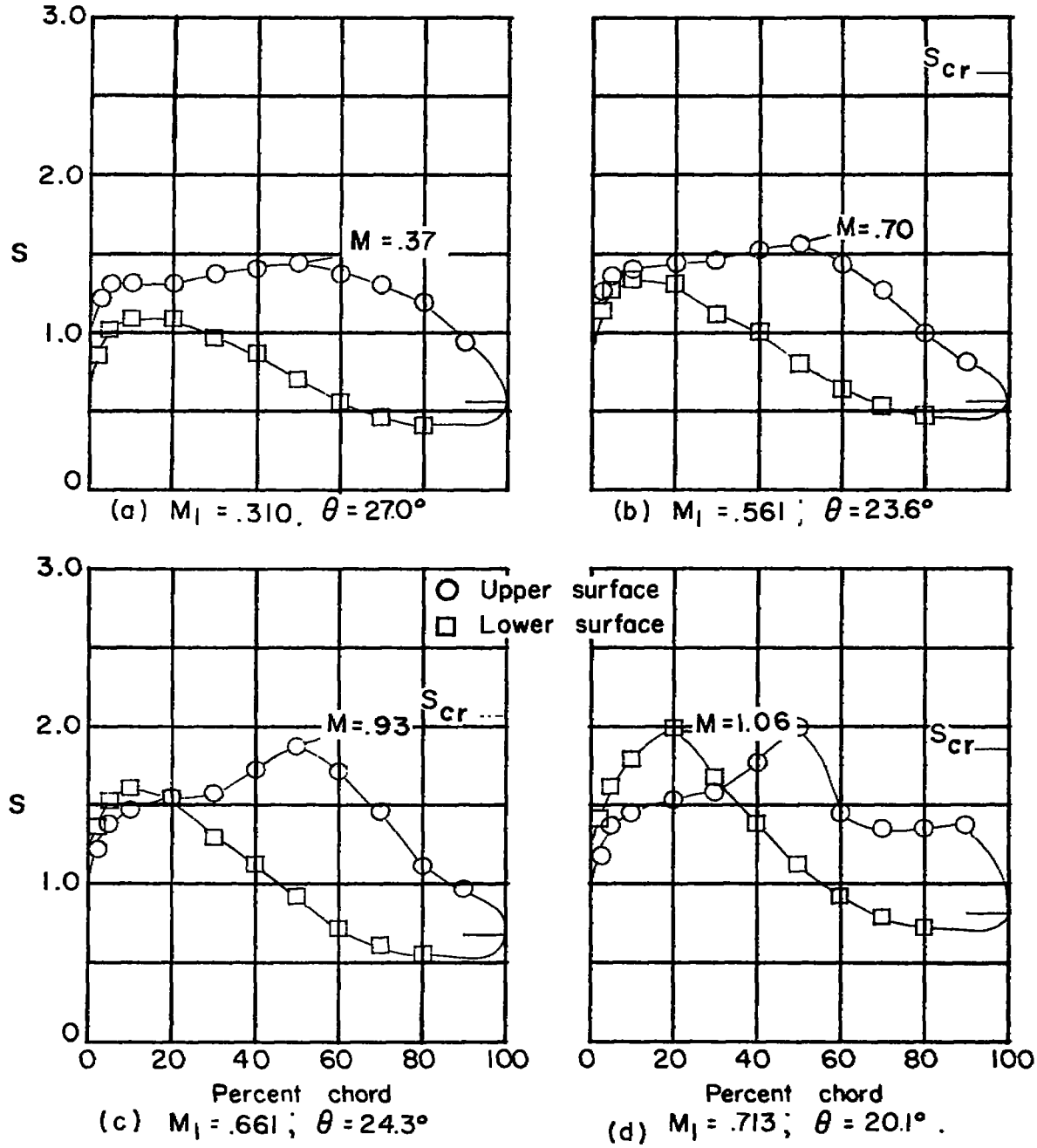

Figure 48.— Blade-surface pressure distributions and section characteristics for the cascade combination. β_1 = 45°; σ = 1.5; α = 13.5°; and blade section, NACA 65-($12A_2I_{8b}$)10.

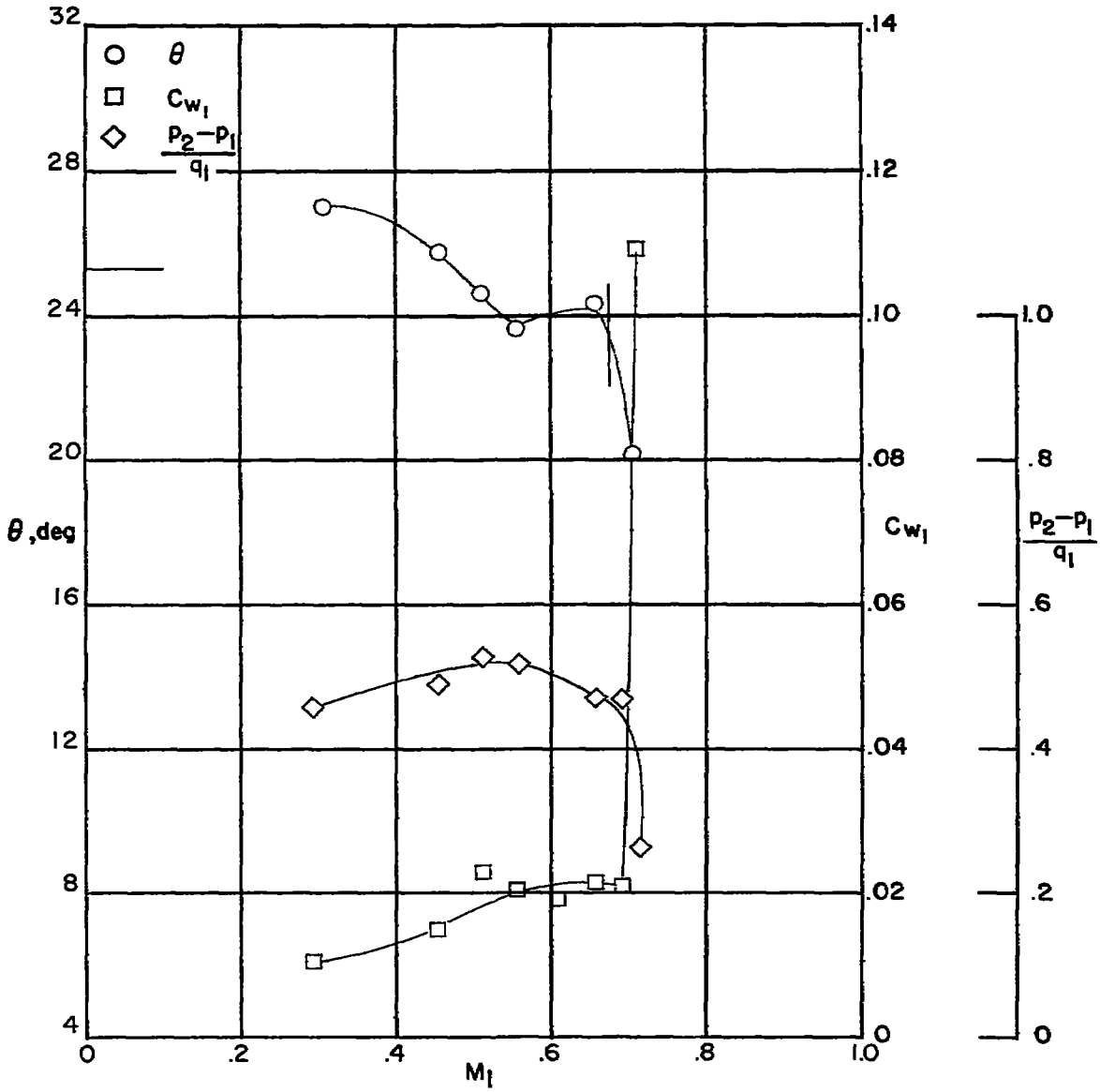

(e) Section characteristics. Tests are two dimensional for Mach numbers up to the vertical line. The horizontal line indicates low-speed turning angle given in reference 2

Figure 48.— Concluded.

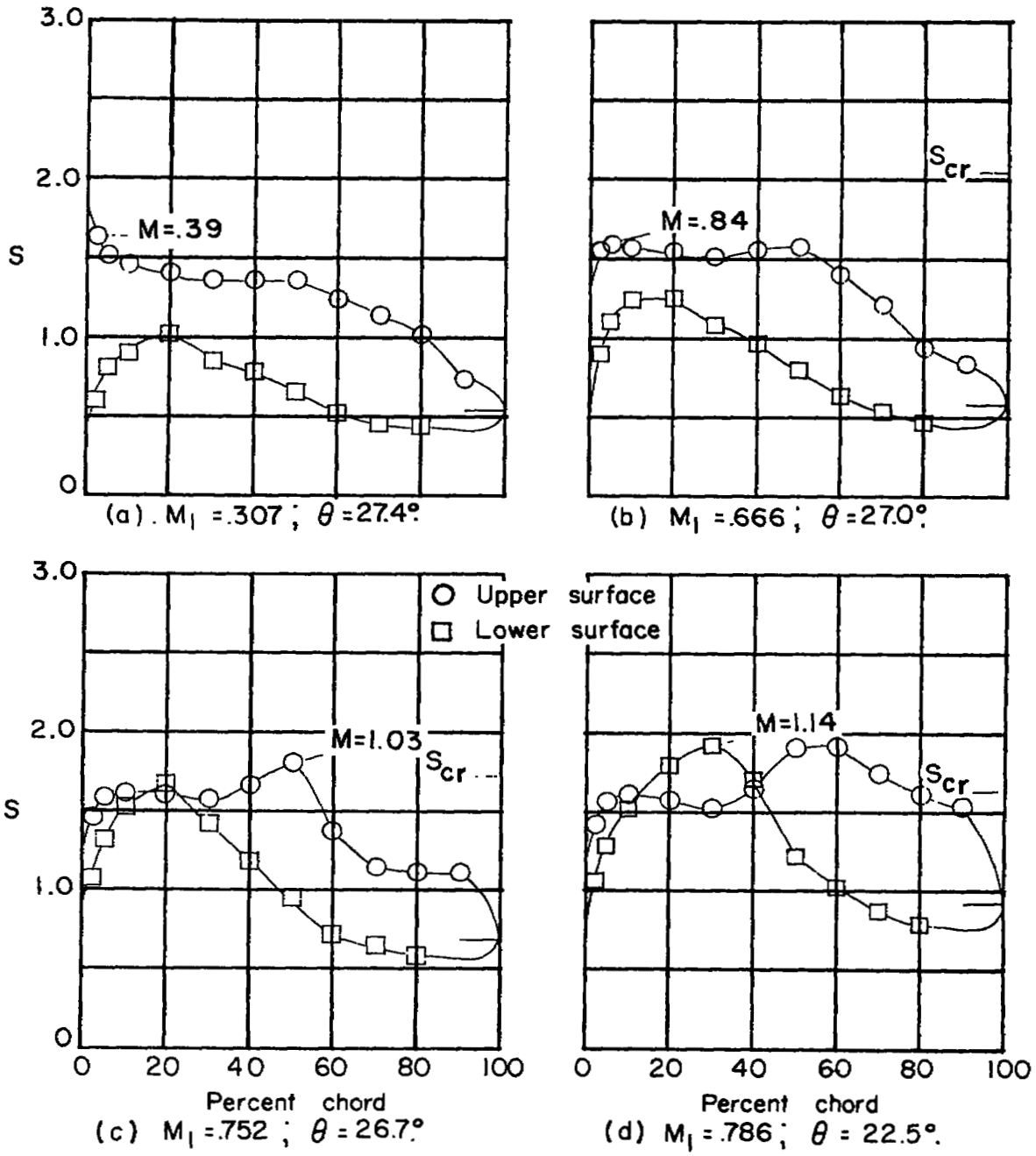

Figure 49 .— Blade-surface pressure distributions and section characteristics for the cascade combination. β_1 = 45°; σ = 1.5 ; α ≈16.5°; and blade section, NACA 65-($12A_2I_{8b}$)10.

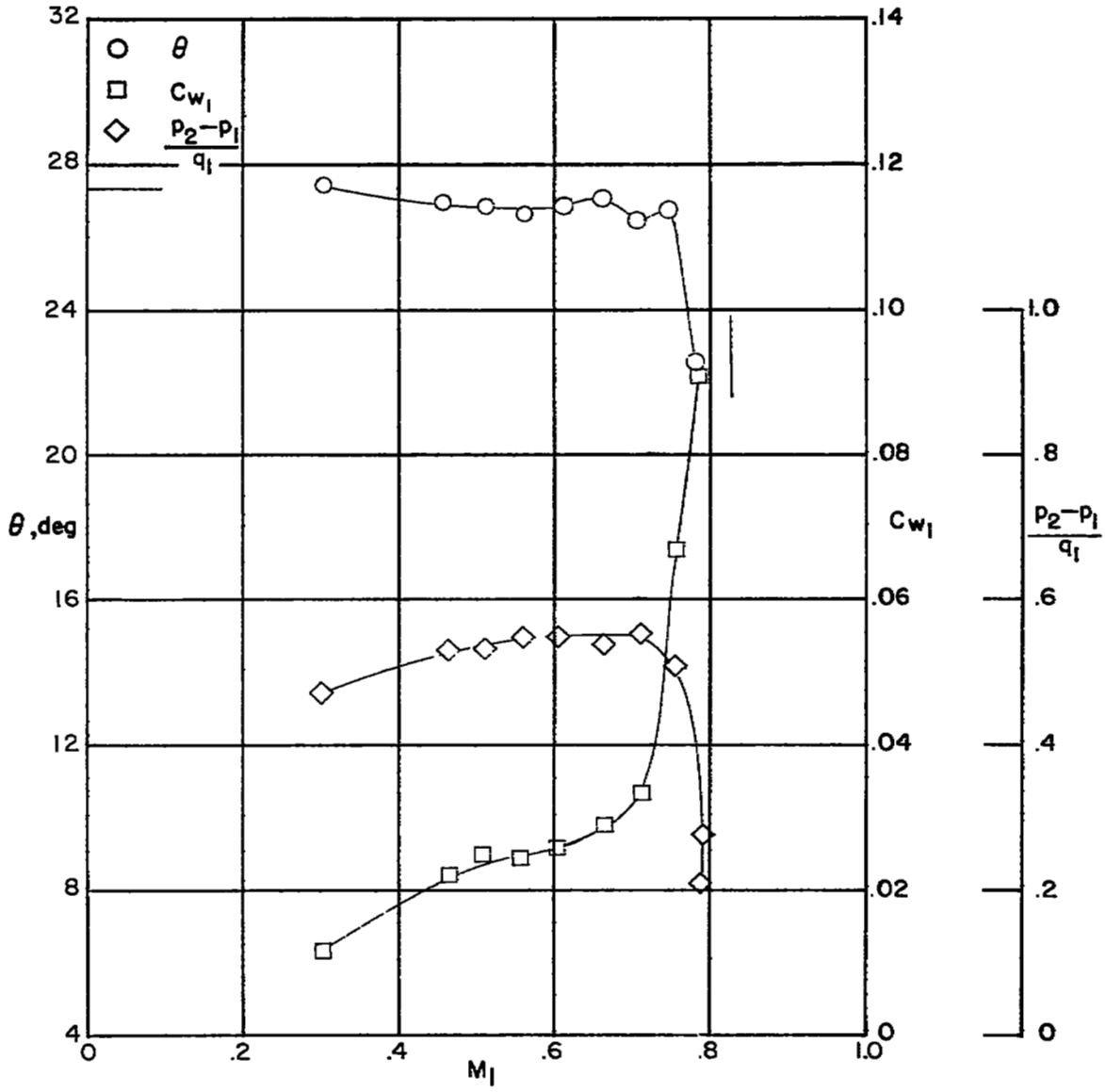

(e) Section characteristics. Tests are two dimensional for Mach numbers up to the vertical line. The horizontal line indicates low-speed turning angle given in reference 2.

Figure 49 .— Concluded.

[redacted]

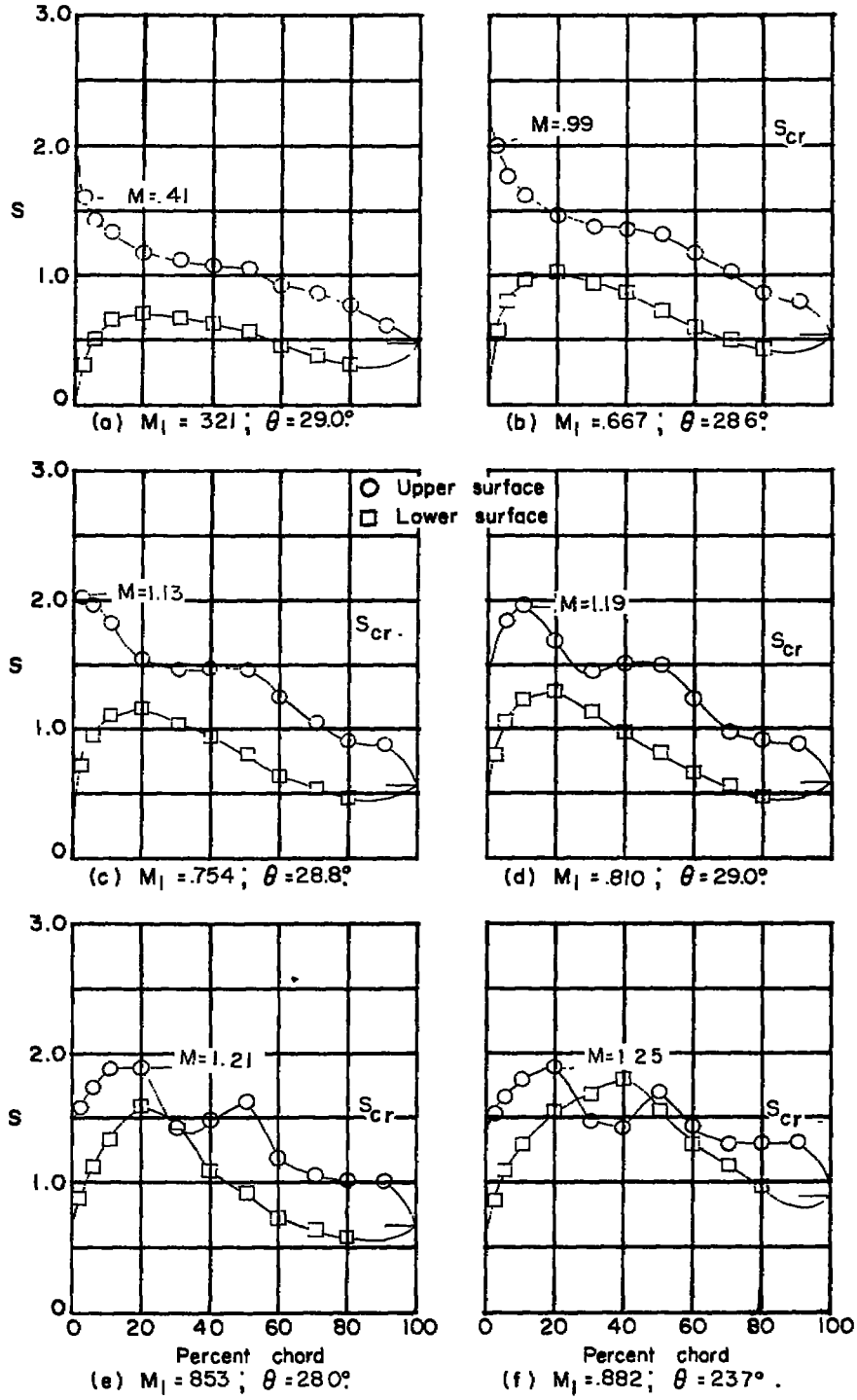

Figure 50.— Blade-surface pressure distributions and section characteristics for the cascade combination. $\beta_1 = 45°$; $\sigma = 1.5$; $\alpha = 19.5°$; and blade section, NACA 65-(12$A_2$$I_{8b}$)10.

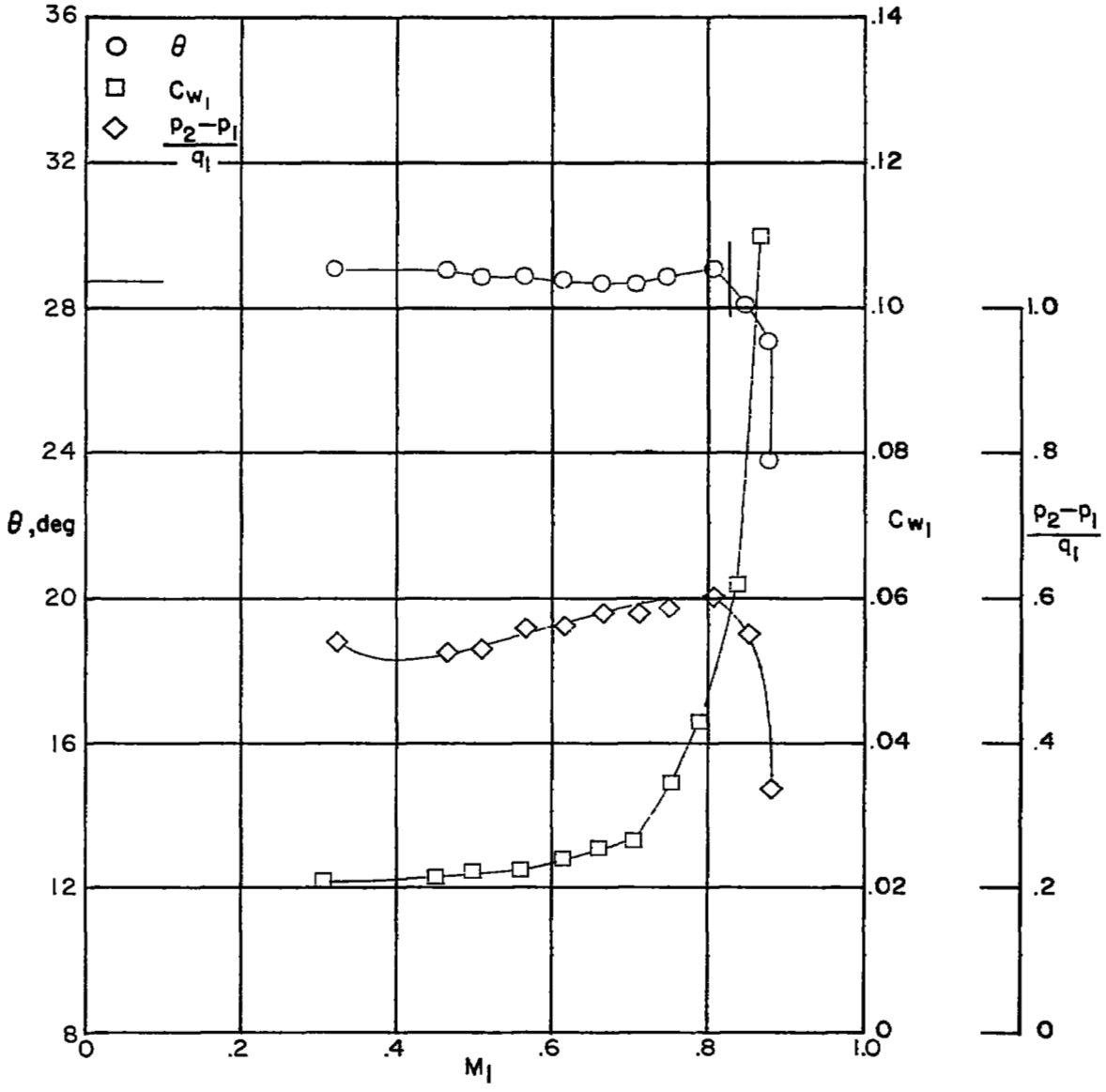

(g) Section characteristics. Tests are two dimensional for Mach numbers up to the vertical line. The horizontal line indicates low-speed turning angle given in reference 2

Figure 50 .— Concluded.

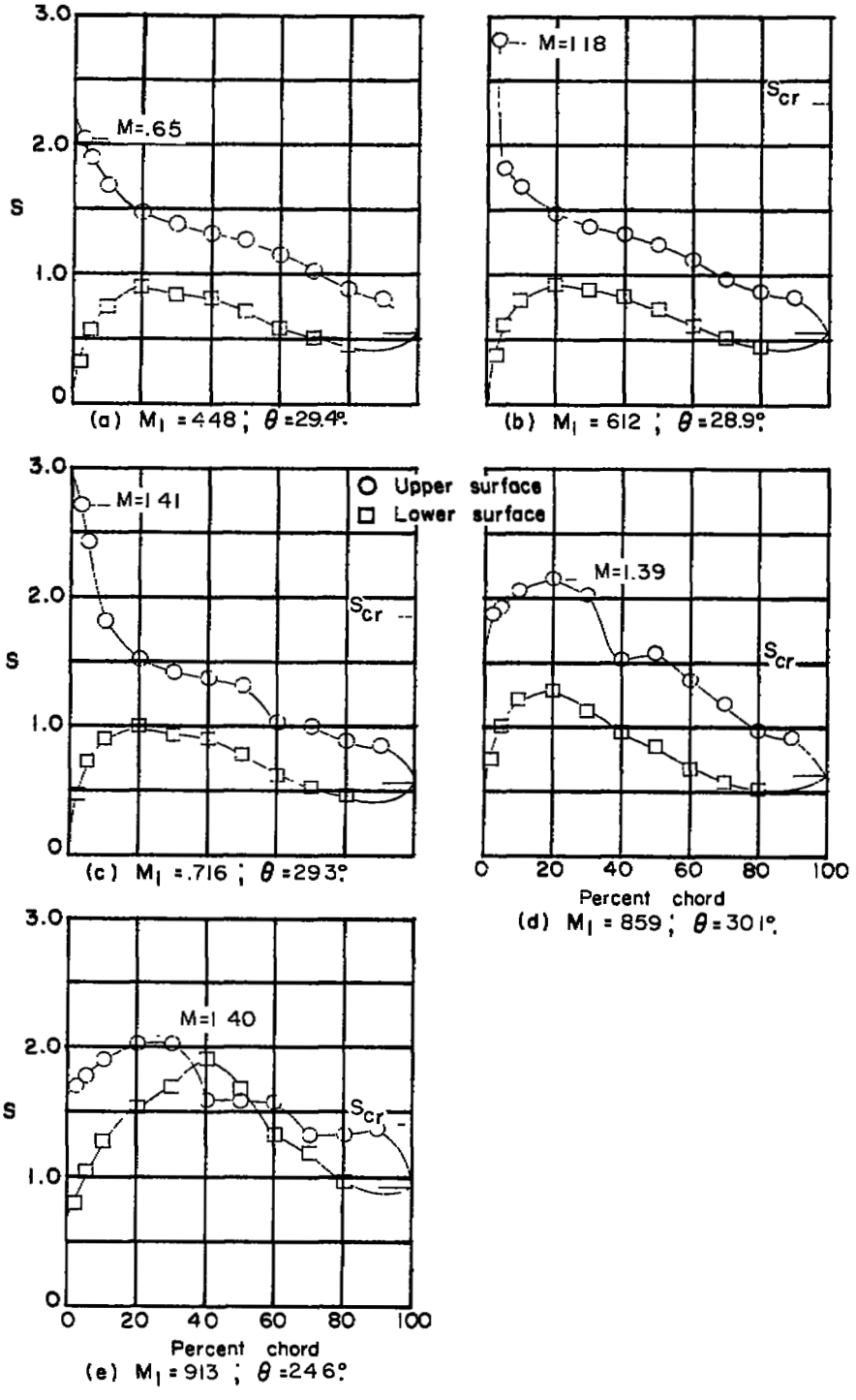

Figure 51 .— Blade-surface pressure distributions and section characteristics for the cascade combination $\beta_1 = 45°$, $\sigma = 1.5$, $\alpha = 22.5°$, and blade section, NACA $65\text{-}(12A_2I_{8b})10$.

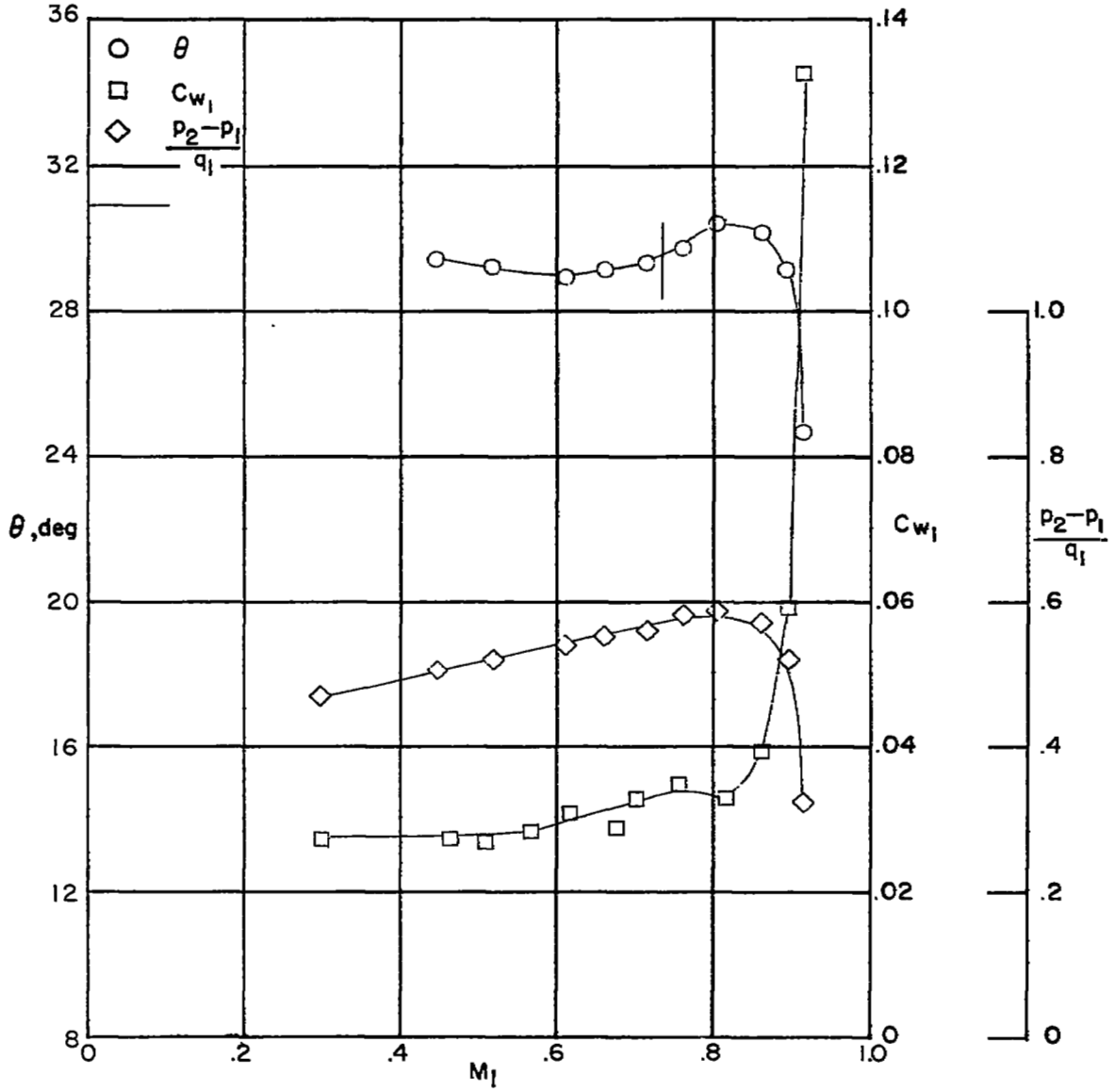

(f) Section characteristics. Tests are two dimensional for Mach numbers up to the vertical line The horizontal line indicates low-speed turning angle given in reference 2

Figure 51 .— Concluded

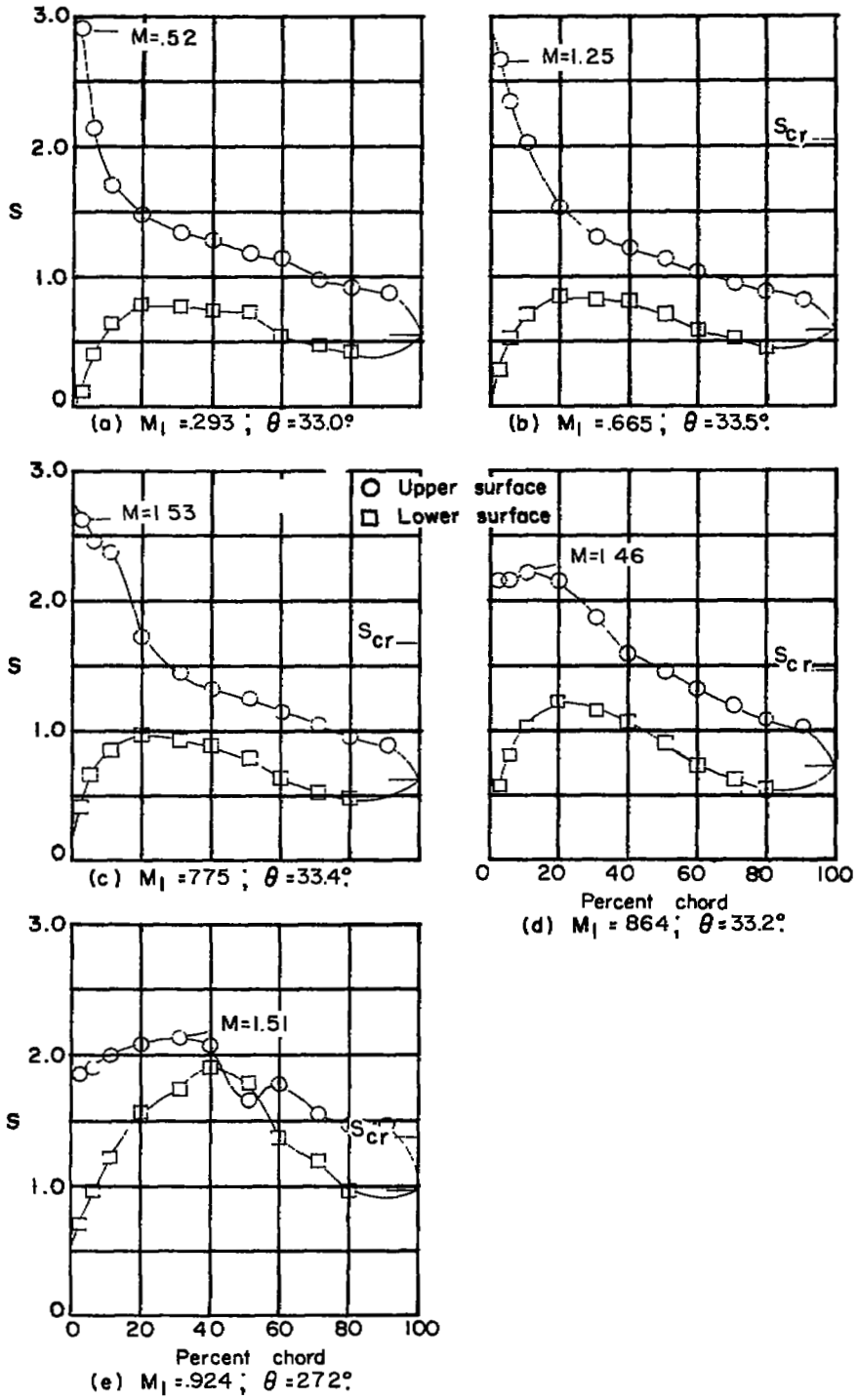

Figure 52 .— Blade-surface pressure distributions and section characteristics for the cascade combination $\beta_1 = 45°$, $\sigma = 1.5$, $\alpha = 25.5°$, and blade section, NACA 65-($12A_2I_{8b}$)10.

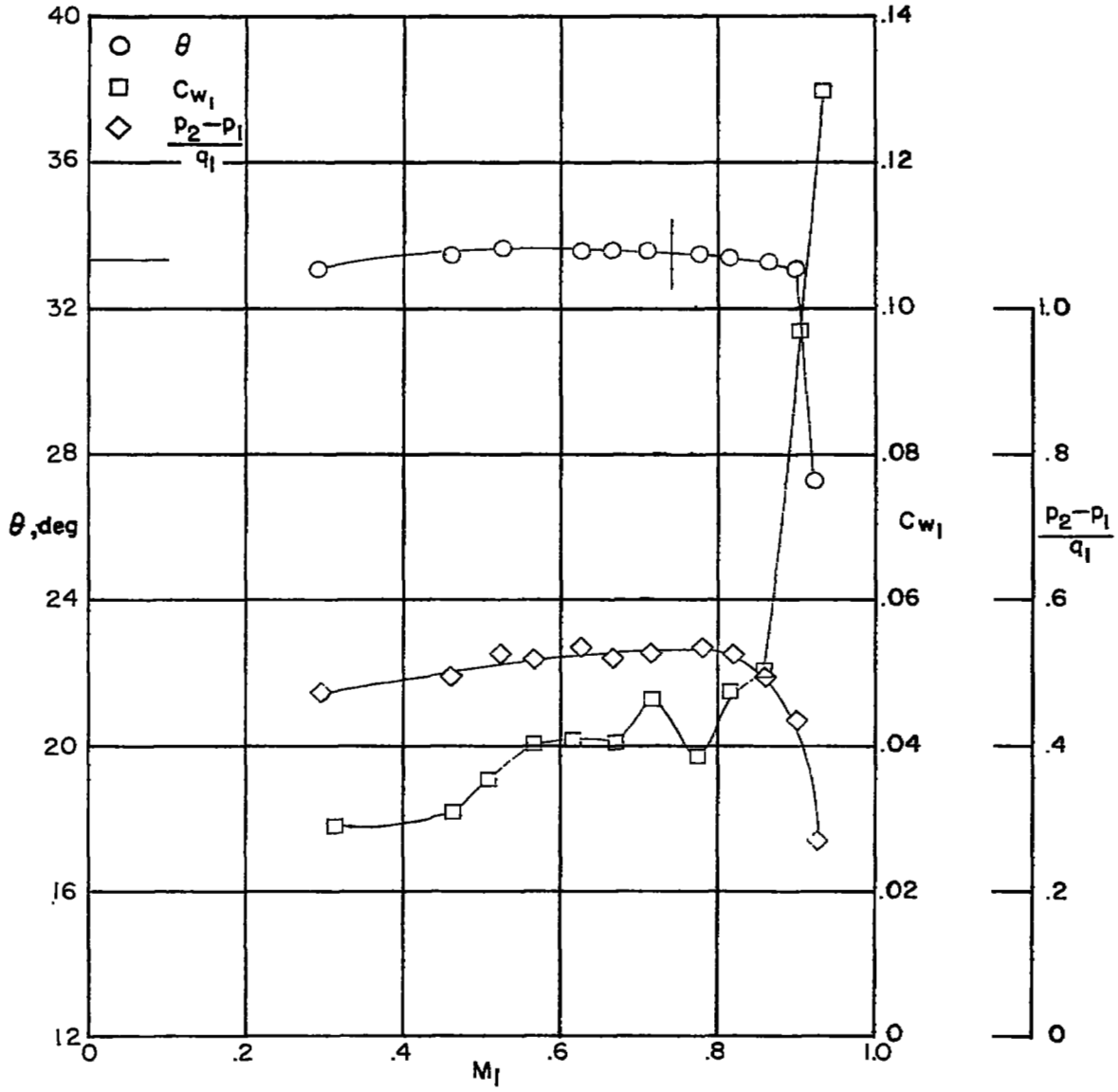

(f) Section characteristics. Tests are two dimensional for Mach numbers up to the vertical line. The horizontal line indicates low-speed turning angle given in reference 2

Figure 52.— Concluded

[redacted]

(a) M_1=0.670 (b) M_1=0.711.

(c) M_1=0.744 (d) M_1=0.816

(e) M_1=0.831. (f) M_1=0868

(g) M_1=0.881

L-90491

Figure 53.- Schlieren photographs and blade-section characteristics for a range of Mach numbers. Cascade of NACA 65-($12A_{10}$)10 compressor blades. $\beta = 60^\circ$; $\sigma = 1.0$; and $\alpha = 9.3^\circ$.

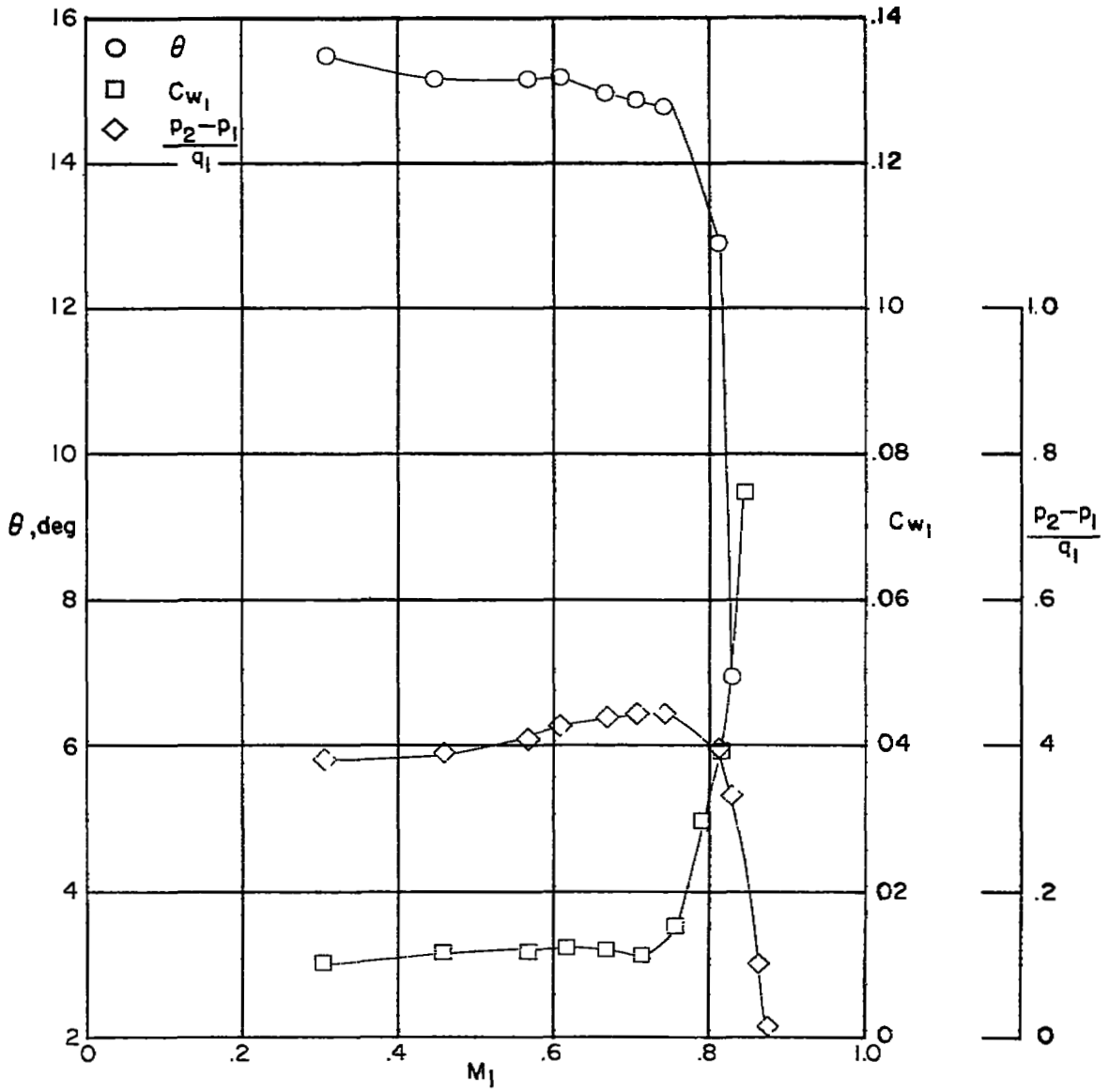

(h) Section characteristics.

Figure 53 .— Concluded.

(a) $M_1 = 0.716$ (b) $M_1 = 0.758$

(c) $M_1 = 0.796$ (d) $M_1 = 0.820$

(e) $M_1 = 0.849$ (f) $M_1 = 0.891$

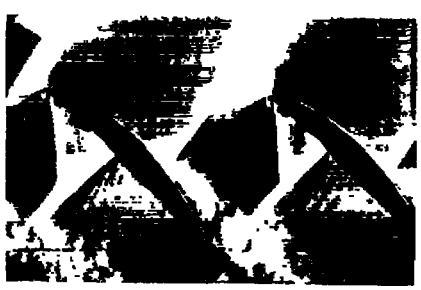

(g) $M_1 = 0.920$

L-90492

Figure 54.- Schlieren photographs and blade-section characteristics for a range of Mach numbers. Cascade of NACA 65-($12A_{10}$)10 compressor blades. $\beta = 60^\circ$; $\sigma = 1.0$; and $\alpha = 12.3^\circ$.

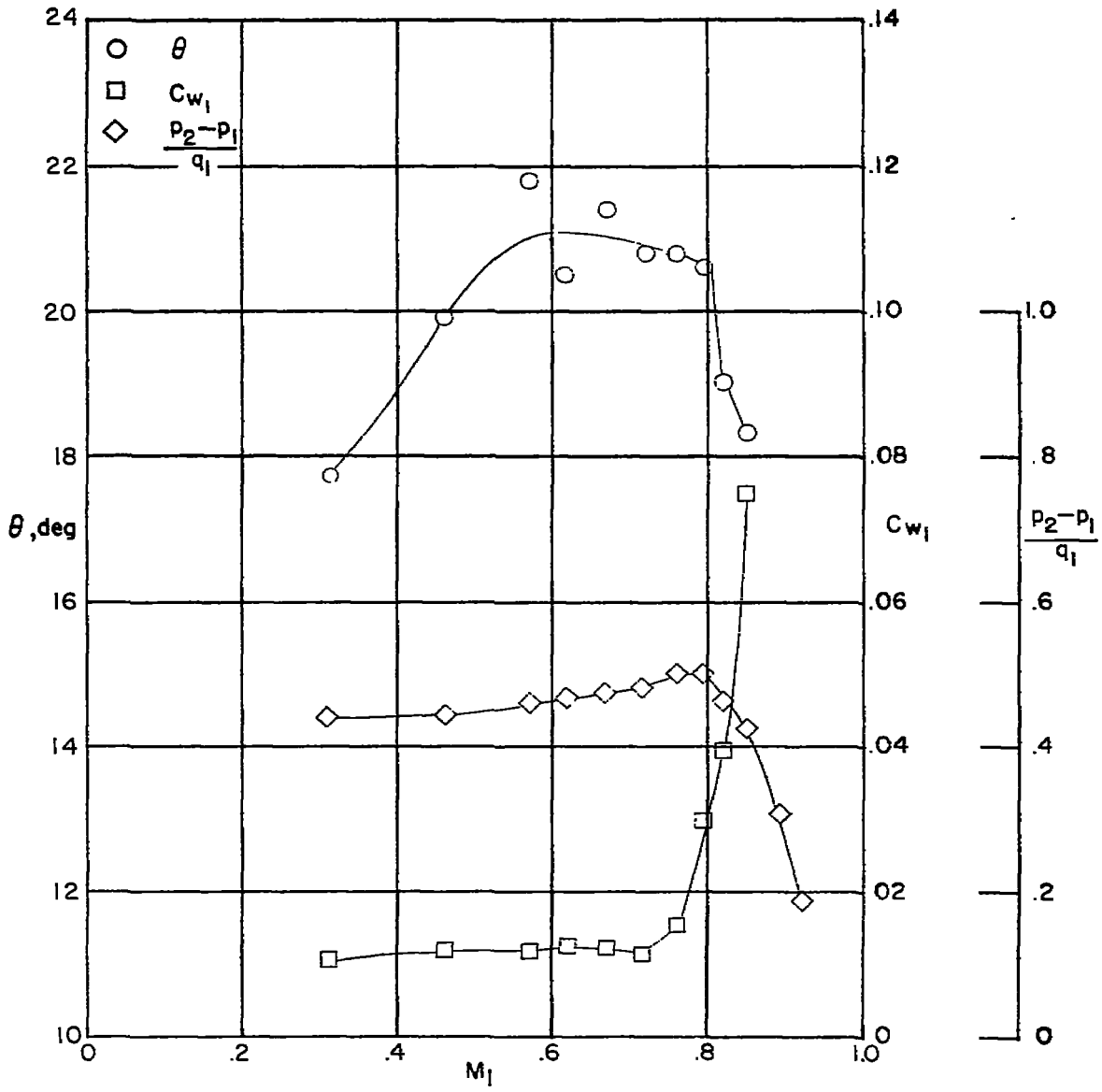

(h) Section characteristics.

Figure 54 .— Concluded.

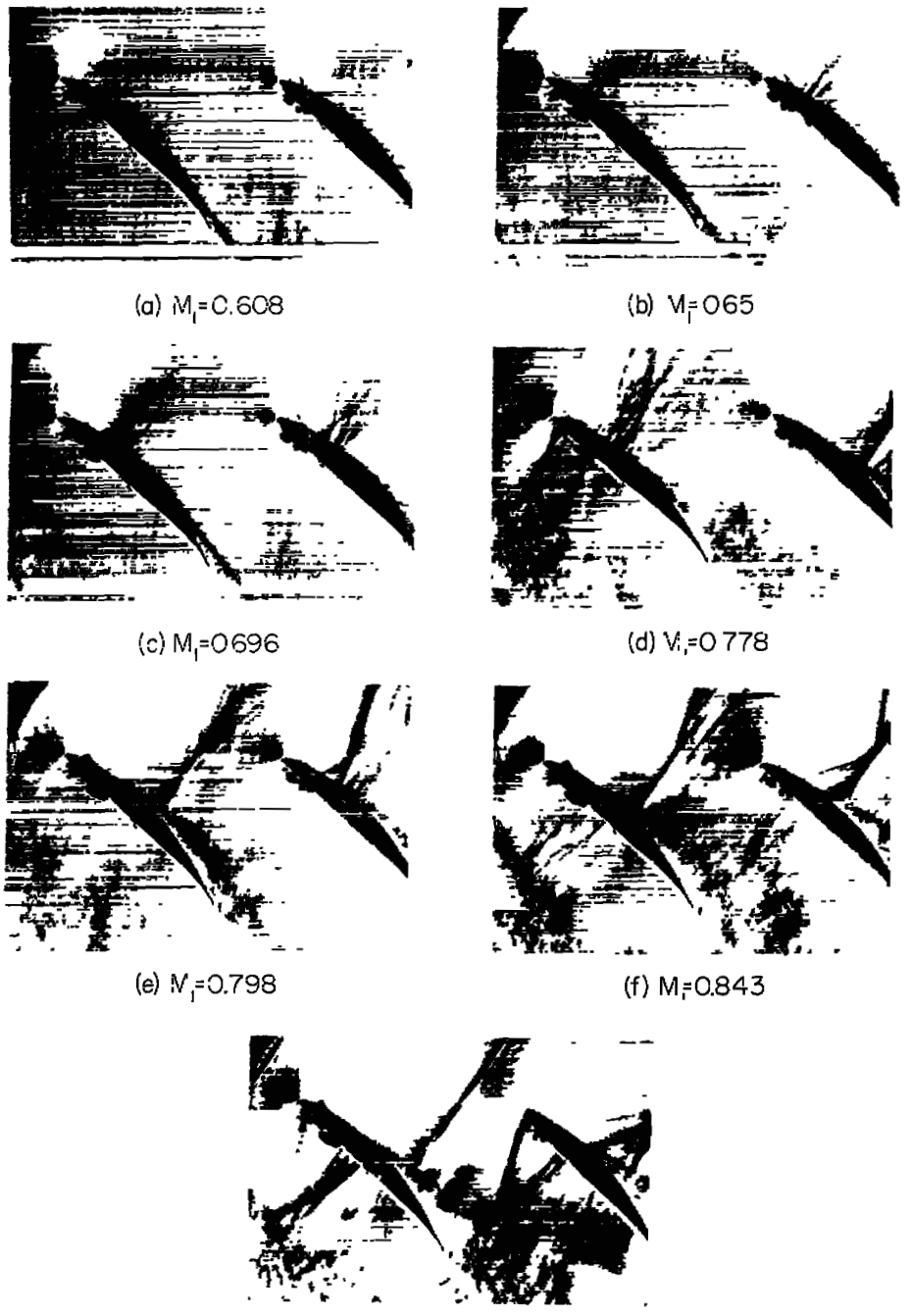

(a) M_1=0.608 (b) M_1=065

(c) M_1=0696 (d) M_1=0 778

(e) M_1=0.798 (f) M_1=0.843

(g) M_1=0.888

L-90493

Figure 55.- Schlieren photographs and blade-section characteristics for a range of Mach numbers. Cascade of NACA 65-$(12A_{10})$10 compressor blades. $\beta = 60^\circ$; $\sigma = 1.0$; and $\alpha = 15.3^\circ$.

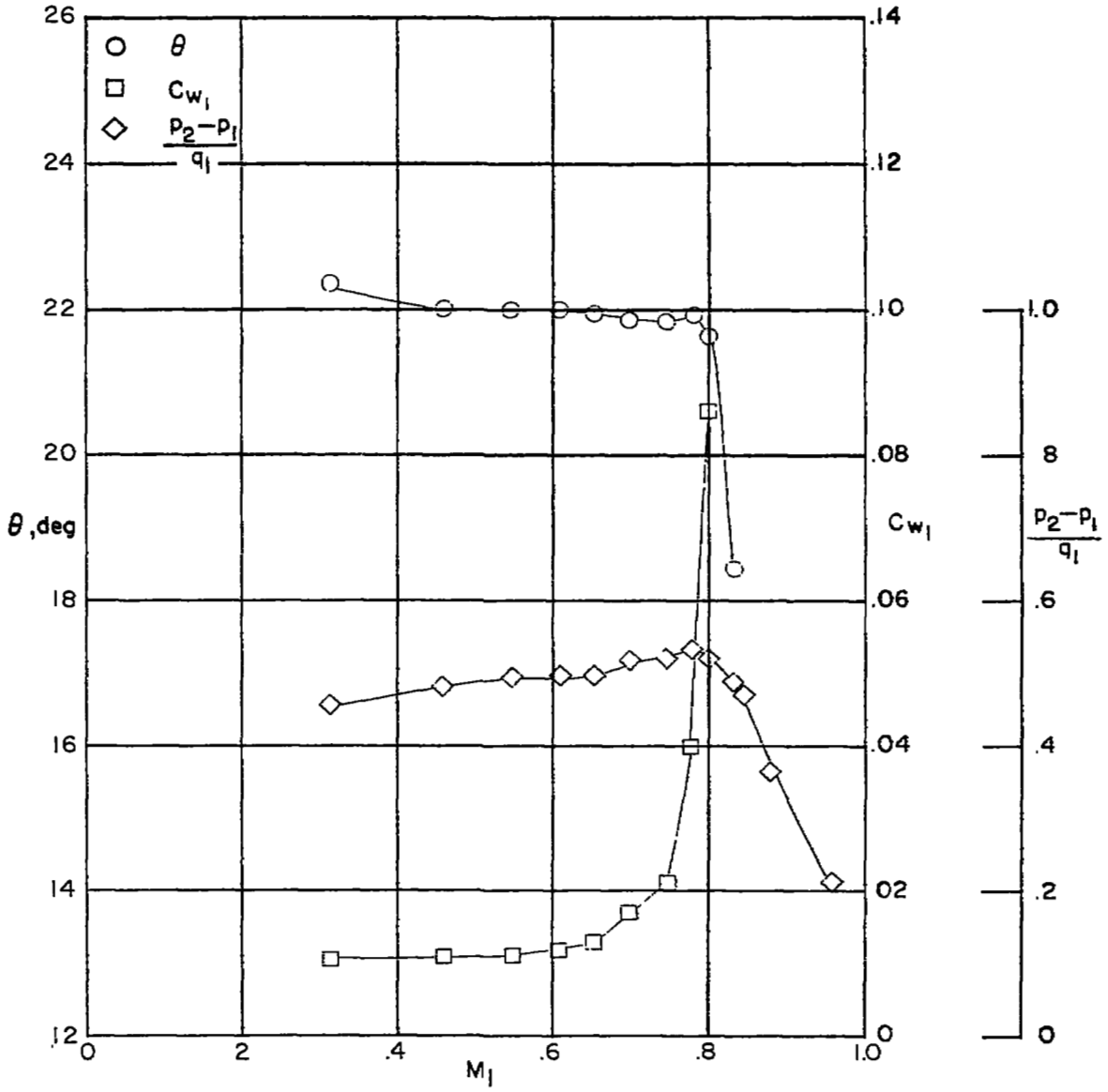

(h) Section characteristics.

Figure 55 .— Concluded.

[redacted]

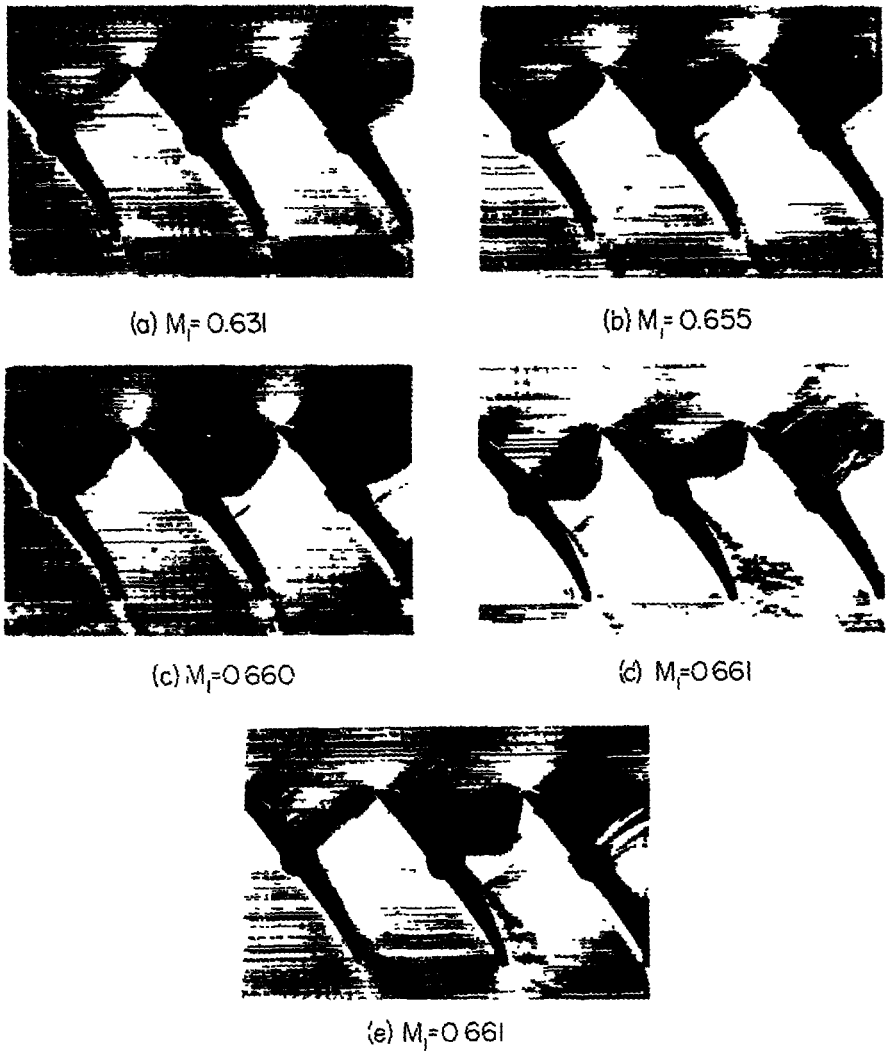

L-90494

Figure 56.- Schlieren photographs and blade-section characteristics for a range of Mach numbers. Cascade of NACA 65-($12A_{10}$)10 compressor blades. $\beta = 45^\circ$; $\sigma = 1.5$; and $\alpha = 8.5^\circ$.

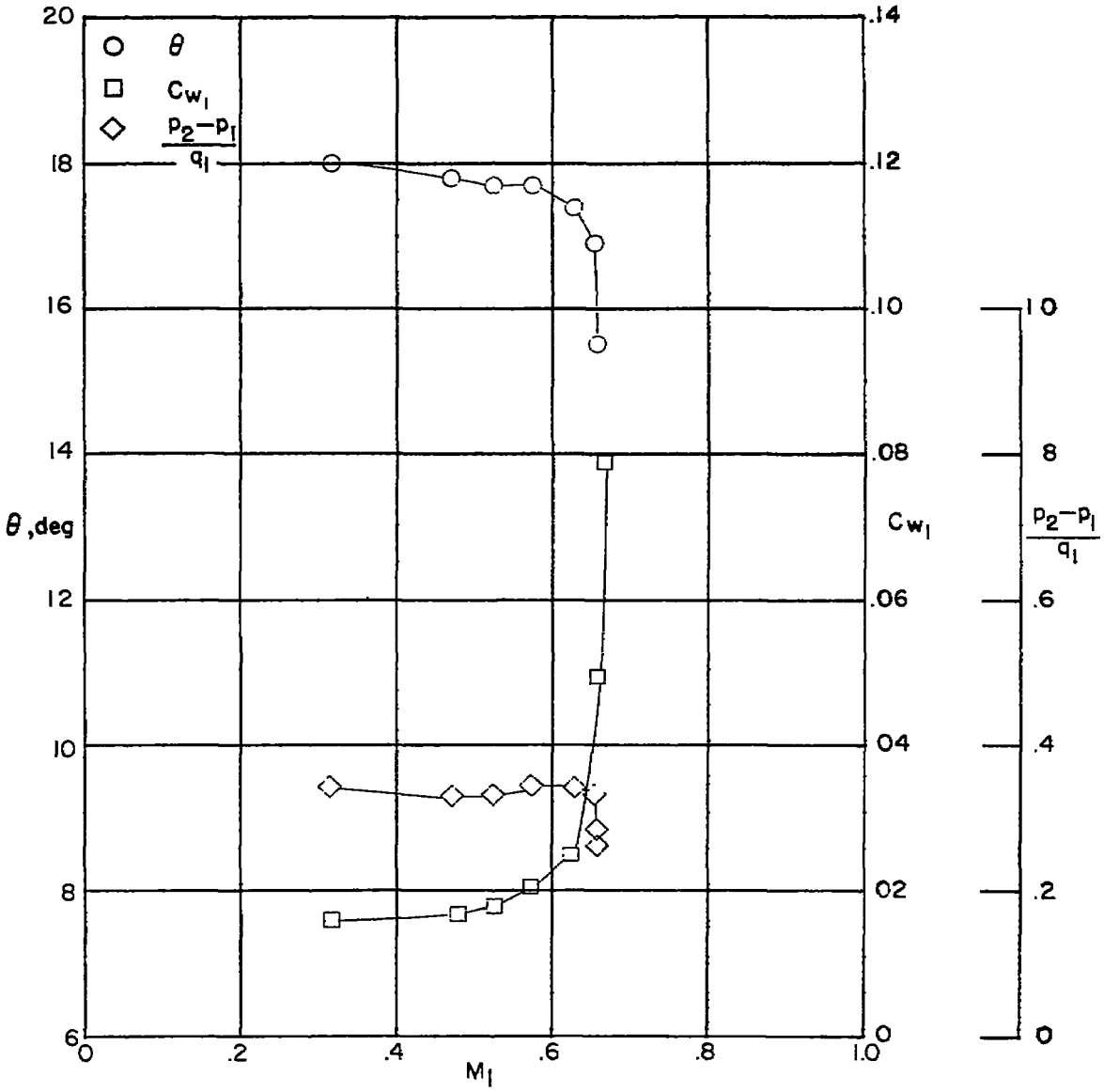

(f) Section characteristics.

Figure 56 .— Concluded.

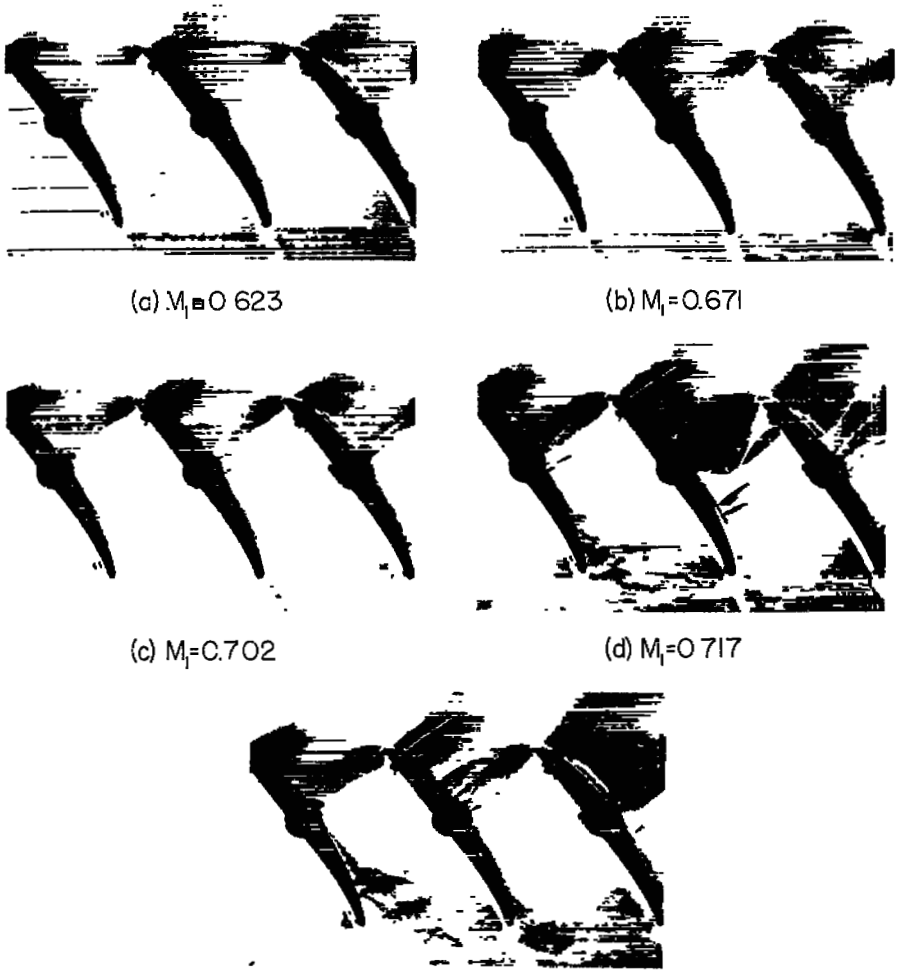

L-90495

Figure 57.- Schlieren photographs and blade-section characteristics for a range of Mach numbers. Cascade of NACA 65-($12A_{10}$)10 compressor blades. $\beta = 45^\circ$; $\sigma = 1.5$; and $\alpha = 11.5^\circ$.

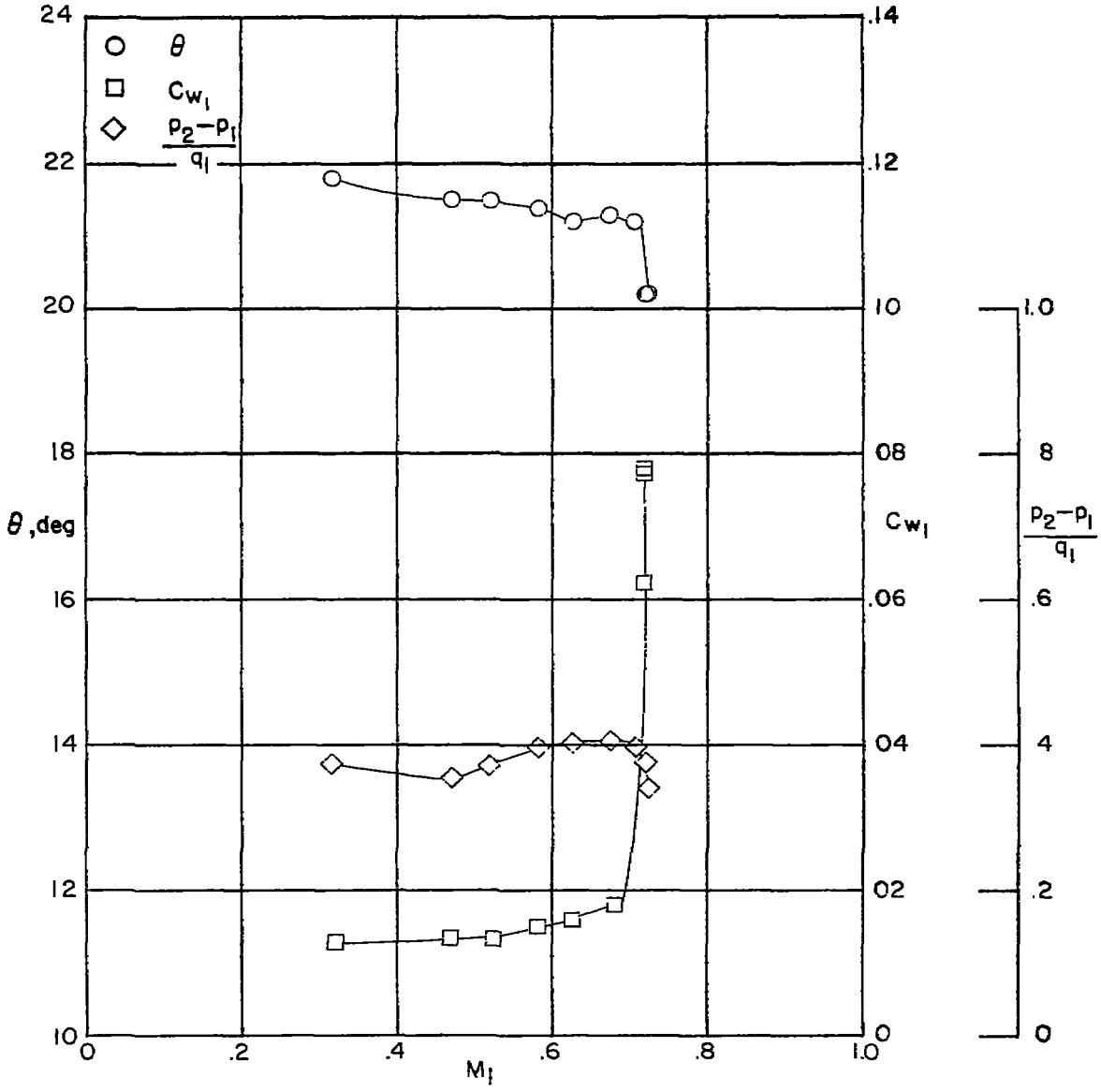

(f) Section characteristics.

Figure 57 .— Concluded.

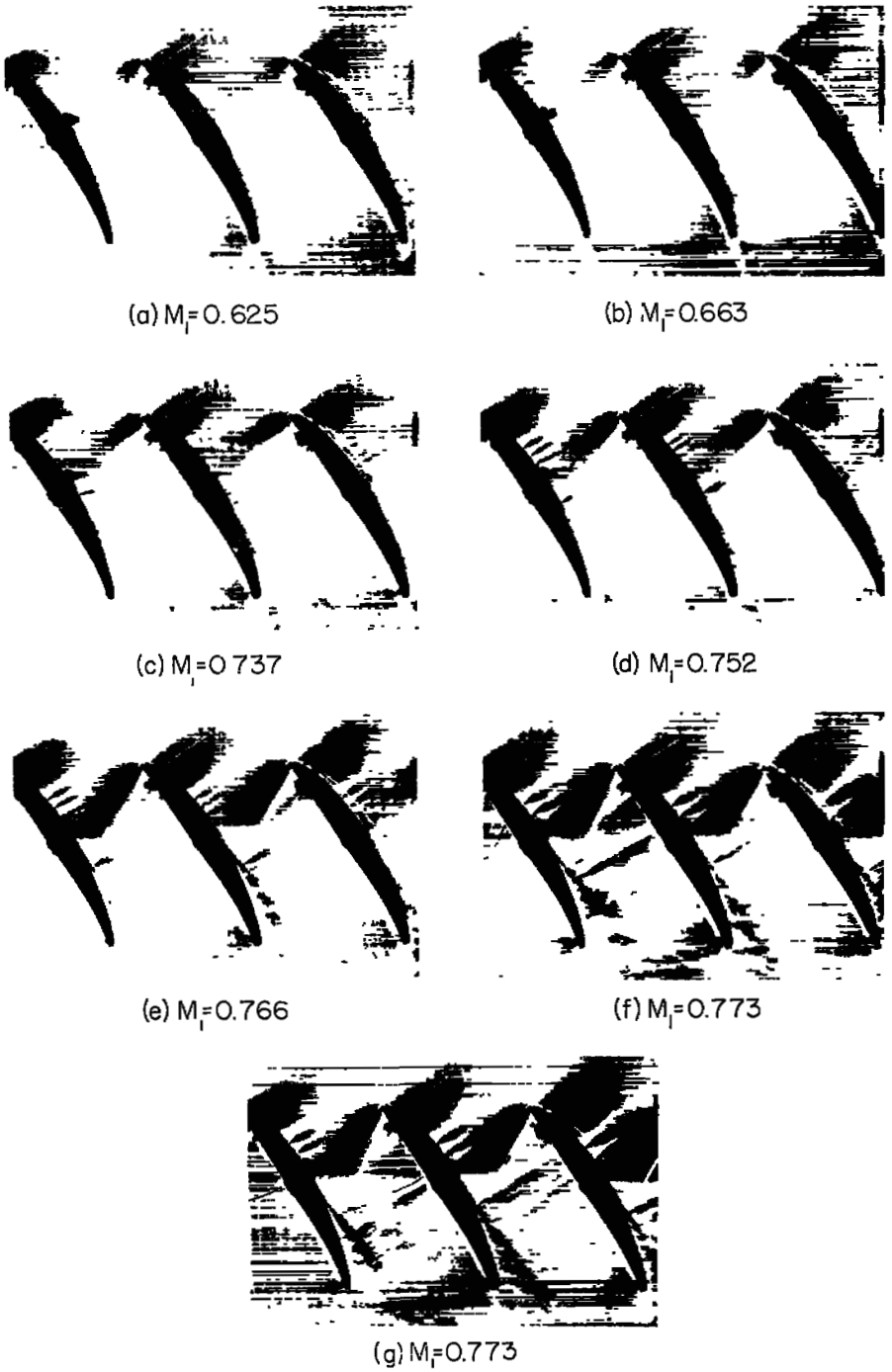

(a) $M_1 = 0.625$ (b) $M_1 = 0.663$

(c) $M_1 = 0.737$ (d) $M_1 = 0.752$

(e) $M_1 = 0.766$ (f) $M_1 = 0.773$

(g) $M_1 = 0.773$

L-90496

Figure 58.- Schlieren photographs and blade-section characteristics for a range of Mach numbers. Cascade of NACA 65-$(12A_{10})10$ compressor blades. $\beta = 45^\circ$; $\sigma = 1.5$; and $\alpha = 14.5^\circ$.

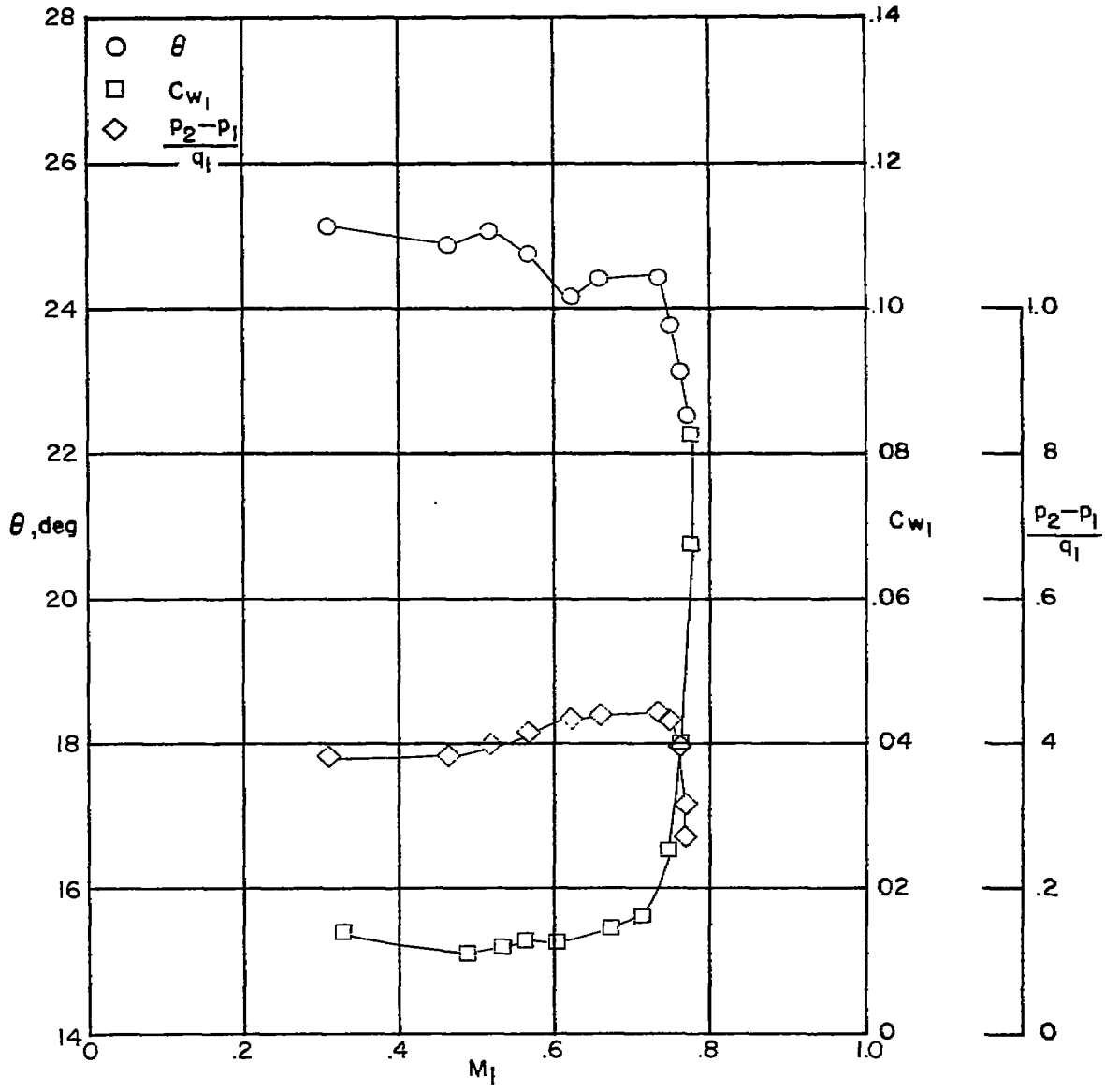

(h) Section characteristics.

Figure 58 .— Concluded.

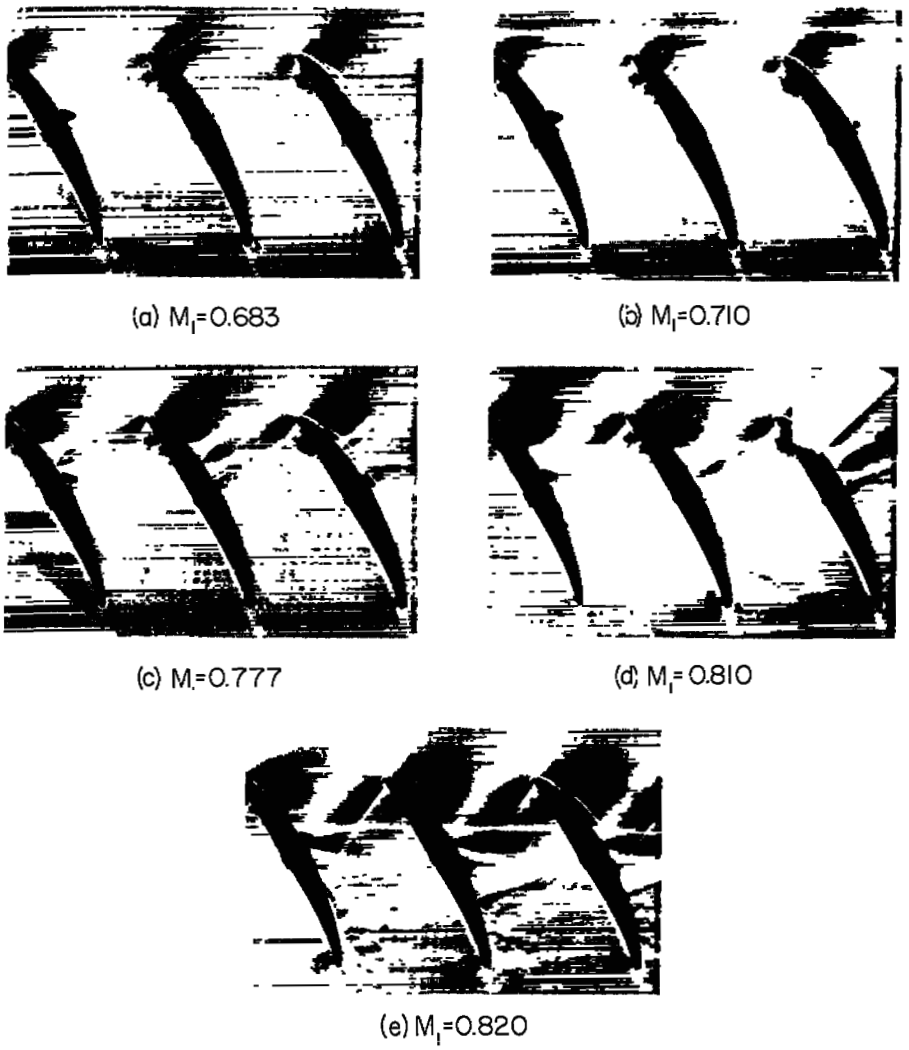

L-90497

Figure 59.- Schlieren photographs and blade-section characteristics for a range of Mach numbers. Cascade of NACA 65-$(12A_{10})$10 compressor blades. $\beta = 45^\circ$; $\sigma = 1.3$; and $\alpha = 17.5^\circ$.

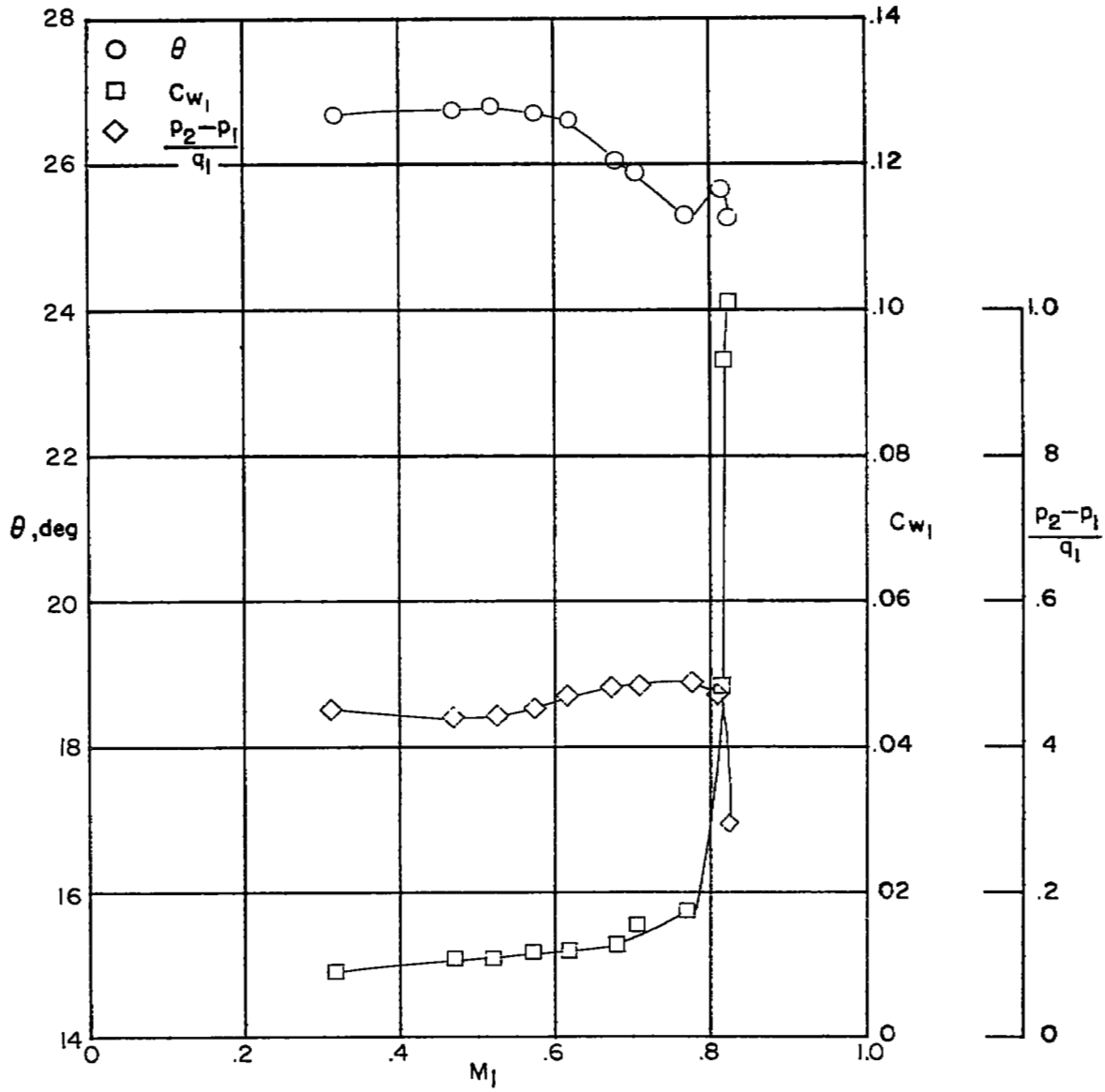

(f) Section characteristics.

Figure 59 .— Concluded.

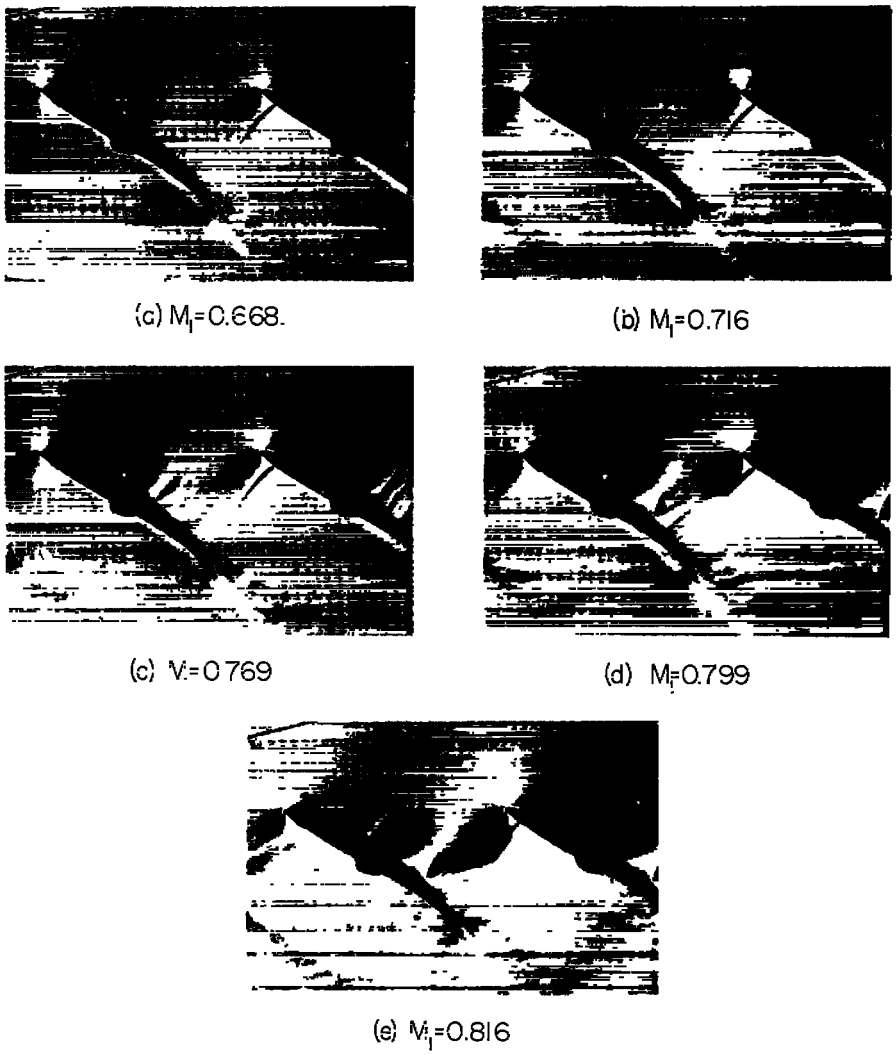

L-90498

Figure 60.- Schlieren photographs and blade-section characteristics for a range of Mach numbers. Cascade of NACA 65-$(12A_2I_{8b})$10 compressor blades. $\beta = 60^\circ$; $\sigma = 1.0$; and $\alpha = 8.1^\circ$.

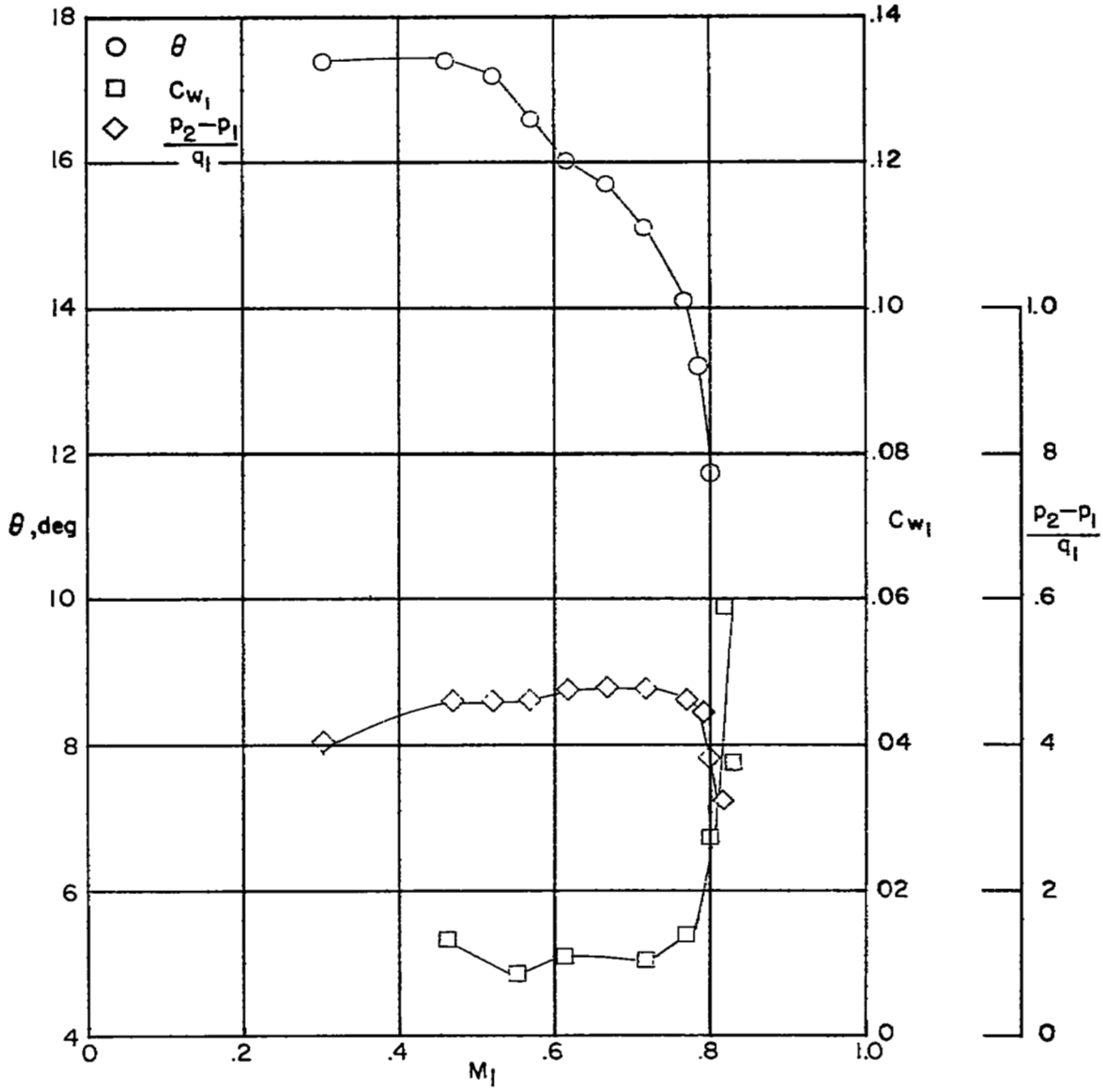

(f) Section characteristics.

Figure 60 .— Concluded.

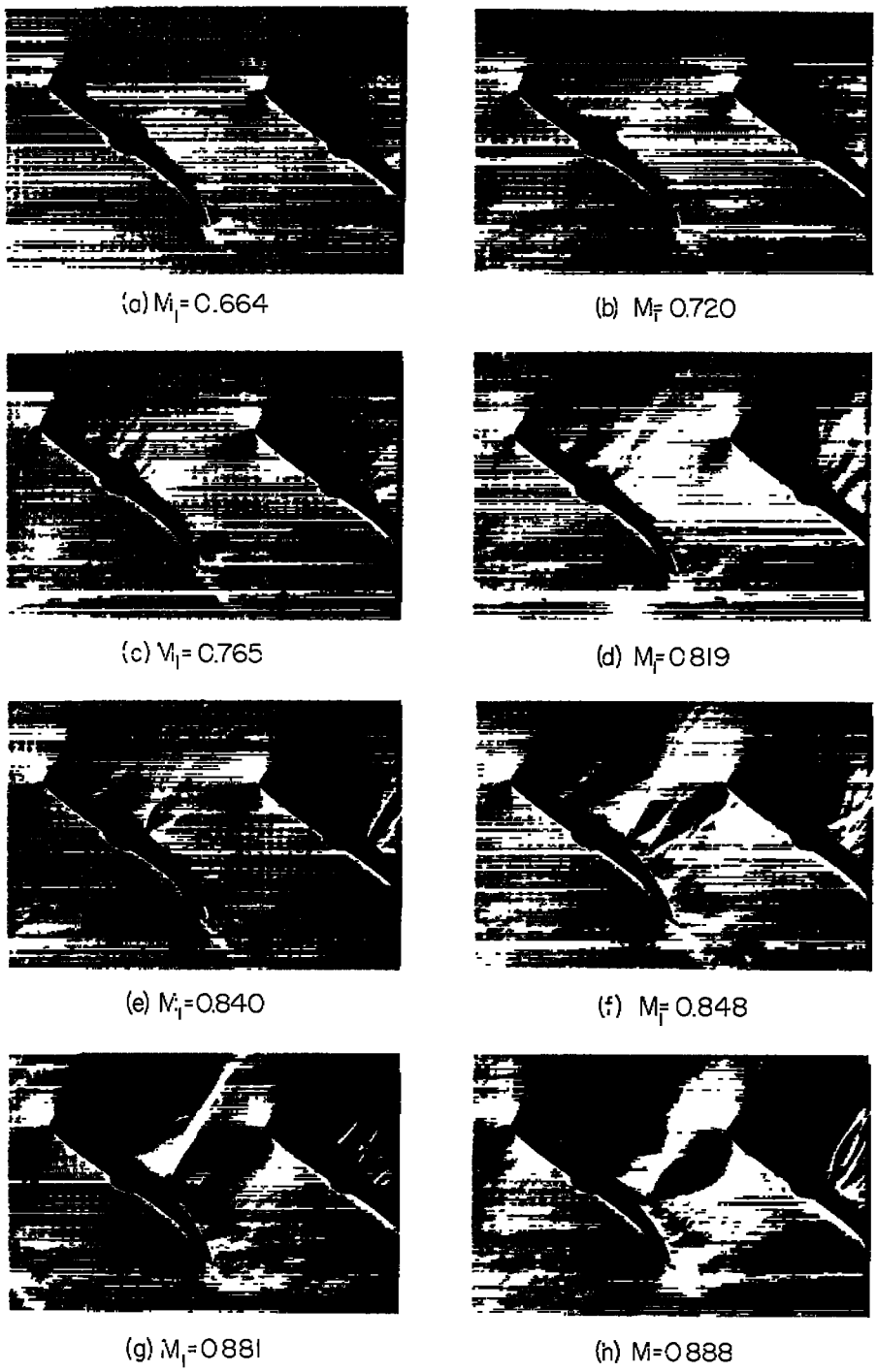

(a) M_1 = 0.664 (b) M_1 = 0.720

(c) M_1 = 0.765 (d) M_1 = 0.819

(e) M_1 = 0.840 (f) M_1 = 0.848

(g) M_1 = 0.881 (h) M = 0.888

L-90499

Figure 61.- Schlieren photographs and blade-section characteristics for a range of Mach numbers. Cascade of NACA 65-$(12A_2I_{8_0})$10 compressor blades. $\beta = 60^\circ$; $\sigma = 1.0$; and $\alpha = 11.0^\circ$.

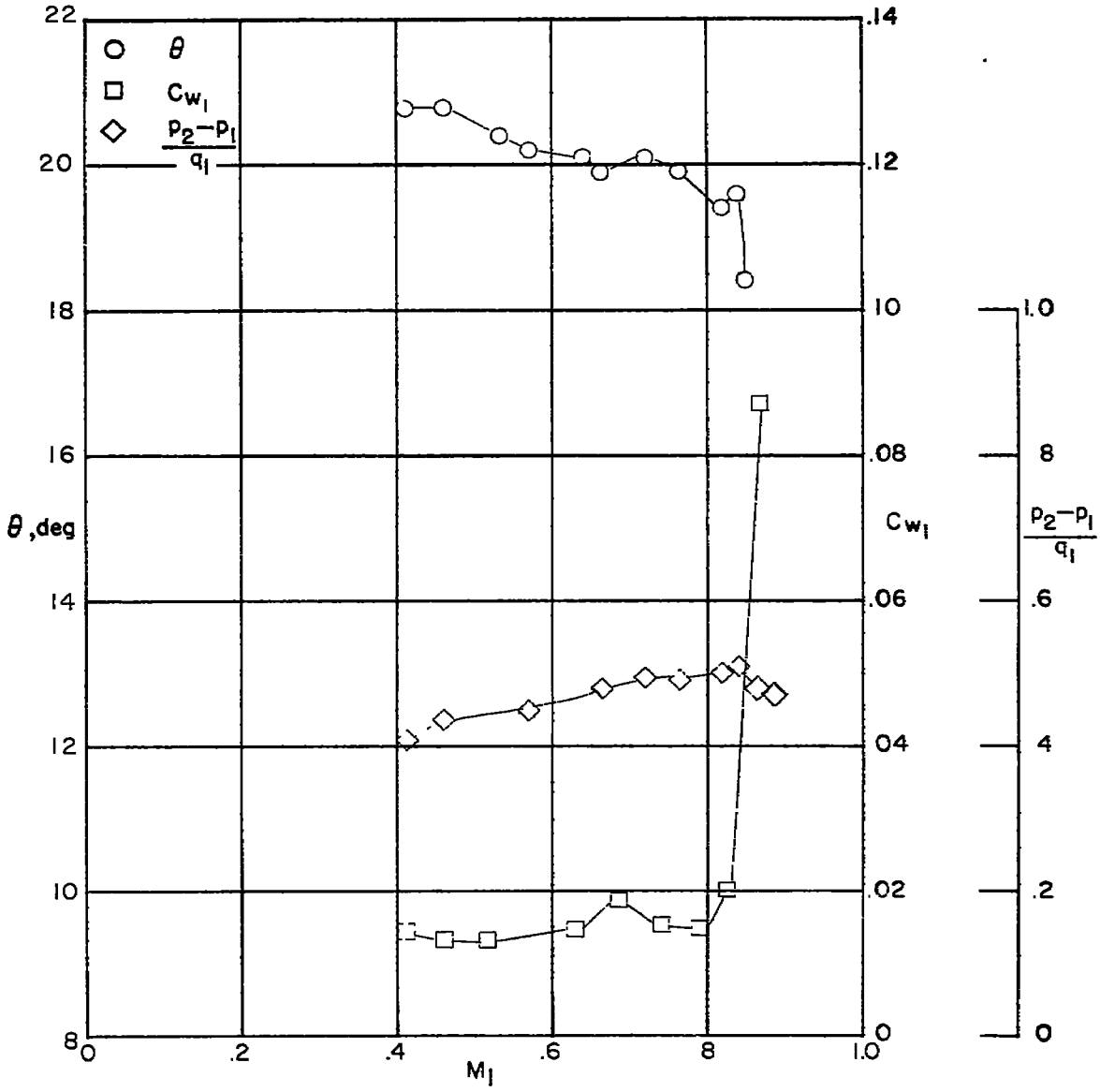

(i) Section characteristics.

Figure 61 .— Concluded.

(a) M = 0.667

(b) M_1 = 0.716

(c) M_1 = 0.767

(d) M_1 = 0.809

(e) M_1 = 0843

(f) M_1 = 0864

(g) M_1 = 0.869

L-90500

Schlieren photographs and blade-section characteristics for Cascade of NACA 65-$(12A_2I_{8b})$10 compressor blade.

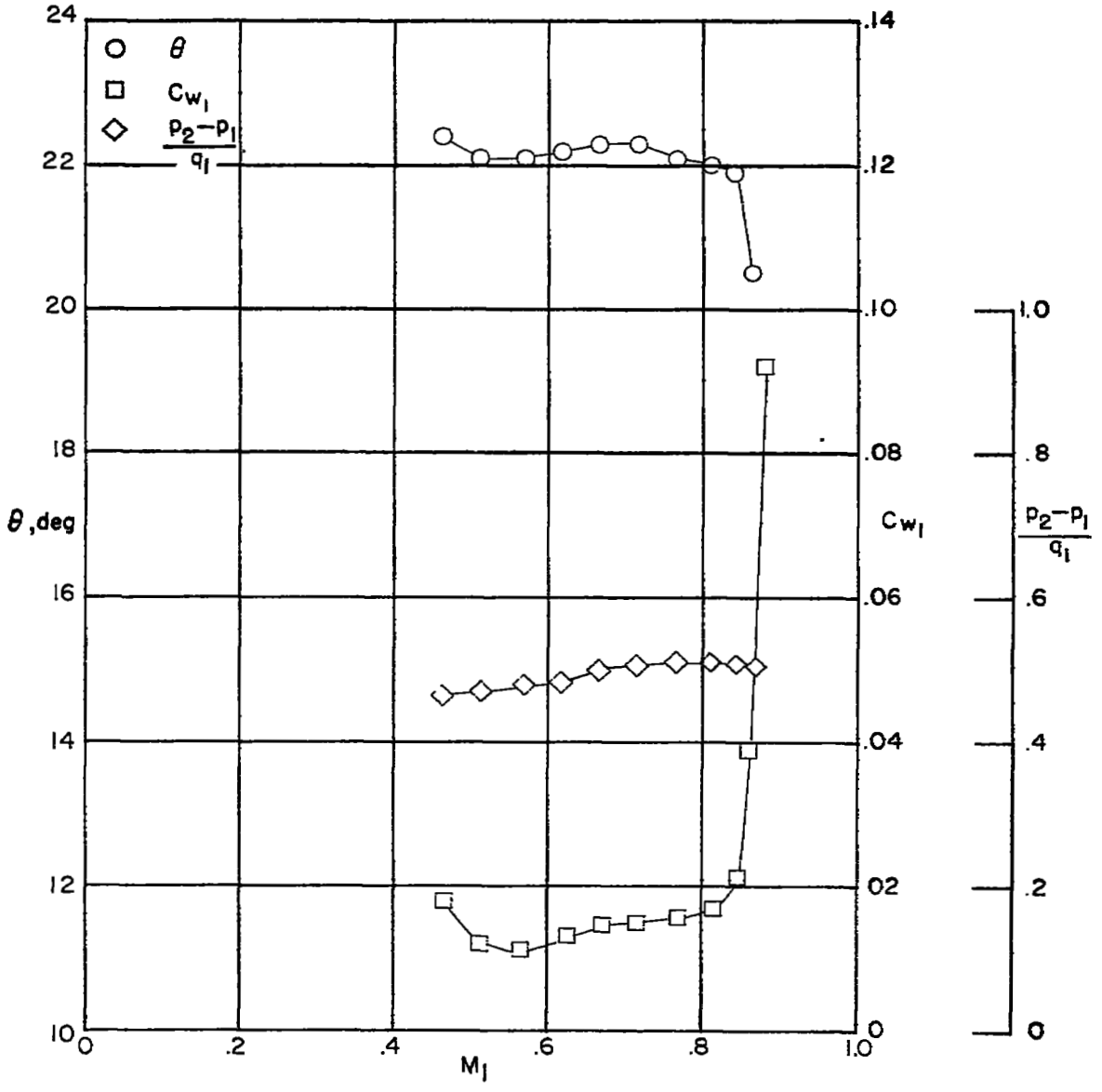

(h) Section characteristics.

Figure 62.— Concluded.

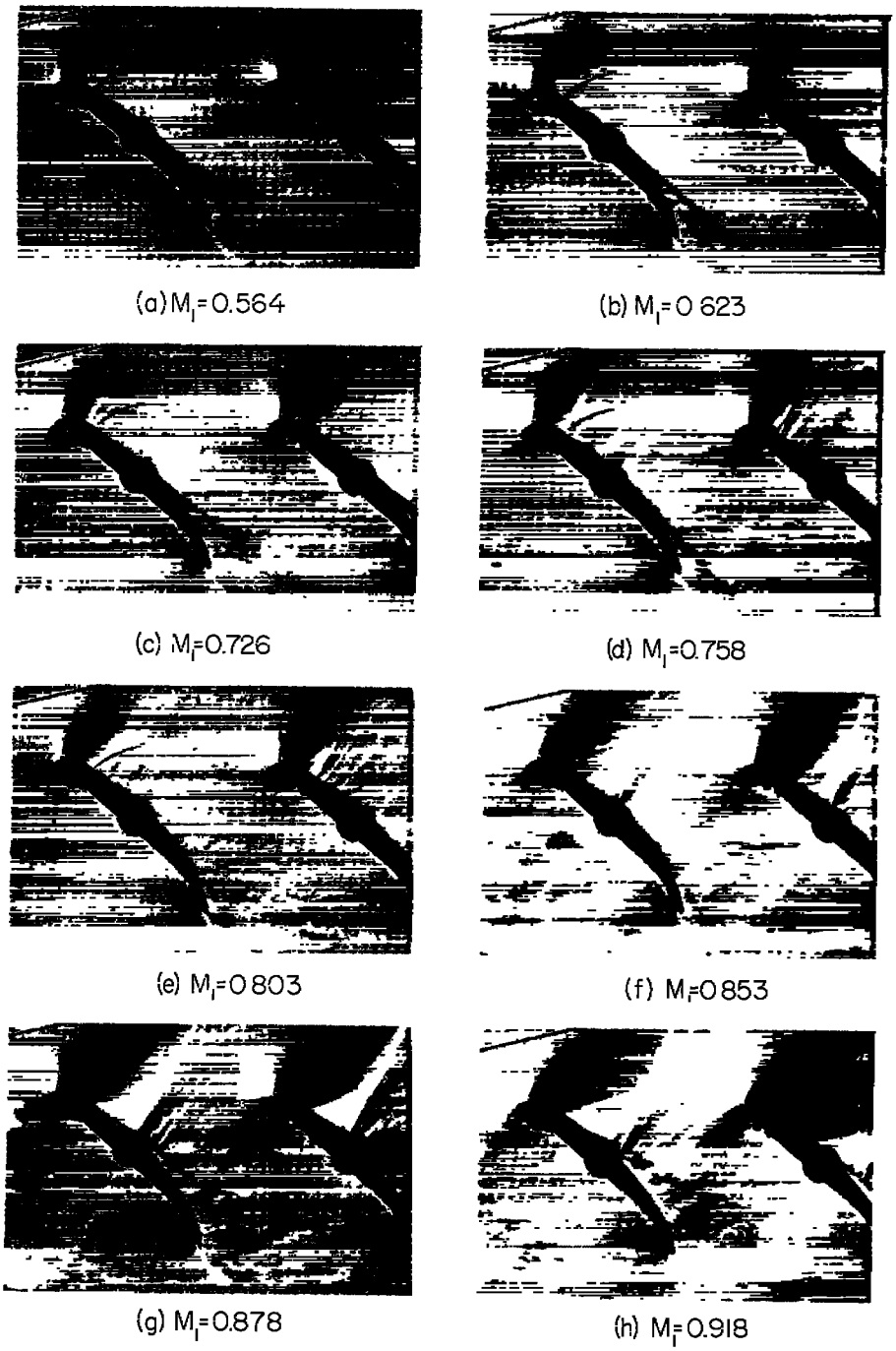

L-90501

Figure 63.- Schlieren photographs and blade-section characteristics for a range of Mach numbers. Cascade of NACA 65-$(12A_2I_{8b})$10 compressor blades. $\beta = 60^\circ$; $\sigma = 1.0$; and $\alpha = 17.1^\circ$.

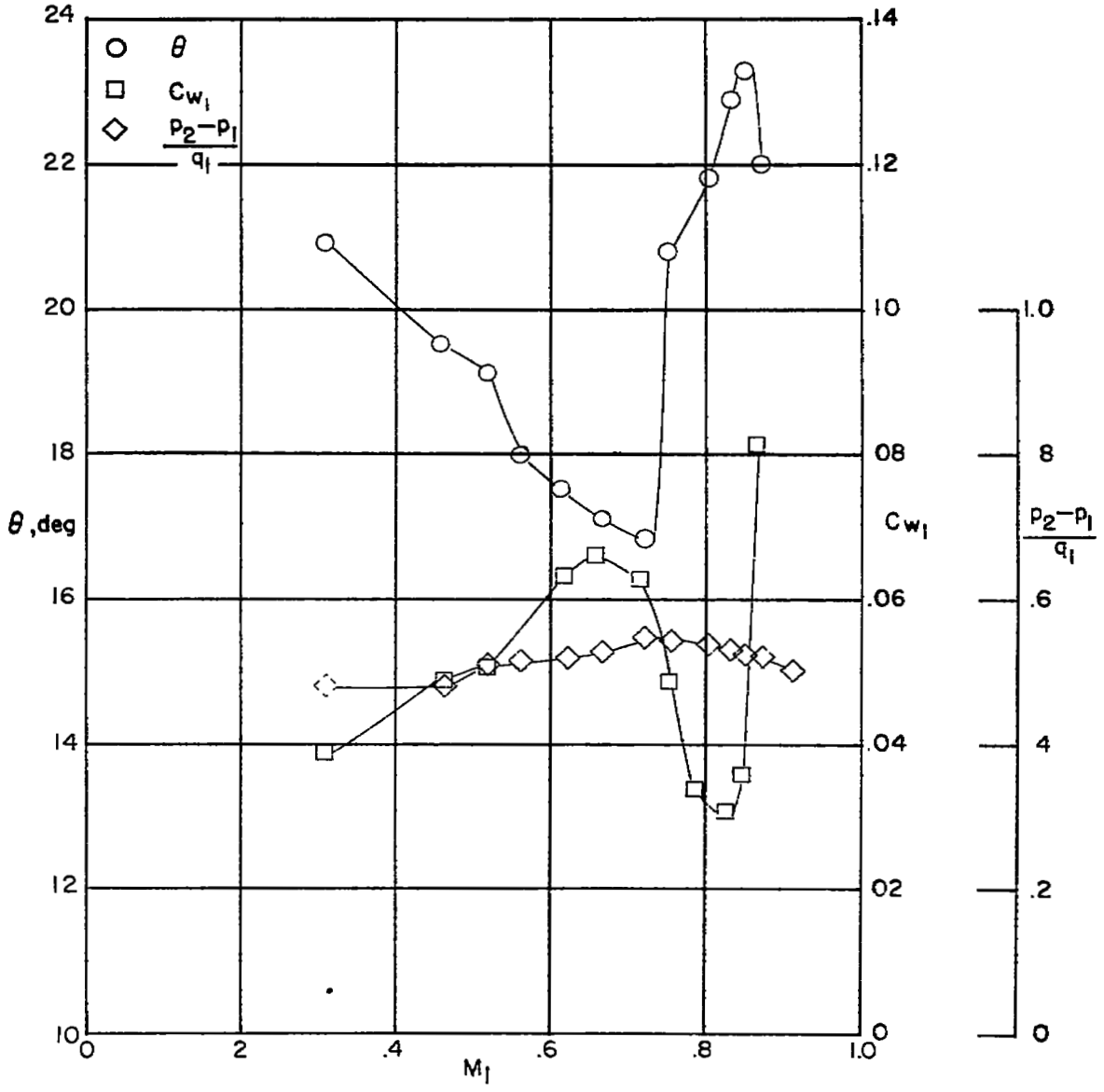

(i) Section characteristics.

Figure 63 .— Concluded.

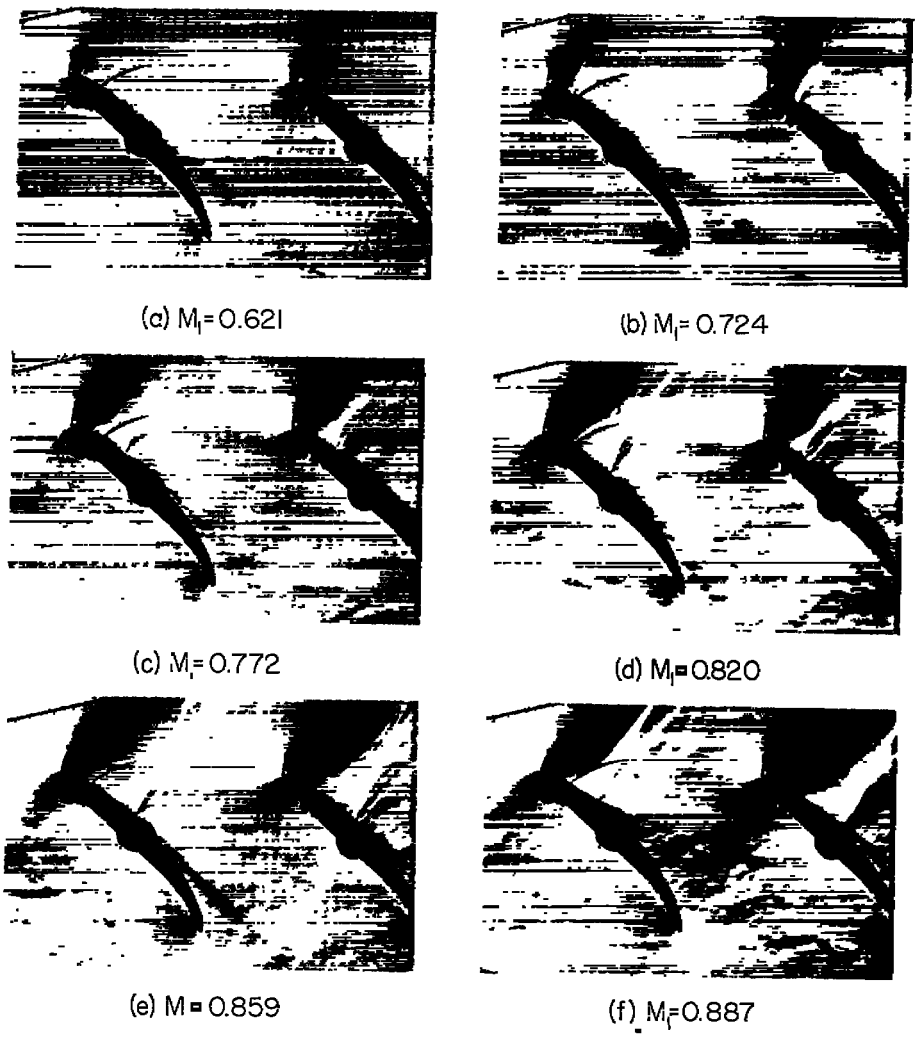

L-90502

Figure 64.- Schlieren photographs and blade-section characteristics for a range of Mach numbers. Cascade of NACA 65-$\left(12A_2I_{8b}\right)$10 compressor blades. $\beta = 60^\circ$; $\sigma = 1.0$; and $\alpha = 19.1^\circ$.

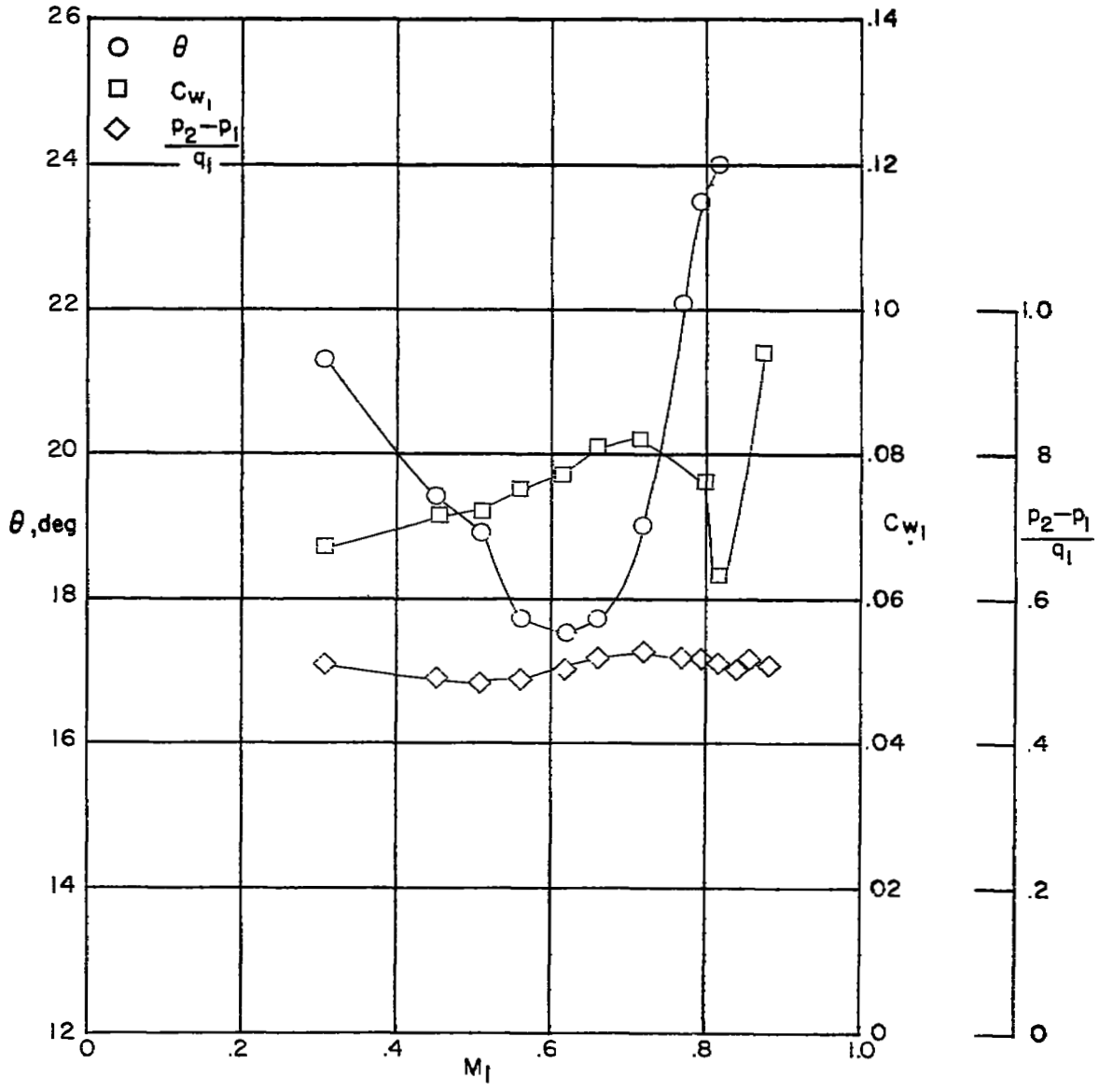

(g) Section characteristics.

Figure 64 .— Concluded.

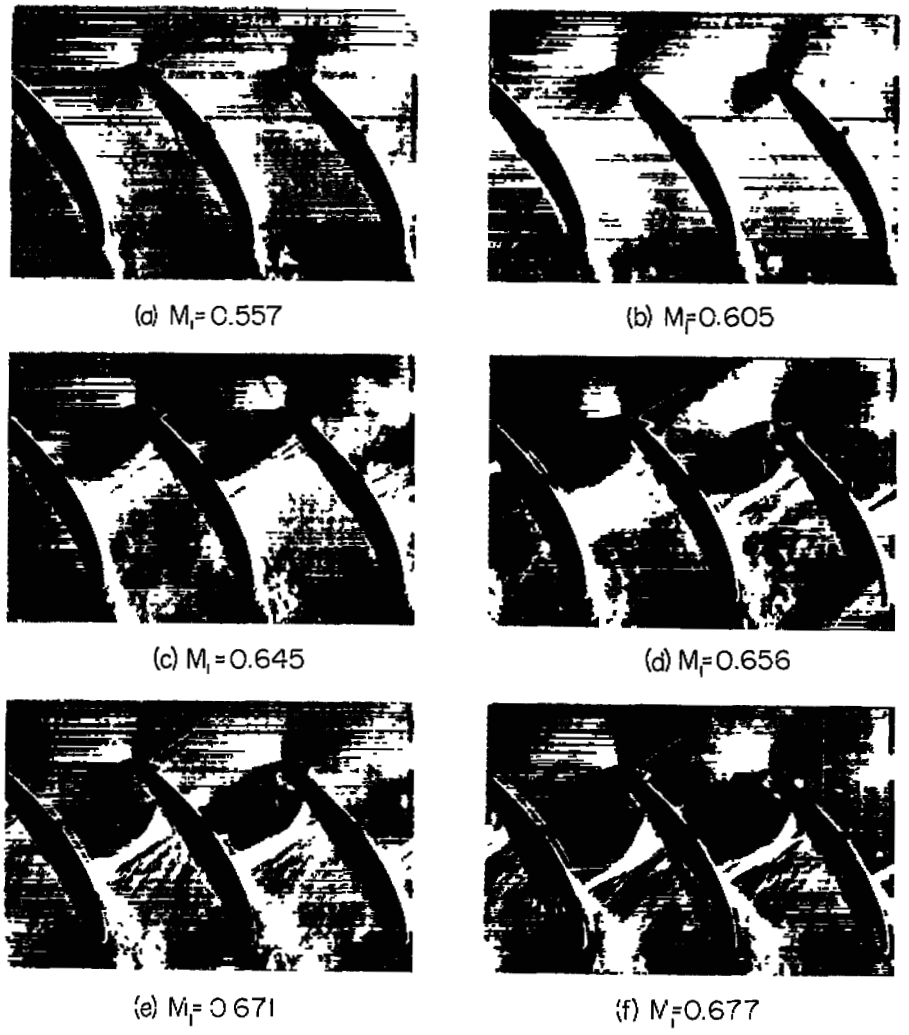

L-90503

Figure 65.- Schlieren photographs and blade-section characteristics for a range of Mach numbers. Cascade of NACA 65-$(12A_2I_{8b})10$ compressor blades. $\beta = 45^\circ$; $\sigma = 1.5$; and $\alpha = 13.5^\circ$.

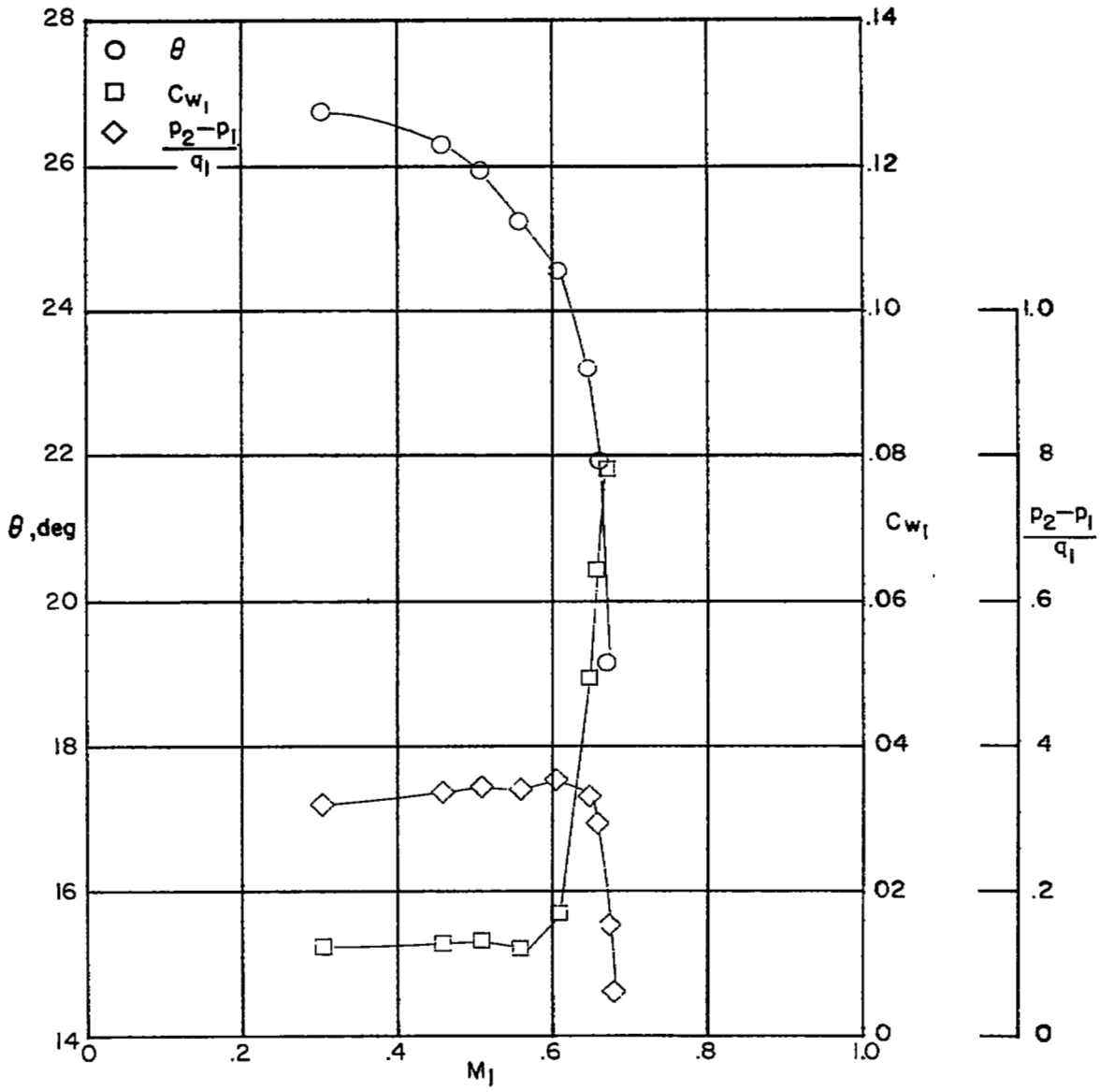

(g) Section characteristics.

Figure 65.— Concluded.

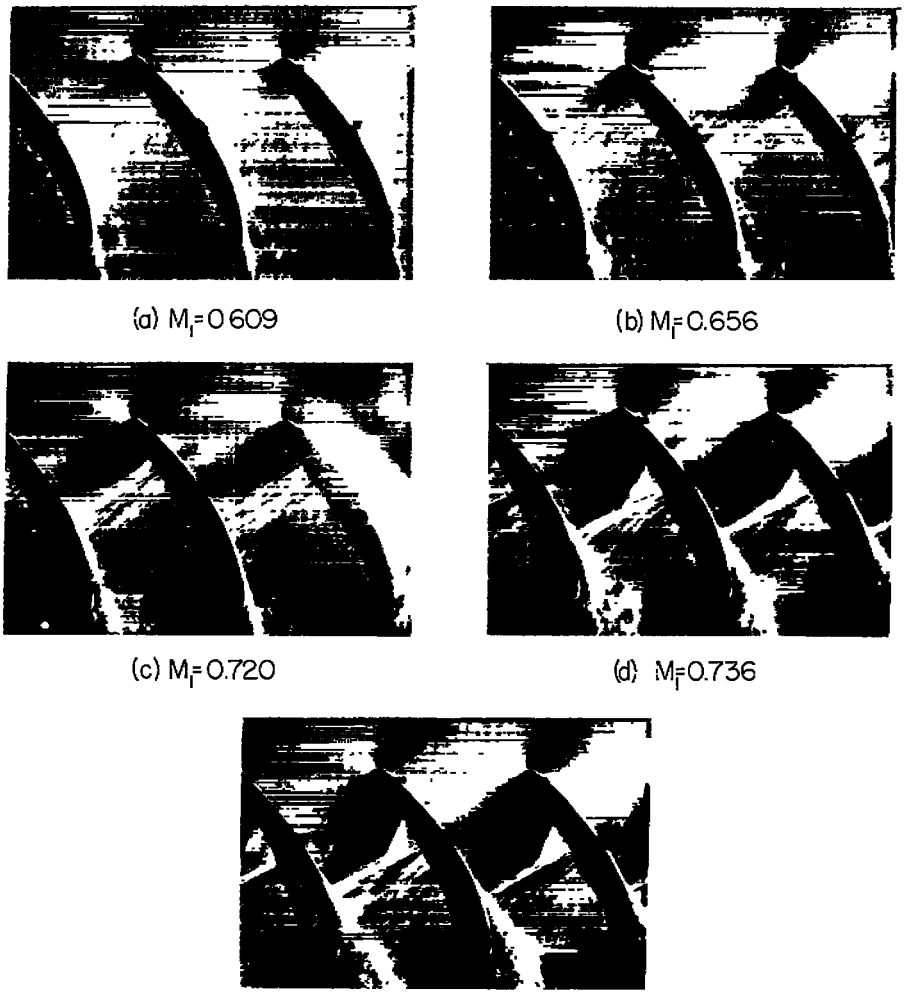

(a) $M_1 = 0.609$

(b) $M_1 = 0.656$

(c) $M_1 = 0.720$

(d) $M_1 = 0.736$

(e) $M_1 = 0.739$.

L-90504

Figure 66.- Schlieren photographs and blade-section characteristics for a range of Mach numbers. Cascade of NACA 65-$(12A_2I_{8b})10$ compressor blades. $\beta = 45°$; $\sigma = 1.5$; and $\alpha = 16.5°$.

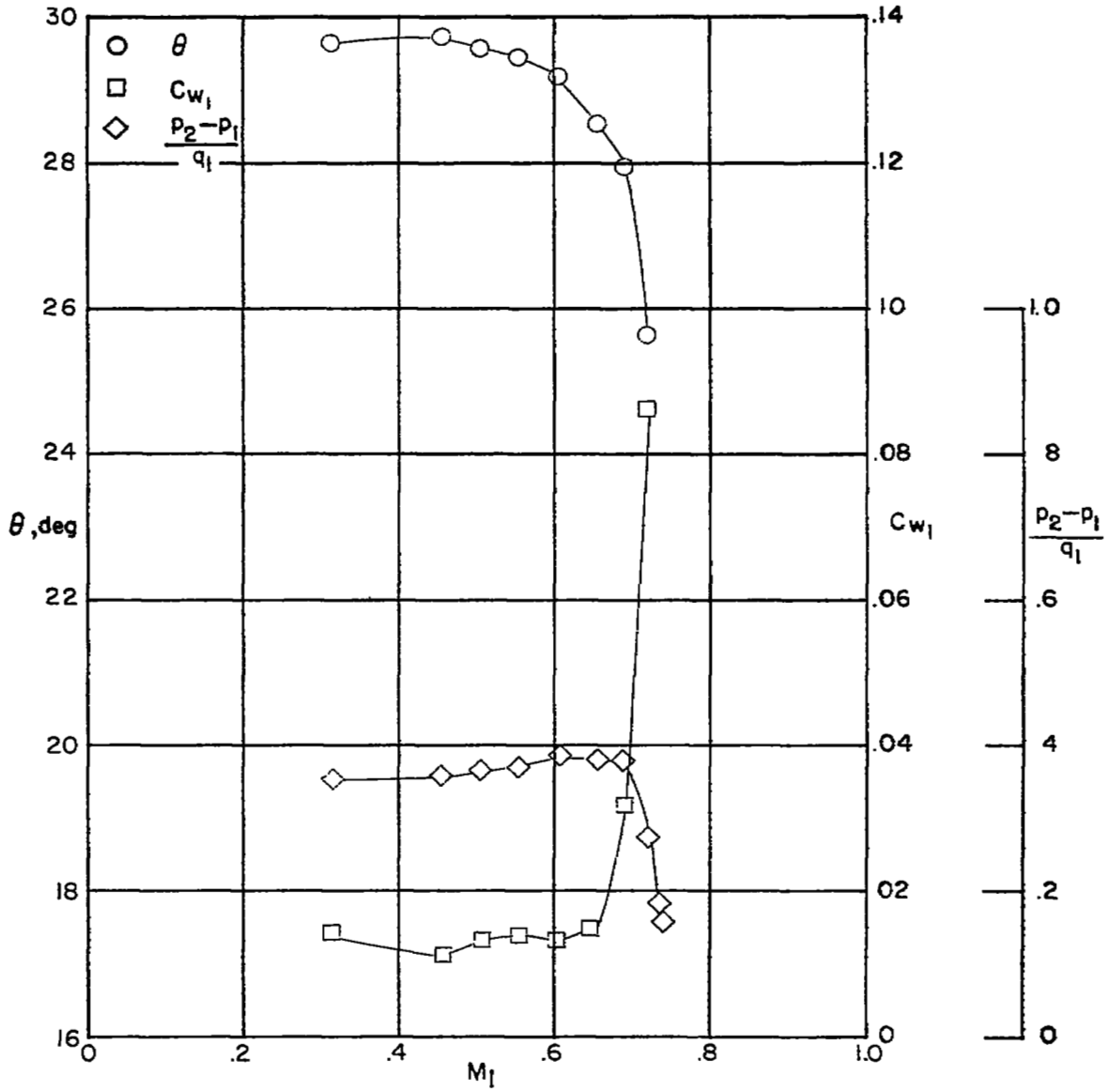

(f) Section characteristics.

Figure 66 .— Concluded.

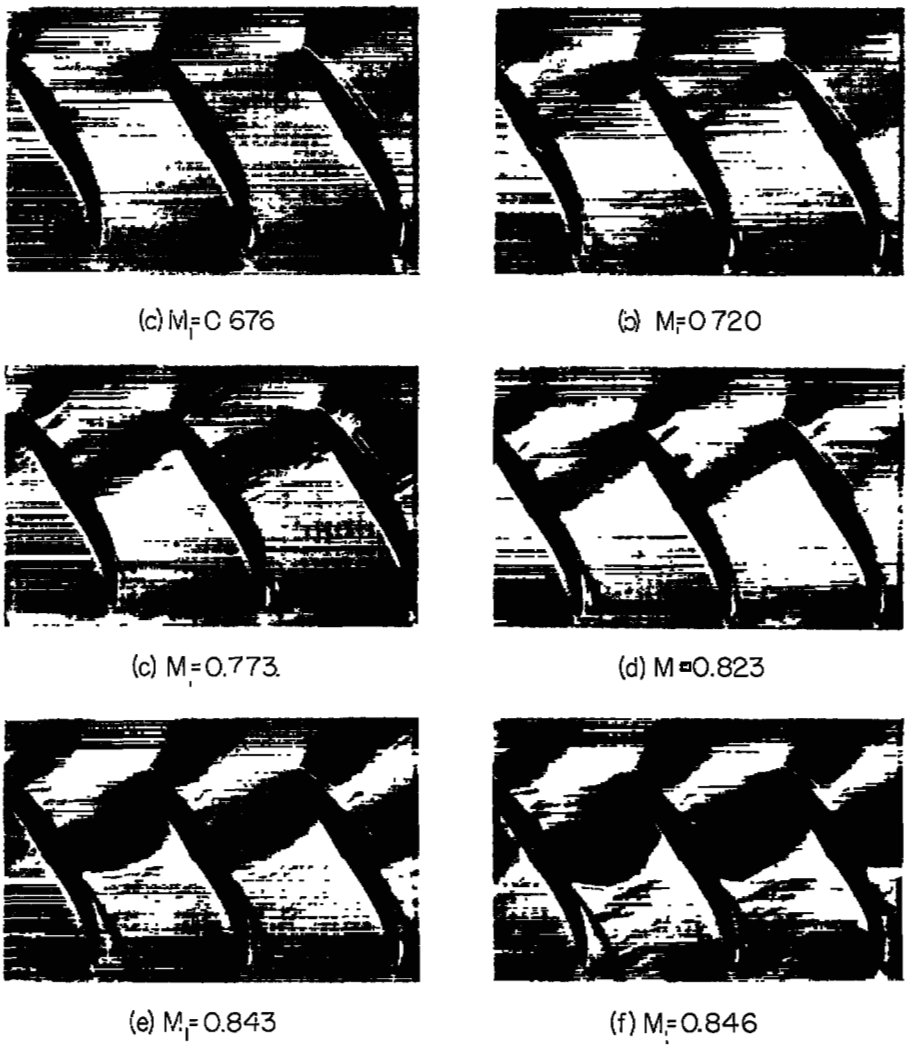

L-90505

Figure 67.- Schlieren photographs and blade-section characteristics for a range of Mach numbers. Cascade of NACA 65-$(12A_2I_{6b})10$ compressor blades. $\beta = 45^\circ$; $\sigma = 1.5$; and $\alpha = 20.5^\circ$.

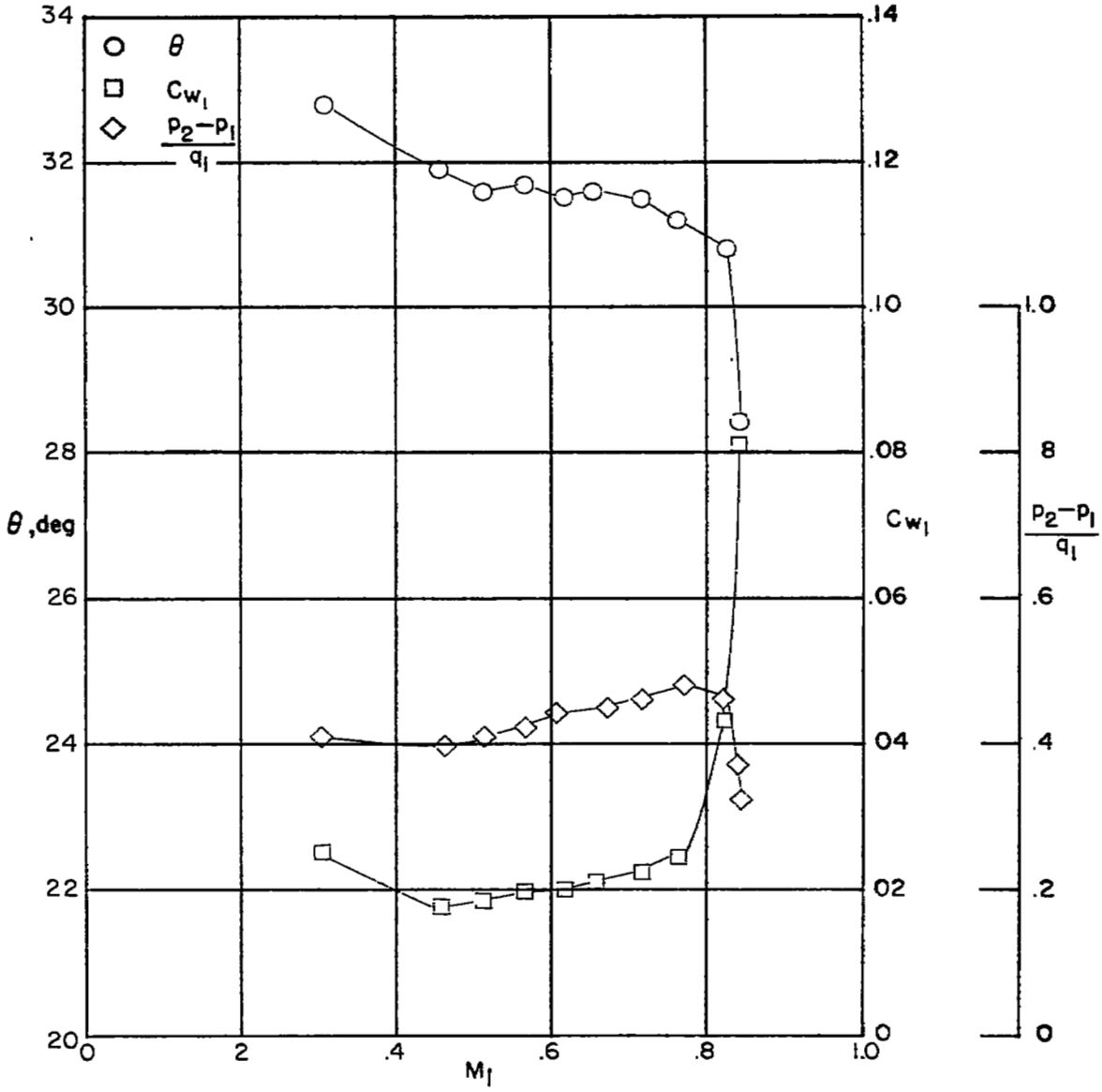

(g) Section characteristics.

Figure 67 .— Concluded.

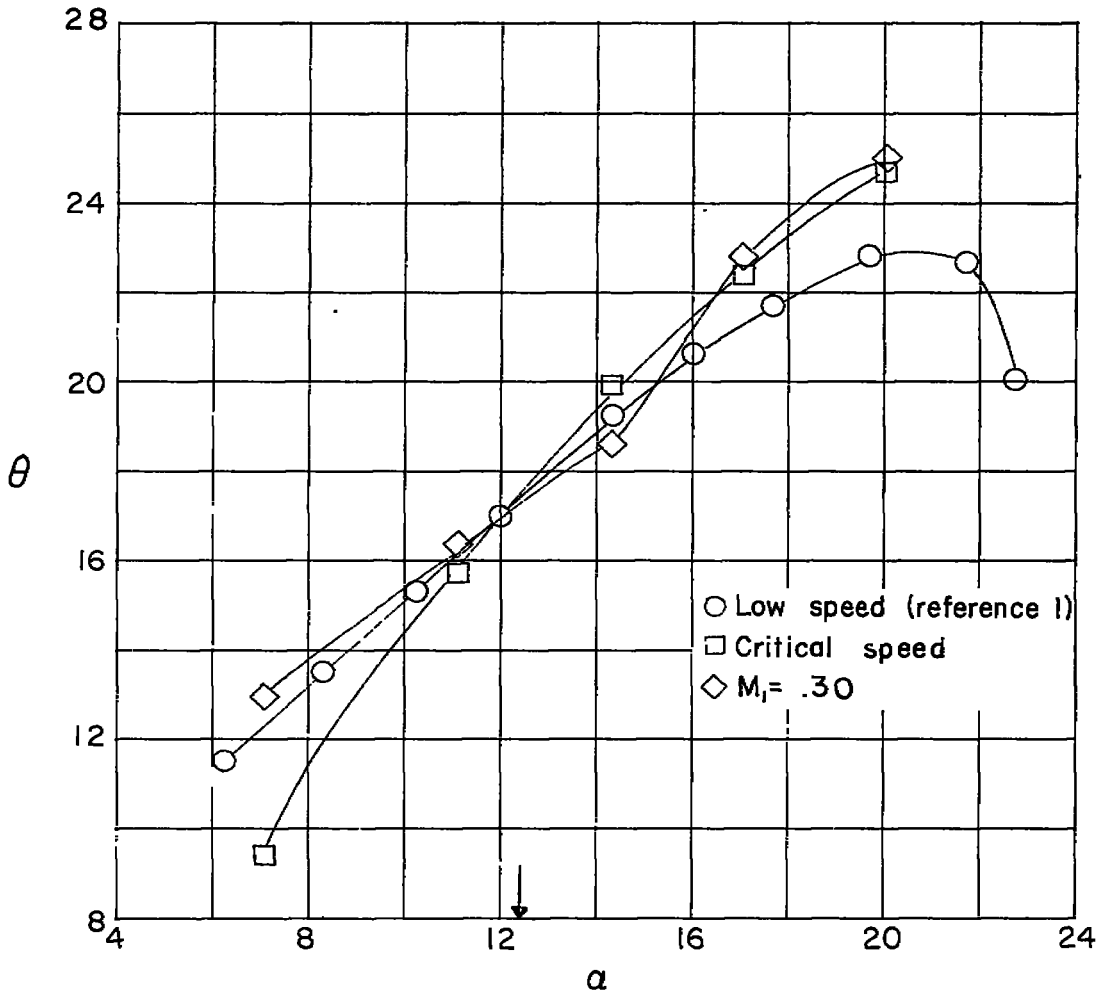

Figure 68.- Comparison of turning angles at high and low speeds for NACA 65-$(12A_{10})$10 blade section at $\beta_1 = 60^\circ$ and $\sigma = 1.0$. Arrow shows low-speed design angle of attack.

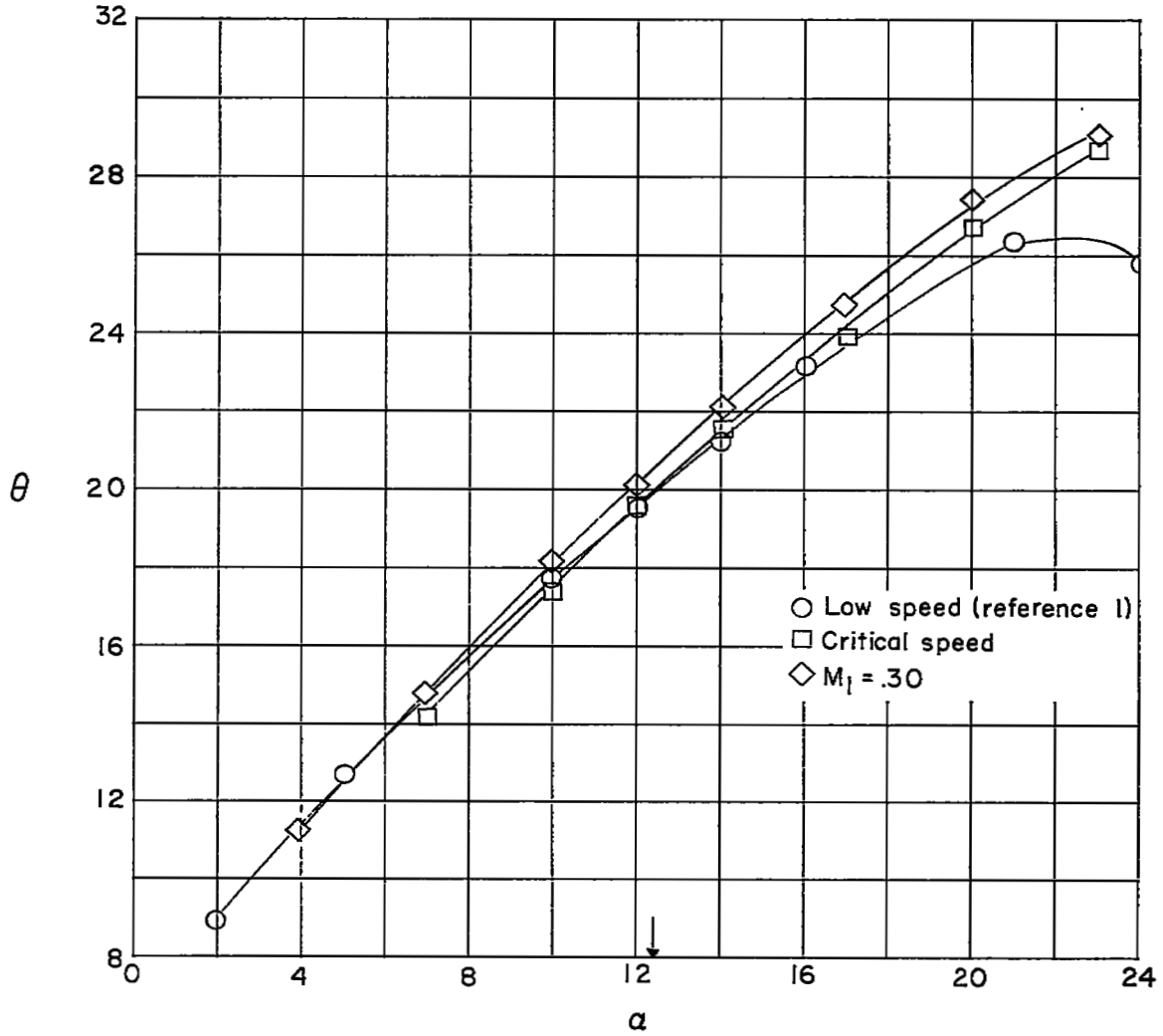

Figure 69.- Comparison of turning angles at high and low speeds for NACA 65-$(12A_{10})10$ blade section at $\beta_1 = 45^\circ$ and $\sigma = 1.0$. Arrow shows low-speed design angle of attack.

[redacted]

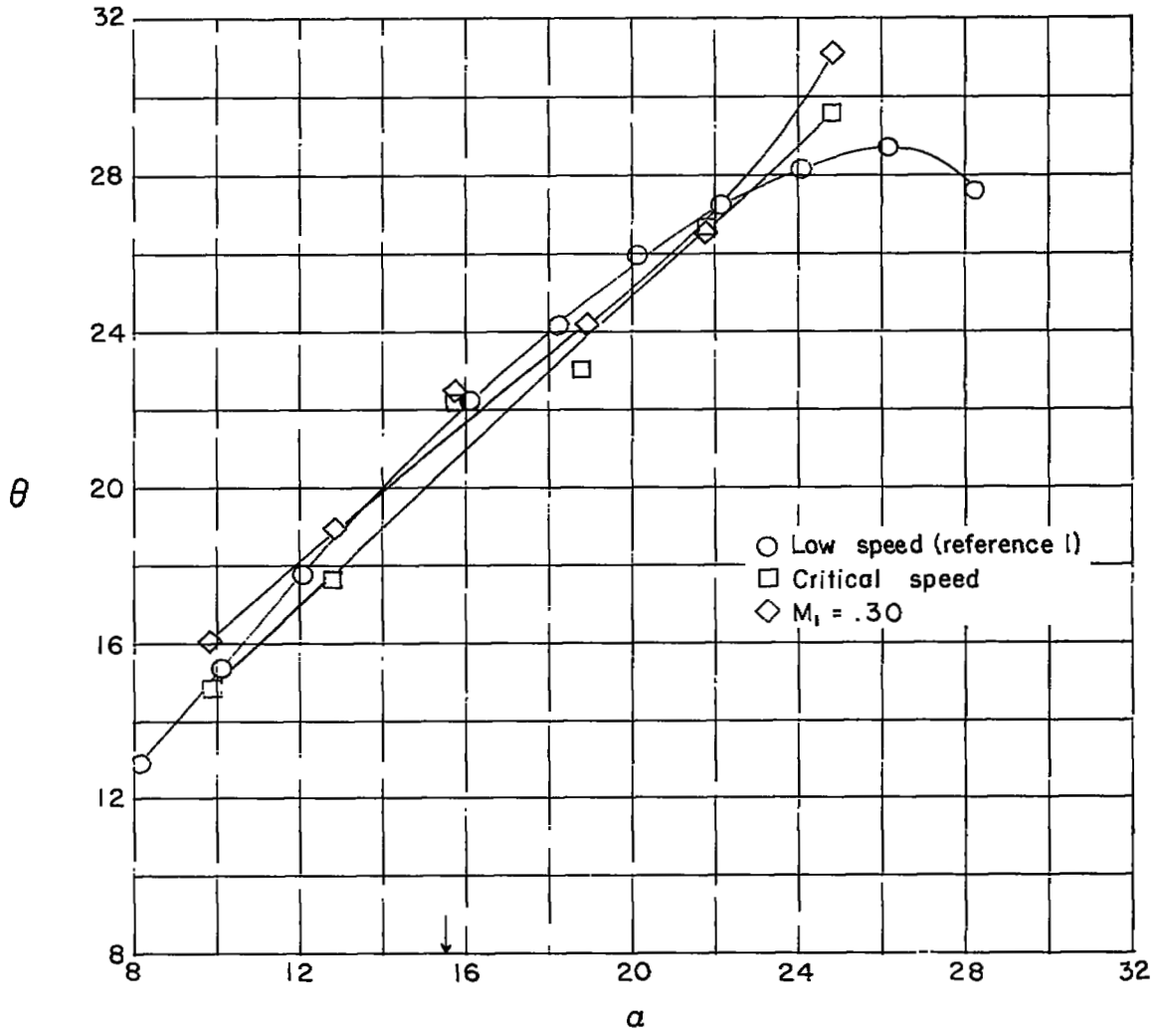

Figure 70.- Comparison of turning angles at high and low speeds for NACA 65-$(12A_{10})$10 blade section at $\beta_1 = 60^\circ$ and $\sigma = 1.5$. Arrow shows low-speed design angle of attack.

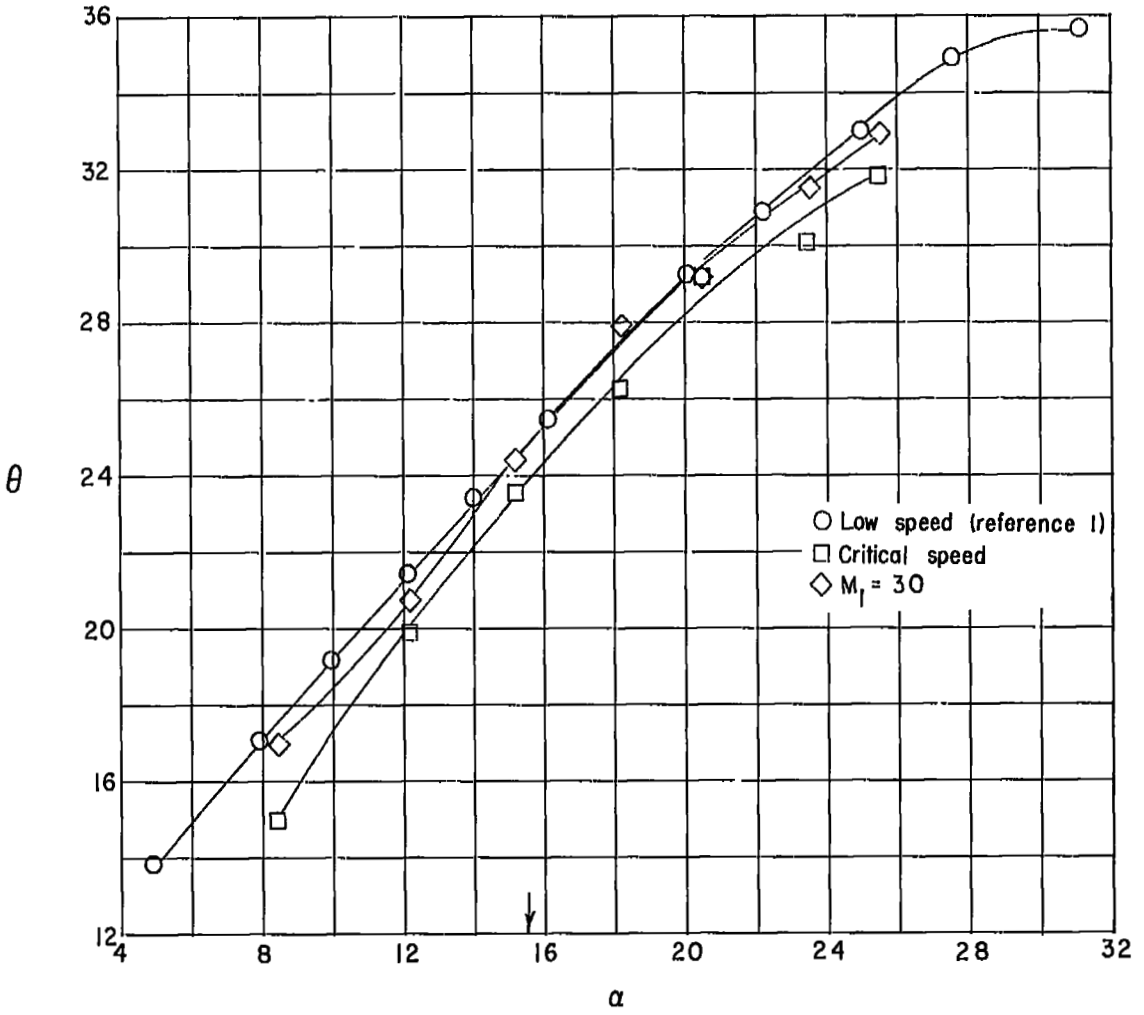

Figure 71.- Comparison of turning angles at high and low speeds for NACA 65-$(12A_{10})10$ blade section at $\beta_1 = 45^\circ$ and $\sigma = 1.5$. Arrow shows low-speed design angle of attack.

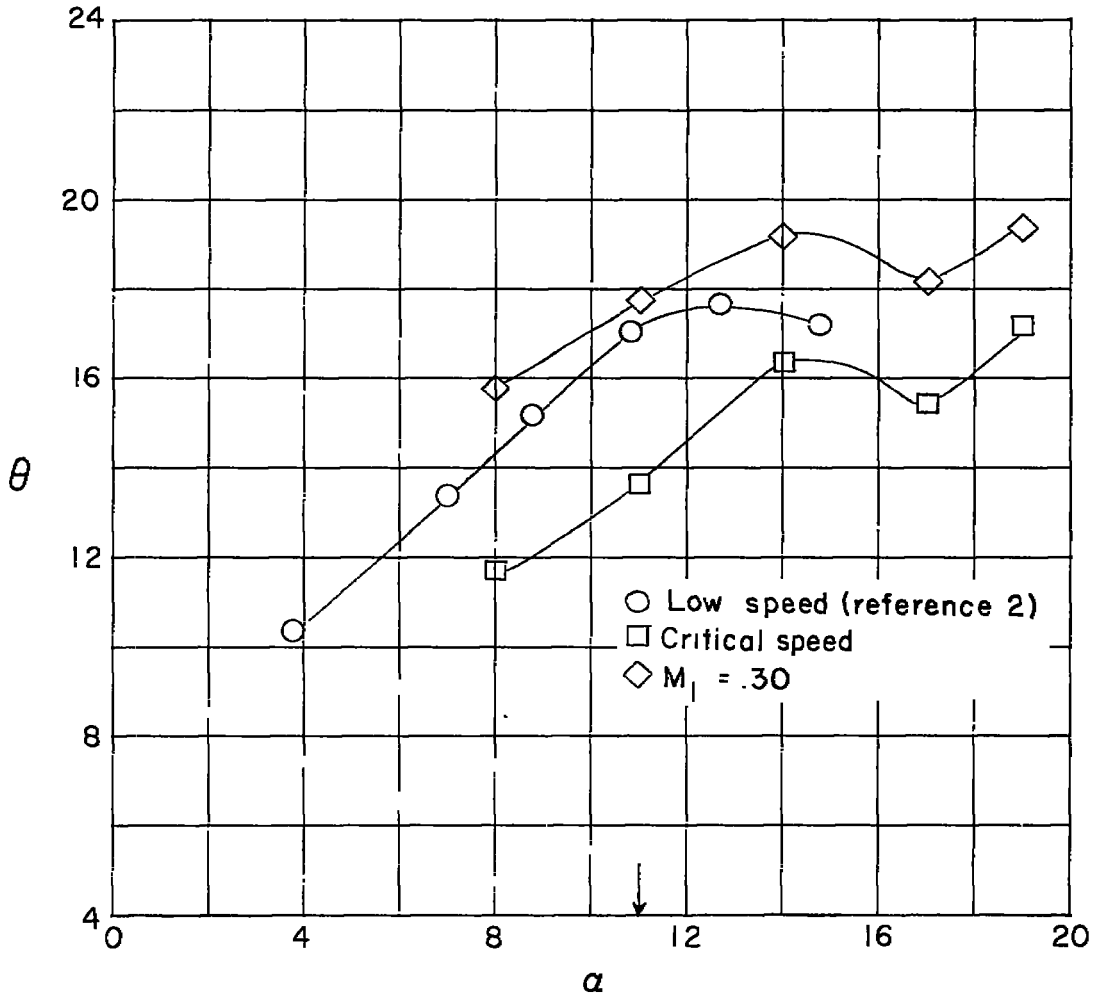

Figure 72.- Comparison of turning angles at low and high speeds for NACA 65-$(12A_2I_{8b})10$ blade section at $\beta_1 = 60^\circ$ and $\sigma = 1.0$. Arrow shows low-speed design angle of attack.

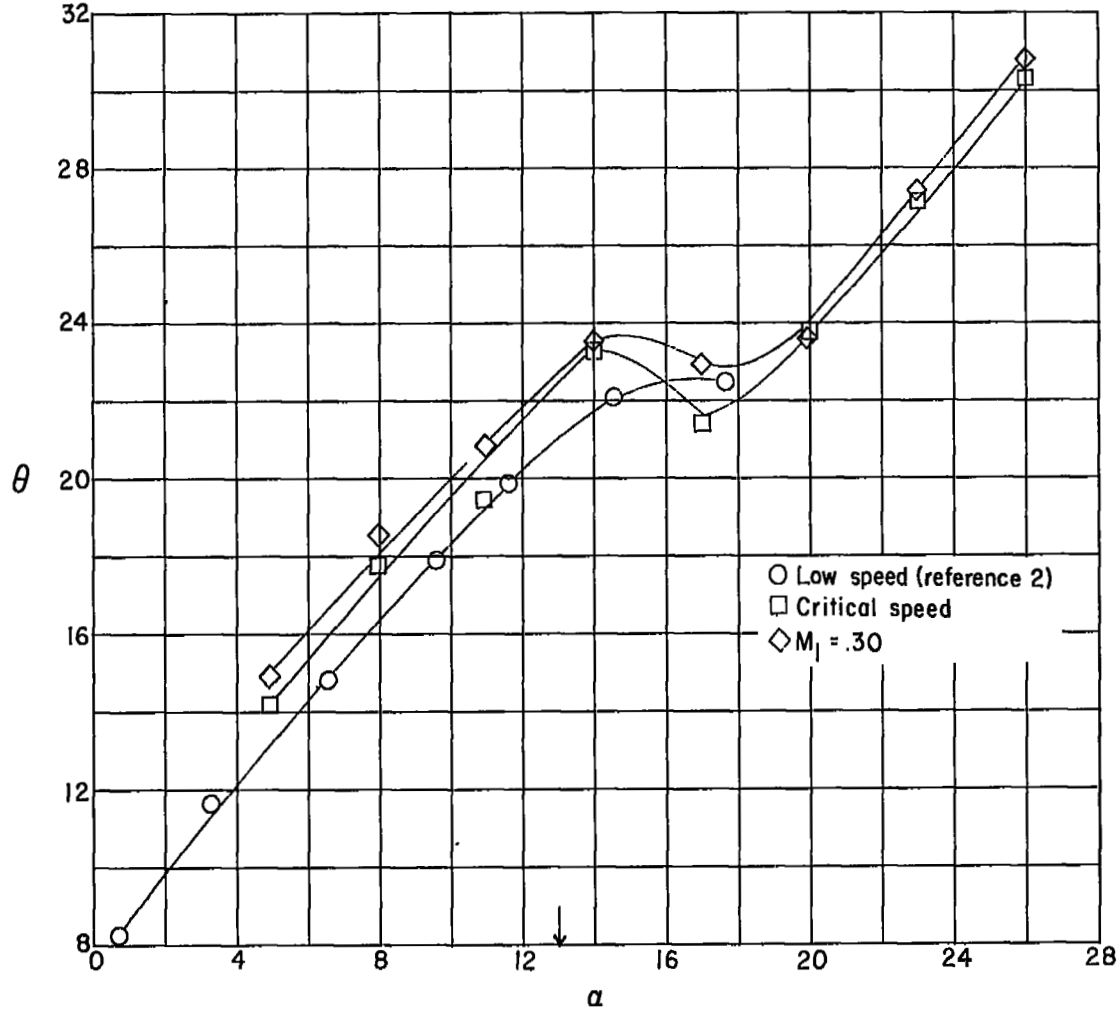

Figure 73.- Comparison of turning angles at high and low speeds for NACA 65-$(12A_2I_{8b})$10 blade section at $\beta_1 = 45^\circ$ and $\sigma = 1.0$. Arrow shows low-speed design angle of attack.

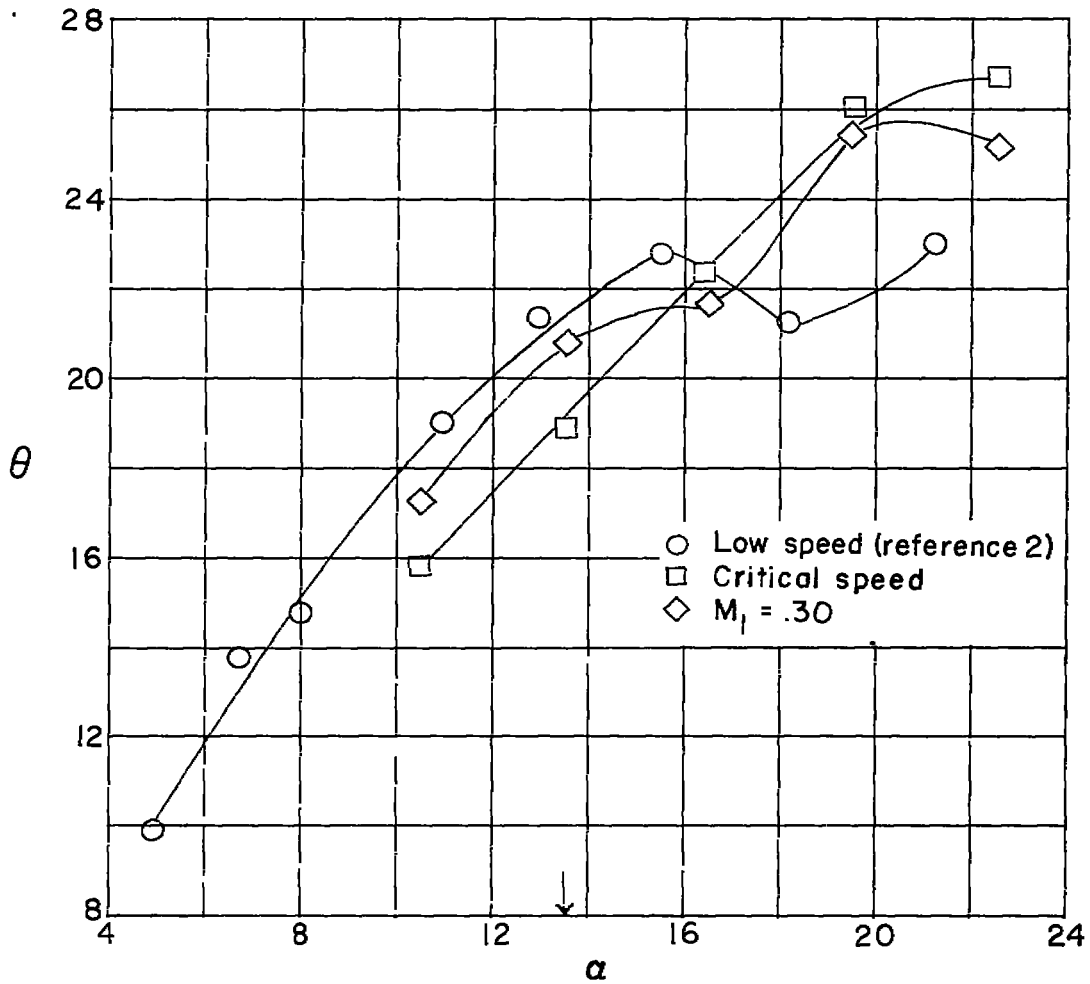

Figure 74.- Comparison of turning angles at high and low speeds for NACA 65-($12A_2I_{8b}$)10 blade section at $\beta_1 = 60°$ and $\sigma = 1.5$. Arrow shows low-speed design angle of attack.

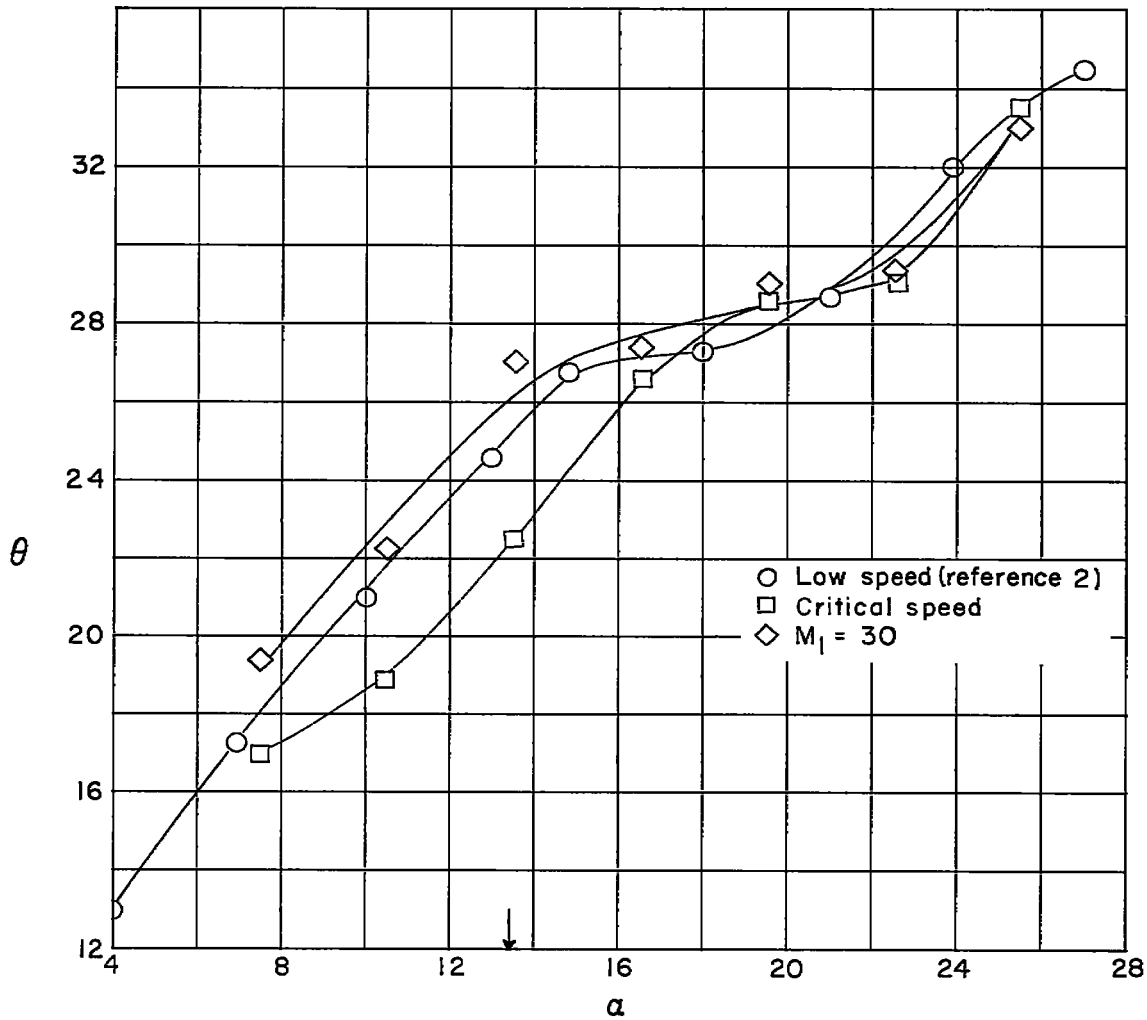

Figure 75.- Comparison of turning angles at high and low speeds for NACA 65-$(12A_2I_{8b})$10 blade section at $\beta_1 = 45^\circ$ and $\sigma = 1.5$. Arrow shows low-speed design angle of attack.

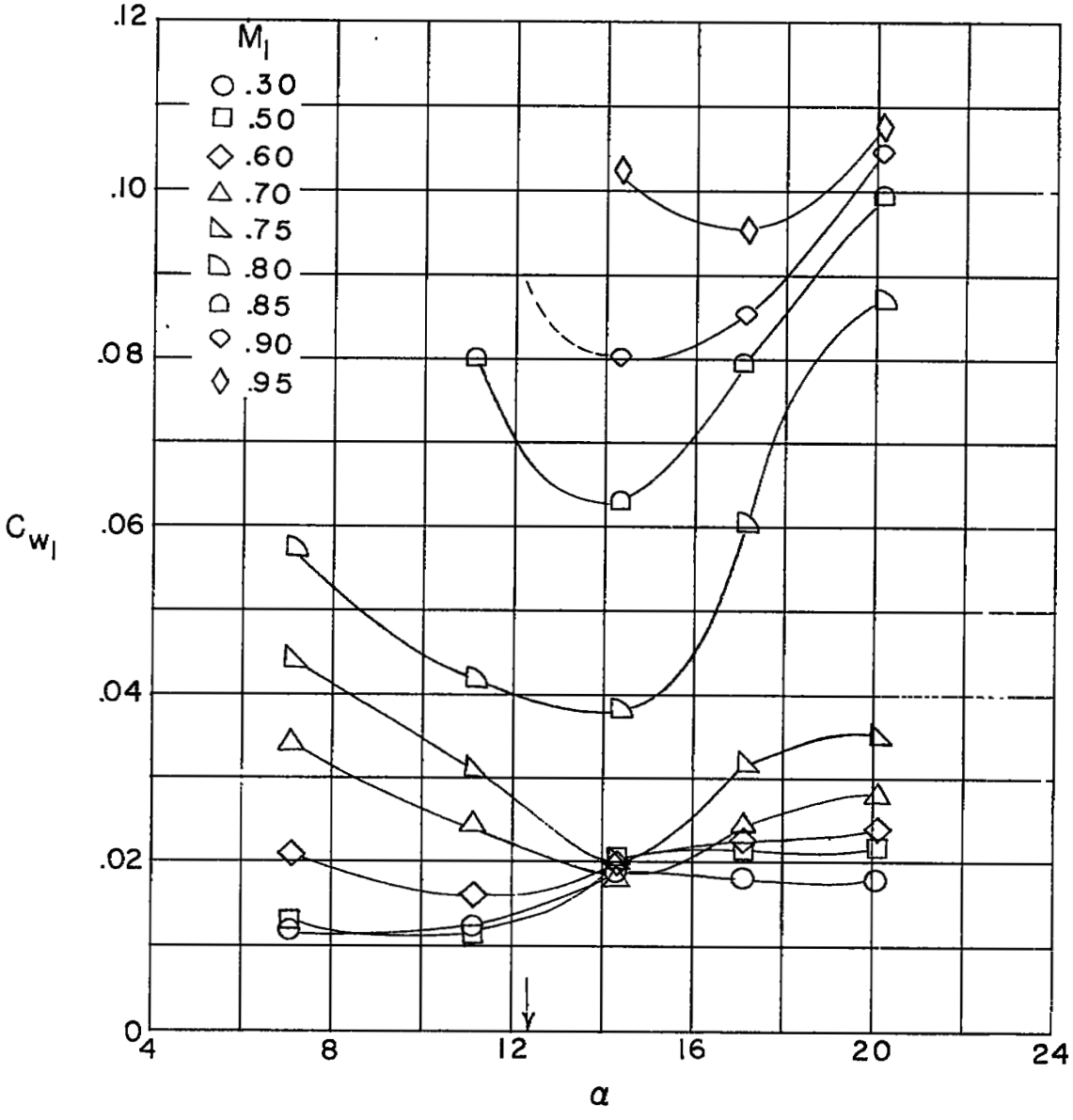

Figure 76.- Variation of momentum loss with angle of attack at constant Mach number for NACA 65-$(12A_{10})$10 blade section at $\beta_1 = 60^\circ$ and $\sigma = 1.0$. Arrow shows low-speed design angle of attack.

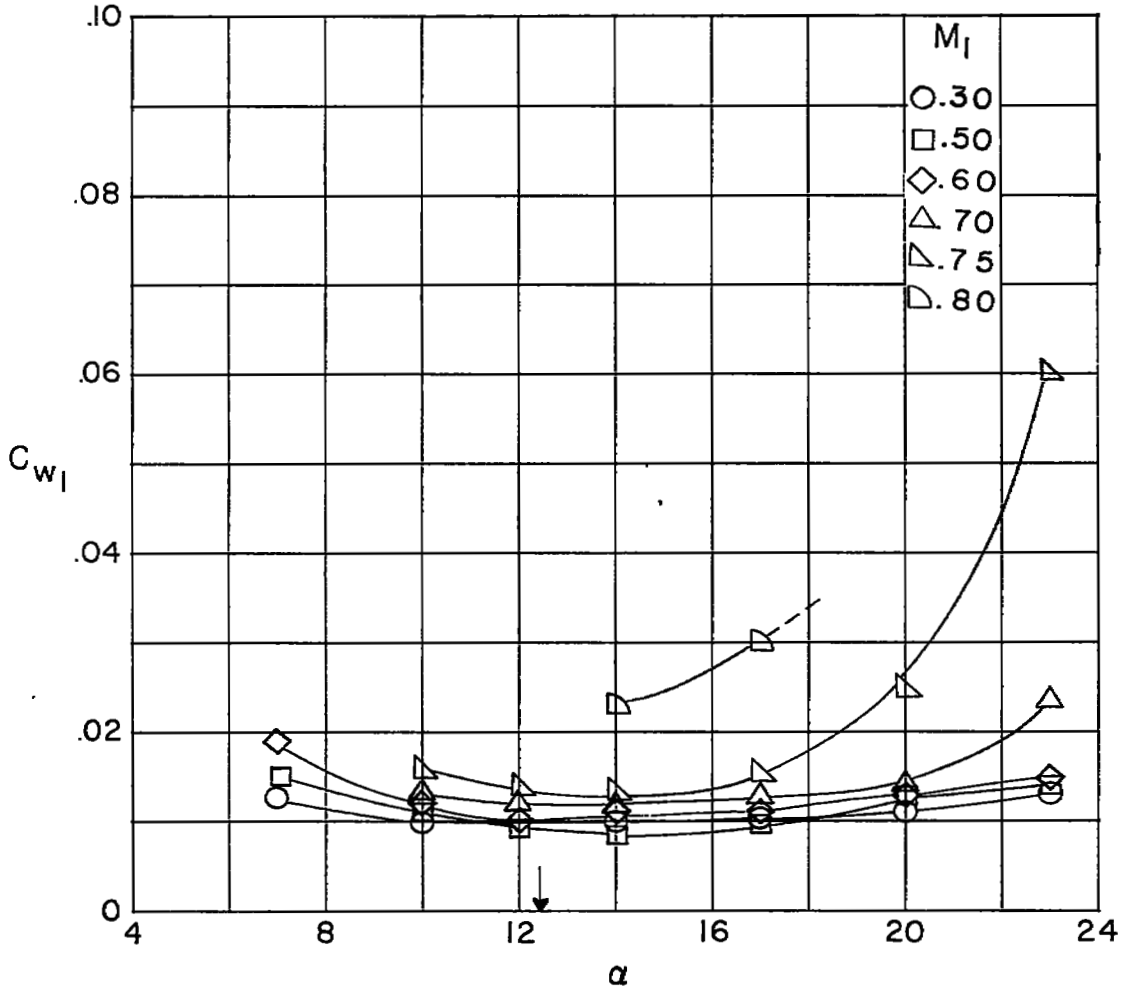

Figure 77.- Variation of momentum loss with angle of attack at constant Mach number for NACA 65-$(12A_{10})$10 blade section at $\beta_1 = 45^\circ$ and $\sigma = 1.0$. Arrow shows low-speed design angle of attack.

[redacted]

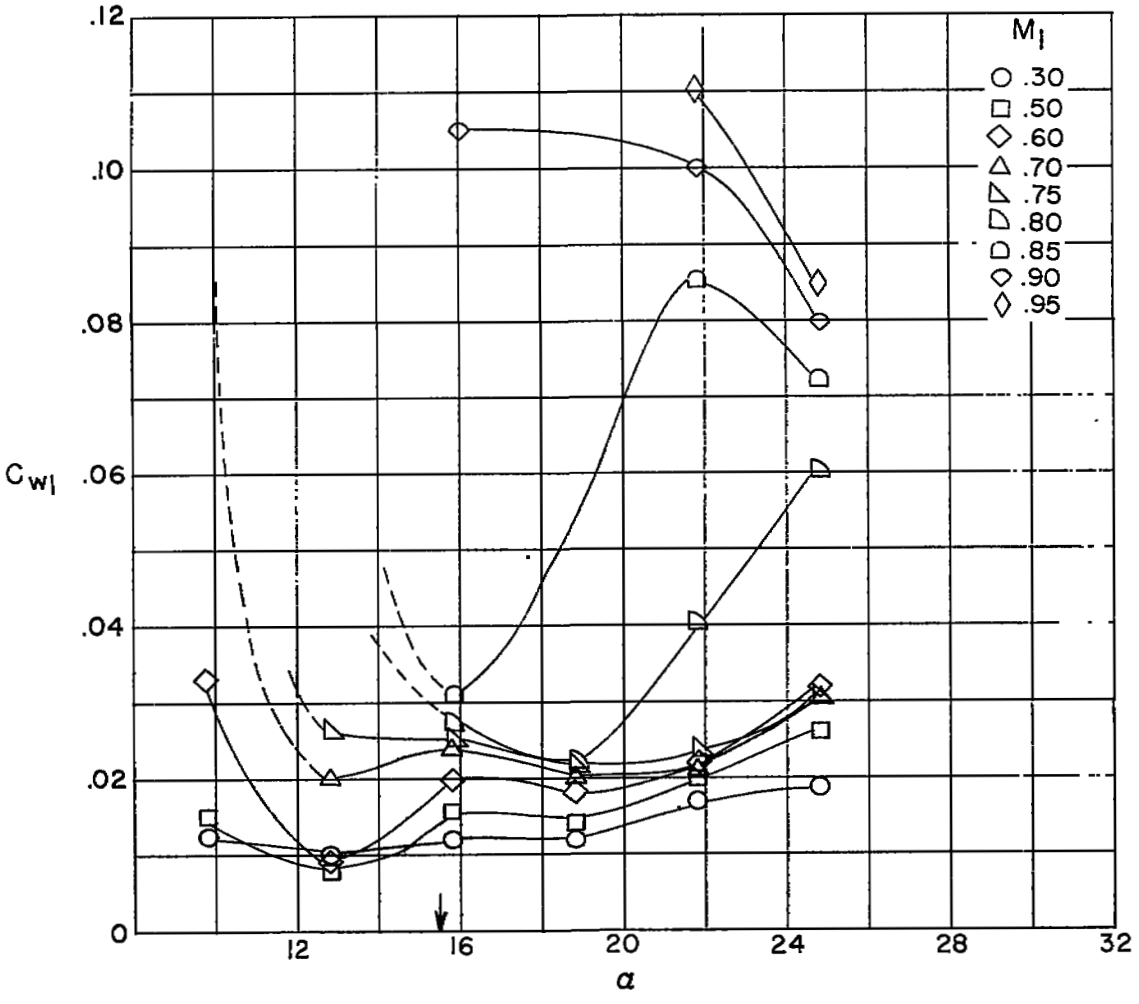

Figure 78.- Variation of momentum loss with angle of attack at constant Mach number for NACA 65-$(12A_{10})$10 blade section at $\beta_1 = 60^\circ$ and $\sigma = 1.5$. Arrow shows low-speed design angle of attack.

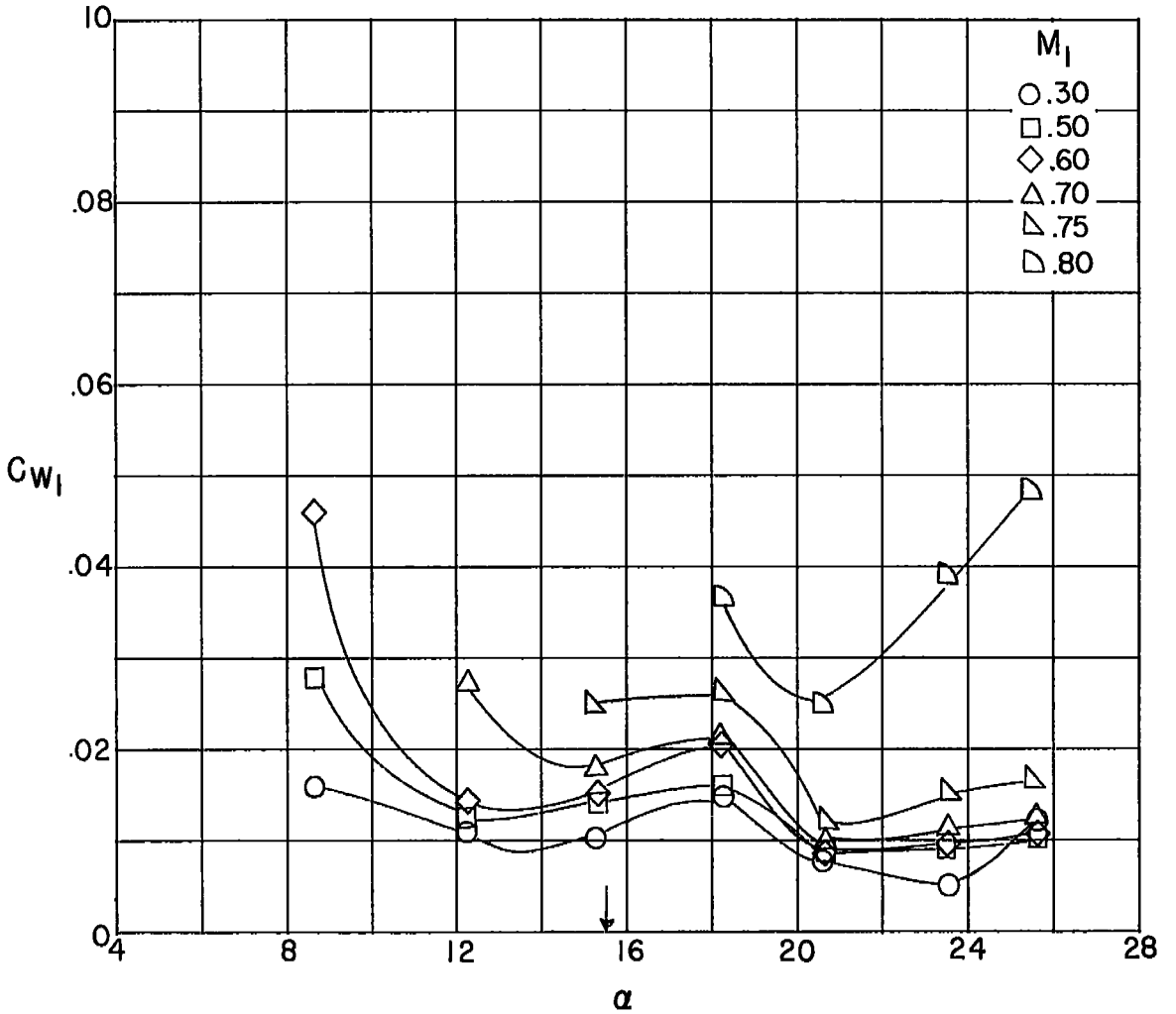

Figure 79.- Variation of momentum loss with angle of attack at constant Mach number for NACA 65-$(12A_{10})$10 blade section at $\beta_1 = 45^\circ$ and $\sigma = 1.5$. Arrow shows low-speed design angle of attack.

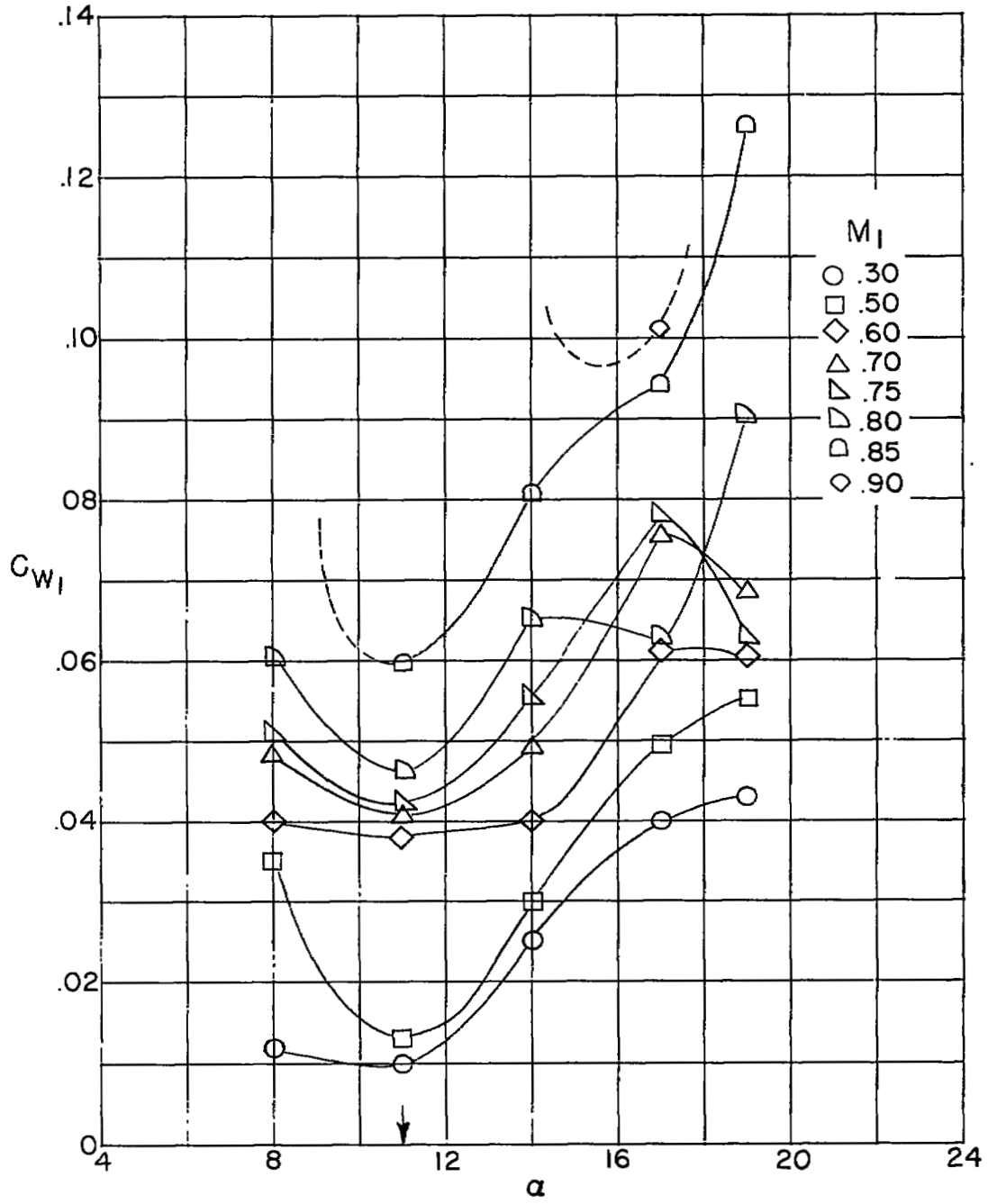

Figure 80.- Variation of momentum loss with angle of attack at constant Mach number for NACA 65-$(12A_2^I{}_{8b})$10 blade section at $\beta_1 = 60^\circ$ and $\sigma = 1.0$. Arrow shows low-speed design angle of attack.

[redacted]

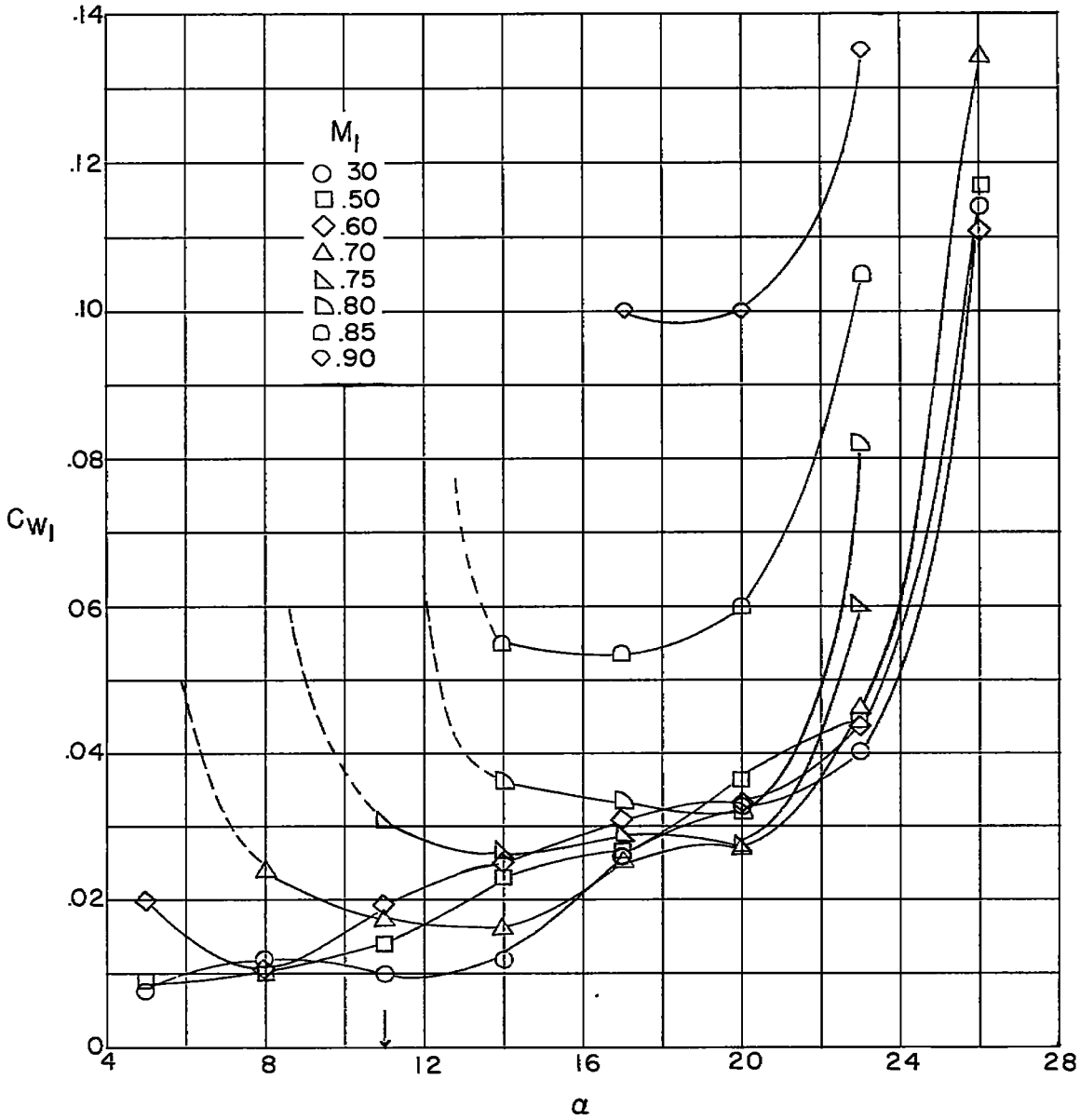

Figure 81.- Variation of momentum loss with angle of attack at constant Mach number for NACA 65-$(12A_2I_{8b})10$ blade section at $\beta_1 = 45^\circ$ and $\sigma = 1.0$. Arrow shows low-speed design angle of attack.

[redacted]

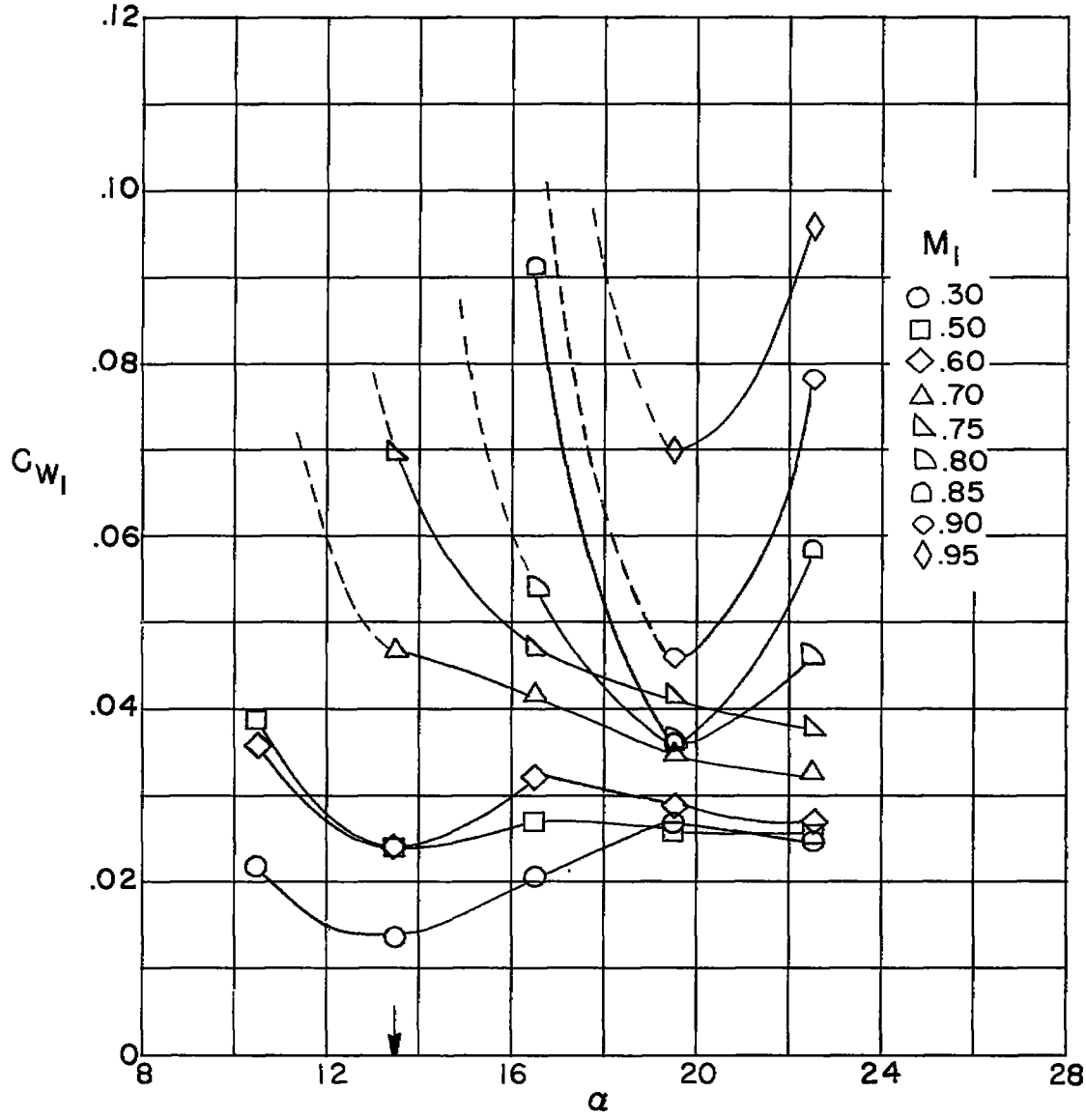

Figure 82.- Variation of momentum loss with angle of attack at constant Mach number for NACA 65-$(12A_2I_{8b})$10 blade section at $\beta_1 = 60^\circ$ and $\sigma = 1.5$. Arrow shows low-speed design angle of attack.

[redacted]

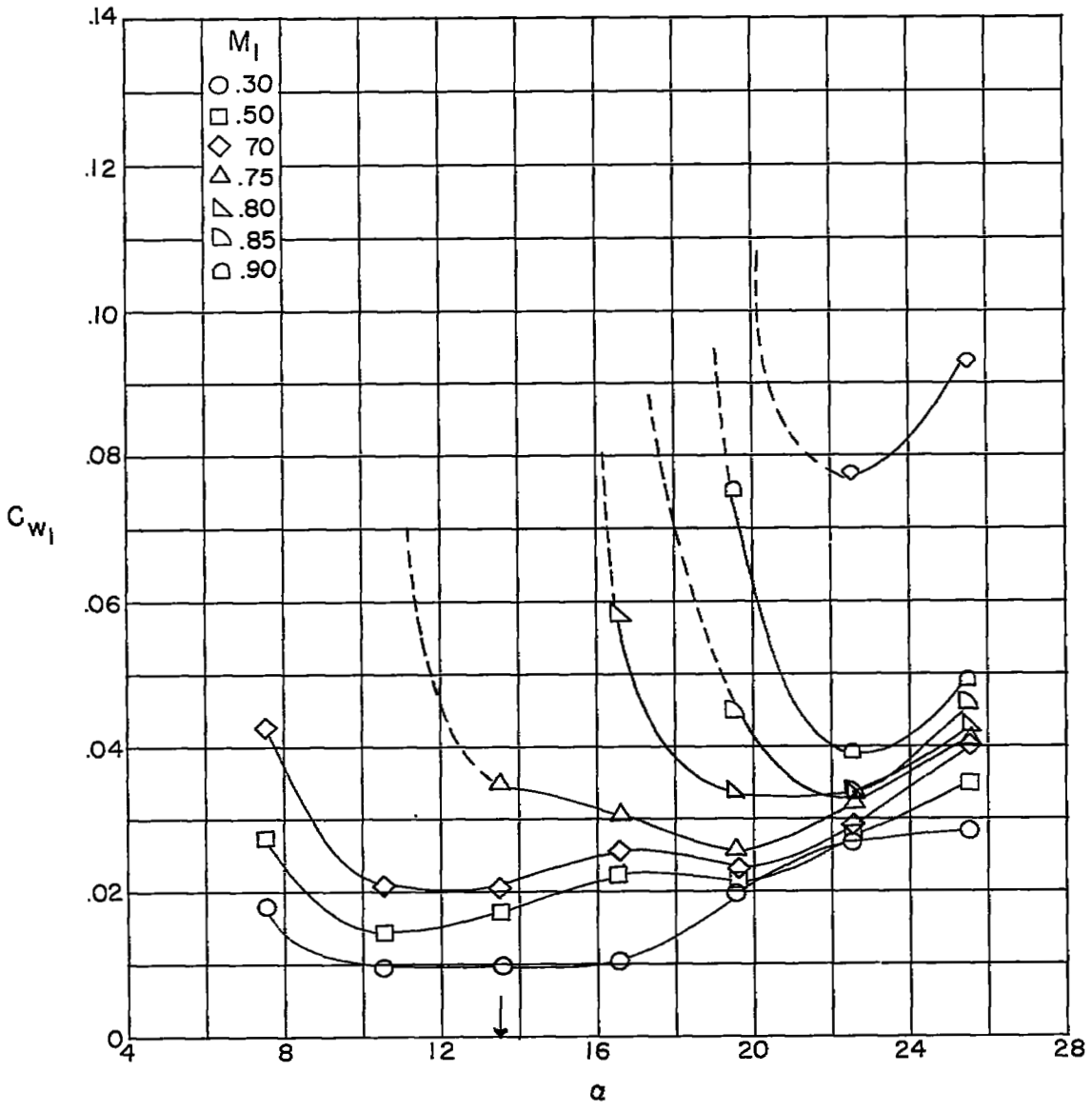

Figure 83.- Variation of momentum loss with angle of attack at constant Mach number for NACA $65(12A_2I_{8b})10$ blade section at $\beta_1 = 45^\circ$ and $\sigma = 1.5$. Arrow shows low-speed design angle of attack.

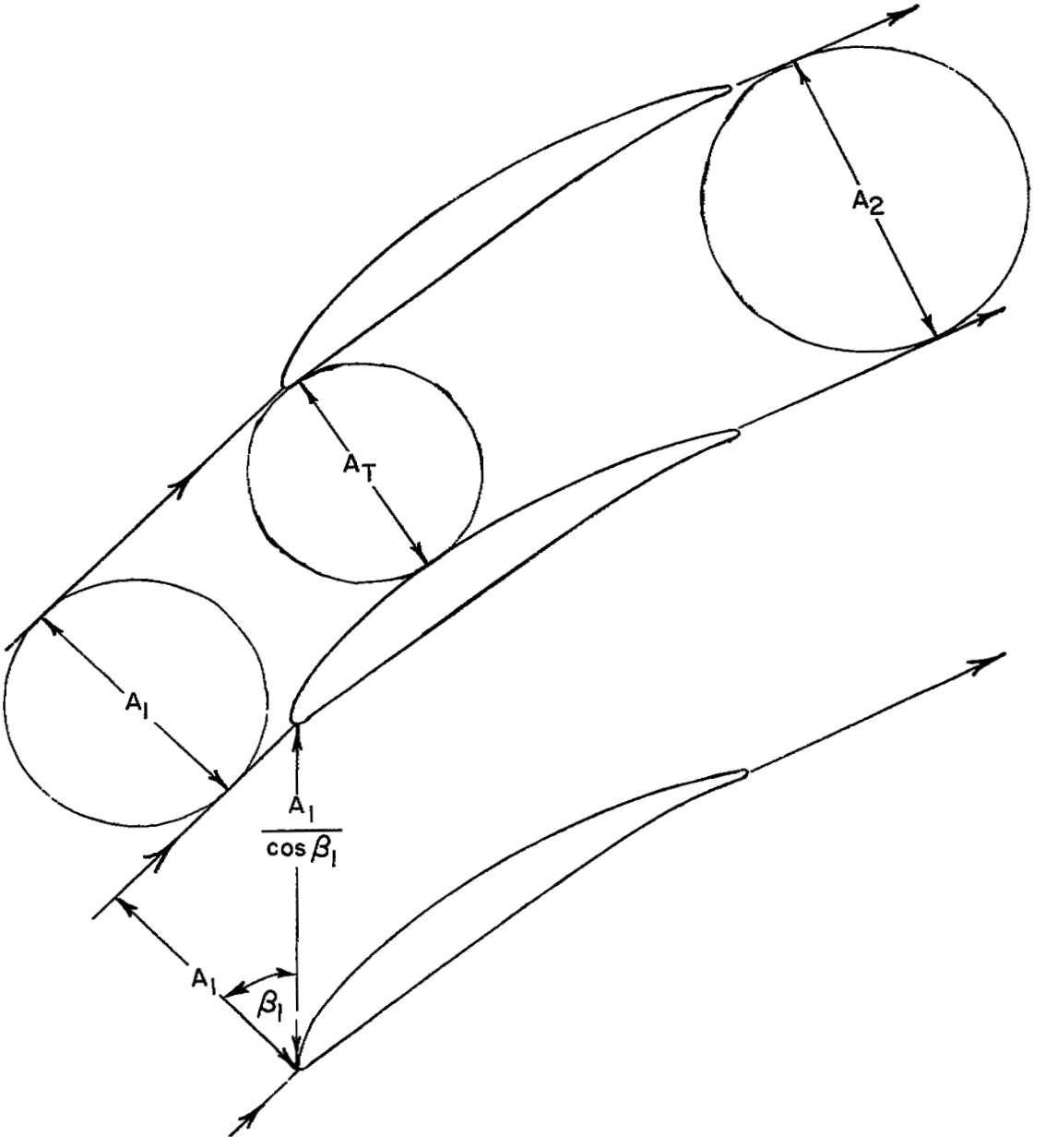

Figure 84.- Blade passage areas.

[redacted]

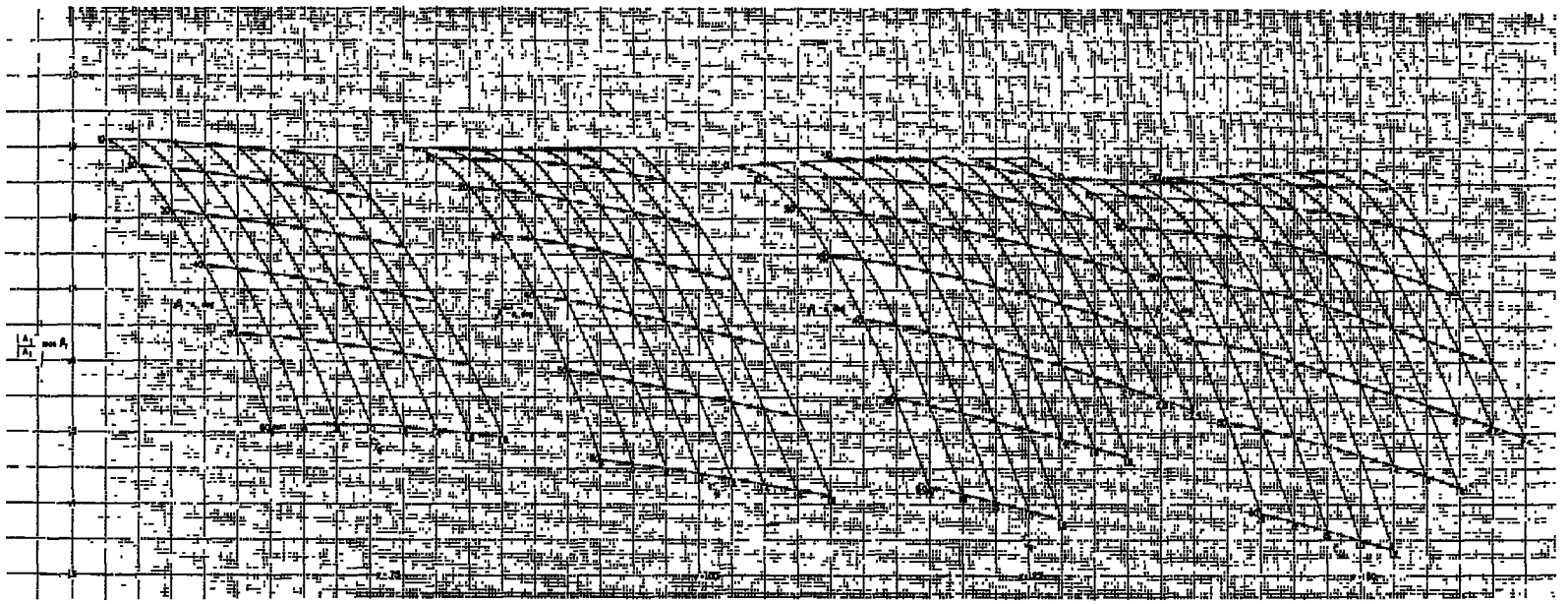

Figure 85.- Throat-area carpet plot of NACA 65-$\left(C_{l_0}A_{10}\right)$10 compressor blade-section cascade configurations.

(A large working copy of this chart may be obtained by using the request card bound in the back of the report.)

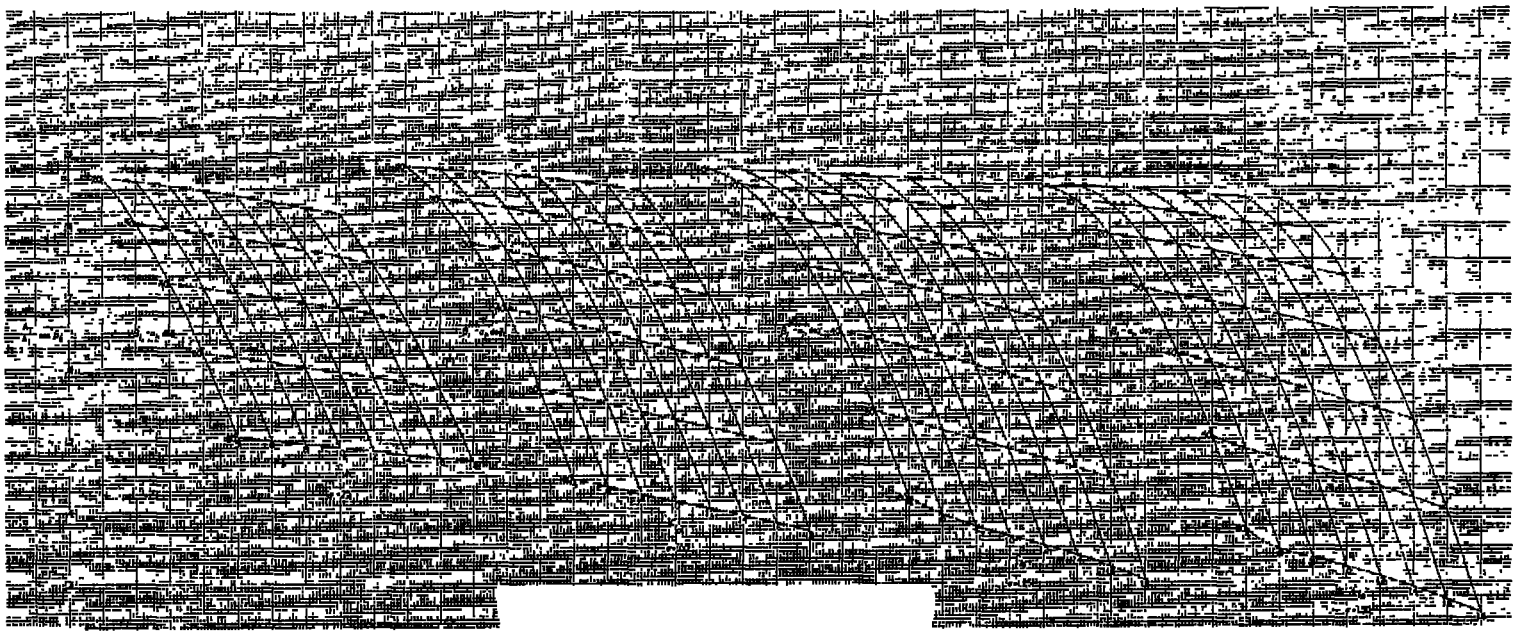

Figure 86.- Throat-area carpet plot of NACA 65-$\left(C_{l_o}A_2I_{8b}\right)$10 compressor blade-section cascade configurations.

(A large working copy of this chart may be obtained by using the request card bound in the back of the report.)

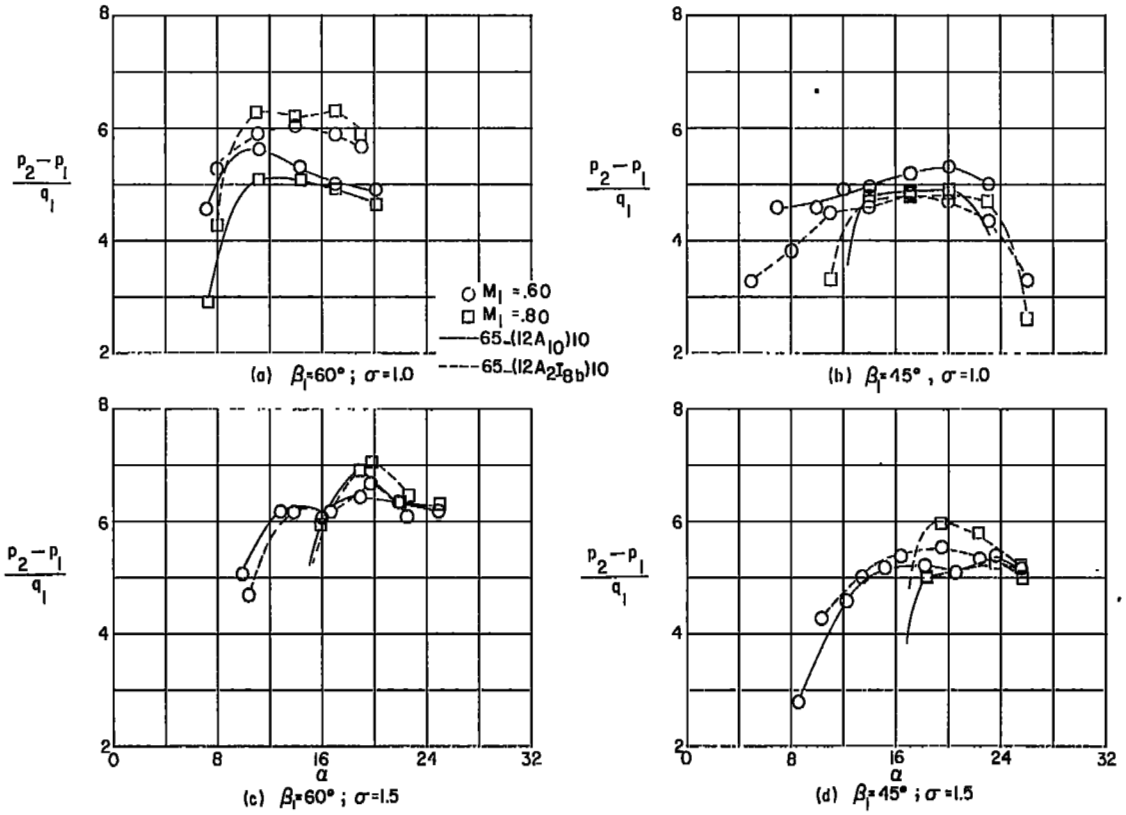

Figure 87.- Static-pressure rise measured across cascades on NACA 65$(12A_{10})10$ and 65-$(12A_2I_{8b})10$ compressor blades at Mach numbers of 0.6 and 0.8.